

**A Thesis Submitted for the Degree of  
Doctor of Philosophy**

**by**

**Sarah Dalibalta**

**Department of Cell Physiology and Pharmacology**

**University of Leicester**

**March 2008**

**Disclaimer:**

**The work presented in this thesis was performed by the author  
at the University of Leicester  
between October 2004 and March 2008.**

UMI Number: U495535

All rights reserved

INFORMATION TO ALL USERS

The quality of this reproduction is dependent upon the quality of the copy submitted.

In the unlikely event that the author did not send a complete manuscript and there are missing pages, these will be noted. Also, if material had to be removed, a note will indicate the deletion.



UMI U495535

Published by ProQuest LLC 2013. Copyright in the Dissertation held by the Author.  
Microform Edition © ProQuest LLC.

All rights reserved. This work is protected against  
unauthorized copying under Title 17, United States Code.



ProQuest LLC  
789 East Eisenhower Parkway  
P.O. Box 1346  
Ann Arbor, MI 48106-1346

**Human ether-a-go-go related gene (hERG) potassium channel gating and drug block**

hERG encodes the  $\alpha$ -subunit of the rapid delayed rectifier potassium current, a crucial current for normal repolarisation of the cardiac action potential. Pharmacological block of hERG is associated with arrhythmias and sudden death. Given its physiological importance, aspects of both the gating and pharmacology of this channel were investigated.

hERG has unusual gating properties characterised by slow activation and deactivation gating. The roles of conserved S6 glycines (Gly648 and Gly657) in hERG as hinges for activation gating were studied. Glycine residues impart flexibility that is thought to be conducive for channel opening. However, mutations at positions 648 and 657 altered gating in a manner consistent with a role in protein packing rather than flexibility. Deactivation gating in hERG is slow due to interactions between the amino-terminus, the voltage sensor, and the pore that stabilise the open state. The pore mutation V659A dramatically slowed channel deactivation and reduced drug block. Replacing Val659 with larger hydrophobic residues resulted in faster deactivation kinetics, but in contrast, V659G hERG was constitutively open. It was concluded that Val659 mutations influence deactivation through hydrophobic interactions with the S4-S5 linker that couples S6 to the voltage sensor. Effects on drug binding correlated with deactivation rates, indicating that Val659 mutations have allosteric rather than direct effects on drug binding.

Tyr652 is thought to be a critical residue for high affinity drug binding. However, this study showed that the contribution of Tyr652 to drug binding varied considerably among 24 compounds tested, with the majority of low affinity blockers being relatively insensitive to the Y652A mutation. Pharmacophore models generated from the results suggest that higher affinity compounds are longer than lower affinity compounds and simultaneously interact with multiple inner cavity residues. The compact structure of low affinity, Y652A-insensitive drugs permits multiple binding modes, making the compounds less reliant on interactions with Tyr652.

## **Acknowledgements**

I dedicate this book to all who believed in me, encouraged and supported me, and gave me the opportunity to pursue my dreams. I would like to thank my supervisor Dr. John Mitcheson for not only his help in creating this manuscript but also for his advice and guidance throughout my PhD. I am grateful for your belief in my potential and giving me the tools to go far in a scientific career. I am also thankful and lucky to have worked with a lovely group of people. I would like to extend my appreciation to Dr. Rachael Hardman, who dedicated countless hours of her time explaining and showing me how to do things in the lab and whose patience I am eternally grateful for. As well as Dr. Sarah Nelson for all the girly chats that I thoroughly enjoyed and looked forward to. I am happy to have spent my time at Leicester with all lab members, past and present, and in CPP, a truly warm and friendly department from which I will cherish many wonderful memories. I would like to thank my supervisors at Pfizer, Dr. Joanne Leaney and Dr. Gareth Waldron, as well as all lab members for giving me the opportunity to carry out some work in their lab and for their time and help while I was there. I also extend my thanks to Dr. Marcel de Groot and Dr. Phill Stansfeld for their contributions in the computational analysis of one of my studies.

The friendships that I have made along the way are ones that I intend to keep for a lifetime. You know who you are, and I thank you from the bottom of my heart, for making my journey worthwhile and unforgettable. To my family, thank you for teaching me that the difference between a successful person and others is not a lack of strength, not a lack of knowledge, but rather a lack of will. Thank you for always being there for me.

*To Mum and Dad*

*Meto and Nano,*

*'Have faith in your dreams and someday, your rainbow will come shining through.  
No matter how your heart is grieving, if you keep believing,  
the dream that you wish will come true' .....*

*With love*

## **Abbreviations**

ATP	<i>adenosine triphosphate</i>
bEAG	<i>bovine ether-a-go-go channel</i>
BK <sub>Ca</sub>	<i>large conductance calcium-activated potassium channel</i>
BSA	<i>bovine serum albumin</i>
CAT	<i>chloramphenicol transferase</i>
CHO	<i>chinese hamster ovary</i>
CMV	<i>cytomegalovirus</i>
C-terminus	<i>carboxy-terminus</i>
DEPC	<i>diethylpycarbonate</i>
DMSO	<i>dimethylsulphoxide</i>
DNA	<i>deoxyribonucleic acid</i>
EAG	<i>ether-a-go-go gene</i>
ECG	<i>electrocardiogram</i>
ECL	<i>enhanced chemiluminescence</i>
<i>E.coli</i>	<i>Escherichia coli</i>
eGFP	<i>enhanced green fluorescence protein</i>
E <sub>K</sub>	<i>potassium equilibrium potential</i>
ELK	<i>ether-a-go-go like potassium channel</i>
ER	<i>endoplasmic reticulum</i>
ERG	<i>ether-a-go-go related gene</i>
FBS	<i>foetal bovine serum</i>
FRET	<i>fluorescence resonance energy transfer</i>
FRT	<i>Flp-Recombination target site</i>
GIRK	<i>G-protein activated inward rectifier potassium channel</i>
HCN	<i>hyperpolarisation-activated, cyclic nucleotide gated channel</i>
HEK-293	<i>human embryonic kidney 293</i>
hERG	<i>human ether-a-go-go related gene</i>
HGNC	<i>Hugo Gene Nomenclature Committee</i>
HRP	<i>horseradish peroxidase</i>

Hsp	<i>heat shock protein</i>
IC <sub>50</sub>	<i>inhibitory concentration of 50 %</i>
IK	<i>intermediate conductance potassium channel</i>
I <sub>Kr</sub>	<i>rapid delayed rectifier potassium channel</i>
I <sub>Ks</sub>	<i>small delayed rectifier potassium channel</i>
I <sub>Kur</sub>	<i>ultra-rapid delayed rectifier potassium channel</i>
IRES	<i>internal ribosome entry site</i>
IUPHAR	<i>International Union of Pharmacology</i>
I-V	<i>current-voltage relationship</i>
K <sub>A</sub>	<i>A-type potassium channel</i>
K <sub>ATP</sub>	<i>ATP-sensitive potassium channel</i>
K <sub>ir</sub>	<i>inward rectifier potassium channel</i>
K <sub>v</sub>	<i>voltage-gated potassium channel</i>
LB	<i>Luria-Bertani</i>
LQTS	<i>long QT syndrome</i>
LQT2	<i>long QT type 2</i>
MEM	<i>minimum essential medium</i>
MESA	<i>MOPS EDTA sodium acetate</i>
<i>minK</i>	<i>minimum conductance potassium channel</i>
<i>MiRP1</i>	<i>minK Related Protein</i>
MTS	<i>methanethiosulfonate</i>
NBF	<i>neutral buffered formalin</i>
NEM	<i>N-ethylmaleimide</i>
NMG	<i>N-methyl-D-glucamide</i>
N-terminus	<i>amino- terminus</i>
NTK	<i>N-terminal truncated</i>
OR2	<i>oocyte ringer solution</i>
PAS	<i>PER-ARNT-SIM domain</i>
PBS	<i>phosphate buffered saline</i>
PCR	<i>polymerase chain reaction</i>
QA	<i>quaternary amine</i>

QSAR	<i>quantitative structure-activity relationship</i>
RIPA	<i>radioimmunoprecipitation assay</i>
RNA	<i>ribonucleic acid</i>
rpm	<i>revolutions per minute</i>
SDS	<i>sodium dodecyl sulphate</i>
SK	<i>small conductance potassium channel</i>
SOC	<i>salt optimised and carbon</i>
SQTS	<i>short QT syndrome</i>
TbuA	<i>tetrabutylammonium</i>
Tdp	<i>torsades de pointes</i>
TEA	<i>tetraethylammonium</i>
TM	<i>transmembrane</i>
TOK1	<i>tandem pore outwardly rectifying potassium</i>
TTBS	<i>tris tween buffered saline</i>
UV	<i>ultraviolet</i>
$V_{0.5}$	<i>half point for the voltage dependence of gating</i>
$V_m$	<i>membrane potential</i>
WT	<i>wild type</i>
3D	<i>three-dimensional</i>

## **Table of Contents**

Abstract	ii
Acknowledgements	iii
Abbreviations	iv
Contents	vii
Publications	x
<b>Chapter 1. Introduction</b>	<b>1</b>
1.1 Potassium channel families	1
1.2 Structure of voltage-gated potassium channels	6
1.2.1 <i>Structure of the pore region</i>	7
1.2.2 <i>Structure of the voltage sensing region</i>	13
1.3 hERG channel structure and functions	18
1.4 Gating properties of hERG channels	20
1.4.1 <i>Structural basis of hERG activation gating</i>	21
1.4.1.1 <i>Interactions between the pore and voltage sensor stabilise the closed state</i>	22
1.4.2 <i>Structural basis of hERG deactivation gating</i>	25
1.4.3 <i>Structural basis of hERG inactivation gating</i>	26
1.5 Role of hERG in the heart	30
1.6 Long QT Syndrome	32
1.7 Structural basis of hERG block	35
1.8 Alternative mechanisms of block	39
1.9 Predicting hERG block	41
1.10 Aims of this thesis	43
<b>Chapter 2. Materials and Methods</b>	<b>45</b>
2.1 Molecular Biology	45
2.1.1 <i>Mutagenesis</i>	45
2.1.2 <i>Transformation of competent cells</i>	47
2.1.3 <i>Preparation of DNA</i>	48
2.1.4 <i>Subcloning of hERG fragments into expression vectors</i>	49
2.1.5 <i>DNA extraction from agarose gels</i>	50
2.1.6 <i>Ligation of DNA fragments</i>	51
2.1.7 <i>Preparation of cRNA by in vitro transcription</i>	52
• <i>Preparation of template DNA</i>	52
• <i>Preparation of cRNA</i>	52

2.2 Two-electrode voltage clamp recordings in <i>Xenopus</i> oocytes	53
2.2.1 <i>Basic characteristics of a Xenopus oocyte</i>	54
2.2.2 <i>Isolation of Xenopus oocytes</i>	54
2.2.3 <i>cRNA injection into Xenopus oocytes</i>	55
2.2.4 <i>Two-electrode voltage clamp recordings</i>	55
2.2.5 <i>Data acquisition and analysis</i>	56
• <i>Current-Voltage (I-V) relationship of hERG</i>	58
• <i>Time dependence of the hERG current</i>	58
• <i>Concentration-response relationships</i>	58
2.2.6 <i>Statistical analysis of the data</i>	59
2.3 Cell Culture	59
2.3.1 <i>Cell lines and their maintenance</i>	59
• <i>hERG-HEK cells</i>	60
• <i>Pore mutant hERG-HEK cells and WT- HEK cells</i>	60
• <i>Flp-In HEK 293 and Flp-In CHO cells</i>	61
2.3.2 <i>Generation of stable cell lines</i>	61
2.4 Western blotting	63
<b><u>Chapter 3. Investigating the glycine hinge hypothesis in hERG</u></b>	<b>65</b>
3.1 Characterisation of WT hERG channels	67
3.1.1 <i>Activation kinetics of WT hERG currents</i>	67
3.1.2 <i>Deactivation kinetics of WT hERG currents</i>	71
3.1.3 <i>Time and voltage dependent kinetics of inactivation in WT hERG channels</i>	73
3.2 Alanine substitution of the gating hinge glycine residues	78
3.3 Substituting the glycine residues with larger amino acid residues	86
3.4 Pharmacology of Gly657 and Gly648 mutants	96
3.5 Discussion	103
<b><u>Chapter 4. Generation of stable cell lines</u></b>	<b>105</b>
4.1 Characterisation of pore helix residues (Thr623 and Ser624)	107
4.2 Flp-In System for generating stable cell lines	112
4.3 Preparation of the pcDNA5/FRT expression vector	113
4.4 Determination of hygromycin sensitivity for HEK-293 and CHO cells	115
4.5 Transfection methods	117
4.6 Assay for hERG protein	117
4.7 Generation of stable cell lines using Lipofectamine	120
4.8 Discussion	124
<b><u>Chapter 5. Investigation of the structural determinants of hERG block using the PatchXpress</u></b>	<b>127</b>

5.1 The PatchXpress 7000A	129
5.2 Solutions	132
5.3 Cell preparation	132
5.4 Compound preparation	134
5.5 Seal formation	136
5.6 Experimental procedure	139
5.7 Data analysis	139
5.8 WT hERG concentration-response relationships	141
5.9 Y652A hERG concentration-response relationships	145
5.10 Structural analysis of the PatchXpress data	149
5.11 Discussion	154
5.12 Comparisons between electrophysiological automated systems	155
<b><u>Chapter 6. The role of inner helix (Val659 and Ile662) residues in hERG gating and pharmacology</u></b>	<b>157</b>
6.1 Characterisation of the activation and deactivation kinetics of V659A currents	159
6.1.1 <i>Activation kinetics of V659A hERG currents</i>	159
6.1.2 <i>Deactivation kinetics of V659A hERG currents</i>	161
6.2 Characterisation of the N-terminal truncated WT and V659A currents	164
6.3 Substituting Val659 with other amino acid residues (Cys, Phe, Ile, Trp)	168
6.3.1 <i>Effects of Val659 mutations on activation gating</i>	168
6.3.2 <i>Effects of Val659 mutations on deactivation kinetics</i>	172
6.3.3 <i>Effects of Val659 mutations on inactivation gating</i>	176
6.4 Substituting Val659 with a glycine residue	180
6.5 Pharmacology of Val659 mutants	182
6.6 Effects of mutations at Ile662 on gating	184
6.6.1 <i>Effects of Ile662 mutants on activation gating</i>	184
6.6.2 <i>Effects of Ile662 mutants on deactivation gating</i>	186
6.7 Effects of I662A on hERG pharmacology	189
6.8 Discussion	191
<b><u>Chapter 7. General Discussion and Summary</u></b>	<b>194</b>
7.1 hERG activation gating	194
7.2 hERG deactivation gating	199
7.3 The hERG drug binding site	204
7.4 Overall Summary	208
<b><u>Chapter 8. Bibliography</u></b>	<b>210</b>

## **Publications**

**'Activation gating of hERG potassium channels: S6 glycines are not required as gating hinges'. J Biol Chem. 2007 Nov 2; 282(44):31972-81**

*Rachael M. Hardman, Phillip J. Stansfeld, Sarah Dalibalta, Michael J. Sutcliffe and John S. Mitcheson*

**Book chapter entitled: "hERG biology and structure-activity relationships" for the book: "Antitargets in drug discovery – Prediction and Prevention of Side Effects", published under the series "Methods and Principles in Medicinal Chemistry", 2008**

*Sarah Dalibalta, John S. Mitcheson*

### **Abstracts:**

**Journal of Molecular and Cellular Cardiology. 39(1) 169-170. 2005 (poster)**

The role of inner helix glycine residues in the activation gating of hERG potassium channels.

*Rachael M. Hardman, Sarah Dalibalta, John S. Mitcheson*

**Biophysical society annual meeting, Salt Lake City, Utah, February 2006 (poster)**

Do hERG potassium channels require a glycine hinge for activation gating?

*Rachael M. Hardman, Sarah Dalibalta, John S. Mitcheson*

**Ion channel symposium, Leeds, UK, July 2007 (talk)**

An investigation of drug interactions with the aromatic residue Tyr652 in the inner cavity of hERG potassium channels.

*Sarah Dalibalta*

**Biophysical society annual meeting, Long Beach, California, February 2008 (poster)**

Role of S6 residues in hERG gating and pharmacology.

*Sarah Dalibalta, John S. Mitcheson*

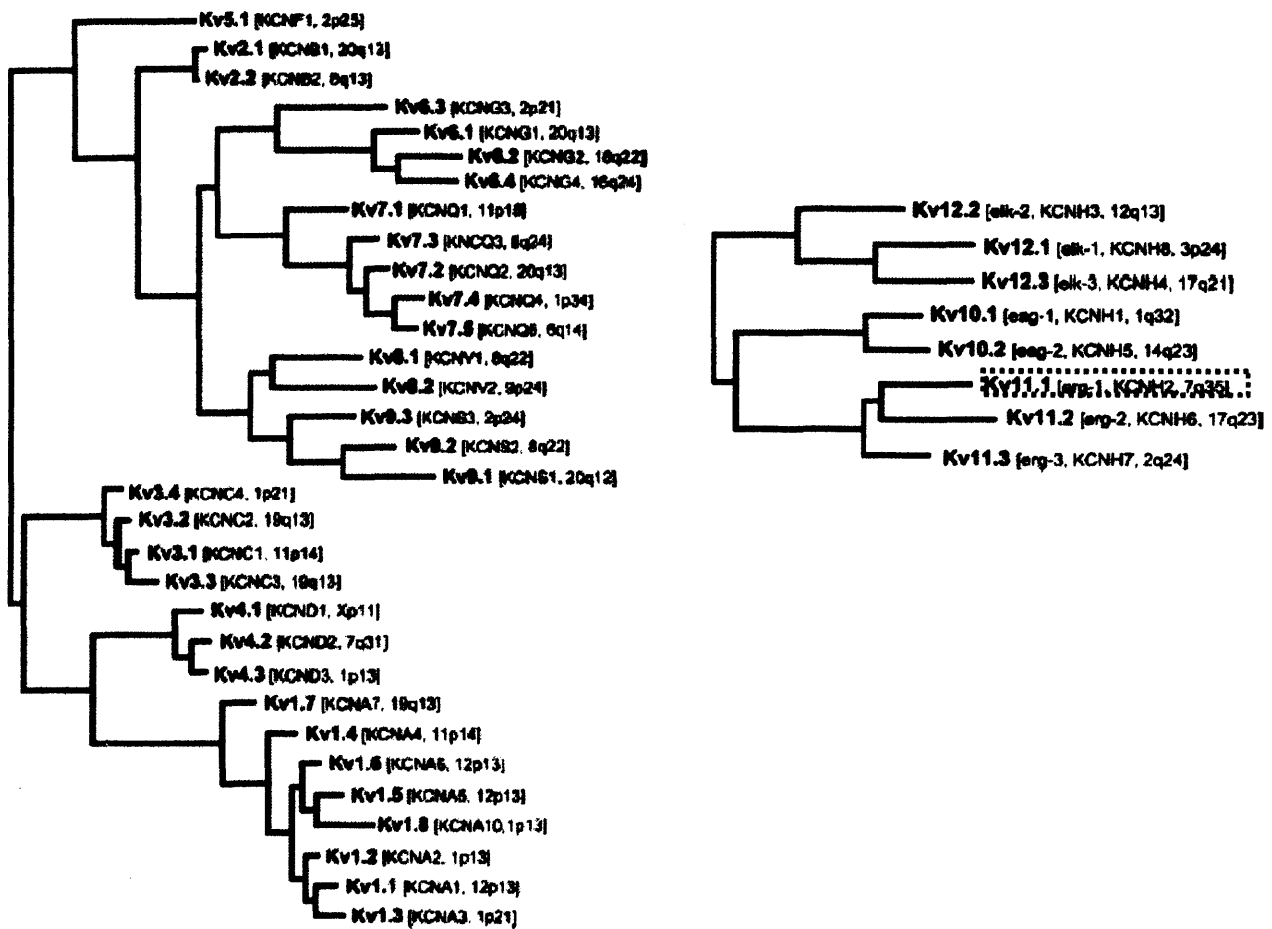
**1.1 Potassium channel families**

Potassium ( $K^+$ ) channels are found in almost all cells and are by far the most diverse family of ion channels. They were initially grouped into subfamilies according to whether they have 2 transmembrane (TM) domains (such as inward rectifier  $K^+$  channels), 4 TM domains (such as twin pore  $K^+$  channels), or 6 TM domains (such as voltage dependent  $K^+$  channels) (Hille, 2001). Some channels though do not conform to this general grouping, such as  $BK_{Ca}$  (large conductance calcium ( $Ca^{+2}$ ) - activated  $K^+$ ) channels that have 7 TM domains and TOK1 (tandem pore domain, outwardly rectifying  $K^+$ ) channels that have 8 TM domains. Since the mapping of the human genome, over 70 genes have been shown to encode  $K^+$  channel subunits hence channel families and subfamilies have been re-grouped based on their sequence homology, as well as structural and functional properties.

The first  $K^+$  channel gene to be cloned was the voltage-gated *Shaker* channel from the fruitfly, *Drosophila melanogaster*. It was so-called due to a shaking wing phenotype caused by a mutation in this gene. Since then, a whole host of voltage and ligand-gated  $K^+$  channels have been identified in a variety of organisms (Jan & Jan, 1997). The voltage-gated channels in mammals consist of over 40 genes and show a high sequence homology with the Shaker channels (Figure 1.1). Shaker channels are referred to as Kv1.1 channels by the International Union of Pharmacology (IUPHAR); where 'K' denotes potassium channel, 'v' denotes voltage-gated, and the first '1' is the *Shaker* subfamily (Gutman *et al.*, 2003; Gutman *et al.*, 2005). The HUGO Gene Nomenclature Committee (HGNC) also assigned *KCNA1* as its gene name. Further diversification arises with the sister channels Kv2.x or *KCNB* (*Shab*), Kv3.x or *KCNC* (*Shaw*), and Kv4.x or *KCND* (*Shal*). Kv5, 6, 8, and 9 include modifier subunits that assemble with other  $K^+$  subunits to form conductive channels. Kv7 channels, also called KCNQ (formerly known

## Chapter 1- Introduction

**Figure 1.1: Classification of Kv channels.** This shows a dendrogram of Kv channel families 1-9 and 10-12. It also gives the human gene name according to the IUPHAR and HGNC as well as the chromosome number. The nomenclature and chromosome localisation for the hERG channel, the subject of study in this thesis, is highlighted by a red box.



From Gutman et al., 2005

## Chapter 1- Introduction

as KvLQT) channels, form interactions with accessory subunits or heterotetramers with other subunits and have major implications in channelopathies such as cardiac arrhythmias, epilepsy, and deafness (Brugada *et al.*, 2007). The KCNH subfamily, which are Kv10-12, are closely related to each other and include the EAG, ERG, and ELK channels. hERG channels (also referred to as human ERG1, Kv11.1, or by the gene product KCNH2) belong to the EAG family and have been subjected to much attention due to their role in long QT type 2 (LQT2) syndrome (Sanguinetti & Tristani-Firouzi, 2006). This voltage-gated K<sup>+</sup> channel is the subject of study in this thesis.

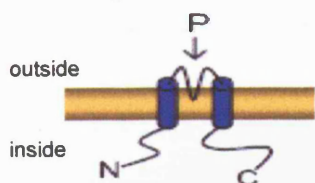
K<sup>+</sup> channels permit K<sup>+</sup> ions through their pore at a rate of up to 10,000 K<sup>+</sup> ions per second and can be identified by a consensus amino acid sequence – TXXTXGY(F)GD – called the K<sup>+</sup> channel ‘signature sequence’ lining the selectivity filter (Yellen, 2002). Mutations of this motif lead to a disruption in channel selectivity. The diversity within K<sup>+</sup> channel families is reflected in their numerous physiological functions. Generally, K<sup>+</sup> channels set the resting membrane potentials of cells, regulate repolarisation of action potentials, and control excitability. Their roles in non-excitabile cells include cellular K<sup>+</sup> recycling for electrolyte balance in the kidney, regulating osmotic flow of gas and water in plants, as well as volume and shape regulation of erythrocytes (Miller, 2000). The activities of K<sup>+</sup> channels are tightly regulated and respond to varying signals. Inward rectifier K<sup>+</sup> channels are gated by intracellular mediators such as G-proteins, polyamines, and nucleotides. Voltage-gated channels respond to depolarising voltage changes, and Ca<sup>+2</sup> - activated K<sup>+</sup> channels respond to changes in intracellular calcium levels and some are also sensitive to voltage.

Structurally, K<sup>+</sup> channels can be grouped according to the number of TM spanning  $\alpha$ -helical domains (Figure 1.2). The 2 TM domain proteins, four of which form one pore, include the inward rectifier K<sup>+</sup> channel family that also contain a TM domain linker forming the selectivity filter. They are formed from Kir subunits and are functionally characterized by large inward currents upon hyperpolarisation and relatively small currents at depolarized potentials (Nichols & Lopatin, 1997). They are generally of two types, strong and weak inward rectifiers. Strong inward rectifiers such as Kir2, Kir3, and

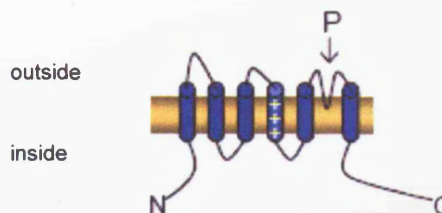
## Chapter 1- Introduction

**Figure 1.2: Membrane topology of K<sup>+</sup> channels.** K<sup>+</sup> channels may be grouped according to the number of TM domains. The Kir family of channels has two TM domains and one pore (P) region as well as intracellular amino (N)- and carboxy (C)-termini. The twin pore family of channels has two P regions and four TM domains while the Kv family has one P region and six TM domains as well as intracellular N- and C-termini. The BK<sub>Ca</sub> family of channels has seven TM domains and one P region. Its N-terminus is located extracellularly and its intracellular C-terminus contains a Ca<sup>+2</sup> - binding domain (Ca-bowl).

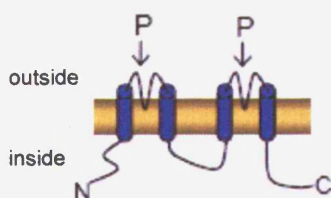
### 2 transmembrane domain Kir family



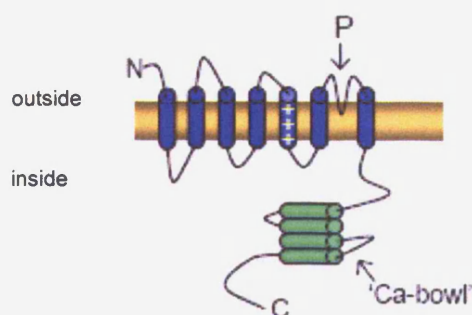
### 6 transmembrane domain Kv family



### 4 transmembrane domain Twin pore family



### 7 transmembrane domain BK<sub>Ca</sub> channels



## Chapter 1- Introduction

Kir4 have a high open probability at hyperpolarizing potentials and are important in maintaining the resting potential in cells. Some are G-protein regulated (Kir3.x) hence open in response to hormones and neurotransmitters (for example, acetylcholine-activated  $K^+$  channels  $K_{ACh}$ ). Weak inward rectifiers such as Kir1, Kir6, and Kir7 show more significant outward current and have diverse roles, such as hyperpolarizing cells when ATP levels are low and regulating insulin secretion from pancreatic  $\beta$ -cells (Kir6.x or  $K_{ATP}$  channels). The 4 TM family includes the twin pore domain  $K^+$  channels, whereby only two subunits are required to form a channel (Farley & Rudy, 1988). They are very weakly voltage dependent and contribute to the 'leak' current often found in recordings of native cells. These channels are regulated by pH, oxygen tension, neurotransmitters, and some anaesthetics. They are important in the modulation of neuronal excitability and possibly act as an oxygen sensor in pulmonary artery smooth muscle (O'Connell *et al.*, 2002; Gurney & Joshi, 2006).

The 6 TM domain voltage-gated  $K^+$  channels are comprised of Kv subunits. They are activated by membrane potential depolarisation and can be functionally grouped into delayed rectifiers or A-type transient outward currents (Hille, 2001):

- a) Delayed rectifiers: These channels show slow or no inactivation (decrease of channel conductance with maintained depolarisation) and exhibit rectification due to their conductance varying with voltage such that they conduct more readily in the outward direction. Fast delayed rectifiers are from the Kv1-4 subfamily and are expressed in unmyelinated axons, motor neurons, and fast skeletal muscle and thus are important in repolarisation of very short action potentials in high firing frequency neurons such as in the auditory system. Slow delayed rectifiers are from the EAG/ERG and KCNQ subfamilies and are expressed in cardiac and neuronal cells. They play important roles in longer action potentials such as repolarisation of the cardiac action potential. In neurons, they influence excitability and adaptation of action potential firing frequency.

## Chapter 1- Introduction

- b) A-type ( $K_A$ ) or transient outward  $K^+$  channels: are closed at normal resting potentials and produce a transient, rapidly activating and fast inactivating current upon depolarisation. They have a sustained conductance within a narrow window of negative sub-threshold potentials from -65 to -40 mV. They therefore play an important role in cells that fire repetitively by dampening interspike depolarisation and in cardiac cells, they partially repolarise action potentials and influence the plateau potential.

$Ca^{+2}$  - activated  $K^+$  channels have 7 TM domains and are divided into three classes depending on ionic conductance; BK channels which are high conductance channels, IK channels which are intermediate conductance channels, and SK channels which are small conductance channels. BK channels are the only voltage dependent channels in this family and respond to membrane depolarisation. These channels are also sensitive to  $[Ca^{+2}]_i$  due to the presence of 'calcium bowls' on their C-termini, which are thought to bind  $Ca^{+2}$ . BK channels provide a hyperpolarizing negative feedback when sufficient calcium has entered or in response to  $Ca^{+2}$  liberation from internal stores.

This project is mainly concerned with hERG, a member of the voltage-gated  $K^+$  channel family. Therefore, I will discuss the broader structural and functional characteristics of these channels and then focus on the specific structure, gating, and physiological properties of hERG  $K^+$  channels.

### **1.2 Structure of voltage-gated potassium channels**

Voltage-gated potassium channels share a common basic architecture (Yellen, 2002). They exist as tetrameric structures, with each subunit containing 6 TM  $\alpha$ -helical segments (denoted S1-S6) and large amino and carboxy termini on the intracellular side. A variable pore (P) segment lies between S5 and S6, which together form the pore domain of the channel. The P segment contains a short pore helix and an extended polypeptide chain that forms the selectivity filter, the narrowest part of the pore. These channels also contain a voltage sensor, which involves the S4 segment and its positively charged

## Chapter 1- Introduction

residues and S1-S3 segments with negatively charged residues. In addition to  $\alpha$ -subunits, these channels usually contain additional subunits whose functions are regulatory or are involved in cytoskeletal interactions. Advances in structural analysis methodologies as well as functional probing of these various domains has led to a much clearer understanding of the structure of the pore domain and the voltage sensing domain of voltage-gated  $K^+$  channels.

### 1.2.1 Structure of the pore region

Studies on drugs and toxins that block  $K^+$  channels have been instrumental in the structural characterisation of their pore region. Early experiments by Armstrong (Armstrong, 1971) using tetraethylammonium (TEA) ions on voltage-gated  $K^+$  channels of the squid axon showed that TEA blocked current through these channels when applied from the intracellular side. TEA was able to bind to its receptor within the channel only when a depolarising pulse to open the channel was applied. Long chain derivatives of TEA also blocked the squid axon delayed rectifier  $K^+$  currents with an increased potency by slowing dissociation from its receptor. In addition, applying  $K^+$  ions to the extracellular side and stepping to negative potentials to generate an inward flux of  $K^+$  ions displaced TEA from its receptor site. Hence, a model for the pore of these channels emerged whereby they have an inner vestibule guarded by a cytoplasmic gate on the intracellular side and a constriction on the extracellular side that stops the drug from passing further once in the pore, but selectively allows  $K^+$  ions to pass through. This inner vestibule was proposed to be formed by the S6 transmembrane segments. Mutations in the S6 helix appeared to alter the binding of quaternary amines (QA) to the pore domain (Choi *et al.*, 1993). Furthermore, cysteine accessibility data on Shaker channels showed that residues on S6 at positions 470-477 line the gated intracellular part of the pore and these positions are protected from reaction by methanethiosulfonate (MTS) reagents when the channel is blocked by tetrabutylammonium (TbuA) in the open state (Liu *et al.*, 1997). This is consistent with these positions lying within the pore of the channel and access is regulated by an intracellular gate. A mutation of I470C in Shaker, which locks the channel in the open state, also allowed the binding of TEA and

## Chapter 1- Introduction

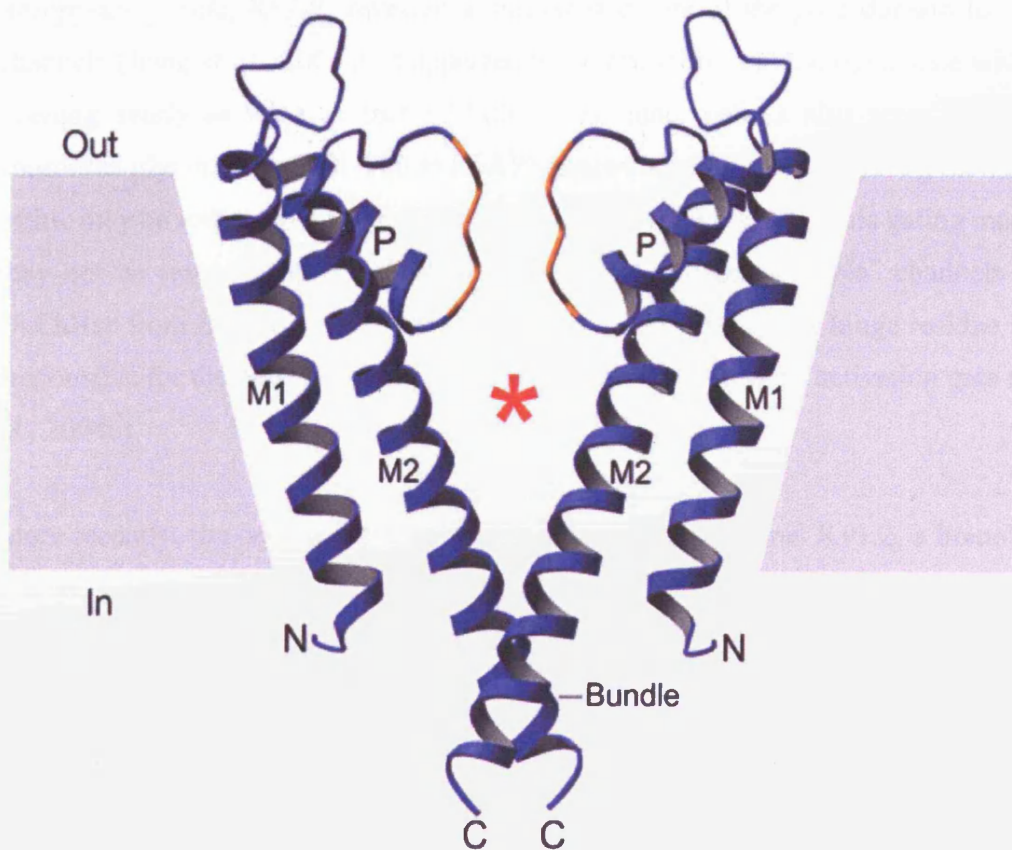
decyltriethylammonium ( $C_{10}$ ) within the pore without interfering with closure of the activation gate also supporting a model of a large inner cavity that can accommodate blockers and where access is controlled by a lid that can open and close (Holmgren *et al.*, 1997). This gate or lid is called the activation gate as it physically opens and closes the ion conduction pathway in response to changes in membrane potential and is formed by the S6 region. Further studies on a type of inactivation in Shaker  $K^+$  channels called N-type inactivation, which involves binding of the N-terminal domain to the pore when the gate is open, further pointed to the location of the activation gate on the intracellular part of channel and the presence of a receptor site behind the gate (Hoshi *et al.*, 1990; Zagotta *et al.*, 1990).

The best evidence of the structure of the pore-forming region of  $K^+$  channels then came from crystal structures of bacterial channels. In 1998, the first crystal structure was solved of the  $K^+$  channel KcsA, from the bacterium *Streptomyces lividans* (Doyle *et al.*, 1998). It is a relatively simple prokaryotic channel with 2 TM domains with sequence homology to S5 and S6 in Kv channels, and is thus not gated by voltage. The crystal structure revealed that this  $K^+$  channel had 4 identical subunits forming an inverted teepee structure surrounding a central pore. The inner helices converge at the cytoplasmic end to form a bundle crossing, proposed to be the activation gate of the channel (Figure 1.3). Since the gate is almost fully closed, this channel was proposed to be crystallized in the closed state. The narrow selectivity filter is on the extracellular side and has carbonyl oxygen atoms from the peptide backbone of the  $K^+$  channel 'signature sequence' amino acids (Gly-Tyr-Gly) that coordinate  $K^+$  ions in a single file. A water-filled cavity lies between the selectivity filter and the bundle crossing. The cavity is lined with hydrophobic residues that limit ion contact with the pore enabling fast ion conduction. Another channel, KirBac1.1 from the inward rectifier family of  $K^+$  channels, was also crystallized in the closed state (Kuo *et al.*, 2003).

Elucidation of the crystal structure of a calcium-gated  $K^+$  channel, MthK, from the archeon *Methanobacterium thermoautotrophicum* illustrated a mechanism for opening of the activation gate (Jiang *et al.*, 2002a). This channel also has a tetrameric, two TM

## Chapter 1- Introduction

**Figure 1.3: Representation of the crystal structure of KcsA.** This structure shows two of the four subunits of the KcsA  $K^+$  channel where M1 is the outer helix and M2 is the inner helix. P refers to the pore helices that position the selectivity filter. The inner helices cross over (Bundle) close to one another on the cytoplasmic side of the membrane to form the intracellular gate that is closed to the movement of  $K^+$  ions. The selectivity filter is shown in orange and the red asterisk marks the central cavity.



## Chapter 1- Introduction

domain structure. Instead of an inner helix bundle crossing, the cytoplasmic ends of the S6 helices are splayed wide open creating a large opening (12 Å in diameter) to the cytoplasm. This would allow K<sup>+</sup> ions to pass through the pore and selectivity filter and therefore, the channel was proposed to be crystallized in the open state. Comparison between the structures of KcsA and MthK suggests that the S6 helices bend at a conserved glycine located just below the selectivity filter. This gating hinge point corresponds to Gly99 in KcsA and Gly83 in MthK. A bend of approximately 30° was observed in MthK at this residue and is thought to induce opening of the channel (Jiang *et al.*, 2002b). The resolved crystal structure of a bacterial Kv channel homolog from *Aeropyrum pernix*, KvAP, revealed a similar structure of the pore domain to other K<sup>+</sup> channels (Jiang *et al.*, 2003a). It appeared to be crystallized in the open state with a pore opening nearly as wide as that of MthK. The inner helices also seem to bend at a conserved glycine hinge (Gly220 in KvAP) suggesting that a similar gating mechanism to MthK may be responsible for opening of the channel (Figure 1.4). This gating mechanism may not be restricted to K<sup>+</sup> channels as bacterial voltage-gated Na<sup>+</sup> channels such as NaChBac from *Bacillus halodurans*, also has a conserved glycine hinge residue in its S6 responsible for the bending of its inner helices and opening of its activation gate (Zhao *et al.*, 2004b).

More recently, the crystal structure of a mammalian Kv channel Kv1.2, a homologue of *Shaker*, was also crystallized in the open state with its inner helices displaying a bend at the cytoplasmic end (Long *et al.*, 2005a). No notable kink was observed at the glycine hinge position in this structure, but rather at the Pro-X-Pro motif found on the lower part of S6 in Shaker family Kv channels but not in prokaryotic channels (Figure 1.5). This motif is highly conserved in Kv1-4 eukaryotic channels and could suggest that the structure of the gate in eukaryotic Kv channels may be different from the observed X-ray structures. Prolines are thought to destabilize α-helices by breaking backbone hydrogen bond networks (Bright *et al.*, 2002). The unusual structure of proline also induces a bend/kink that breaks helices. These properties thus confer hinge-like properties that are proposed to allow movement of S6 during activation gating (Yellen, 1998; del Camino *et al.*, 2000). Mutating this motif leads to a loss of function or channels that favor the

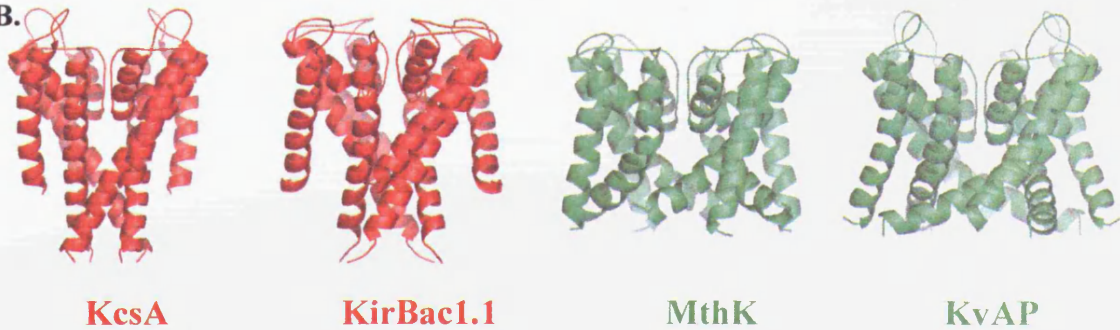
## Chapter 1- Introduction

**Figure 1.4: Crystal structures of K<sup>+</sup> channels.** **A.** Sequence alignments of the pore helix and inner helices of hERG and prokaryotic K<sup>+</sup> channels that have been crystallized. Grey boxes indicate conserved areas between these sequences. **B.** Crystal structures of K<sup>+</sup> channels. KcsA and KirBac1.1 were crystallized in the closed state while MthK and KvAP were crystallized in the open state. The inner helices bend at a conserved glycine (indicated by the green box in the sequence alignment), proposed to form a hinge for activation gating. hERG also has a conserved glycine at this position.

**A.**

	Pore helix	Inner Transmembrane Helices
<b>hERG</b>	ALYFTFSLSLTSVGFQNVSPNTNSEKIF	SICVMLIGSLMYASIPGNVSAIIQRLY
<b>KcsA</b>	ALWWSVETATTVGYGDLYPVTTLWGRCVAVVVMVAGITSEFGLVTAALATWVFGRE	
<b>KirBac1.1</b>	AFFESVETLATVGYGDMHPQTVYAHAIATLEIFVGM	SGIALSTGLVFARFARPR
<b>MthK</b>	SLYWTFVTTIATVGYGQDYS	PSTPLGMYFTVTLIVIGIGTFAVAVERLLEFLINRE
<b>KvAP</b>	ALWAVVTATTVGYGDVVPATPIGK	VIGIAVMLTGISALTTLLIGTVSNMFQKIL

**B.**



## Chapter 1- Introduction

**Figure 1.5: Sequence alignment of K<sup>+</sup> channel inner helices.** This alignment of K<sup>+</sup> channel inner helices shows the conserved glycines (in green) that are proposed to form the hinge point at which the channel bends during opening of the intracellular activation gate. Also indicated in blue is the PXP motif, which is conserved in the Kv channel family.

### 1.3.4 Structure of the Voltage-Sensing Region

The voltage-sensing region (VSR) of a voltage-gated K<sup>+</sup> channel is a domain of approximately 100 amino acids that is located in the intracellular part of the channel. It is thought to be responsible for the opening of the intracellular activation gate during depolarization. The VSR is composed of several conserved motifs, including the PXP motif and the glycine hinge point.

### 1.3.4.1 The Voltage-Sensing Region

	K <sup>+</sup> signature sequence	Inner helices
hERG	LTSVGF <sup>GNVSPNTNSEKIF</sup> SICVMLI <sup>CS</sup> LMYASIF <sup>GNVSAIIQR</sup> LY	
hEAG	LTSVGF <sup>GNIAPSTDIEKIFAVAIMMI</sup> CSLLYATIF <sup>GNVTTFQOM</sup> Y	
HCN	MLCIGYGRQAPESMTDIWLTMLSMIV <sup>ATCYAMFI</sup> GHATALIQSLD	
hKv1.1	MTTVGYGDMYPVTIGGKIVGSLCAIA <sup>CVLTIAL</sup> <b>PVP</b> VIVSNFNFY	
Shaker	MTTVGYGDMTPVGF <sup>WGKIVGSLCVIA</sup> CVLTIAL <b>PVP</b> VIVSNFNFY	
KcsA	ATTVGYGDLYPVTLWGRCVAVVVMVA <sup>ITSEGLVT</sup> ALATWFGRE	
KvAP	ATTVGYGDVVPATPIGKVI <sup>GIAVMLI</sup> GISALTL <sup>LLIGTVSNMFQ</sup> KIL	
MthK	IATVGYGDYSPSTPLGMYFTVTL <sup>LIVIG</sup> IGTFAVAVERLLEFLINRE	
KirBacl.1	LATVGYGDMHPQTVYAHAIATLEIFV <sup>MSGIALST</sup> GLVFARFARPR	

## Chapter 1- Introduction

open state (Labro *et al.*, 2003). In addition to the structure of the pore region, the crystal structures of KvAP and Kv1.2 revealed the conformation of the voltage sensor of Kv channels that permits us to understand how the activation gate is controlled by the voltage sensing domain.

### 1.2.2 Structure of the voltage sensing region

The voltage sensor is central to the function of voltage-gated K<sup>+</sup> channels. The S4 region has long been proposed to be critical to function due to the identification of positively charged residues, conserved in voltage-gated Na<sup>+</sup>, K<sup>+</sup>, and Ca<sup>+2</sup> channels, that were proposed to move in response to changes in the electric field (Sigworth, 1994). The S4 segment contains 4 - 8 positively charged arginine or lysine residues, spaced regularly at every third position (Liman *et al.*, 1991; Aggarwal & MacKinnon, 1996; Yellen, 1998; Bezanilla, 2000). Movement of these charges across the membrane electric field with gating generates small outward gating currents that can be detected when ionic currents are eliminated. Accessibility studies on Shaker established that the S4 domain spans the membrane and upon depolarisation, conformational changes expose these positively charged residues that have moved from the intracellular part of the membrane with channel opening (Larsson *et al.*, 1996; Yusaf *et al.*, 1996; Wang *et al.*, 1999; Milligan & Wray, 2000; Li *et al.*, 2004; Wray, 2004; Li *et al.*, 2005). This translated to the movement of 12 - 14 gating charges across the electric field (Schoppa *et al.*, 1992; Aggarwal & MacKinnon, 1996; Seoh *et al.*, 1996). Fluorimetry techniques are one way of measuring local protein movements, by attaching fluorescent molecules to specific residues. Changes in fluorescence can report on structural rearrangements due to changes in the surrounding environment. Site-specific fluorescent labeling of residues on the S4 of Shaker showed a movement of at least 7 amino acids residues from the intracellular to the extracellular environment upon channel activation (Mannuzzu *et al.*, 1996; Loots & Isacoff, 1998). Mutations that neutralized the charged residues in S4 altered both the voltage dependence of activation of K<sup>+</sup> channels (Papazian *et al.*, 1991; Smith-Maxwell *et al.*, 1998b, a; Ledwell & Aldrich, 1999) and the amount of gating current (Perozo *et al.*, 1994). Histidine scanning mutagenesis also showed that certain S4 arginines (R365,

## Chapter 1- Introduction

R368, R371) in Shaker enable proton transport through the membrane in the presence of a pH gradient when they shuttle across the electric field in response to a depolarized potential (Starace *et al.*, 1997; Starace & Bezanilla, 2001). Results of these studies are consistent with the S4 arginines facing a polar protein crevice. Mutations of these residues to smaller amino acids allow permeability to metal ions, not through the selectivity filter but within the voltage sensor domains (omega current), suggesting that the arginine side chains normally occlude this pathway and therefore face a water-filled inner cavity (Tombola *et al.*, 2005). Fluorescence resonance energy transfer (FRET) measurements and proton transport studies suggest that a very small distance separates intracellular and extracellular solvent accessible crevices. Thus, relatively small conformational changes are required to move charges across the electric field.

The crystal structure of KvAP showed that S4 was not present in the protein core but rather it was located in the outer perimeter of the protein facing the hydrophobic core of the lipid bilayer (Jiang *et al.*, 2003a). This was inconsistent with previous studies and it was speculated that the antibody Fab fragments crystallized in complex with KvAP may have distorted its original conformation. A more recent structure of KvAP in the absence of antibody showed that the voltage sensing domain is loosely attached to the pore domain and the initial conformation observed was not due to the Fab fragments, rather due to the absence of a lipid membrane necessary for stabilizing the native structure (Lee *et al.*, 2005). The crystal structure of Kv1.2 also shows the voltage sensing domain as an independent entity, weakly attached to the pore domain (Long *et al.*, 2005b). It shows the voltage sensing domain of one subunit coming close to the pore-forming domains of the neighbouring subunit, consistent with mutagenesis studies on Shaker that show S4 in close proximity with S5 of a neighbouring subunit as well as to residues in S6 (Li-Smerin *et al.*, 2000; Laine *et al.*, 2003; Neale *et al.*, 2003; Elliott *et al.*, 2004; Neale *et al.*, 2007).

There are several possible models for the voltage sensor structure and movement derived from studies of S4 on cysteine accessibility as well as from changes in the fluorescence of probes attached to S4 upon channel activation. In most models, the S4 helix has been proposed to insert into a groove between the pore helices and the S1-S3 helices. This

## Chapter 1- Introduction

allows S4 to move its charged residues across the membrane without exposing them to the lipid environment (Long *et al.*, 2005b). Gating dependent reactivity of cysteine residues with sulfhydryl reagents suggested that S4 undergoes large movements (15 Å translations) for the channel to go from the open to the closed state. However, FRET measurements then suggested much smaller movements of S4 across the membrane. The isolated crystal structure of KvAP showed that the voltage sensor can act as an independent entity and is highly flexible. The KvAP studies also demonstrated that S4 is not in a canalculus but may also be exposed to the lipid environment.

A description of the models proposed above is as follows (Figure 1.6):

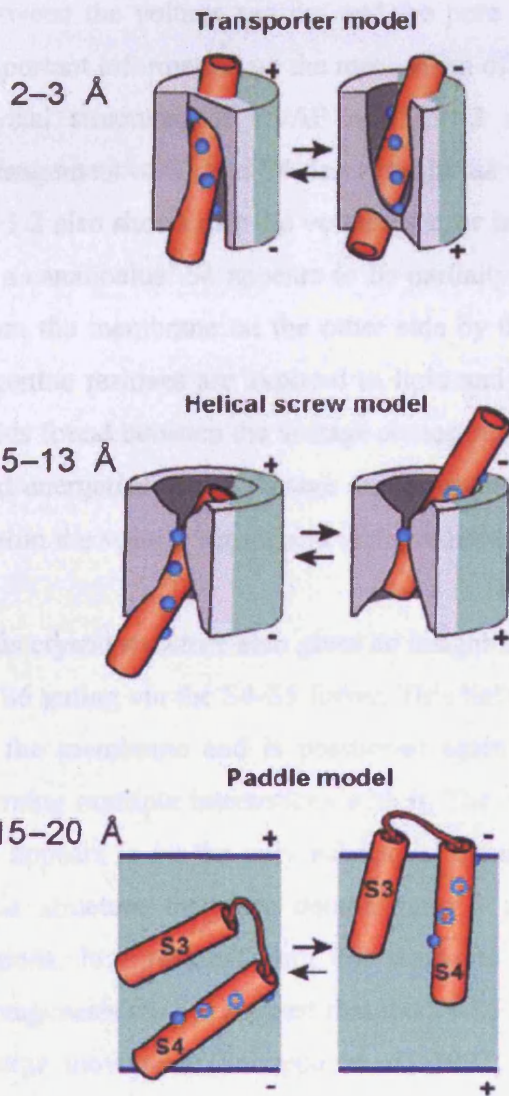
- 1) The helical screw model: suggests that upon depolarisation, each S4 helix screws outwards towards the extracellular surface through a narrow vestibule between the pore domain and the S1-S3 helices. This vestibule is proposed to provide an aqueous environment. This would move each charge to the position of the next charge producing an overall translocation of charge across the membrane (Gandhi & Isacoff, 2002). The S4 charges are thought to move 13 Å along the axis of the helix.
- 2) The twist and tilt (transporter) model: suggests that S4 is found in between 2 crevices; an internal water-filled crevice made by S1 and S5 and an external hydrophobic crevice made by S2 and S3. Upon depolarisation, the electric field acts on charges facing the inside forcing S4 to move towards the outside by rotating 180° and tilting a little. This exposes the basic residues to the outside crevice and involves a small (2 - 3 Å) movement of S4. The mechanism of twisting and tilting pulls on S5, which in turn pulls apart the S6 segments thus opening the channel (Bezanilla, 2000).
- 3) The voltage paddle model: is derived from comparison of the crystal structure of the voltage sensor domain of KvAP and of the intact KvAP channel (Jiang *et al.*, 2003b). It describes a paddle-like structure formed by S4 and its antiparallel relationship to the carboxy-terminal half of the S3 helix (S3b). MacKinnon's

## Chapter 1- Introduction

**Figure 1.6: Models of voltage sensing.** Three different models have been proposed to explain movements of the S4 helix (seen as an orange tube) through the membrane electric field. The transporter model suggests a twist and tilt conformation coupled with small movements of S4 through the membrane. The helical screw model suggests a larger translocation of charges (blue spheres) as S4 screws outwards towards the extracellular surface. The paddle structure formed by S3 and S4 helices are suggested to translocate through the entire membrane bilayer in the voltage paddle model.

The most recent study by MacKinnon (Lang et al., 2005) investigates the movements of the voltage sensor from the crystal structure of Kv1.2. Unlike KvAP, the conformational changes in the Kv1.2 structure were subtle providing evidence that they may not have the substantial movements suggested by the transporter and helical screw models. The crystal structure of Kv1.2 also shows a self-associated domain, which is not linked to the membrane as the other side by the helix S3. The two of the charged residues in the S4 helix are shown to interact with residues in the S3 helix. The movement of the S4 helix is suggested to be a small movement of the helix towards the extracellular surface.

The transporter model suggests a twist and tilt conformation coupled with small movements of S4 through the membrane. The helical screw model suggests a larger translocation of charges (blue spheres) as S4 screws outwards towards the extracellular surface. The paddle structure formed by S3 and S4 helices are suggested to translocate through the entire membrane bilayer in the voltage paddle model.



*Adapted from Tombola et al, 2006*

## Chapter 1- Introduction

group suggested that the paddle lies near the intracellular side when the channel is closed and that the paddle moves from inside to outside when the channel opens. So the paddles translocate their gating charges across the entire bilayer in response to changes in membrane potential. The net transmembrane movement was measured to be 15 - 20 Å (Ruta *et al.*, 2005). This model however, does not fit with a lot of experimental evidence and has been highly controversial.

The most recent study by MacKinnon (Long *et al.*, 2005b) investigates the movements of the voltage sensor from the crystal structure of Kv1.2. Unlike KvAP, the connections between the voltage sensors and the pore in the Kv1.2 structure were intact providing important information on the mechanism of voltage dependent gating. Comparing the two crystal structures of KvAP and Kv1.2 shows that they both have the antiparallel arrangement of S3 and S4 described in the voltage paddle model. The crystal structure of Kv1.2 also shows that the voltage sensor is a self-contained domain, which is not buried in a canaliculus. S4 appears to be partially exposed to lipid on one side and is shielded from the membrane on the other side by the S1 and S2 helices. So two of the charged arginine residues are exposed to lipid and the other two can interact with acidic amino acids found between the voltage sensor paddle and the S1 and S2 helices. The movement and energetics of the voltage sensor involves hydrophobic and electrostatic interactions within the voltage sensor and with the lipid environment.

This crystal structure also gives an insight into the coupling of voltage sensor movements to S6 gating via the S4-S5 linker. This linker is an amphipathic  $\alpha$ -helix that runs parallel to the membrane and is positioned against the S6 helix from the same subunit thus forming multiple interactions with it. The close proximity between the S4-S5 linker and S6 appears to be the only substantial contact between the voltage sensor and the pore. This structure therefore demonstrates a mechanism of coupling between these two regions. In agreement with this structural basis of voltage coupling to gating, several mutagenesis studies suggest that the S4-S5 linker influences activation gating and gating charge movement (Schoppa *et al.*, 1992; Slesinger *et al.*, 1993; Shieh *et al.*, 1997), interacts with S6 in Shaker and hyperpolarisation-activated cyclic nucleotide-gated

## Chapter 1- Introduction

(HCN) channels, and lies near the channel's permeation pathway (Isacoff *et al.*, 1991; Sanguinetti & Xu, 1999; Chen *et al.*, 2001; Lu *et al.*, 2002; Caprini *et al.*, 2005). A chimera substituting the pore domain (S5 to S6) of Shaker with the KcsA pore results in a functional, voltage sensitive, K<sup>+</sup> selective channel suggesting that the KcsA pore can be gated by Shaker's voltage sensor (Lu *et al.*, 2001). However, mutations in either the C-terminal end of S6 or the S4-S5 linker result in a non-conducting channel due to the uncoupling between these two regions (Caprini *et al.*, 2001; Lu *et al.*, 2002). The importance of the S4-S5 linker in the coupling between the voltage sensor and the S6 in hERG has also been shown (Tristani-Firouzi *et al.*, 2002) and will be discussed in more detail in a later section. Similarly, alanine scanning mutagenesis of the S4-S5 linker of HCN2 pacemaker channels identified residues that disrupted normal channel closure, also suggesting a coupling between the voltage sensor and activation gating (Chen *et al.*, 2001). Cysteines introduced into the S4-S5 linker of HCN1 channels and the S6 C-linker region showed a possible cross-linking interaction between these regions leading to profound changes in channel gating and a reversed voltage dependence (Prole & Yellen, 2006). The motions in S4 appear to be transmitted to the pore through the S4-S5 linker. A working model of the coupling between the voltage sensor and the activation gate proposes that the S4-S5 linker moves downwards when S4 moves towards the intracellular side, compressing the inner helices and closing the pore. On the contrary, when S4 moves towards the extracellular side, it relieves the inner helices from the constriction formed by the S4-S5 linker ring thus opening the channel. In order to properly elucidate the movements of the voltage sensing domain, a closed conformation of the voltage sensor would be necessary.

### 1.3 hERG channel structure and functions

hERG was first cloned by homology screening with *Drosophila* EAG from a human hippocampal library (Warmke & Ganetzky, 1994). Its structure is similar to other Kv channels and consists of four pore forming  $\alpha$ -subunits, each with six TM spanning domains and large intracellular N- and C-termini. The fully glycosylated form of the protein is a 155 kDa structure with 1159 amino acids. An early study on outward delayed

## Chapter 1- Introduction

rectifier  $K^+$  currents in guinea pig ventricular myocytes revealed two components, which could be distinguished due to varying sensitivities to block by E-4031, a class III antiarrhythmic agent. These currents represented a slow activating delayed rectifier  $K^+$  current ( $I_{Ks}$ ), that was insensitive to drug, and a rapidly activating delayed rectifier  $K^+$  current ( $I_{Kr}$ ) that was blocked by drug (Sanguinetti & Jurkiewicz, 1990). Two research groups then identified hERG (*erg1*) as the pore forming  $\alpha$ -subunit of channels that conduct  $I_{Kr}$  (Sanguinetti *et al.*, 1995; Trudeau *et al.*, 1995). hERG is most abundantly expressed in the heart and contributes to the outward  $K^+$  current during the plateau and repolarisation phases of the cardiac action potential. It plays a role in atrial and ventricular myocyte action potential repolarisation and also conducts current during the diastolic depolarisation in pacemaker cells (Ono & Ito, 1995; Mitcheson & Hancox, 1999). hERG channels have also been found in neuronal, epithelial, and smooth muscle tissues as well as some cancerous tissues, where they are thought to be involved in the regulation of tumour development and apoptosis (Wang *et al.*, 2002; Vandenberg *et al.*, 2004; Arcangeli, 2005; Sanguinetti & Tristani-Firouzi, 2006). Two other genes, *erg2* and *erg3*, were found to be expressed in rat and human nervous systems, but not in atrial or ventricular muscle, and contribute to cell excitability in neuronal tissues (Shi *et al.*, 1997). *Erg 2* had similar kinetic properties to *erg1*, although its midpoint of activation was shifted to more positive potentials. *Erg3* currents, on the other hand, had a large transient component at positive potentials and exhibited much faster activation rates, slower inactivation kinetics, and had a midpoint of activation that was substantially left-shifted. The considerable window of *erg3* current at more negative potentials could influence sub-threshold firing properties of neurons.

The hERG1 subunits exist as two isoforms, hERG1a and hERG1b, that are identical except for variation in the N-terminus (Robertson *et al.*, 2005). hERG1b has a unique N-terminus that is shorter than that of hERG1a. *In vivo* and in heterologous systems, both subunits assemble to form heteromeric channels. The interaction between these subunits is mediated by their N-terminal interactions during the early stages of channel biogenesis (Phartiyal *et al.*, 2007). There is also evidence that hERG is found associated with auxiliary subunits, that may modify its function. In particular, a class of subunits encoded

## Chapter 1- Introduction

by *KCNE* genes, *minK* (*KCNE1*) and *MiRP1* (*KCNE2*). These  $\beta$ -subunits are single transmembrane domain peptides and have been reported to co-assemble with hERG in heterologous systems. *MinK* is not thought to be the subunit responsible for forming native  $I_{Kr}$  channels but may upregulate hERG current by increasing surface expression of channels without altering current density and gating kinetics (McDonald *et al.*, 1997). The *MiRP1*/hERG complex, on the other hand, appears to have similar characteristics to  $I_{Kr}$  channels, in terms of conductance and activation gating, although the coassembly of *MiRP1* and hERG subunits confers other properties such as accelerating  $I_{Kr}$  deactivation and the rate of onset of drug block and decreased trafficking to the cell surface (Abbott *et al.*, 1999; Schroeder *et al.*, 2000; Tinel *et al.*, 2000). Mutations in *MiRP1* have also been associated with LQTS pointing to the possibility that *MiRP1* and hERG may constitute native  $I_{Kr}$ . However, *MiRP1* also co-assembles with other  $K^+$  channels such as Kv4.2 and KvLQT1, as well as some expressed in the brain such as KCNQ2 and KCNQ3. This suggests that *MiRP1* does not specifically co-assemble with hERG, but rather modifies the functions of a number of ion channels (Weerapura *et al.*, 2002). The discrepancies seen in the biophysical and pharmacological properties between the *MiRP1*/hERG complex and native  $I_{Kr}$  raises doubt about the extent of their role in human cardiac  $I_{Kr}$  channels.

### 1.4 Gating properties of hERG channels

The hERG channel can exist in 3 different states: closed, open, or inactivated controlled by two separate yet voltage dependent gating processes that occur simultaneously: activation and inactivation (Vandenberg *et al.*, 2004). Activation describes the transition from the closed to the open state and is thought to involve the opening of an intracellular activation gate. The reverse process is called deactivation and in hERG, both activation and deactivation are slow. The process of inactivation describes the transition into an inactive state during depolarisation due to closure of an inactivation gate. Recovery from inactivation is the opening of the inactivation gate and in hERG, both inactivation and its reverse process are rapid (Zhou *et al.*, 1998; Tristani-Firouzi & Sanguinetti, 2003). As a consequence of this fast inactivation process, hERG  $K^+$  channels function as inward

## Chapter 1- Introduction

rectifiers by passing little current in the outward direction upon depolarisation but then passing significant current in the inward direction upon repolarisation to potentials negative to  $E_K$  (potassium equilibrium potential) (Smith *et al.*, 1996). The kinetics of hERG are very unusual and are considerably different to the kinetics of Shaker channels that carry the A-type  $K^+$  currents characterized by fast activation and two different types of inactivation gating (Hille, 2001; Kerschbaum *et al.*, 2002), which will be discussed in the subsection 1.4.3. The structural basis of hERG activation, deactivation, and inactivation gating will now be explored.

### 1.4.1 Structural basis of hERG activation gating

The existence of an intracellular gate that controls access to the inner cavity of the hERG channel is supported by studies using methanesulfonanilides such as MK-499 and dofetilide (Spector *et al.*, 1996a; Zou *et al.*, 1997; Mitcheson *et al.*, 2000b). These compounds block the inner cavity from the intracellular side, where access is gained only when the channel opens. The S6 of hERG also has two glycines, one at position 648 analogous to the conserved putative glycine hinge and the other at position 657 analogous to the second proline residue in the Pro-X-Pro motif in Kv channels (refer to Figure 1.5). Thus, there are two potential sites of flexibility for activation gating. Mutation of Gly648 to an alanine showed little change to the voltage and time dependence of channel activation and deactivation (Mitcheson *et al.*, 2000a). This suggests that the glycine residue is not crucial for hERG's activation gating. This is very different to what has been observed with other channels since there is usually a loss of channel function when the glycine is mutated to various other amino acids. Mutations of the putative glycine hinge point (Gly466) in Shaker channels result in channels that are nonfunctional or slower to open (Labro *et al.*, 2003; Ding *et al.*, 2005). Only a mutation at Gly466 to proline was able to rescue channel function (Magidovich & Yifrach, 2004). Prolines also favor bending of  $\alpha$ -helices. Introducing a glycine at an adjacent position (G466A/V467G) also restored  $K^+$  current, supporting the role of a glycine as a hinge point (Ding *et al.*, 2005). Similar conclusions have been reached for voltage-gated  $K^+$  channels and  $BK_{Ca}$  channels (Magidovich & Yifrach, 2004), G-protein dependent  $K^+$  (GIRK) channels (Jin *et al.*,

## Chapter 1- Introduction

2002), as well as bacterial Na<sup>+</sup> channels (Zhao *et al.*, 2004b). Results from these mutagenesis studies combined with observations from the crystal structures of bacterial K<sup>+</sup> and Na<sup>+</sup> channels led to the prediction of a ubiquitous glycine hinge model for activation gating.

However, there were several difficulties with this model of activation gating. The crystal structure of the eukaryotic Kv1.2 channel revealed a pronounced bend at a Pro-X-Pro motif further down from the proposed glycine hinge point, and mutagenesis studies also indicated that the Pro-X-Pro motif may be important in gating. Furthermore, there are some K<sup>+</sup> and cyclic-nucleotide gated channels that lack a glycine in the putative glycine hinge position. For example, EAG and KCNQ1 channels have an alanine at the hinge position. Mutating Ala336 in KCNQ1 channels to a glycine shifted the voltage dependence of activation to more negative potentials, consistent with it performing a role as a gating hinge for channel activation (Seeböhm *et al.*, 2006). However, mutating this alanine to a cysteine or threonine also gave functional currents, although with a rightward shift in their voltage dependence of activation. It was concluded that a glycine at this position may be able to facilitate bending but is not an absolute requirement for KCNQ1 channel function. EAG and KCNQ1 channels also have an Ile-Phe-Gly or Pro-Ala-Gly respectively in place of the Pro-X-Pro motif (Shealy *et al.*, 2003). Mutating the glycine or proline in the Pro-Ala-Gly motif to alanine resulted in nonfunctional channels, suggesting the importance of this motif in inducing flexibility for channel activation. Hence, the universality of the glycine hinge hypothesis has been called into question. An alanine scanning mutagenesis study had found that G648A and G657A hERG were functional, indicating differences between activation gating in hERG compared to other Kv channels (Mitcheson *et al.*, 2000a). The roles of the S6 glycines in hERG were studied in this project and are discussed in Chapter 3 of this thesis. It was important to investigate whether either or both of these glycines form the gating hinge in hERG, responsible for its activation gating, since the hinge point has implications for the structure of the inner cavity and therefore, the drug binding site of hERG.

### 1.4.1.1 Interactions between the pore and the voltage sensor stabilise the closed state

## Chapter 1- Introduction

The crystal structure of Kv1.2 suggested that the voltage sensor is coupled to the activation gate through the S4-S5 linker (Long *et al.*, 2005b). A point mutation in the S4-S5 linker of hERG (D540K) resulted in a channel with highly unusual gating properties, in which the channel can open upon stepping to hyperpolarised as well as to depolarised potentials (Mitcheson *et al.*, 2000b). This mutant was shown to destabilise the closed state of hERG by disrupting a salt bridge between Asp540 on the S4-S5 linker and Arg665 on the C-terminal end of S6 (Tristani-Firouzi *et al.*, 2002). These findings suggest that an interaction between the voltage sensor and the activation gate in hERG via the S4-S5 linker is necessary to keep the channel in the closed state at hyperpolarised potentials. This is further confirmed by using chimeras constructed from hERG and the related bovine ether-a-go-go (bEAG) channel. Substituting the S6 in hERG with that of bEAG rendered the channel constitutively open at negative potentials. Thus, the stable closed state was disrupted despite 81 % sequence homology between the S6 domains (Ferrer *et al.*, 2006). Normal channel closure was achieved by restoring two specific residues on the C-terminal end of S6, Arg665 and Leu666, into the background of the chimera. Moreover, introducing cysteines in the S4-S5 linker and C-terminal end of S6 permitted the formation of a disulfide bond between D540C and L666C under oxidising conditions that locked the hERG channel in the closed state concordant with a pairing between these two regions (Ferrer *et al.*, 2006). This interaction also reduced gating currents, confirming that the movement of the voltage sensor was restricted due to a direct coupling between the S4-S5 linker and S6. Other residues in the S6 of hERG have been shown to disrupt channel closure, such as the mutation of Val659 to alanine (Mitcheson *et al.*, 2000a). V659A dramatically slows channel deactivation and appears to alter the sensitivity of the channel to drug block. This residue is predicted to be close to where the S6 helices bundle together and may be a possible location for interaction with the S4-S5 linker. As part of this project, I investigate the role of this Val659 residue in hERG gating.

## Chapter 1- Introduction

Voltage dependent activation involves an outward movement of S4 coupled to opening of the activation gate. The slow activation of hERG may be due to the slow movement of the voltage sensor or the slow opening of the activation gate. Voltage clamp fluorimetry measurements showed that fluorophores attached to the extracellular end of S4 undergo both rapid and slow voltage dependent changes in fluorescence (Smith & Yellen, 2002). The slow component correlated well with the voltage dependence of activation and the rapid component had similar kinetics to inactivation. However, the addition of extracellular TEA that slows inactivation or the presence of the G628C:S631C mutation, that abolishes inactivation, did not lead to changes in the fluorescence signals. It was suggested that the fast component was reporting rapid voltage sensor movements, which drive the inactivation process. Other experiments measured slow and fast components to gating charge movements of hERG (Piper *et al.*, 2003). The time constant for the slow gating current of hERG was found to be 70 ms, which is about two orders of magnitude slower than that for Shaker and was attributed to activation gating. The slow component accounted for most of the hERG gating current. The time constant for the fast gating component was a few ms but did not seem to directly report on the fast inactivation process. These results were consistent with the voltage clamp fluorimetry measurements, which led to the conclusion that the main reason for the slow activation kinetics of hERG is the slow movement of the S4 voltage sensor upon depolarisation. This may be due to hERG having only three positive charges on S4 that act as gating charges during activation (Zhang *et al.*, 2004). On the other hand, the first four charges in the S4 of Shaker (R362, R365, R368, R371) have been shown to carry the gating charges (Starace & Bezanilla, 2001, 2004). Having one less gating charge per subunit in hERG may indicate that the membrane is less sensitive to depolarisation, slowing the movement of S4 and subsequently slowing activation gating. In addition, negative charges in Shaker, as well as EAG channels, were shown to form salt bridges with positively charged residues, thus stabilising S4 (Schonherr *et al.*, 2002; Liu *et al.*, 2003). hERG has a greater number of negatively charged residues on the S1, S2, and S3 domains compared to most other voltage-gated K<sup>+</sup> channels. Salt bridges between the negatively charged residues on S1 and S2 were shown to stabilise hERG in the closed state, contributing to its slow activation kinetics (Liu *et al.*, 2003; Subbiah *et al.*, 2004; Zhang *et al.*, 2004). A direct

## Chapter 1- Introduction

interaction was determined between a residue on the outer end of S2 (D456) in hERG and the outer most positive charge (K525) on S4. Another residue on the inner end of S1 (D411) was also shown to couple to the inner most positive charge (K538) on S4 (Zhang *et al.*, 2005). This type of coupling between charged residues in the voltage sensing domain is suggested to slow the activation process in hERG.

An alanine scan of S4 then identified residues localised to a spiral thread on S4 that perturbed charge movement (Piper *et al.*, 2005). Mutations that affected activation gating were spread throughout, except at one helical face of S4. Interestingly, mutations that altered inactivation gating were localised at a distinct face of S4 suggesting that different regions in S4 contribute differentially to activation or inactivation gating.

### 1.4.2 Structural basis of hERG deactivation gating

hERG has a slow deactivation process that is physiologically important. Some LQT2-associated mutations reduce  $I_{Kr}$  current at the end of the cardiac action potential by accelerating channel deactivation (Chen *et al.*, 1999). The N-terminus plays an important role in the deactivation process. Deletion of the first 354-370 amino acids of hERG resulted in a channel with substantially faster deactivation (Schonherr & Heinemann, 1996; Wang *et al.*, 1998). In these channels, slow deactivation could be restored by the addition of a peptide corresponding to the first 16 amino acid residues of the channel to the intracellular surface of the truncated channel (Wang *et al.*, 2000). The first 25 residues of hERG are conserved among the EAG/ERG/ELK superfamilies of channels and deletion of these residues resulted in accelerated deactivation (Terlau *et al.*, 1997). This region has two positively charged arginine residues, which suggests that electrostatic forces contribute to binding of the N-terminal deactivation peptide (Liu *et al.*, 2003).

In Shaker channels, the N-terminus has been shown to bind to a receptor site within the pore causing N-type inactivation (Hoshi *et al.*, 1990; Zagotta *et al.*, 1990). The N-

## Chapter 1- Introduction

terminus of hERG does not block the pore and slows deactivation by increasing the channel open time (Wang *et al.*, 1998; Wang *et al.*, 2000). The N-terminal domain is also thought to bind to sites in the S4-S5 linker that are exposed following channel opening and slow the subsequent closure of the channel. A mutation at Gly546 on the S4-S5 linker of hERG to cysteine significantly altered the channel's deactivation rate when modified by N-ethylmaleimide (NEM) treatment similar to the ability of the N-terminal deletion of slowing deactivation, suggesting a possible interaction between the linker and the N-terminal domain (Wang *et al.*, 1998).

The N-terminus of hERG includes a region that folds in a manner comparable to a eukaryotic PAS domain (Morais Cabral *et al.*, 1998). PAS is the acronym for the products of the genes, *PER*, *ARNT*, and *SIM*. These domains are frequently found in eukaryotic proteins with roles in circadian rhythm. The PAS domain in hERG appears to be important in the normal trafficking of hERG channels to the surface membrane, as mutations in this domain impair the trafficking process. Functionally, the PAS domain seems to modulate the deactivation process. LQT-associated mutations of residues within this domain also resulted in faster deactivation kinetics (Chen *et al.*, 1999). The PAS domain is thought to interact with the pore stabilising the open state. Weakening this binding therefore leads to the acceleration of hERG deactivation (Wang *et al.*, 1998). Interactions between the N-terminus and the pore of hERG are explored further in Chapter 6 of this thesis.

### 1.4.3 Structural basis of hERG inactivation gating

hERG channels exhibit inward rectification that is not due to the block of outward current by  $Mg^{+2}$  or polyamines as shown for inward rectifier  $K^+$  channels, but rather due to the rapid onset of a voltage dependent inactivation process (Ficker *et al.*, 1994; Lu & MacKinnon, 1994; Spector *et al.*, 1996b). The inactivation processes in Shaker channels have been well studied and shown to be of two types, referred to as N- and C-type inactivation (Lopez-Barneo *et al.*, 1993). N-type inactivation in Shaker is fast and due to

## Chapter 1- Introduction

the N-terminus acting as a tethered particle that binds to its receptor site within the inner vestibule of the channel, blocking the pore in the open state (ball and chain model) (Hoshi *et al.*, 1990; Zagotta *et al.*, 1990; MacKinnon *et al.*, 1993). Deletion of the N-terminus still allows a slow inactivation process, described as C-type, because of mutations to the C-terminal half of the channel that disrupt inactivation (Hoshi *et al.*, 1991). C-type inactivation is thought to involve conformational changes in the outer mouth of the channel for a number of reasons: (1) Mutation of Thr449 close to the extracellular side of the selectivity filter altered inactivation gating. (2) When TEA is applied extracellularly, a slowing of the kinetics of C-type inactivation is observed due to TEA binding to a site in the outer mouth of the channel (MacKinnon & Yellen, 1990; Choi *et al.*, 1991). In contrast, intracellular TEA slows N-type inactivation by competing with the ball peptide in the intracellular binding site. (3) C-type inactivation in Shaker is influenced by the concentration of external cations and (4) Inactivation affects the selectivity and permeability of the pore to ions (Lopez-Barneo *et al.*, 1993; Yellen *et al.*, 1994; Starkus *et al.*, 1997). Fluorescent probes attached to S4 and the P-region reported structural rearrangements within these regions during the onset and recovery from slow inactivation (Loots & Isacoff, 1998). The onset of inactivation showed two sequential rearrangements; the first rapidly closed the external gate in a process termed P-type inactivation and the second stabilised the closed conformation in a slower process termed C-type inactivation. P-type and C-type differ in that only C-type inactivation is associated with modifications in the conformation of the voltage sensor, thus inducing shifts in the voltage dependence of gating charge movement (Olcese *et al.*, 1997; Loots & Isacoff, 1998). C-type inactivation described in Shaker channels has also been shown for other Kv channels such as Kv1.3 (Panyi *et al.*, 1995), Kv1.4 (Rasmusson *et al.*, 1995), Kv1.5 (Fedida *et al.*, 1999), and Kv2.1 (Klemic *et al.*, 1998). In all these channels, this type of inactivation is slow and has no intrinsic voltage dependence, but rather derives its voltage sensitivity from coupling to the voltage sensitive activation process induced by the movement of S4 upon depolarisation (Gandhi *et al.*, 2000). The slow inactivation kinetics in these channels has been ascribed to the presence of hydrogen bonds around the outer mouth of the channel that stabilise the open conformation of the selectivity filter.

## Chapter 1- Introduction

Breaking of these bonds then allows the collapse of the selectivity filter during P-type inactivation (Larsson & Elinder, 2000; Ortega-Saenz *et al.*, 2000).

Inactivation in hERG however is intrinsically voltage dependent and is much faster than C-type inactivation in Shaker (Sanguinetti *et al.*, 1995; Smith *et al.*, 1996; Spector *et al.*, 1996b; Rasmusson *et al.*, 1998). hERG channels exhibit inward rectification with a voltage of half maximal ( $V_{0.5}$ ) inactivation equal to -85 mV compared to activation with a  $V_{0.5}$  of -20 mV (Schonherr & Heinemann, 1996; Smith *et al.*, 1996; Spector *et al.*, 1996b; Zou *et al.*, 1998). The P-loop region also appears to be critical for the inactivation of hERG. This has been verified by studies of chimeras between hERG and homologues in the EAG superfamily that lack inactivation. Point mutations within this region, such as S620T (Ficker *et al.*, 1998) and S631A (Smith *et al.*, 1996; Zou *et al.*, 1998), abolished or substantially shifted inactivation to positive potentials. A number of other mutations in the P-region have also been shown to abolish inactivation, such as W585C, L586C, H587C, L589C, G590C, D591C, I593C, and G594C (Liu *et al.*, 2002). Most of these mutants also altered  $K^+$  selectivity; analogous to the effects of mutations in Shaker near the extracellular mouth of the pore on selectivity and C-type inactivation, suggesting similar mechanisms underlie inactivation in the two channels (Liu *et al.*, 1996; Yellen, 1998). It is worth noting that the selectivity filter has been proposed to be a second gate in KcsA, inward rectifier and cyclic nucleotide gated channels (Flynn & Zagotta, 2001; Claydon *et al.*, 2003; Blunck *et al.*, 2006). Whilst fluorescence spectroscopy might be able to detect different changes in movement at the selectivity filter compared to the lower bundle crossing, these gates are not totally independent. Further studies are needed to elucidate the coupling between these two gates.

It has been proposed that the fast inactivation in hERG is due to the outer mouth of hERG being narrower and more flexible than of the Shaker channel (Fan *et al.*, 1999). So during inactivation, a smaller motion of the outer mouth of hERG is required (Tseng, 2001; Piper *et al.*, 2005). In Shaker, as well as most  $K^+$  channels, the Gly-Tyr-Gly sequence forms the selectivity filter (Doyle *et al.*, 1998). It has been suggested that the tyrosine of

## Chapter 1- Introduction

the selectivity filter forms hydrogen bonds with two tryptophans in the pore helix, thus stabilising the selectivity filter. Mutation of this tyrosine in Shaker to phenylalanine (Y445F) resulted in accelerated C-type inactivation (Ranganathan *et al.*, 1996). In hERG channels, the tyrosine of the selectivity filter is a phenylalanine. Kir6.x channels, which contain a Gly-Phe-Gly selectivity filter, also undergo a fast form of C-type inactivation. Mutating the phenylalanine in Kir6.2 to a tyrosine resulted in a non-functional channel, confirming the importance of this residue for the functional conformation of the pore. It seems likely that the presence of a phenylalanine in the selectivity filter of hERG and the absence of tryptophan residues in the pore helix and hence, the lack of the hydrogen bonds in hERG between the selectivity filter and the pore helix, results in a more flexible and narrower selectivity filter than Shaker. hERG also has an unusually long S5-P linker that forms an amphipathic  $\alpha$ -helix (Torres *et al.*, 2003; Tseng *et al.*, 2007). Its central portion has also been shown to be extremely dynamic, capable of forming intersubunit disulfide bonds that can contribute to its fast inactivation process as well as forming interactions with residues on the outer mouth of the selectivity filter affecting channel selectivity (Jiang *et al.*, 2005).

Voltage clamp fluorimetry experiments first showed that fluorescent probes attached to residues on S4 moved with depolarisation with voltage dependence and kinetics similar to inactivation gating (Smith & Yellen, 2002). S4 itself may therefore act as a voltage sensor for inactivation gating or else charged residues close to the extracellular end of S4, such as those in the extracellular S5 - pore helix linker, may move in response to changes in voltage. Mutations of some of the charged residues in this region resulted in either non-functional channels (such as K595C), or channels which do not inactivate (such as D591C) (Liu *et al.*, 2002). Although a fast change of fluorescence with kinetics similar to that of inactivation has been detected, the voltage dependence of this fast fluorescent component was much more positive than that of inactivation ( $V_{0.5}$  equal to +15 mV compared to -85 mV). Furthermore, extracellular TEA altered the kinetics of inactivation but not those of the fast fluorescent component. Hence the fast fluorescent component may not be reporting channel inactivation but is possibly reporting rearrangements connected to this process (Smith & Yellen, 2002). The charged residues on the S5-P

## Chapter 1- Introduction

linker in hERG has been shown to significantly affect the voltage dependence of inactivation (Clarke *et al.*, 2006). A subset of residues on S4 was later mapped as being sensitive to hERG inactivation and appears to be longitudinally distributed across the entire length of S4, consistent with a small tilt in S4 causing rearrangements that close the inactivation gate (Piper *et al.*, 2005).

The hERG channel's complex and distinctive gating processes are critical to its functional role in the body. The next section will demonstrate this by discussing physiological roles of hERG in the heart.

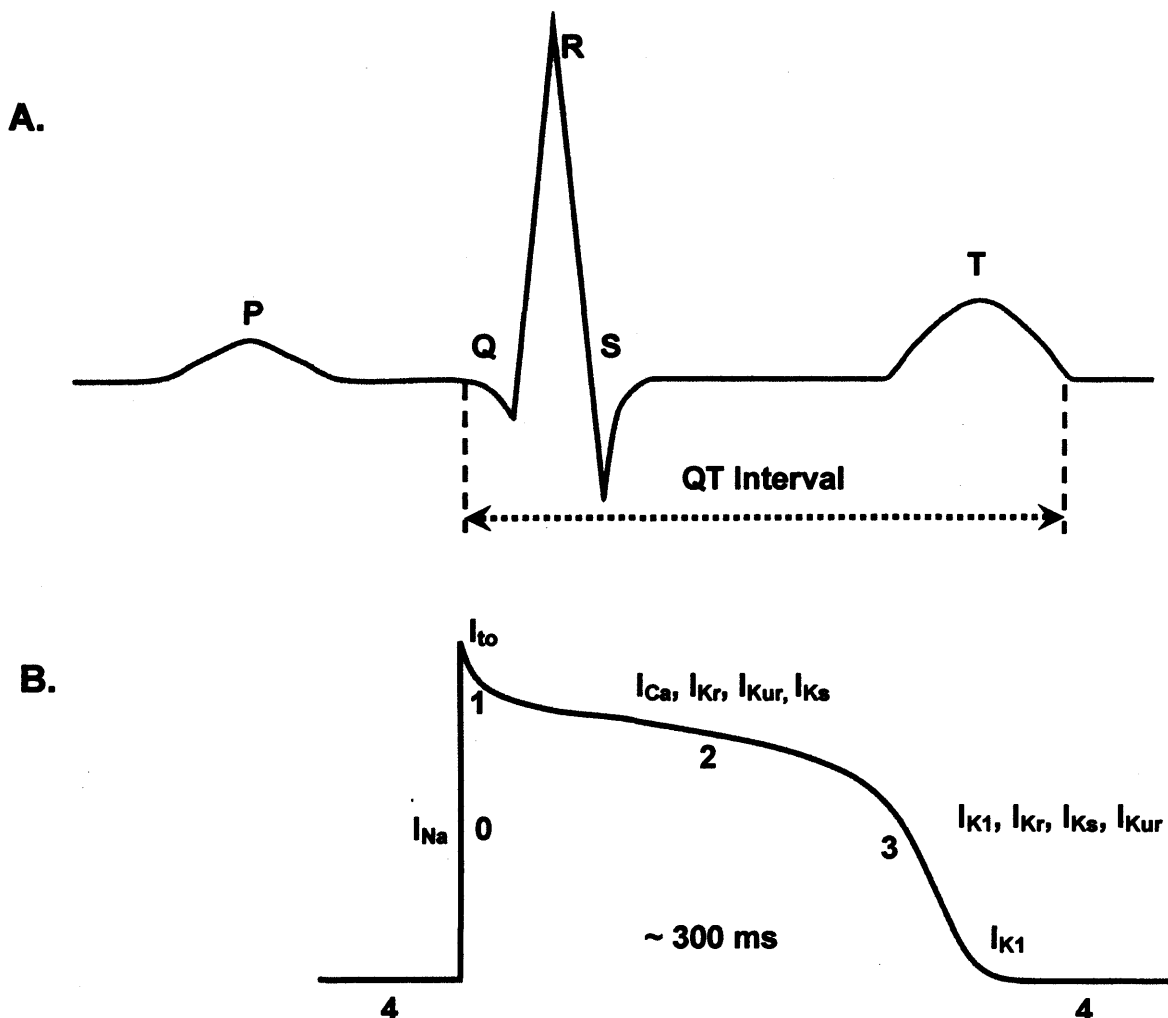
### 1.5 Role of hERG in the heart

This project focuses on the role of hERG in the ventricular action potential and the cardiac arrhythmias that may occur as a consequence of genetic mutations to the hERG channel or block by pharmacological agents.

The duration of an action potential is much longer in cardiac cells than in nerve and skeletal muscle cells. The action potential shape varies in different regions of the heart, but in non-pacemaker cells it can be defined by 5 phases: phase 0 is the action potential upstroke, phase 1 is the notch due to partial repolarisation, phase 2 which is a long plateau phase, followed by phase 3 which is the repolarisation phase, and finally phase 4 which is the return to the resting membrane potential (Roden *et al.*, 2002). The various phases of the cardiac action potential are due to changes in the ionic conductance of the cell membrane mainly due to the interplay between  $\text{Na}^+$ ,  $\text{K}^+$ , and  $\text{Ca}^{+2}$  currents (Figure 1.7). Propagating action potentials cause a depolarisation of the membrane potential. This is sensed by voltage-gated  $\text{Na}^+$  channels, which open allowing a large rapid influx of  $\text{Na}^+$  ions to produce the rapid upstroke of the action potential. The process is so rapid because of the abundance of  $\text{Na}^+$  channels and the electrochemical gradient, which produces a large driving force for  $\text{Na}^+$  entry into the cell. However, the  $\text{Na}^+$  channels inactivate very

## Chapter 1- Introduction

**Figure 1.7: Representation of an ECG and a ventricular cardiac action potential.** A. A representation of an ECG trace showing its five typical deflections (PQRST waves). The QRS wave denotes ventricular depolarisation, while the T wave denotes ventricular repolarisation. The QT interval is therefore a crude estimate of ventricular action potential duration. B. Diagram showing a ventricular action potential and the ionic currents underlying the five different phases.



## Chapter 1- Introduction

soon after they open so the influx of  $\text{Na}^+$  ions ceases within 1 or 2 msec after the excitation of the cell. A rapid phase 1 repolarisation then follows because of the outward movement of  $\text{K}^+$  ions via transient outward  $\text{K}^+$  channels (Kv1.4 with its slow inactivating component, Kv4.2 and Kv4.3 with their fast inactivating component). These  $\text{K}^+$  channels open briefly producing the notch at the very beginning of the plateau. L-type  $\text{Ca}^{+2}$  channels also open during phase 0 and phase 1. These two phases correspond to the QRS wave on an electrocardiogram (ECG) and denote ventricular muscle depolarisation. Phase 2 is the long plateau phase (hundreds of milliseconds long) due to a balance between the inward currents, largely through L-type  $\text{Ca}^{+2}$  channels, and outward current, largely through delayed rectifier  $\text{K}^+$  channels. There are 3 major delayed rectifier currents in the heart that are named according to their relative rates of activation: rapid delayed rectifier current ( $I_{Kr}$ ), slow delayed rectifier current ( $I_{Ks}$ ), and ultra-rapid delayed rectifier current ( $I_{Kur}$ ). hERG encodes the  $\alpha$ -subunit underlying  $I_{Kr}$ . Phase 3 is the final rapid repolarisation achieved due to a much greater efflux than influx of cations across the cell membrane. This is due to the inactivation of  $\text{Ca}^{+2}$  channels and the actions of delayed rectifier and inward rectifier  $\text{K}^+$  channels. The spread of action potential repolarisation produces the T wave on an ECG, which represents ventricular repolarisation. The QT interval therefore estimates the duration of a ventricular action potential. Phase 4 is the stable resting membrane potential, which is accomplished by the outward movement of  $\text{K}^+$  ions through Kir2.1 channels. The relatively high conductance to  $\text{K}^+$  ensures that the membrane potential is clamped close to  $E_K$  at rest.

### 1.6 Long QT Syndrome

Long QT syndrome (LQTS) is a group of disorders that are diagnosed on the basis of a prolongation of the QT interval on an ECG because of abnormalities in ventricular action potential repolarisation. They carry the increased risk of early after-depolarisations, which are highly arrhythmogenic (Tristani-Firouzi *et al.*, 2001). LQTS is also characterised by syncope and seizures, due to cardiac arrhythmias such as *Torsades de pointes* (Tdp), a polymorphic ventricular tachyarrhythmia with a characteristic twist of the QRS complex around the isoelectric line. Degeneration of Tdp into ventricular

## Chapter 1- Introduction

fibrillation may then lead to sudden cardiac death. LQTS can be divided into two main types: familial (inherited or congenital) and acquired (drug-induced). Inherited LQTS involves mutations to a number of cardiac ion channel  $\alpha$  and  $\beta$  subunits. These are hERG, *MiRP1*, *KvLQT1*, *minK*, and *SCN5A* (Curran *et al.*, 1995; Wang *et al.*, 1995a; Wang *et al.*, 1995b; Chen *et al.*, 1998; Splawski *et al.*, 1998; Abbott *et al.*, 1999; Splawski *et al.*, 2000; Priori *et al.*, 2001). Other LQTS mutations are in *Kir2.1*, *Cav1.2*, and Ankyrin B, a scaffolding protein involved in ion channel and transporter localization.

Over 200 mutations in hERG have been associated with LQT2. They lead to a reduction of  $I_{Kr}$  by causing a suppression of hERG function by alteration of channel gating, permeation, or trafficking to the cell surface (Sanguinetti *et al.*, 1996; Keating & Sanguinetti, 2001). These mutations appear to cluster in a few regions within hERG, namely around the pore and the surrounding membrane spanning regions, the amino terminal domain (Splawski *et al.*, 2000), the pore helix (Huang *et al.*, 2001), and the P-region in the outer mouth of the channel (Nakajima *et al.*, 1998). The majority of mutations are missense mutations (single base pair change) that result in subunit misfolding and defective protein trafficking to the cell surface (Tristani-Firouzi *et al.*, 2001). These mutations are found throughout the hERG protein and include T65P in the N-terminus, R752W and N861I in the C-terminus, F805C, V822M, and R823W in the cyclic-nucleotide binding domain, N470D in the S2 domain, A561V in the S5 domain, and several mutations such as G601S, Y611H, V612L, T613M, and L615V in the pore region (Delisle *et al.*, 2004). A number of methods have been identified in order to induce export of trafficking defective proteins from the endoplasmic reticulum (ER) and increase cell surface expression. These strategies are selective for certain mutants and include lowering the incubation temperature, adding high concentrations of glycerol, or by pharmacological rescue with drugs such as E-4031, cisapride, astemizole, quinidine, and fexofenadine (Zhou *et al.*, 1999; Rajamani *et al.*, 2002; Gong *et al.*, 2006; Robertson & January, 2006). These methods are thought to stabilise intermediate states of the protein, thus promoting native protein folding. Rescue of LQT2 mutants by pharmacological agents has obvious therapeutic implications, however the concentrations needed of these drugs also blocks hERG current, increasing the risk of arrhythmias. One exception is the

## Chapter 1- Introduction

drug fexofenadine that rescues the N470D and G601S mutations at drug concentrations that do not block the hERG current (Rajamani *et al.*, 2002). In contrast, a number of compounds have been identified that disrupt hERG channel trafficking and contribute to drug-induced LQTS (Wible *et al.*, 2005; Rajamani *et al.*, 2006).

The net effect of LQT2 mutations is a loss of hERG channel function and reduction of current magnitude leading to a prolongation in cardiac action potential repolarisation. Interestingly, a single mutation in the S5-P loop region of hERG (N588K) has been identified as a gain-of-function substitution, which reduces inactivation and increases the magnitude of repolarising current, thus shortening the QT interval (Brugada *et al.*, 2004). Mutations in two other genes, KCNQ1 and KCNJ2 encoding K<sup>+</sup> ion channels, have also been linked to short QT syndrome (SQTS), which can cause atrial fibrillation and cardiac arrhythmias (Brugada *et al.*, 2005). Hence, mutations in hERG that cause both a loss of its function and a gain of its function can lead to potentially life threatening cardiac arrhythmias.

A far more common form of LQTS is the drug-induced form due to medications that directly block hERG current or disrupt channel trafficking to the membrane (Sanguinetti & Tristani-Firouzi, 2006). A wide variety of drugs have been linked with acquired LQTS and Tdp. These range from antiarrhythmics, typically Class IA and III drugs, to antihistamines, antipsychotics, antimalarials, and antibiotics (Clancy *et al.*, 2003). In the mid-1990s, a number of non-cardiac drugs such as terfenadine and astemizole (antihistamines), cisapride (gastrointestinal agent), sertindole (antipsychotic), and grepafloxacin (antibiotic) were withdrawn from the market or had severe restrictions added to their use due to their associated risk of causing arrhythmias (Witchel & Hancox, 2000; Brown, 2004). Drug regulatory authorities then deemed it necessary for every drug to be tested for the liability to prolong QT intervals. Companies have responded by testing compounds against hERG at progressively earlier stages of drug development. Difficulty arises as hERG channel blockers are not only therapeutically diverse but also structurally very diverse. The development of higher throughput electrophysiological techniques as well as screening assays such as radioligand binding, rubidium flux, and

## Chapter 1- Introduction

fluorescence based assays and the advancement of *in silico* techniques have aided in the screening and assessment of hERG block (Finlayson *et al.*, 2004). Nevertheless, it is estimated that 40-70 % of compounds are still discarded during the early stages of drug development (Mitcheson *et al.*, 2005; Witchel, 2007). This approach does have its limitations as many therapeutically valuable compounds with minimal arrhythmogenic risks may also be discarded. Progress in the use of *in silico* approaches may aid this issue and enable the identification of hERG blocking compounds (Mitcheson *et al.*, 2005; Recanatini *et al.*, 2005). In addition, advances in the understanding of the structure of the hERG channel and its drug binding site help in the explanation of the pharmacological promiscuity of this channel.

### 1.7 Structural basis of hERG block

The unusual susceptibility of hERG to block by drugs in comparison with other Kv channels indicates a unique drug binding site. Early experiments revealed that drugs blocked Kv channels when applied from the intracellular side and only when the channel was open. Moreover, larger blockers prevented channel closure upon repolarisation and slowed deactivation kinetics. This type of block was termed 'foot in the door' (Armstrong, 1971). These channels could only close the activation gate (door) when the drug (foot) dissociated from the inner cavity and exited the channel. Another type of block was revealed with smaller compounds that blocked the channel without changing the deactivation rate and without exiting the channel. This phenomenon was called 'drug trapping' (Yellen, 1998). In this case, drugs are trapped within the inner cavity by closure of the activation gate and are only permitted to exit the pore when the channel reactivates. Studies on hERG blockers have revealed that drugs block the pore of the channel from the intracellular side and in the open state (Spector *et al.*, 1996a; Zou *et al.*, 1997). Recovery from block for a lot of these drugs is also extremely slow and almost nonexistent at negative voltages, consistent with a drug trapping mechanism (Perry *et al.*, 2004; Perry *et al.*, 2006). This was confirmed with the D540K hERG channels, which open at negative potentials, allowing recovery from block with MK-499, an antiarrhythmic compound and a potent hERG blocker (Mitcheson *et al.*, 2000b). The

## Chapter 1- Introduction

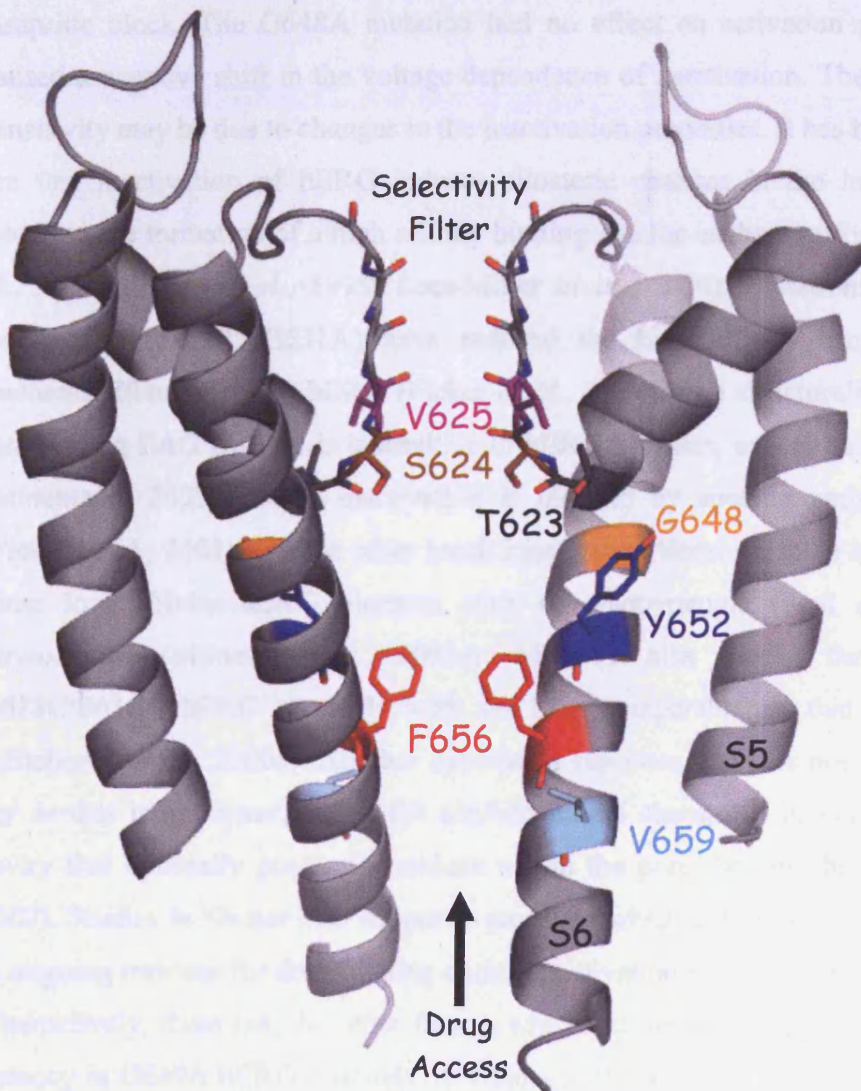
strong hyperpolarisation favors the unbinding of the positively charged drug from the inner vestibule, thus promoting rapid recovery from MK-499 block. This provided evidence that the slow recovery from block of WT channels is due to trapping of drug molecules within the inner cavity by closure of the activation gate.

The ability of hERG to trap methanesulfonanilides as well as many other compounds, despite their large size, suggests that the size of its inner cavity is larger than that of other Kv channels (Mitcheson *et al.*, 2000a). Modelling of its pore region based on the structure of KcsA reveals two unique properties of the inner pore of hERG not predicted to be shared by any other K<sup>+</sup> channel. First is the absence of the Pro-X-Pro motif in the C-terminal end of S6 of hERG. This motif is predicted to kink S6 and limit the size of the inner vestibule (del Camino *et al.*, 2000). Hence, many drugs can fit into the inner cavity of hERG but not other Kv channels. Second, is the presence of two aromatic residues, Tyr652 and Phe656, which are predicted to face the inner pore and are crucial to drug binding (Mitcheson *et al.*, 2000a). These residues are unique to the EAG/ERG K<sup>+</sup> channel family, as most other Kv channels have an Ile and Val in the equivalent positions. Alanine mutagenesis of these residues markedly decreases drug block for the majority of compounds studied so far, indicating an important role in drug binding to hERG (Mitcheson *et al.*, 2000a; Perry *et al.*, 2004; Witchel *et al.*, 2004; Perry *et al.*, 2006). These aromatic residues on S6 are hydrophobic and are therefore capable of forming hydrophobic interactions with drug molecules. The  $\pi$ -electron faces are also capable of overlapping with aromatic groups on drugs and forming  $\pi$ -stacking interactions as well as cation- $\pi$  interactions with charged amines. Further mutagenesis at these positions indicated that Phe656 is important for forming hydrophobic interactions with drugs while the aromatic properties of Tyr652 are important for high affinity binding to drugs (Fernandez *et al.*, 2004).

Site-directed mutagenesis has revealed a number of other key amino acid residues involved in drug binding to hERG (Figure 1.8) (Mitcheson *et al.*, 2000a). Individual residues on S6 and some pore helix residues were mutated to alanine and the sensitivity to block by MK-499 was determined for each mutant channel. In most of the mutant

## Chapter 1- Introduction

**Figure 1.8: Key residues involved in drug binding.** Homology model of hERG based on the crystal structure of KcsA in the closed state. It shows only two of its four subunits, each with S5 and S6 inner helices, and in colour highlights the key residues involved in drug binding identified by mutagenesis studies. The aromatic residues Tyr652 and Phe656 are important in most drug binding. Other residues include Gly648, Val659, Thr623, Ser624, and Val625. The point of drug access is indicated by an arrow.



## Chapter 1- Introduction

channels, current was reduced in a similar manner to WT hERG indicating that the mutated residue is not involved in drug binding to MK-499. However, a number of residues showed decreased sensitivity to block by MK-499 enabling the characterisation of specific residues that are important for the binding of MK-499. As discussed above, the aromatic residues Tyr652 and Phe656 appeared to be highly important for drug binding within the inner cavity. Gly648 also appeared to be important for MK-499 block of hERG by giving a 55-fold increase in the concentration of MK-499 required to block the current by 50 % ( $IC_{50}$ ). However, G648A did not have an effect on terfenadine and cisapride block. The G648A mutation had no effect on activation gating, however it caused a negative shift in the voltage dependence of inactivation. The reduction in drug sensitivity may be due to changes in the inactivation properties. It has been suggested that the fast inactivation of hERG induces allosteric changes in the inner mouth region allowing the formation of a high affinity binding site for methanesulfonanilides (Wang *et al.*, 1997; Ficker *et al.*, 1998; Lees-Miller *et al.*, 2000). Mutations that disrupt this inactivation (S620T, S631A) have reduced the high affinity drug binding of the methanesulfonanilides to hERG (Ficker *et al.*, 1998). The structurally related yet non-inactivating EAG channel is insensitive to hERG blockers, except clofilium (Gessner & Heinemann, 2003), unless inactivation is induced by specific amino acid mutations (Ficker *et al.*, 2001). On the other hand, inactivation does not seem to be necessary for some low affinity hERG blockers such as disopyramide (Paul *et al.*, 2001) and fluvoxamine (Milnes *et al.*, 2003a). MK-499 also blocks the non-inactivating G628C:S631A hERG channels with an  $IC_{50}$  comparable to that in WT channels (Mitcheson *et al.*, 2000a). Another hypothesis supposes that it is not inactivation gating *per se* that is important, rather the conformational changes it induces within the inner cavity that optimally positions residues within the pore for drug binding (Chen *et al.*, 2002). Studies in Shaker also support a model in which conformational changes are key in aligning residues for drug binding during inactivation gating (Panyi & Deutsch, 2007). Alternatively, there may be other factors which influence the apparent increase in drug potency in G648A hERG channels. It is thought that the drug binds to a pocket between the pore helix and the S6 domain that the alanine at position 648 might occlude. This

## Chapter 1- Introduction

mutation may also hamper interactions with other residues such as Thr623 and Tyr652. The role of this glycine residue in drug binding was studied as part of this thesis.

Other residues that appeared to form part of the drug binding site for MK-499 were Thr623, Ser624, Val625, and Val659. These residues are conserved in K<sup>+</sup> channels and so cannot explain the unusual pharmacology of hERG. Thr623 and Ser624 are polar and can interact with halogen and methanesulfonamide groups present on many high affinity blockers. Changing the *para*-substituent on phenyl rings of ibutilide, clofilium, and their analogues was sufficient to alter the potency of drugs by over 100-fold, most likely via differential interactions with Thr623 and Ser624 (Perry *et al.*, 2004; Perry *et al.*, 2006). The double mutation T623A:S624A showed an increase in the IC<sub>50</sub> of compounds of more than a 1000-fold. The Val625 side chain points away from the inner cavity and is therefore unlikely to be involved directly in drug binding (Stansfeld *et al.*, 2007). However, mutating this residue may result in changes to the folding around the selectivity filter and thus disrupting drug interactions with Thr623 and Ser624. Similarly, Val659 appears to have an impact on the potency of some drugs. V659A hERG channels exhibit extremely slow deactivation kinetics, which may allow for recovery from block and hence the reduced sensitivity to drug block. This project also attempts to distinguish between the effects observed on drug potency due to direct interactions with compounds or effects on channel gating.

### 1.8 Alternative mechanisms of block

For a small selection of drugs, one or both of the aromatic Phe656 and Tyr652 residues do not seem to be an important requirement for block of hERG channels. These blockers include some low affinity hERG blockers such as vesnarinone (Kamiya *et al.*, 2001), propafenone (Witchel *et al.*, 2004), and bepridil (Kamiya *et al.*, 2006) as well as some high affinity blockers such as dronedarone (Ridley *et al.*, 2004), thioridazine (Milnes *et al.*, 2006), and quinidine (Sanchez-Chapula *et al.*, 2003), which preferentially interact with Phe656 side chains with only minor interactions with Tyr652. Fluvoxamine, on the

## Chapter 1- Introduction

other hand, appears to be insensitive to mutations at both Phe656 and Tyr652 (Milnes *et al.*, 2003a), suggesting alternative sites of block.

The external mouth of the channel has also been shown to be the binding site for some drugs. In particular, toxins such as ergotoxin, BeKm1, and CnErg1 have been shown to block hERG and native  $I_{K_r}$  channels from the extracellular side of the membrane (Gurrola *et al.*, 1999; Pardo-Lopez *et al.*, 2002a; Pardo-Lopez *et al.*, 2002b; Milnes *et al.*, 2003b). BeKm1 toxin has also been shown to block the channel preferentially in the closed state, distinct from the open state dependent mechanism described for most hERG blockers (Milnes *et al.*, 2003b). Toxins have also been used to gain further insight into the structure of the outer mouth of the channel and were used to create a model for hERG's unusual S5-P linker as it bears no sequence similarity to that of other  $K^+$  channels (Zhang *et al.*, 2003; Tseng *et al.*, 2007). The model shows that residues 585-597, in the middle part of the S5-P linker in hERG, form a very dynamic amphipathic  $\alpha$ -helix with its hydrophobic face capable of interacting with other channel subunits and forming intersulfide bonds when residues are replaced by cysteines. In the open state, the S5-P linkers interact with pore loops to influence ion permeation through the pore. Toxins have therefore proved to be useful tools in probing the structure of the outer vestibule and raise the question of whether there are alternative binding sites and blocking mechanisms for small molecule blockers of hERG.

Some compounds indirectly suppress hERG current by reducing hERG trafficking to the cell surface. Long term exposure (for 24 hours) to arsenic trioxide, used for the treatment of acute promyelocytic leukaemia, was the first example of a compound that showed a reduction in hERG surface expression (Ficker *et al.*, 2004). Then a number of other compounds such as geldanamycin (Roe *et al.*, 1999; Ficker *et al.*, 2003) and pentamidine (Kuryshv *et al.*, 2005) exhibited inhibition of hERG protein trafficking to the cell surface. These compounds appear to interfere with the function and binding of hERG to cytosolic chaperones, such as Hsp70 and Hsp90. Chaperones play a crucial role in the proper folding, assembly, and processing of hERG channels in the ER (Ficker *et al.*,

## Chapter 1- Introduction

2003). The net result is an inhibition in hERG surface expression and reduction of  $I_{Kr}$  current, producing a novel form of acquired LQTS.

In contrast to the reduction in hERG current magnitude observed by most hERG blockers, a few hERG channel activators have recently been identified, such as RPR260243, PD-118057, and NS1643 (Kang *et al.*, 2005; Zhou *et al.*, 2005; Casis *et al.*, 2006). These compounds share the ability to shorten action potential duration and thus may have some therapeutic significance when treating cardiac disorders. RPR260243 causes a slowing of hERG channel deactivation leading to almost a 20 % increase in hERG current magnitude (Kang *et al.*, 2005). RPR260243 and PD-118057 mediate their effects by binding at a site distinct to that of dofetilide, hence not within the inner cavity. The binding site of RPR260243 has been shown to involve a cluster of residues near the cytoplasmic ends of the S5 and S6 helices, facing away from the ion conduction pathway (Perry *et al.*, 2007). In contrast, NS1643 affects the rates of onset and voltage dependence of inactivation rather than deactivation and acts as a partial agonist, which may form  $\pi$ - $\pi$  interactions with the Phe656 residue in hERG (Casis *et al.*, 2006).

### 1.9 Predicting hERG block

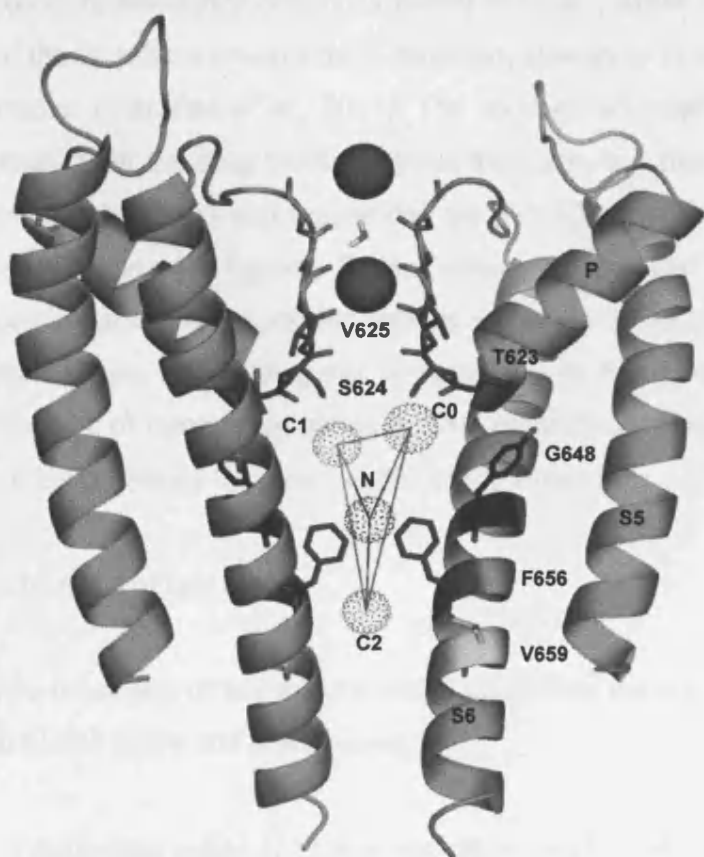
Advances in *in silico* techniques offer the potential for predicting possible hERG blocking entities and designing drugs with reduced QT liability (Sanguinetti & Mitcheson, 2005). These methods have so far involved a combination of ligand docking, hERG homology models, and quantitative structure-activity relationship (QSAR) studies.

QSAR studies have been useful in identifying the physicochemical features of hERG blockers. Two 3-dimensional (3D) QSAR models have been described and reveal a number of shared features (Cavalli *et al.*, 2002; Ekins *et al.*, 2002). These pharmacophores differ in the shape of the pyramidal structure representing each pharmacophore. The common pharmacophoric features are a central charged nitrogen (N) linked to a phenyl ring (C0) and potentially one or two other hydrophobic groups, which may be aromatic (C1 and C2) (Figure 1.9). The homology models of hERG have been

## Chapter 1- Introduction

### Figure 1.9: Interactions of the Cavalli pharmacophore within inner cavity of hERG.

This shows a model of hERG with the inner helices of two of its four subunits and the Cavalli pharmacophore model positioned within the inner cavity. The main features of the Cavalli pharmacophore are a central nitrogen (N), an aromatic group (C0), and the presence of hydrophobic groups (C1 and C2). The pharmacophore is manually positioned according to data from a variety of mutagenesis and *in silico* modelling studies. The N feature possibly forms cation- $\pi$  interactions with Tyr652 and Phe656, C1 may form  $\pi$ - $\pi$  or hydrophobic interactions with Tyr652. C2 is predicted to bind to Phe656 and C0 may interact with Thr623 and/or Ser624. The solid spheres in the selectivity filter represent K<sup>+</sup> ion sites.



## Chapter 1- Introduction

based on crystal structures of the closed and open states of KcsA and MthK or KvAP respectively. Although useful in explaining the structural interaction between hERG blockers and key amino acid residues in the pore identified by mutagenesis, these models are not predictive. The key features of hERG blockers can be identified as the protonated nitrogen atom that can form cation- $\pi$  interactions with Tyr652, and the phenyl rings that may form a variety of hydrophobic or electrostatic  $\pi$ -electron interactions with Tyr652 or Phe656 (Fernandez *et al.*, 2004; Stansfeld *et al.*, 2006). Polar groups attached to the *para*-substituent may also interact with Thr623 and Ser624. Some of the homology models of hERG however are at odds with results from mutagenesis studies. For instance, two serine residues Ser649 and Ser660 would be predicted from homology models to interact with drug moieties and yet mutation of these residues indicates they have no impact on drug potency. The key amino acid residues Tyr652 and Phe656 identified in mutagenesis studies are also not correctly orientated to favor drug interactions within the pore. A recent rotated-hinge homology model of hERG, which incorporates a clockwise rotation of the S6 helices towards the C-terminus, appears to be more consistent with mutagenesis studies (Stansfeld *et al.*, 2007). The imposed S6 rotation displaces the serine residues away from the drug binding site as they have not been shown to be involved in drug binding in hERG and repositions the Tyr652 and Phe656 residues to optimally favor interactions with ligands. Recent studies suggest that inactivation gating may induce conformational changes that include a rotation of S6 (Chen *et al.*, 2002). Thus, during inactivation, key binding site residues may be repositioned relative to the inner cavity. The lack of inactivation gating in EAG channels may explain the low potency of blockers for EAG, despite the identical homology within S6.

### 1.10 Aims of this thesis

The broad aim of this project was to understand the contribution of inner cavity residues to hERG gating and pharmacology.

1) Activation gating in Shaker and other Kv channels pointed to a glycine hinge model for channel opening, whereby conserved glycines facilitated bending of the inner helices.

## Chapter 1- Introduction

hERG channels have two glycines, Gly648 and Gly657, analogous to the sites of flexibility found in other Kv channels. This project addressed the roles of S6 glycines in hERG activation gating by firstly mutating these residues, individually or simultaneously, to alanine and then denoting changes to the kinetics of channel gating. Glycines are also the smallest amino acid residues and so mutations to larger amino acids were investigated in order to determine packing of the channel around these regions.

2) Deactivation gating in hERG has been shown to involve the N-terminal end of the channel. This gating process is slowed due to possible interactions between the pore, the voltage sensing domain, and the N-terminus, which stabilise the open state of the channel. Since V659A hERG slows deactivation kinetics, the aim was to investigate the role of Val659 in deactivation gating and test possible interactions with the N-terminus. Deactivation kinetics were therefore compared between N-terminal truncated V659A and WT hERG channels. Ile662 may also be crucial in channel gating due to its key position near the putative activation gate in hERG. The effects of mutations of Ile662 were also investigated.

3) The contributions of Gly648, Gly657, Val659, and Ile662 to the hERG drug binding site were investigated. The role of the aromatic Tyr652 residue for high affinity drug binding in hERG was also studied by using an automated planar electrode patch clamp system. A set of 24 compounds with varying structures and potencies were studied using WT hERG then compared to Y652A hERG channels. The aim was to use the consistent datasets from these experiments to build pharmacophore models that could identify chemical and structural moieties on drugs that interact with important components of the drug binding site of hERG.

## **2.1 Molecular Biology**

Molecular biology techniques were used in this thesis to create numerous mutant hERG constructs in order to investigate structure-function relationships in a number of different cell types. These techniques primarily involved site-directed mutagenesis of the DNA that coded for the hERG protein by using polymerase chain reaction (PCR), and then inserting it into the appropriate expression vector. This plasmid was then transformed into bacterial cells to express high levels of the hERG protein. Cloned plasmid DNA had to be extracted from the host bacterial cells and purified using different kits and protocols, which will be described in sections to follow. RNA could also be synthesised *in vitro* by linearising the DNA template then allowing transcription to occur with the use of a transcription kit.

The hERG protein was expressed in *Xenopus* oocytes as well as mammalian HEK-293 cells. A number of expression vectors were used in this study dependent upon the purpose of the experiments and the types of cells used. Mutations involving the glycine residues (Gly648 and Gly657), the pore helix residues (Thr623 and Ser624), and the Val659 residue were all made in the psp64 vector. The Ile662 mutants were made in the pcDNA3 vector. Both these vectors were suitable for *in vitro* transcription with RNA polymerase. They contain promoter sites (SP6 for psp64 and T7 for pcDNA3) for RNA transcription and sequences such as the polyadenylation sequence at its 3'-end stabilising transcribed RNA, therefore effective for studies with *Xenopus* oocytes. G648A and T623A:S624A mutant hERG channels were subcloned into the pIRES2-eGFP-hERG expression vector for transfection into HEK-293 cells. This vector was used to allow selection for hERG transfected cells on the basis of eGFP expression.

### **2.1.1 Mutagenesis**

## Chapter 2- Materials and Methods

Site-directed mutagenesis is a widely used technique allowing the manipulation of the genetic code and the alteration of specific amino acid residues in order to understand protein structure-function relationships. In this study, this technique was used to make mutations within the S6 region of the hERG channel. The point mutations introduced into the hERG gene were achieved via PCR by using the Stratagene Quikchange mutagenesis kit (Stratagene, La Jolla, CA, USA).

The *wild-type* (WT) construct used, consisted of the hERG sequence, which contained a silent Sall restriction site at nucleotide position 1393 within the S2 encoding sequence (a gift from Dr. Harry Witchel, University of Sussex). The region between the Sall and XhoI restriction sites encoding S2 - S6 of hERG was subsequently subcloned into pBlueScript KSII+. Its extensive range of restriction enzyme recognition sites and its small size (3 kb) made it ideal for subcloning hERG fragments.

The Quikchange method involved the preparation of a PCR reaction consisting of primers (100 ng) with the desired mutation, DNA template (50 ng), dNTP mix (100 mM), and *Pfu turbo* DNA polymerase ( $2.5 \text{ U } \mu\text{l}^{-1}$ ) (Stratagene, CA, USA) per 50  $\mu\text{l}$  reaction. Oligonucleotide primers were specifically designed using Vector NTI software (Invitrogen) to contain the mutation of interest and anneal to complementary sequences of the plasmid. They were between 25 and 45 bases long, with a GC content of about 40 – 60 % and a melting temperature  $\geq 78 \text{ }^\circ\text{C}$  (Stratagene Quikchange manual). Each PCR cycle involved the denaturation of the double stranded DNA at  $95 \text{ }^\circ\text{C}$ , annealing of the oligonucleotide primers at a temperature usually  $5 \text{ }^\circ\text{C}$  lower than their melting temperature, and then DNA elongation by DNA polymerase at  $68 \text{ }^\circ\text{C}$ . These steps were repeated 18 times in an automated thermal cycler and led to the exponential amplification of the DNA fragment and the generation of a mutant plasmid containing staggered nicks. The restriction enzyme DpnI (10 units per 50  $\mu\text{l}$ ), was then added to digest the methylated, template (non-mutated) double stranded DNA. The non-methylated DNA, carrying the mutation, could then be transformed into competent cells to produce bacterial clones containing the desired mutated plasmid.

## Chapter 2- Materials and Methods

### 2.1.2 Transformation of competent cells

Bacterial transformation is defined as the process of insertion of new genetic material, which results in the genetic alteration of a bacterial cell. This procedure therefore allows the uptake and expression of plasmids by bacterial cells. These plasmids contain an antibiotic resistance gene required for the growth of bacteria in antibiotic-containing selection media and for identifying which cells have successfully taken up the plasmid. The purpose of this technique was to amplify the plasmid DNA and thus, was used following a PCR mutagenesis reaction or after DNA ligation when subcloning fragments into plasmid constructs.

Mutant DNA was transformed into library efficiency competent DH5a *Escherichia coli* (*E.coli*) cells (Invitrogen). Competent cells are cells that have been suspended in a high concentration of calcium to create small holes in the membrane, which then allows DNA uptake. The cells purchased were already chemically pre-treated to encourage DNA uptake. Falcon 2059 tubes were cooled and competent cells slowly thawed on ice. 50  $\mu$ l of cells were used in each transformation. 2 - 4  $\mu$ l of PCR product or 5  $\mu$ l of ligation product was slowly added to each aliquot of competent cells. A positive control, such as pUC18 plasmid DNA (0.1 ng), was added to an aliquot of cells to test transformation efficiency. The competent cells and DNA were first incubated on ice for 30 minutes. Cells were then placed in a 42 °C water bath for 45 seconds then rapidly replaced on ice for 2 minutes (heat-shock). The salt optimised and carbon (SOC) media (Invitrogen) was also warmed to 42 °C. 900  $\mu$ l of SOC media was then added to each transformation sample, and tubes were placed in a 37 °C shaker at 225 rpm for 1 hour to allow transformed bacteria to express the plasmid gene for antibiotic resistance.

Luria-Bertani (LB) agar plates were made by adding 8.75 g LB agar powder (Sigma) to 250 ml milliQ water and then autoclaving it. After cooling to approximately 55 °C (hand-held hot), antibiotic selection reagents such as ampicillin (100  $\mu$ g ml<sup>-1</sup>) or kanamycin (30  $\mu$ g ml<sup>-1</sup>) were then added to select for cells containing either the ampicillin or kanamycin

## Chapter 2- Materials and Methods

resistance genes respectively. LB agar solution was poured into each plate and allowed to set for 20 minutes. 200  $\mu\text{l}$  of the transformed bacteria in SOC media was spread onto the agar plates using sterile techniques and then placed in a 37 °C incubator overnight. The presence of colonies indicated that the bacterial clone had successfully taken up the plasmid DNA and had antibiotic resistance. The next stage was to pick single colonies and grow them in liquid broth, after which plasmid DNA could be extracted from the bacterial culture.

### 2.1.3 Preparation of DNA

Commercially available kits were used to purify plasmid DNA from bacterial culture. The experimental procedure was based on the alkaline lysis of bacterial cells and the removal of bacterial protein lipid and genomic DNA. Plasmid DNA was then adsorbed onto silica resin columns in the presence of a high salt buffer, after which purified DNA could be easily eluted.

Single bacterial colonies were picked then transferred to 5 ml LB broth with 100  $\mu\text{g ml}^{-1}$  ampicillin or 30  $\mu\text{g ml}^{-1}$  kanamycin and left overnight at 37 °C. The Qiaprep Spin mini-prep kit (Qiagen, CA, USA) was then used to extract plasmid DNA from bacterial cultures. Cells were first centrifuged at 3000 rpm at 4 °C for 5 minutes and the supernatant carefully removed. The pellet was then resuspended in buffer, before the addition of lysis buffer for 3 minutes. This breaks the bacterial cell wall and releases its DNA contents. The lysate was neutralised by using neutralisation buffer, which precipitated chromosomal DNA and denatured proteins, while leaving the plasmid DNA in solution. The cell lysate was then cleared by centrifugation and the supernatant containing the plasmid DNA was filtered through the Qiaprep columns. These columns contained silica-gel membranes and were fitted into microcentrifuge tubes. They facilitated the selective binding of plasmid DNA to the column in the presence of a high salt buffer, while the rest of the reaction by-products passed through the column and were later discarded. The column was then washed with an ethanol-containing buffer to

## Chapter 2- Materials and Methods

remove excess salts. DNA was extracted from the column by the addition of an elution buffer.

Samples were quantified by comparison to a standard DNA ladder, DNA hyperladder I (Bioline, London), by using a 1 % agarose gel with 0.003 % ethidium bromide. Typically, a miniprep would yield 6 µg of DNA. DNA samples were then sent for sequencing at the Protein and Nucleic Acid Chemistry Laboratory (PNACL, University of Leicester). The Vector NTI software was used to compare sequences to WT hERG. Once the desired sequences were confirmed, DNA was prepared on a larger scale (midiprep), which could yield 20 – 100 µg of DNA, using similar methods. DNA was stored at -20 °C until required.

### 2.1.4 Subcloning of hERG fragments into expression vectors

In order to insert the mutant DNA fragment from pBluescript KSII+ into the vector of interest, restriction digests must first be made using the relevant restriction enzymes (New England Biolabs, Hertfordshire, UK). These enzymes recognise specific sequences in the DNA molecule, cleaving the DNA at these particular sites. A whole host of restriction enzymes were used in this study, so I have presented one pair as an example. Sall and BglII are two restriction enzymes found in both the pBluescript KSII+ and pcDNA3 vectors. A double digestion with these two enzymes simultaneously would cleave the vectors along with the mutated fragments in pBluescript KSII+ at these positions after incubation at 37 °C in the presence of bovine serum albumin (BSA) and with the recommended NEB buffer 3 (New England Biolabs, UK). This buffer was selected because it provided optimal reaction conditions for the activity of both enzymes. Sall leaves an overhang of 5' – TCGA (sticky-end) and BglII leaves an overhang of 5' – GATC. It is important that enzymes do not produce compatible ends, which can bind to one another. For instance, both Sall and XhoI produce an overhang of 5' – TCGA, hence they could not be used simultaneously.

## Chapter 2- Materials and Methods

Another consideration when using restriction endonucleases is their ability to display star activity, or relaxed sequence specificity. That is the ability to cleave sequences which are similar but not identical to their recognition sequence. Some restriction enzymes are more inclined to induce star activity than others; however this can be also produced under extreme reaction conditions. High glycerol concentrations (> 5 % of total reaction volume), high pH (> pH 8), and a high ratio of enzyme units to DNA concentration (usually > 100 units  $\mu\text{g}^{-1}$ ) may all contribute to the possibility of star activity. To combat these issues, the enzymatic reaction could be run for a longer time period or the reaction volume may be increased to dilute the glycerol content. Certain enzyme combinations may not be amenable to perform a double digest, e.g. Sall and KpnI. In these cases, a sequential digest with each enzyme separately would be required.

The temperature used and the length of incubation varied according to the type and amount of enzyme used. Typically, 1 unit of enzyme is needed to digest 1  $\mu\text{g}$  of DNA in 1 hour. The complete digestion of the DNA was then confirmed by loading a small amount of cut DNA on a 1 % agarose gel, which was then subjected to electrophoresis.

### 2.1.5 DNA extraction from agarose gels

Gel electrophoresis was used to separate DNA fragments according to size by the application of an electric current. The DNA molecules in the agarose gel were stained by ethidium bromide so that the DNA bands may be visualised under ultraviolet (UV) light. These bands containing the DNA molecules of interest could then be isolated and purified.

Cut DNA samples were run on an agarose gel stained with 0.003 % ethidium bromide for a sufficient period of time to ensure that the DNA fragments were clearly separated. The DNA bands of interest were cut from the gel with a sterile scalpel blade. The required DNA bands included the mutated fragment in pBluescript KSII+ (insert) and the hERG coding sequence in the vector of interest (psp64 or pcDNA3) after it was cut with the

## Chapter 2- Materials and Methods

same restriction enzymes (vector). The gel slice was dissolved in a heating block at 50 °C. DNA was then extracted from the gel by using the Qiaquick gel extraction kit (Qiagen, USA), following the manufacturer's protocol.

### 2.1.6 Ligation of DNA fragments

The two cut DNA fragments (insert and vector) each containing sticky-ends, were then ligated by using T4 DNA ligase (New England Biolabs, UK), so as to insert the fragment containing the necessary mutation in pBluescript KSII+ into the psp64 or pcDNA3 hERG vector. DNA ligase can form covalent phosphodiester bonds between the 3'- hydroxyl groups of one nucleotide and the 5'- phosphate groups of another nucleotide. Restriction digests produced double stranded DNA with complementary single stranded overhangs. The ligase enzyme catalysed the covalent link between these cohesive sticky-ends producing continuous DNA strands.

The ligation mixture contained 2 µl of T4 ligase, 1 µl of 10x T4 buffer, and a 5:1 molecular ratio of insert to vector (e.g. insert : vector size ratio was 1:12 then needed 5 ng of insert for every 12 ng of vector ). The reaction was incubated at 16 °C overnight. Ligated DNA was then transformed into bacteria. Successful ligations would yield colonies on agar plates, due to the presence of an antibiotic resistance gene marker on the ligated circular construct. Colonies were then picked as detailed earlier in section 2.1.3 and the DNA prepared. Several control reactions were also set up. One contained no DNA ligase to test for the presence of uncut vector DNA, one with no insert to test for self-ligation of the vector, and another in the absence of the vector to test for self-hybridisation of the mutant DNA inserts. No colonies would be expected for any of the control samples on the agar plates. The resultant DNA was then amplified, purified, and the fragment encompassing where the mutation would be expected to reside was sent for sequencing to ensure that the desired mutation was present and that no extra random mutations had occurred. It was important to ensure that the sequencing primers included the restriction sites, as that is where mutations frequently occur.

## Chapter 2- Materials and Methods

### 2.1.7 Preparation of cRNA by *in vitro* transcription

*In vitro* transcription is the process by which a DNA sequence can be enzymatically copied by RNA polymerase in the laboratory to synthesise a complementary RNA strand.

#### Preparation of template DNA

DNA template was used to make cRNA from plasmid DNA. EcoRI restriction enzymes (New England Biolabs, UK) were used to linearise DNA as they cut the plasmid at a single specific site downstream of the 3'-end, to increase the efficiency of RNA synthesis. The DNA template contains an RNA polymerase promoter site to which the enzyme can bind and initiate RNA synthesis. 10  $\mu\text{g}$  of DNA was incubated with 5  $\mu\text{l}$  of 100 U  $\mu\text{l}^{-1}$  of EcoRI for 1 hour at 37 °C. Once linearization was complete, 100  $\mu\text{g ml}^{-1}$  of Proteinase K and 0.5 % SDS was added to the DNA and incubated for 30 minutes at 50 °C. This denatures contaminating proteins, especially RNAases, and care must subsequently be taken to minimise contamination. The Qiaquick gel extraction kit (Qiagen, USA) was used to purify the linearised DNA by passing the solution through the provided column. DNA was eluted using elution buffer and quantified using gel electrophoresis. It was then diluted using diethylpyrocarbonate (DEPC) - treated water to a final concentration of 0.2  $\mu\text{g } \mu\text{l}^{-1}$  and stored at -20 °C until required.

#### Preparation of cRNA

*In vitro* transcription, to make cRNA, was carried out at room temperature using the mMessage mMachine kit (Ambion, USA). Extreme care was exercised at all stages in this process in order to avoid contamination by RNAases, such as using autoclaved glassware, wearing a clean lab coat and gloves, and using filter pipette tips. The reaction was assembled in the following order: 1  $\mu\text{l}$  of nuclease-free water, 10  $\mu\text{l}$  of NTP/CAP mix, 2  $\mu\text{l}$  of 10x reaction buffer, 2  $\mu\text{l}$  of RNA polymerase enzyme mix, and 1  $\mu\text{g}$  of DNA template. The solution was then incubated at 37 °C for 2 hours. This should give

## Chapter 2- Materials and Methods

approximately 20  $\mu\text{g}$  of capped RNA. The cap structure, also found in eukaryotic mRNA at the 5'-end, is necessary for the initiation of protein synthesis and the protection of synthesised RNA from ribonuclease digestion. It also increases the stability of the RNA making it ideal for oocyte microinjection.

After incubation, 1  $\mu\text{l}$  of DNAase1 was added to the reaction and incubated for 15 minutes at 37 °C to digest the template DNA. To assess the quality and yield of RNA, a sample was heated to 85 °C for 3 minutes then run on a 1 % denaturing formaldehyde agarose gel at 80 mV for 50 minutes. This gel contained 10x MOPS EDTA sodium acetate (MESA) buffer made up of MOPS (2 M), sodium acetate (50 mM), EDTA (10 mM), pH 7. RNA was quantified on the gel relative to RNA standards, then diluted to a concentration of 500 ng  $\mu\text{l}^{-1}$  and aliquoted into 3.2  $\mu\text{l}$  samples. If the RNA appeared smeared when run on a denaturing gel, this would indicate contamination and the RNA would be discarded. RNA aliquots were stored at -80 °C until required for injection into *Xenopus* oocytes.

### 2.2 Two-electrode voltage clamp recordings in *Xenopus* oocytes

Oocytes from *Xenopus laevis* frogs are commonly used as an expression system for ion channel proteins. Oocytes were used extensively in this study to investigate the gating and pharmacological properties of WT and mutant hERG channels due to the fact that they offer many advantages over other expression systems. They can efficiently translate exogenous mRNA into proteins. They also express a relatively low number of endogenous transporters and channels and have a large diameter (1 - 1.2 mm) making them an easy system to inject and record from. In comparison to other electrophysiological techniques, recording from oocytes is relatively straightforward and only requires coarse movement manipulators and low powered microscopes. Recordings are also stable over prolonged periods of time (1 – 2 hours). Oocytes are simple to isolate and manipulate, and faithfully express the desired protein. The level of expression can also be regulated by adjusting the amount of cRNA injected. cDNA may also be injected into the nucleus of oocytes.

## Chapter 2- Materials and Methods

### 2.2.1 Basic characteristics of a *Xenopus* oocyte

An oocyte is an immature egg stored in the abdominal cavity of adult females in clumps called ovarian lobes that include oocytes, connective tissue, blood vessels, and follicle cells. They go through six maturation stages (I - VI). Oocytes at stages V and VI, which were the largest in size, were used for electrophysiological recordings. They have a black pigmented region called the animal pole and a white non-pigmented vegetal pole. A vitelline membrane surrounds the oocyte, but does not affect electrophysiological recordings as it is devoid of channels and transporters. Another layer of cells, called the follicular membrane, surrounds the vitelline membrane and separates the oocyte from its external environment. The follicular membrane expresses ion channels and transporters, is hard to pierce with microelectrodes, and must be removed prior to injection.

### 2.2.2 Isolation of *Xenopus* oocytes

Oocytes were extracted from adult female *Xenopus laevis* frogs. Frogs were humanely killed by anaesthetic and pithing followed by an incision made in the lower abdominal wall to expose the ovarian lobes. Oocytes were separated into clumps of 10 - 20 oocytes and placed in oocyte Ringer (OR2) solution, containing (in mM): NaCl 82.5, KCl 2.5, Na<sub>2</sub>HPO<sub>4</sub> 1, MgCl<sub>2</sub> 1, HEPES 5 (pH 7.5). Normally, 15 - 20 ml of oocytes could be collected per frog. Oocytes were then washed with OR2 solution 6 - 7 times, or until solution was clear. Oocytes were treated with 25 ml of sterile-filtered 1 mg ml<sup>-1</sup> collagenase (Sigma), and gently rocked until the follicular layer could be easily removed (approximately 30 minutes). Oocytes were then washed with Barth's solution containing (in mM): NaCl 88, KCl 1, CaCl<sub>2</sub> 0.41, Ca(NO<sub>3</sub>)<sub>2</sub> 0.33, MgSO<sub>4</sub> 1, NaHCO<sub>3</sub> 2.4, HEPES 10 (pH 7.4), until the solution was clear. Oocytes were placed in a petri dish with fresh Barth's solution, and the follicular cell layer was removed manually with forceps. The defolliculated oocytes were cultured at 18 °C in Super Barth's solution (Barth's solution supplemented with 1 mM Na-pyruvate and 50 µg ml<sup>-1</sup> gentamicin). The following day, these oocytes were injected with cRNA for hERG channel expression.

## Chapter 2- Materials and Methods

### 2.2.3 cRNA injection into *Xenopus* oocytes

Glass pipettes filled with mineral oil (Sigma) were used for cRNA injection into the oocytes. These pipettes were first pulled and tips broken to approximately 30  $\mu\text{m}$  wide with a sharp tip to enable its insertion into the oocyte with minimal damage. The pipette was mounted onto the microinjection apparatus (Nanoliter 2000, World Precision Instruments), and RNA was pulled into the tip of the injection pipette. The pipette was pushed into the cell and the RNA injected, while observing a slight swelling of the oocyte. The amount of cRNA injected ranged from 5 - 30 ng of cRNA per oocyte in a volume of 20 – 60 nl depending on the expression levels of the hERG mutant channels being tested. Each aliquot of RNA was used to inject 30 oocytes. Oocytes were cultured in Super Barth's solution, which was replaced every 24 hours.

### 2.2.4 Two-electrode voltage clamp recordings

The voltage clamp technique was used to measure macroscopic currents across cell membranes in response to an applied voltage. There are a number of different variations of this technique, however the one used extensively to record from *Xenopus* oocytes was the two-electrode voltage clamp method. Macroscopic membrane currents were recorded between 1 and 7 days after oocytes had been injected with cRNA. This technique permits recording of relatively large currents and is well-suited for studies in *Xenopus* oocytes that express large numbers of ion channels. In brief, the two-electrode voltage clamp set-up has two electrodes; one electrode measures the membrane potential relative to ground, while the other passes current. When a command potential is set, a pre-amplifier connected to the electrodes records the membrane potential and sends the output to a feedback amplifier. This amplifier acts as a negative feedback system to maintain the cell at this voltage. It subtracts the membrane potential from the command potential, magnifies any difference, and sends an output to the current electrode. So a current equal and opposite to the ionic current is produced and measured.

## Chapter 2- Materials and Methods

The microelectrodes were made from 1 mm filamented borosilicate thin walled glass (TW150F-4, World Precision Instruments) and pulled using a horizontal puller (Sutter Instruments). They were filled with 3 M KCl at least 48 hours before use to enable air bubbles in the fine tips to dissipate and the tips were broken to a resistance of 1 - 2 M $\Omega$ .

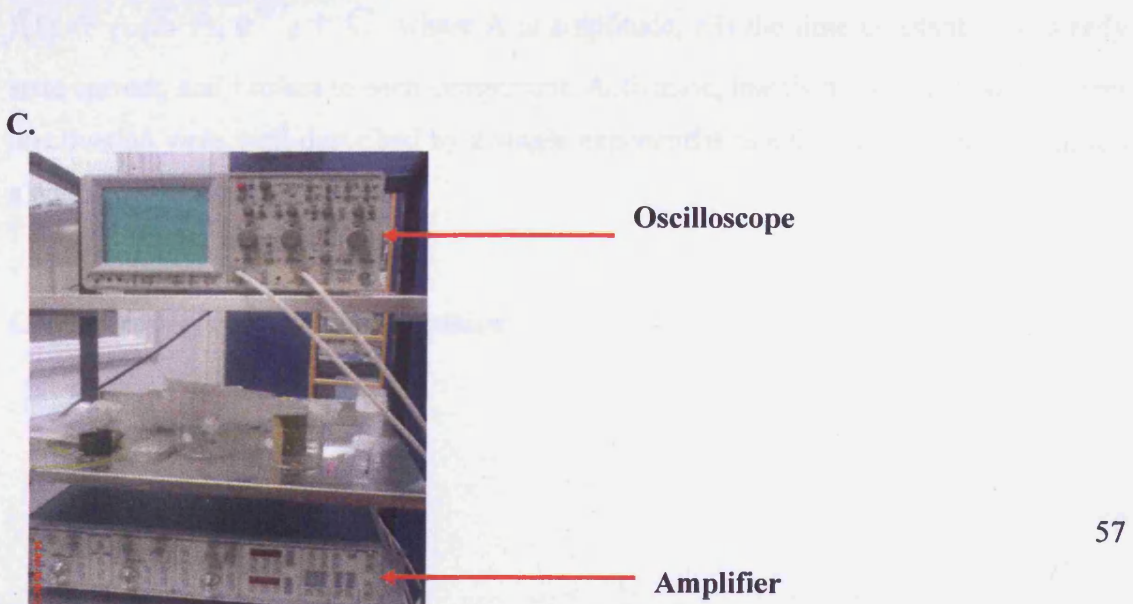
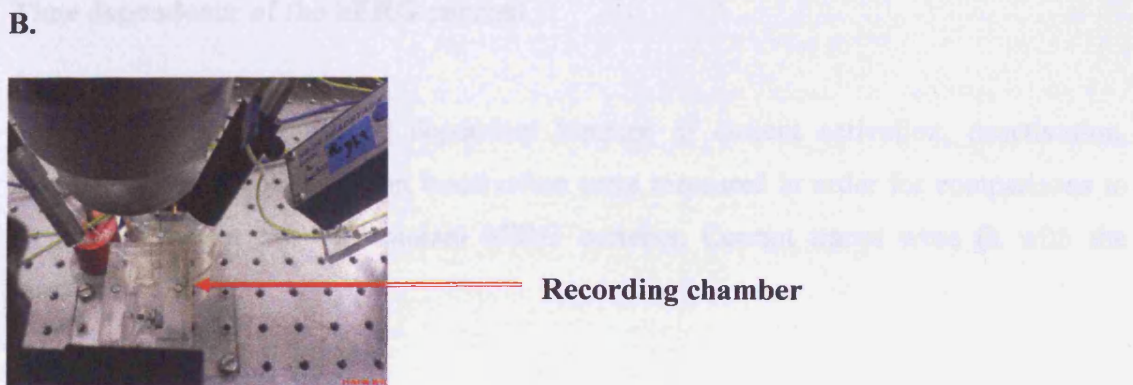
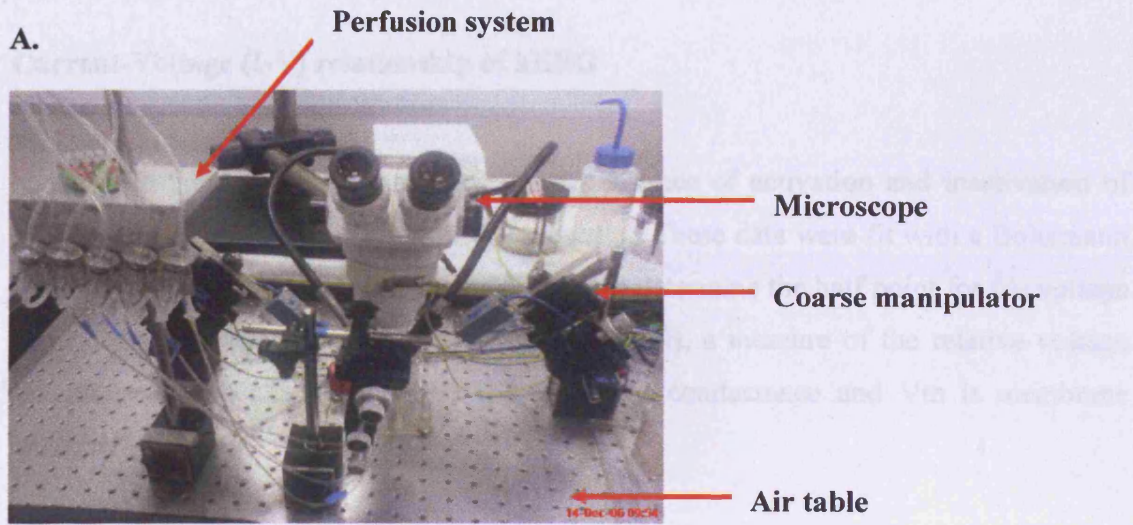
The oocyte was placed in the recording chamber and the bath perfused with a low Cl<sup>-</sup>, 2 mM K<sup>+</sup> oocyte recording solution to attenuate endogenous chloride currents. This solution contained 96 mM Na 2-(N-Morpholino)ethanesulfonic acid (MES), 2 mM KMES, 2 mM Ca(MES)<sub>2</sub>, 5 mM HEPES, 1 mM MgCl<sub>2</sub> (pH 7.6). To record currents from hERG channel mutants that exhibit a negative shift in the voltage dependence of inactivation, a 96 mM K<sup>+</sup> recording solution was used containing 2 mM NaMES, 96 mM KMES, 2 mM Ca(MES)<sub>2</sub>, 5 mM HEPES, 1 mM MgCl<sub>2</sub> (pH 7.6). Extracellular solutions were applied from a solution-switching device that controlled 5 separate perfusion lines. Figure 2.1 shows how the equipment was set up. Build up of extracellular K<sup>+</sup> would change the voltage dependence and kinetics of hERG currents. It is postulated that the presence of a vitelline membrane and foldings in the plasma membrane prevent the rapid equilibration of K<sup>+</sup> outside the oocyte membrane. Removal of the vitelline membrane, measuring smaller currents, and pre-swelling the oocyte in a hypo-osmotic solution are ways of combating this problem. The easiest method of facilitating diffusion and minimising extracellular K<sup>+</sup> accumulation is by placing the outlet of the manifold close to the oocyte during recordings. Recordings were done at room temperature.

### 2.2.5 Data acquisition and analysis

Voltage clamp recordings were made with a Geneclamp 500B amplifier (Molecular Devices, USA) coupled to a computer by a Digidata 1322A digital to analogue converter (Molecular Devices, USA). pCLAMP 9 software (Molecular Devices) was the data acquisition and analysis software used. Prism 4.0 (GraphPad Software) was used for data presentation and fitting Hill functions to concentration–response curves. Voltage and current signals were low pass filtered at 1 - 2 kHz and recorded to disk with a sampling

## Chapter 2- Materials and Methods

**Figure 2.1: Two-electrode voltage clamp setup.** A. Coarse manipulators hold the two electrodes and a perfusion system controls extracellular solution. The rig is placed on an air table. B. Oocytes are placed in a recording chamber and the rig is connected to an oscilloscope and amplifier (C).



## Chapter 2- Materials and Methods

frequency of 5 kHz. Some currents with faster kinetics necessitated filtering at 5 kHz and sampling with a frequency of up to 20 kHz. A detailed description of the voltage protocols and analysis of elicited currents will be discussed in the results chapters. Commonly utilised curve-fitting functions are briefly described in the following section.

### Current-Voltage (I-V) relationship of hERG

Normalised conductances for the voltage dependence of activation and inactivation of hERG were plotted as a function of test potential. These data were fit with a Boltzmann function [ $G(V) = 1 / (1 + \exp((V_{0.5} - V_m) / k))$ ] to determine the half point for the voltage dependence of gating ( $V_{0.5}$ ) and the slope factor ( $k$ ), a measure of the relative voltage sensitivity of the channels.  $G(V)$  is normalised conductance and  $V_m$  is membrane potential.

### Time dependence of the hERG current

Time constants for the time dependent kinetics of current activation, deactivation, inactivation, and recovery from inactivation were measured in order for comparisons to be made between WT and mutant hERG currents. Current traces were fit with the function:

$f(t) = \sum_{i=1}^n A_i e^{-t/\tau_i} + C$  where  $A$  is amplitude,  $\tau$  is the time constant,  $C$  is steady state current, and  $i$  refers to each component. Activation, inactivation, and recovery from inactivation were well-described by a single exponential function. Deactivation required a double exponential function.

### Concentration-response relationships

## Chapter 2- Materials and Methods

Peak tail current amplitudes, after they have stabilised in control solutions or after reaching steady state block at each drug concentration, were corrected for leak. Current amplitudes at each drug concentration were normalised to control ( $I_{Drug}/I_{Control}$ ). The corresponding concentration-response relationships were fitted with a sigmoidal curve using the Hill function  $[(I_{Drug}/I_{Control}) = 1 / (1 + ([D] / IC_{50})^h)]$  where  $IC_{50}$  is the concentration at which the drug inhibits the current by 50 % and  $[D]$  and  $h$  correspond to the drug concentration and Hill coefficient respectively.

All drug solutions were prepared daily by dilution of a concentrated stock to the required experimental concentration in extracellular recording solution. Drugs were dissolved in dimethylsulphoxide (DMSO) and the stock solution was kept at -20 °C.

### 2.2.6 Statistical analysis of the data

Data are presented as mean  $\pm$  standard error of the mean (S.E.M) between WT and mutant hERG channels. Statistical comparisons of WT and mutant hERG current results were performed using ANOVA with Dunnet's test for multiple comparisons. This test compares group means for 3 or more groups against the mean of a reference group (control). Differences were considered statistically significant for  $p \leq 0.05$  with a 95 % confidence interval. Prism 4.0 (GraphPad, San Diego, USA) was used for statistical analysis and to plot results.

## 2.3 Cell Culture

### 2.3.1 Cell lines and their maintenance

A number of different mammalian cell lines were recorded from in this study:

- A) Stably transfected Human Embryonic Kidney 293 (HEK-293) cells, expressing hERG (hERG-HEK cells), kindly provided by Professor Craig January, University of Wisconsin.

## Chapter 2- Materials and Methods

- B) Stably transfected HEK-293 cells expressing hERG with the following mutations within the pore: G648A, T623A:S624A, and Y652A. Y652A hERG-HEK cells were kindly provided by Dr. Harry Witchel, University of Sussex.
- C) HEK-293 and Chinese Hamster Ovary (CHO) cells incorporating the Flp-In technology (Invitrogen).
- D) *Wild-type* HEK-293 cells (WT-HEK cells).

### **hERG-HEK cells**

hERG-HEK cells were maintained in Dulbecco's Minimum Essential Medium (MEM with Earle's salts, Gibco) supplemented with 10 % foetal bovine serum (FBS, Gibco), 2 mM L-glutamine (Gibco), 1 mM sodium pyruvate (Gibco), and 400  $\mu\text{g ml}^{-1}$  geneticin (G418, Gibco). Cells were stored in an incubator at 37 °C maintained in an atmosphere of 5 % CO<sub>2</sub>. They were grown in 25 cm<sup>2</sup> flasks and passaged every 3 - 4 days. To passage cells, they would first be washed twice with 5 ml of phosphate buffered saline (PBS, Gibco), before the addition of 1 ml of Trypsin-EDTA (Gibco) and incubation for approximately 2 minutes, to dissociate cells from the bottom of the flask. Cells were centrifuged at 250 rpm for 2 minutes and the pellet was then resuspended in 3 ml of medium, before a 1:4 split. Cells were allowed to adhere for 24 hours before gently removing the medium and replacing it with 10 ml of fresh medium to remove any residual trypsin.

### **Pore mutant hERG-HEK cells and WT- HEK cells**

Stable cell lines expressing the pore mutant hERG channels were generated using the Lipofectamine-based transfection method. Pore mutant hERG-HEK cells and WT-HEK 293 cells were maintained in MEM alpha medium without nucleosides (Gibco) supplemented with 10 % FBS, and 1 % penicillin-streptomycin. Mutant hERG-HEK cells

## Chapter 2- Materials and Methods

were further supplemented with 500  $\mu\text{g ml}^{-1}$  geneticin (G418, Gibco). Cells were grown in 25  $\text{cm}^2$  flasks and passaged every 3-4 days as described above.

### **Flp-In HEK 293 and Flp-In CHO cells**

Methods describing the generation of stable cell lines using the Flp-In expression system will be explained in results chapter 4. Flp-In HEK 293 cells were cultured in Dulbecco's MEM with high glucose, and supplemented with 2 mM L-glutamine (Gibco), 10 % FBS, 1 % penicillin-streptomycin (Gibco), and 100  $\mu\text{g ml}^{-1}$  Zeocin (Invitrogen), at 37 °C under 5 %  $\text{CO}_2$ . Flp-In CHO cells were cultured in Ham's F12 media (Gibco), supplemented with 2 mM L-glutamine, 10 % FBS, 1 % penicillin-streptomycin, and 100  $\mu\text{g ml}^{-1}$  Zeocin, at 37 °C under 5 %  $\text{CO}_2$ . Cells were grown in 25  $\text{cm}^2$  flasks and passaged every 3 - 4 days. When cells were confluent, they were washed twice with 10 ml PBS and a 1:10 split was carried out. Medium was changed every 2 - 3 days.

### **2.3.2 Generation of stable cell lines**

Transfection is a method of introducing plasmid DNA into eukaryotic cells by using a cationic lipid reagent. Positively charged groups on the lipid molecule interact with negatively charged phosphates on DNA forming complexes. These complexes fuse with the cell plasma membrane and deliver DNA into the cell.

A stable cell line constitutively expresses the protein of interest because the exogenous DNA is incorporated into chromosomal DNA and becomes part of the genome. This is a low probability event, particularly for incorporation into active regions of the genome. Clones have to be grown up from single cells and expression levels tested. The aim of making a stable cell line was to ensure that all cells expressed the hERG protein, giving hERG currents of sufficient size for electrophysiological recordings with minimal cell to cell variation in current density. Although transient transfection is less laborious and time consuming, expression only lasts from 1 – 7 days after transfection due to DNA

## Chapter 2- Materials and Methods

degradation. The efficiency of DNA uptake and the level of expression also vary between transiently transfected cells.

The two mutant hERG channels (G648A and T623A:S624A) were subcloned into the pIRES2-eGFP-hERG expression vector (kindly donated by Dr. Jamie Vandenberg, University of New South Wales) using the techniques previously described (section 2.1). The pIRES2 vector permits the co-translation of the protein of interest and the enhanced green fluorescent protein (eGFP), thus allowing easy and efficient selection of transfected cells on the basis of eGFP expression. It is able to do so because it contains an internal ribosome entry site (IRES) of the encephalomyocarditis virus (ECMV) that drives the translation of two open reading frames from a single bicistronic mRNA. So hERG expression should correlate with eGFP expression. This vector also has antibiotic resistance genes, which would allow for stably transfected cells to be selected for using G418.

Lipofectamine 2000 (Invitrogen, UK) was used to transfect HEK-293 cells, expressing mutant hERG channels (G648A and T623A:S624A). Cells were cultured on a 6-well plate until they were approximately 80 % confluent. 3  $\mu$ l of Lipofectamine was added to 95  $\mu$ l of serum-free media and left at room temperature for 5 minutes. 1  $\mu$ g of DNA was then added to the solution and the transfection mixture was left to equilibrate for a further 20 minutes. The lipid-DNA complex was subsequently slowly added to the cells. Transfection media was replaced after 5 hours by culture media, without selection antibiotic. Cells were split into G418-containing media 48 hours after transfection.

Cells selected for using the G418 selection media were plated into 96-well plates using serial dilution. Wells were closely observed so that only those containing single cells were used to generate clones for selection based on eGFP expression. Green fluorescence was used as a marker of transfection and therefore an indicator of hERG-expressing cells. When the cells of those particular wells divided to form colonies, they were removed by using a Gilson pipette tip and grown in a 25 cm<sup>2</sup> flask. Cells were then maintained and hERG expression levels were tested in patch clamp experiments. Clones were finally

## Chapter 2- Materials and Methods

selected on the basis of expression levels and suitability for use in electrophysiological recordings.

### 2.4 Western blotting

This technique was used in this study to detect the presence and level of expression of hERG protein in the stable cell lines. In brief, proteins are separated on a polyacrylamide gel according to molecular weight and then transferred onto a nitrocellulose membrane for analysis. A primary antibody is first used to bind to the protein of interest. Then a secondary antibody, conjugated to a reporter molecule such as horse radish peroxidase (HRP), detects the location of the primary antibody and creates a visible band when a substrate is added.

Cells were split into 6-well plates overnight so as to achieve ~ 70 % confluency. Each well of cells was washed with 1 ml PBS and lysed with 200  $\mu$ l RadioImmunoPrecipitation Assay (RIPA) buffer (Sigma) for 10 minutes on ice. Cells were scraped off the plate and centrifuged at 16,000 g for 5 minutes at 4 °C. The Lowry protein assay was performed on the supernatant to determine the amount of total protein in cell lysates. A standard curve was created using BSA at concentrations of 25, 50, 100, 200, 250, and 400  $\mu$ g ml<sup>-1</sup>. The data points were fitted with a linear regression curve (Prism 4.0). To enable accurate measurement, the cell lysates were diluted by a factor of 20 and light absorbance at 750 nm measured using a Beckman Du-65 spectrophotometer. The concentration of total protein in the cell lysates was calculated from the BSA standard curve. Sample volumes were then adjusted to ensure uniform protein loading in each lane of a western blot.

30  $\mu$ g of total protein from each sample was added to an equal volume of Laemmli buffer (Sigma). Samples were heated for 2 minutes at 60 °C to denature the protein. These samples, along with coloured molecular weight markers (Biolone, London), were loaded onto an 8 % sodium dodecyl sulfate (SDS) polyacrylamide gel and separated by electrophoresis at 200 V for 2 - 3 hours. The gel was then transferred to a nitrocellulose

## Chapter 2- Materials and Methods

membrane using a Trans-blot SD semi-dry transfer cell (Biorad, CA, USA) for 20 minutes at 15 V. Samples were then blocked for 1 hour to reduce non-specific binding in blocking buffer, consisting of 5 % Marvel milk powder in a 0.3 M Tris-Tween buffered saline (TTBS) containing, 137 mM NaCl, 2.7 mM KCl, 25 mM Trizma Base, and 0.05 % Tween (pH 8). The membrane was washed several times with 0.3 M TTBS then incubated overnight at 4 °C with a 1:10,000 dilution of rabbit anti-hERG serum. The next day, after several washes, a 1:7000 dilution of secondary anti-rabbit antibody conjugated to HRP (Sigma) prepared in 0.3 M TTBS, was incubated with the blot for 1 hour at room temperature.

Protein detection was carried out using enhanced chemiluminescence (ECL, Amersham), according to the manufacturer's protocol. Addition of the ECL detection agents onto the membrane elicits a peroxidase catalysed oxidation of luminol resulting in a chemiluminescent signal. Excess ECL solution was removed from the nitrocellulose membrane which was placed in a hypercassette and exposed on an ECL Hyperfilm (Amersham) for seconds or minutes then developed using a hyperprocessor. The luminescence produced as a reaction product is in proportion to the amount of protein.

## **Chapter Three** Investigating the glycine hinge hypothesis in hERG

Crystallographic studies carried out on bacterial channels have provided information on the structural characteristics of the pore-forming region of  $K^+$  channels. The first crystal structure solved was that of the bacterial  $K^+$  channel KscA, a relatively simple prokaryotic channel with 2 transmembrane domains that are similar to S5 and S6 in Kv channels (Doyle *et al.*, 1998). The inner helices were straight and formed a bundle near the intracellular side creating a closed channel that was impermeable to  $K^+$  ions. Another bacterial  $K^+$  channel, the inward rectifier KirBac1.1, was also crystallised in the closed state (Kuo *et al.*, 2003). In contrast, the crystal structures of MthK, KvAP, and Kv1.2 all corresponded to the open state (Jiang *et al.*, 2002a; Jiang *et al.*, 2002b; Jiang *et al.*, 2003a; Long *et al.*, 2005a). Instead of a bundle crossing, the homologues of the S6 helices were splayed open creating a wide opening to the cytoplasm. Comparison between the closed and open state structures revealed a bend at a glycine hinge point located just below the selectivity filter.

A sequence alignment of a variety of  $K^+$  selective channels showed that this glycine was conserved in most  $K^+$  channels as well as many other ion channels (Shealy *et al.*, 2003). This suggested a universal mechanism, known as the 'gating hinge', for opening of  $K^+$  channels through bending of the inner helices at this glycine position. An essential feature of a glycine is its ability to confer flexibility in protein structures because of its small size and its ability to adopt a wide range of angles (Bright *et al.*, 2002). Further studies demonstrated the role of glycine as a gating hinge for the opening of ligand and voltage dependent  $K^+$  channels. Substituting this glycine with an alanine and other amino acids in Shaker and  $BK_{Ca}$  channels hindered channel opening (Magidovich & Yifrach, 2004; Ding *et al.*, 2005). However, by introducing another glycine at an adjacent position in Shaker, the channel recovered its ability to open. Also substituting the glycine with a proline favoured the open state of Shaker by introducing a rigid kink that reduced channel

### Chapter 3- Glycine hinge study

flexibility. This data supported the role of the glycine gating hinge, necessary in pore opening.

A Pro-X-Pro motif found on the lower part of S6 is also conserved in many members of the Kv family of channels (Shealy *et al.*, 2003). This PXP motif is absent in KcsA, MthK, and KvAP, which indicates that the structure of the gate in eukaryotic Kv channels may be different from the observed X-ray structures. Prolines tend to kink  $\alpha$ -helices due to the lack of a hydrogen bond normally formed by the amide nitrogen and also by steric constraints. So the bend in the S6  $\alpha$ -helices in eukaryotic channels may be due to this PXP motif, which could create a flexible hinge allowing the movement of the lower S6 segment during channel gating. Substituting these prolines in Shaker channels with other residues gave non-functional channels or channels with dramatically impaired gating properties, which suggested that these prolines may create a gating hinge in the S6  $\alpha$ -helices, thus playing an essential role in gating (Labro *et al.*, 2003). Simulation studies on Shaker also proposed a similar gating mechanism at this motif (Bright *et al.*, 2002).

Many K<sup>+</sup> channels have a second glycine in place of the second proline found on the PXP motif in S6 that may also act as a gating hinge point. hERG K<sup>+</sup> channels have two glycine residues on S6, Gly648 and Gly657, each occupying a putative hinge site. A previous alanine scan of S6 inner helices in hERG showed that the mutation of either glycine residue did not appear to significantly alter gating, indicating a discrepancy with the data obtained from other channels (Mitcheson *et al.*, 2000a). The aim of this study was therefore to establish the role of these glycines in hERG activation gating and to determine whether they function as gating hinges. The two glycine residues were mutated to a range of amino acid residues of different sizes and properties and the effects on activation and deactivation gating were studied. hERG blockers were also used as a tool to probe for changes in the structure of the pore of the channel with these mutations.

## Chapter 3- Glycine hinge study

### 3.1 Characterisation of WT hERG channels

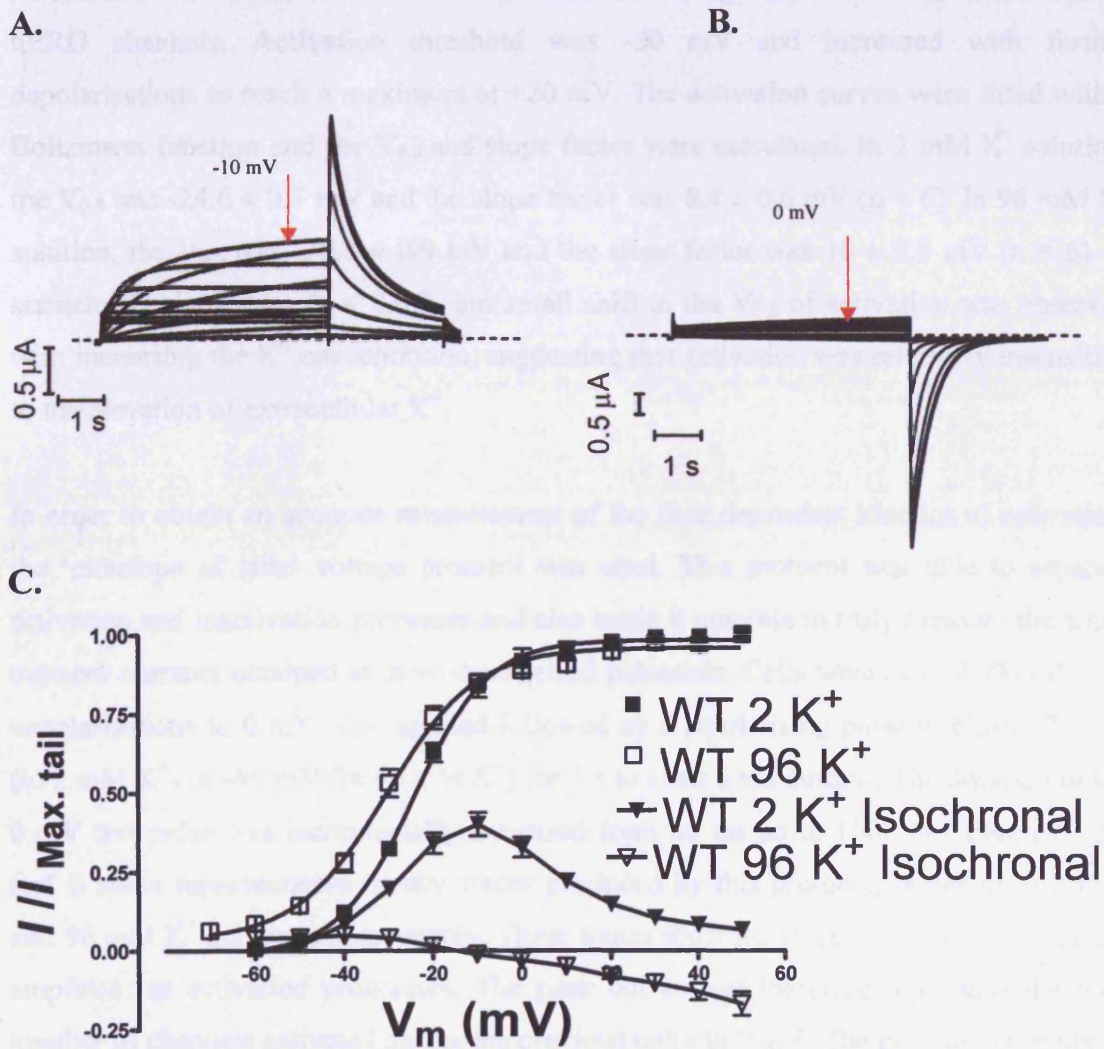
The kinetic behaviour of hERG channels is very unusual. It is characterised by comparatively slow activation and deactivation kinetics but very rapid and voltage dependent inactivation kinetics. As a consequence, these channels function as inward rectifiers by passing little current in the outward direction upon depolarisation but then passing significant current in the inward direction upon repolarisation (Schonherr & Heinemann, 1996; Smith *et al.*, 1996; Spector *et al.*, 1996b). By using different voltage protocols, we were able to separate these processes and measure the time and voltage dependence of hERG activation and inactivation. Inactivation of hERG is C-type and is sensitive to extracellular  $K^+$  concentrations (Zhou *et al.*, 1998; Tseng, 2001). The gating properties of hERG were studied in 2 mM and 96 mM extracellular  $K^+$  solutions to enable direct comparison with mutant channels recorded under the same conditions.

#### 3.1.1 Activation kinetics of WT hERG currents

To measure the voltage dependence of activation of the WT hERG current expressed in *Xenopus* oocytes, current-voltage (I-V) protocols were used. The cell was held at a membrane potential of -90 mV, which was then stepped to varying voltages between -60 and +50 mV in 10 mV increments for 5 s. This was followed by a 2.5 s repolarisation to -70 mV in 2 mM  $K^+$  solution or -90 mV in 96 mM  $K^+$  solution. Figures 3.1A and B show representative WT hERG currents recorded in 2 mM and 96 mM  $K^+$  solutions respectively. Upon depolarisation, there was a slow increase of outward current, which then began to decrease at more depolarised potentials. Upon repolarisation, large tail currents were observed, which then slowly decayed. This protocol allowed the activation gate to slowly open with depolarisation in a process called activation. At more depolarised potentials, the current amplitude began to decrease because of the rapid closure of the inactivation gate, a process called inactivation. However, upon repolarisation, large tail currents were observed due to the channel rapidly recovering from inactivation, hence both the activation and inactivation gates were open. This current then slowly decayed as the activation gate closed, in a process called deactivation.

### Chapter 3- Glycine hinge study

**Figure 3.1: Current-voltage relationship of hERG currents in 2 mM and 96 mM extracellular  $K^+$  solutions.** **A.** Representative current traces recorded using an I-V protocol in 2 mM  $K^+$  solution. A series of 5 s depolarising pulses from a holding potential of -90 mV to potentials ranging from -60 mV to +50 mV were applied followed by a 2.5 s pulse to -70 mV. The dashed line indicates the zero current line. **B.** Representative current traces recorded using a similar I-V protocol in 96 mM  $K^+$ . The only difference was that the tail potential was -90 mV. **C.** Mean data showing the voltage dependence of the isochronal currents and the peak tail currents in 2 and 96 mM  $K^+$  solutions. Current amplitudes were normalised to maximum peak tail current ( $I_{Max. tail}$ ) amplitudes. The peak tail currents were fitted with a Boltzmann function ( $n = 6$ ).



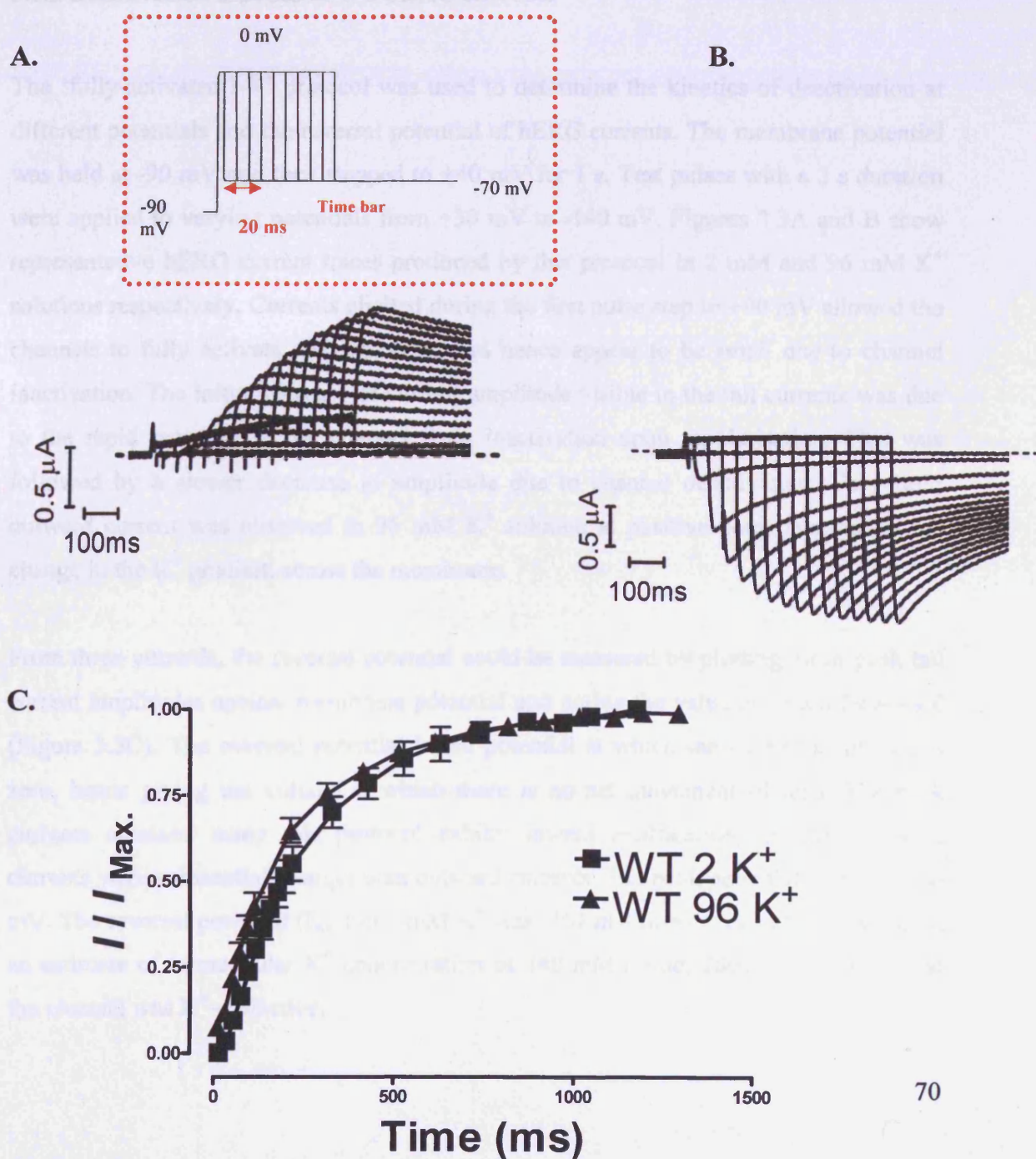
### Chapter 3- Glycine hinge study

Peak tail current amplitudes were normalised to the maximum value and plotted against the test potential. The current amplitude at the end of the 5 s test depolarisation is referred to as the isochronal current. This was also normalised to the maximum amplitude of each cell and plotted as a function of voltage. Figure 3.1C shows the voltage dependence of the isochronal currents recorded at the end of the test depolarisations as well as peak tail currents in 2 mM and 96 mM K<sup>+</sup> solutions. The isochronal end-pulse current recorded in 2 mM K<sup>+</sup> solution peaked at -10 mV and then decreased due to the augmentation of channel inactivation. Very little isochronal current was observed in 96 mM K<sup>+</sup> solution due to a change in the K<sup>+</sup> gradient across the membrane, such that the equilibrium potential ( $E_K$ ) is nearly zero indicating a minimal net flux of K<sup>+</sup> ions across the membrane. The peak tail currents represent the voltage dependence of activation of hERG channels. Activation threshold was -50 mV and increased with further depolarisations to reach a maximum at +20 mV. The activation curves were fitted with a Boltzmann function and the  $V_{0.5}$  and slope factor were calculated. In 2 mM K<sup>+</sup> solution, the  $V_{0.5}$  was  $-24.6 \pm 0.7$  mV and the slope factor was  $8.4 \pm 0.6$  mV ( $n = 6$ ). In 96 mM K<sup>+</sup> solution, the  $V_{0.5}$  was  $-30.8 \pm 0.9$  mV and the slope factor was  $10 \pm 0.8$  mV ( $n = 6$ ). A statistically significant ( $p < 0.05$ ), but small shift in the  $V_{0.5}$  of activation was observed with increasing the K<sup>+</sup> concentration, suggesting that activation was relatively insensitive to the elevation of extracellular K<sup>+</sup>.

In order to obtain an accurate measurement of the time dependent kinetics of activation, the 'envelope of tails' voltage protocol was used. This protocol was able to separate activation and inactivation processes and also made it possible to truly measure the small outward currents obtained at more depolarised potentials. Cells were held at -90 mV and depolarisations to 0 mV were applied followed by a repolarising pulse to either -70 mV (in 2 mM K<sup>+</sup>) or -90 mV (in 96 mM K<sup>+</sup>) for 1 s to elicit a tail current. The duration of the 0 mV test pulse was incrementally increased from 20 ms up to 1500 ms. Figures 3.2A and B show representative current traces produced by this protocol, recorded in 2 mM and 96 mM K<sup>+</sup> solutions respectively. These traces show the increase in peak tail current amplitude as activation progresses. The peak tail current therefore represents the total number of channels activated during the previous pulse to 0 mV. The peak tail currents

### Chapter 3- Glycine hinge study

**Figure 3.2: The time dependence of hERG activation in 2 mM and 96 mM K<sup>+</sup> solutions.** A. Representative current traces recorded using the 'envelope of tails' protocol in 2 mM K<sup>+</sup> solution. The voltage protocol (inset) is described in the main text. B. Representative current traces in 96 mM K<sup>+</sup> solution elicited using a similar protocol but with tail currents measured at -90 mV. C. Mean tail currents normalised to maximum and plotted against 0 mV pulse duration. Mean results in each recording solution were fit with a single exponential function (n = 5).



## Chapter 3- Glycine hinge study

were normalised to the maximum tail current value and then plotted as a function of the test pulse duration (Figure 3.2C). Results for the time course of activation were fit with a single exponential function to give a time constant of activation of  $248 \pm 33$  ms in 2 mM  $K^+$  solution ( $n = 5$ ) and  $214 \pm 29$  ms in 96 mM  $K^+$  solution ( $n = 5$ ). The time course of hERG activation was not significantly affected by the increase in  $K^+$  concentration ( $p > 0.05$ ).

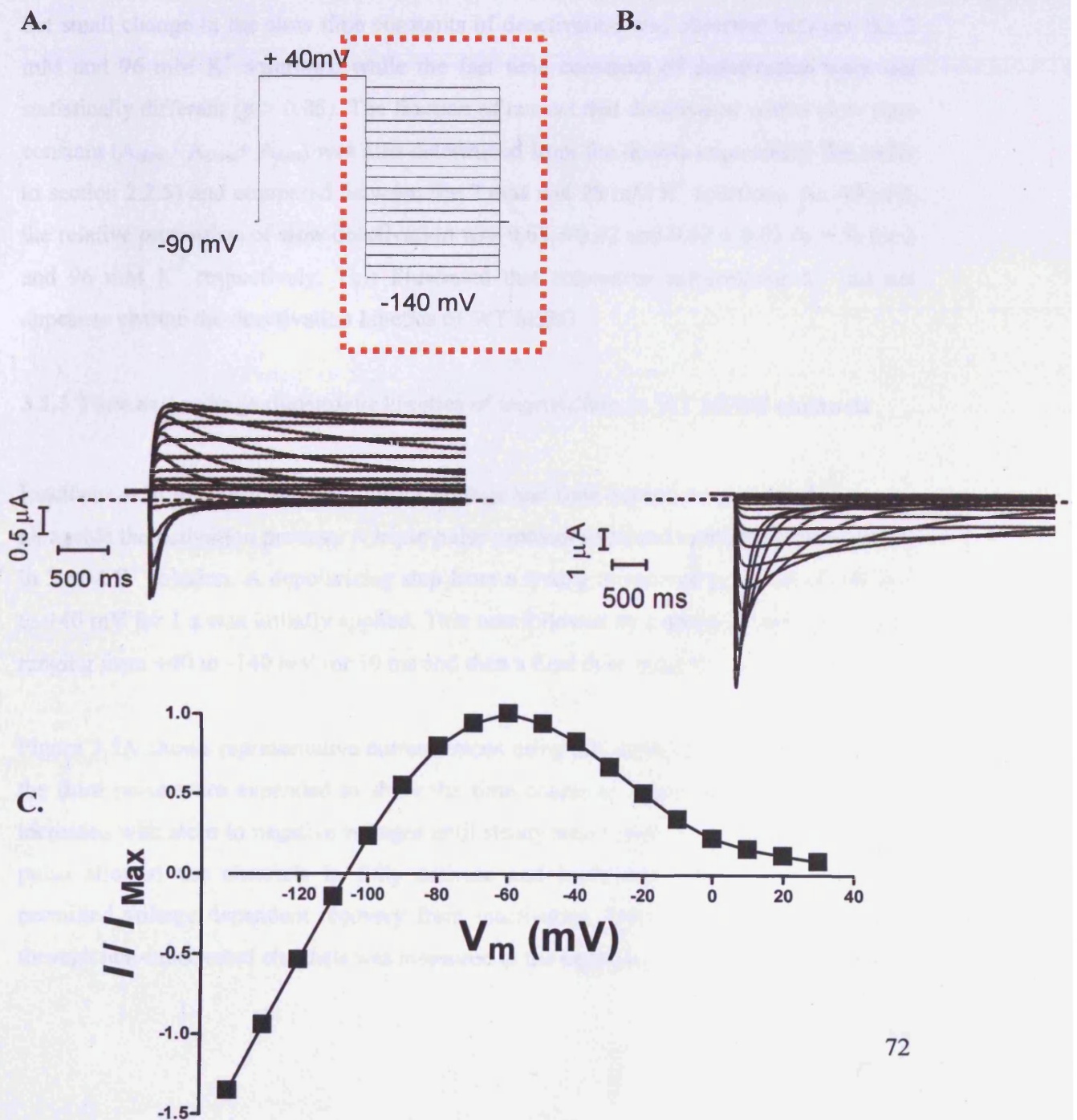
### 3.1.2 Deactivation kinetics of WT hERG currents

The 'fully-activated I-V' protocol was used to determine the kinetics of deactivation at different potentials and the reversal potential of hERG currents. The membrane potential was held at -90 mV and then stepped to +40 mV for 1 s. Test pulses with a 3 s duration were applied to varying potentials from +30 mV to -140 mV. Figures 3.3A and B show representative hERG current traces produced by this protocol in 2 mM and 96 mM  $K^+$  solutions respectively. Currents elicited during the first pulse step to +40 mV allowed the channels to fully activate and inactivate and hence appear to be small due to channel inactivation. The initial increase of current amplitude visible in the tail currents was due to the rapid recovery of the channel from inactivation upon repolarisation. This was followed by a slower decrease in amplitude due to channel deactivation. Very little outward current was observed in 96 mM  $K^+$  solution at positive potentials due to the change in the  $K^+$  gradient across the membrane.

From these currents, the reversal potential could be measured by plotting mean peak tail current amplitudes against membrane potential and noting the value at which  $I$  equals 0 (Figure 3.3C). The reversal potential is the potential at which the current amplitude is zero, hence giving the voltage at which there is no net movement of ions. The peak currents obtained using this protocol exhibit inward rectification, in which inward currents were substantially larger than outward currents. The peak potential occurs at -60 mV. The reversal potential ( $E_{rev}$ ) in 2 mM  $K^+$  was -107 mV ( $n = 5$ ), close to  $E_K$  based on an estimate of intracellular  $K^+$  concentration of 140 mM (Hille, 2001), confirming that the channel was  $K^+$  - selective.

### Chapter 3- Glycine hinge study

**Figure 3.3: Properties of hERG currents using the 'fully-activated I-V' protocol.** **A.** Representative family of currents in 2 mM  $K^+$  solution using the 'fully-activated I-V' protocol illustrated in inset. Currents were plotted from part of the protocol indicated by the dashed line box. **B.** Representative hERG currents in 96 mM  $K^+$  solution from the same cell using the same protocol. **C.** Mean peak tail current amplitudes in 2 mM  $K^+$  solution plotted against membrane potential and normalised to maximal outward current ( $n = 5$ ). Error bars were smaller than symbols.



### Chapter 3- Glycine hinge study

The time constants of deactivation were also measured from this protocol by fitting the tail current decay with a double exponential, which separated deactivation into a fast and a slow component (Figure 3.4). Deactivation is a voltage dependent process that is most rapid at more negative potentials. The deactivating pulse is too short to obtain accurate measurements of the slow time constants at more depolarised potentials, hence the data plotted is at potentials negative to -60 mV. At -90 mV, the slow and fast time constants in 2 mM K<sup>+</sup> were 349 ± 30 ms and 84 ± 8 ms respectively (n = 5) and in 96 mM K<sup>+</sup> were 579 ± 66 ms and 108 ± 33 ms respectively (n = 5). A statistically significant (p < 0.05), but small change in the slow time constants of deactivation was observed between the 2 mM and 96 mM K<sup>+</sup> solutions, while the fast time constants of deactivation were not statistically different (p > 0.05). The fraction of current that deactivated with a slow time constant ( $A_{\text{slow}} / A_{\text{slow}} + A_{\text{fast}}$ ) was also determined from the double exponential fits (refer to section 2.2.5) and compared between the 2 mM and 96 mM K<sup>+</sup> solutions. At -90 mV, the relative proportion of slow deactivation was 0.63 ± 0.02 and 0.62 ± 0.02 (n = 5) for 2 and 96 mM K<sup>+</sup> respectively. This illustrated that increasing extracellular K<sup>+</sup> did not appear to change the deactivation kinetics of WT hERG.

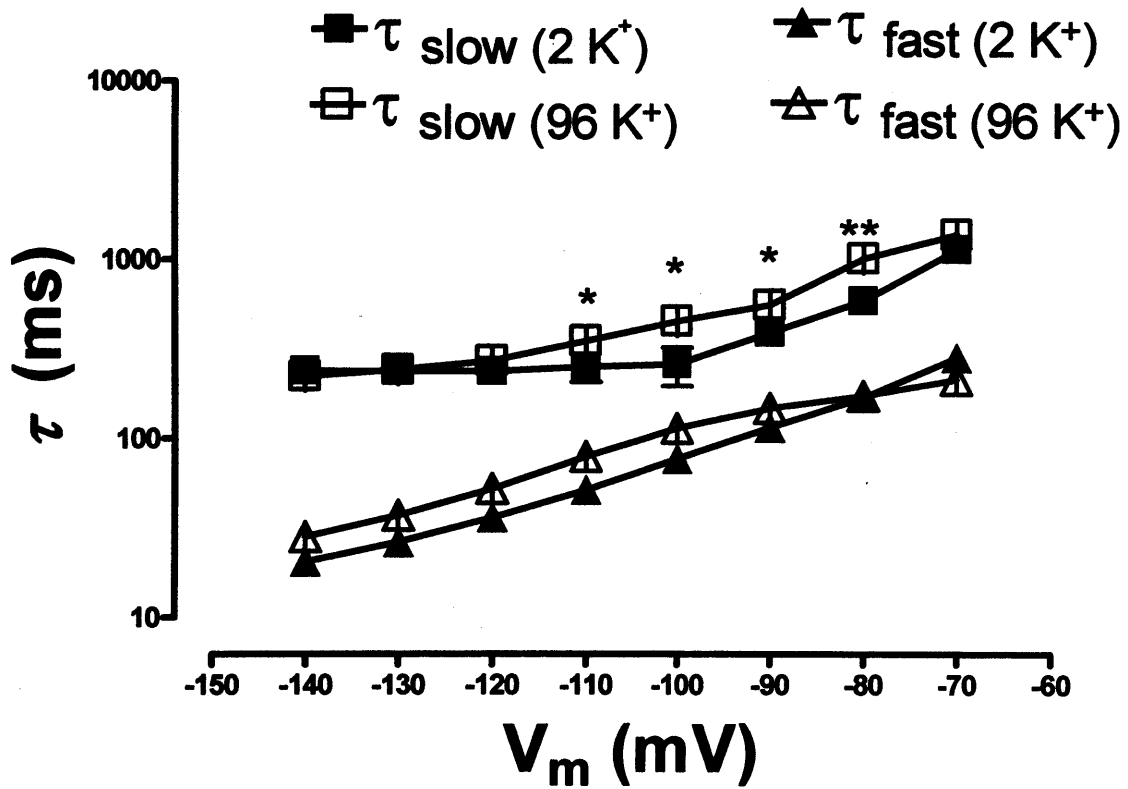
#### 3.1.3 Time and voltage dependent kinetics of inactivation in WT hERG channels

Inactivation in hERG channels is also a voltage and time dependent process that occurs alongside the activation process. A triple pulse protocol was used to measure inactivation in 2 mM K<sup>+</sup> solution. A depolarizing step from a resting membrane potential of -90 mV to +40 mV for 1 s was initially applied. This was followed by a second step to potentials ranging from +40 to -140 mV for 10 ms and then a final third pulse to +40 mV.

Figure 3.5A shows representative current traces using this protocol. The currents during the third pulse were expanded to show the time course of inactivation. These currents increased with steps to negative voltages until steady state current was achieved. The first pulse allowed the channels to fully activate and inactivate, then the second pulse permitted voltage dependent recovery from inactivation. Instantaneous current passing through non-inactivated channels was measured at the beginning of the third pulse. An

### Chapter 3- Glycine hinge study

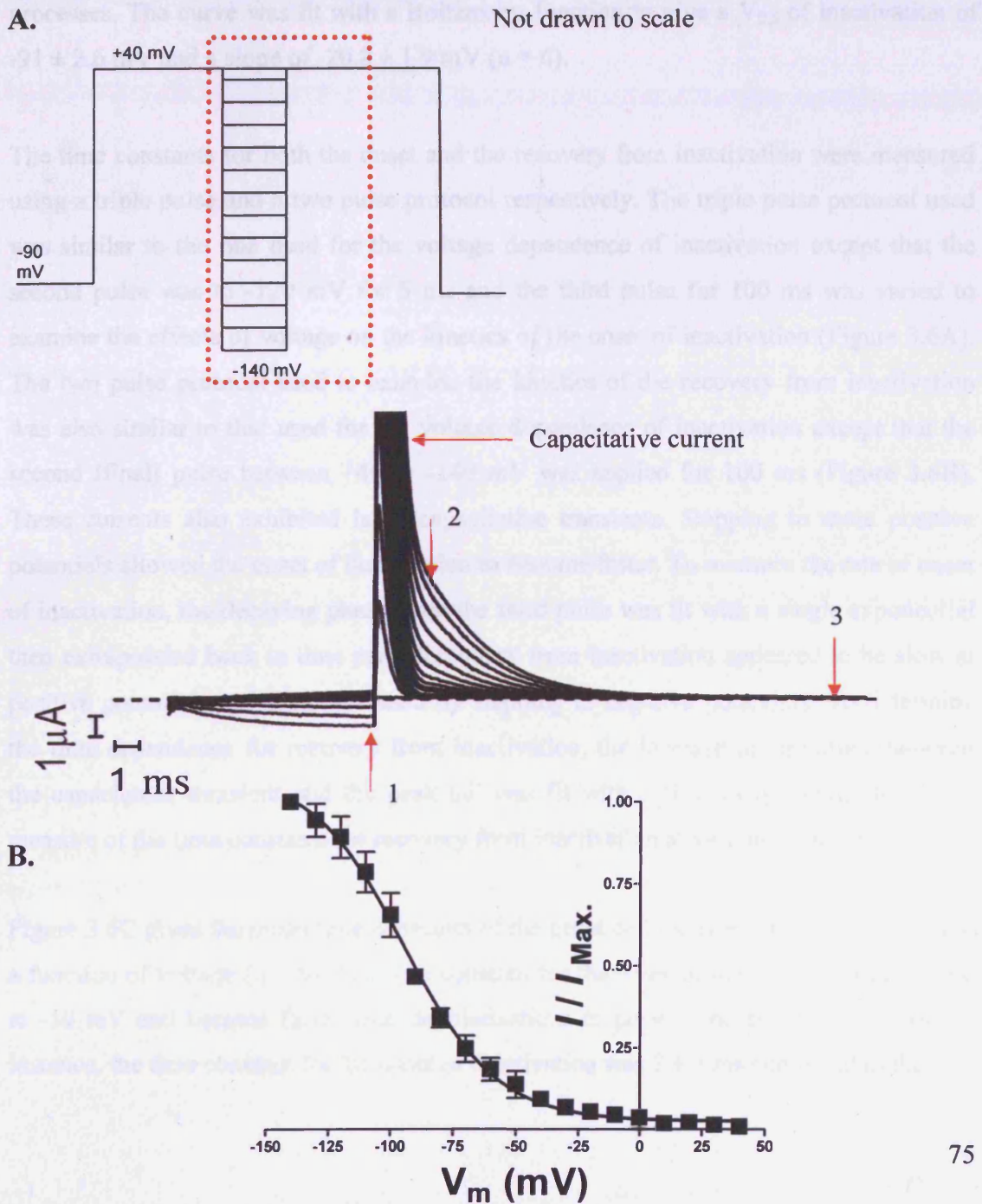
**Figure 3.4: Time constants of WT hERG current deactivation in 2 and 96 mM K<sup>+</sup> solutions.** Deactivation was fit with a double exponential function giving the fast and slow time constants of deactivation (n = 5). Mean time constants ( $\tau$ ) of deactivation are plotted on a log<sub>10</sub> scale against membrane potential in 2 mM K<sup>+</sup> solution and 96 mM K<sup>+</sup> solution. Voltages exhibiting a statistical difference are indicated by (\*) whereby (\*) means p < 0.05 and (\*\*) means p < 0.01.



Chapter 3- Glycine hinge study

**Figure 3.5: Voltage dependence of steady state inactivation of WT hERG currents.**

**A.** Representative current traces using the triple pulse protocol. Currents during the second and third pulses are expanded as indicated by a box on the inset to show the time course of the currents. Onset of inactivation of the hERG current was fit between cursors 2 and 3 then extrapolated back to cursor 1. **B.** Currents, normalised to maximum, were plotted as a function of test potential, then fitted with a Boltzmann function to give the voltage dependence of inactivation ( $n = 6$ ).



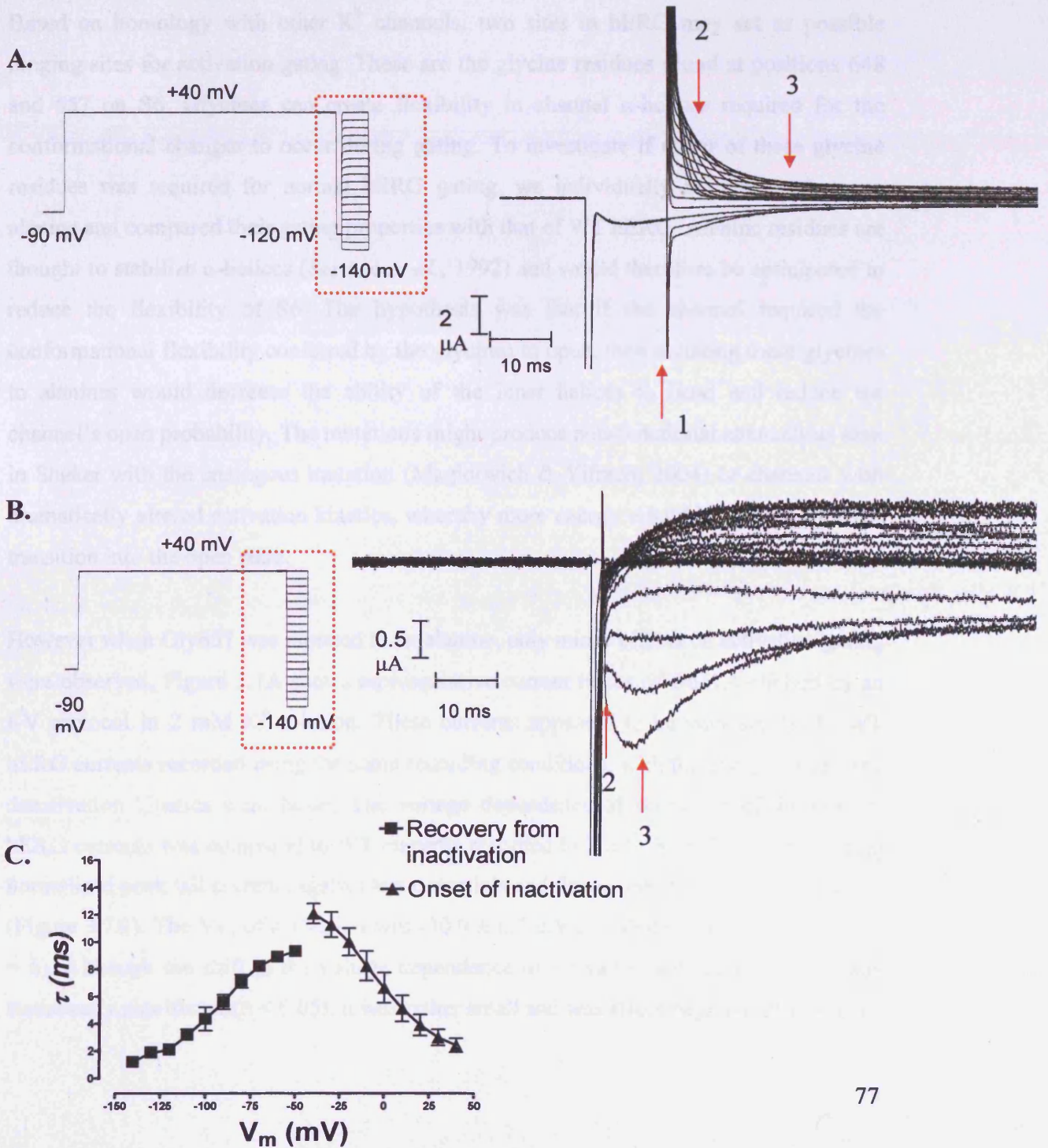
### Chapter 3- Glycine hinge study

important feature is the presence of a large capacitive current during depolarisation to positive potentials. The decaying phase of the current was fit after the capacitive current with a single exponential and extrapolated back to the start of the pulse. This current was normalised to the maximum current to give current availability, which was then plotted as a function of membrane potential from the second pulse (Figure 3.5B). The value of steady state inactivation was greater at more negative potentials, and had a voltage dependence independent from that of activation showing that they are two distinct processes. The curve was fit with a Boltzmann function to give a  $V_{0.5}$  of inactivation of  $-91 \pm 2.6$  mV and a slope of  $-20.8 \pm 1.9$  mV ( $n = 6$ ).

The time constants for both the onset and the recovery from inactivation were measured using a triple pulse and a two pulse protocol respectively. The triple pulse protocol used was similar to the one used for the voltage dependence of inactivation except that the second pulse was to  $-120$  mV for 5 ms and the third pulse for 100 ms was varied to examine the effects of voltage on the kinetics of the onset of inactivation (Figure 3.6A). The two pulse protocol used to examine the kinetics of the recovery from inactivation was also similar to that used for the voltage dependence of inactivation except that the second (final) pulse between  $+40$  to  $-140$  mV was applied for 100 ms (Figure 3.6B). These currents also exhibited large capacitive transients. Stepping to more positive potentials allowed the onset of inactivation to become faster. To measure the rate of onset of inactivation, the decaying phase from the third pulse was fit with a single exponential then extrapolated back to time zero. Recovery from inactivation appeared to be slow at positive potentials and then increased by stepping to negative potentials. To determine the time dependence for recovery from inactivation, the increase in amplitude between the capacitance transient and the peak tail was fit with a single exponential to give a measure of the time constants for recovery from inactivation at various voltages.

Figure 3.6C gives the mean time constants of the onset and recovery from inactivation as a function of voltage ( $n = 6$ ). The time constant for the onset of inactivation was slowest at  $-50$  mV and became faster with depolarisations to positive potentials. At 0 mV for instance, the time constant for the onset of inactivation was  $7 \pm 1$  ms compared to the

**Figure 3.6: Time constants of onset and recovery from inactivation of WT hERG currents.** Representative current traces using the triple pulse (A.) and two pulse protocols (B.) expanded from part of the protocol indicated by a box on the inset. C. Time constants ( $\tau$ ) of the onset (from A) and recovery from inactivation (from B) plotted as a function of voltage by fitting the decaying components of the curve between cursors 2 and 3 with a single exponential ( $n = 6$ ).



## Chapter 3- Glycine hinge study

time constant of activation of  $248 \pm 33$  ms at the same potential. On the other hand, the time constant for recovery from inactivation was fastest at more negative potentials and slowed with depolarization to reach maximum value at -50 mV.

### 3.2 Alanine substitution of the gating hinge glycine residues

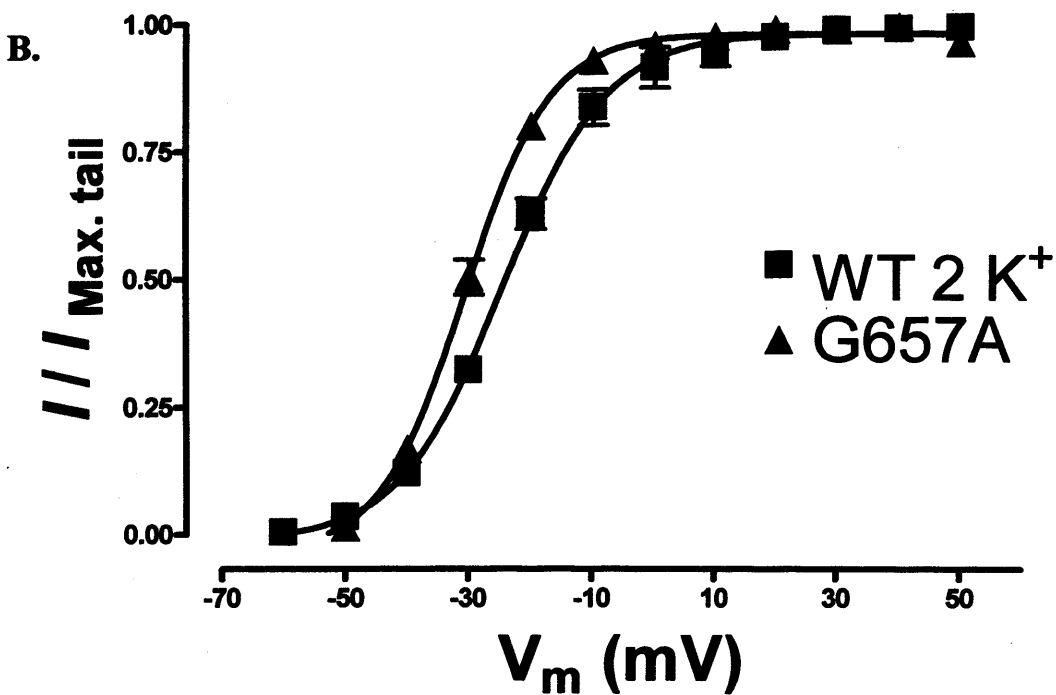
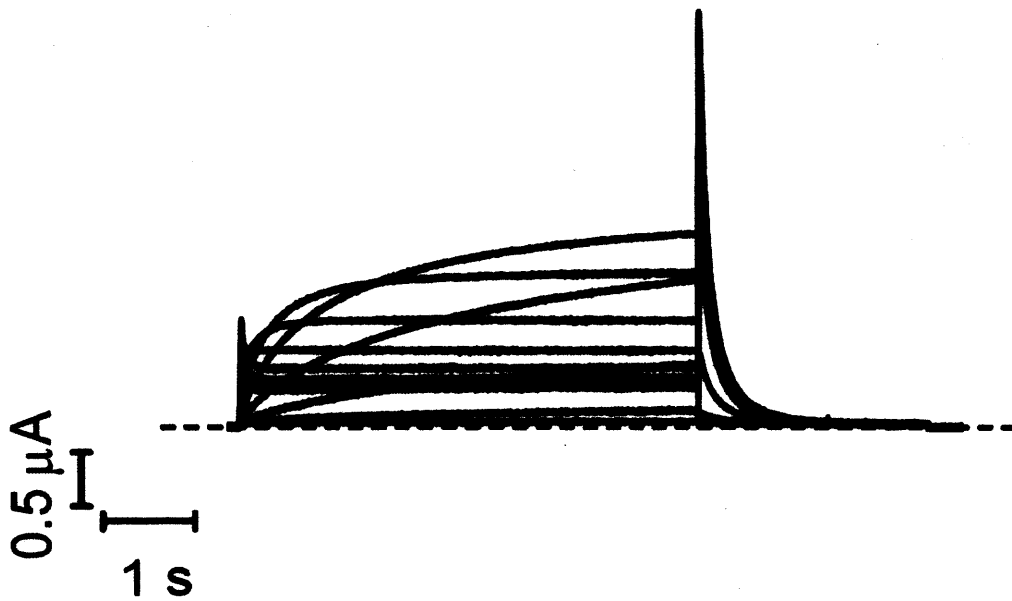
Based on homology with other  $K^+$  channels, two sites in hERG may act as possible hinging sites for activation gating. These are the glycine residues found at positions 648 and 657 on S6. Glycines can create flexibility in channel  $\alpha$ -helices required for the conformational changes to occur during gating. To investigate if either of these glycine residues was required for normal hERG gating, we individually mutated each to an alanine and compared their gating properties with that of WT hERG. Alanine residues are thought to stabilize  $\alpha$ -helices (Serrano *et al.*, 1992) and would therefore be anticipated to reduce the flexibility of S6. The hypothesis was that if the channel required the conformational flexibility conferred by the glycines to open, then mutating these glycines to alanines would decrease the ability of the inner helices to bend and reduce the channel's open probability. The mutations might produce non-functional channels as seen in Shaker with the analogous mutation (Magidovich & Yifrach, 2004) or channels with dramatically altered activation kinetics, whereby more energy would be required for the transition into the open state.

However when Gly657 was mutated to an alanine, only minor effects on activation gating were observed. Figure 3.7A shows representative current traces of G657A elicited by an I-V protocol in 2 mM  $K^+$  solution. These currents appeared to be very similar to WT hERG currents recorded using the same recording conditions, with the exception that the deactivation kinetics were faster. The voltage dependence of activation of the G657A hERG currents was compared to WT currents recorded in 2 mM  $K^+$  solution by plotting normalised peak tail currents against test potentials and fitting with a Boltzmann function (Figure 3.7B). The  $V_{0.5}$  of activation was  $-30.9 \pm 0.5$  mV and slope was  $6.9 \pm 0.4$  mV ( $n = 6$ ). Although the shift in the voltage dependence of activation with this mutation was statistically significant ( $p < 0.05$ ), it was rather small and was also a negative shift of 6.3

Chapter 3- Glycine hinge study

**Figure 3.7: Minor effects of G657A on the current-voltage relationship of hERG channels.** A. Representative currents from G657A hERG recorded in 2 mM  $K^+$  solution. B. Mean normalised peak tail currents were plotted as a function of test potential and fitted with a Boltzmann function to give the voltage dependence of activation ( $n = 6$ ). The activation curve for WT hERG is shown for comparison.

A.



### Chapter 3- Glycine hinge study

mV instead of a loss of function or a large positive shift, which would be more consistent with the gating hinge hypothesis.

For G648A channels, no currents were observed in 2 mM K<sup>+</sup> solution due to the voltage dependence of inactivation becoming shifted to more negative potentials. Therefore, recordings were done using high K<sup>+</sup> solution (96 mM K<sup>+</sup>) which shifted inactivation to positive potentials, but as shown previously (Figure 3.1), has minor effects on the voltage dependence of activation. Figure 3.8A shows representative current traces of G648A elicited by an I-V protocol in 96 mM K<sup>+</sup> solution. Tail currents appear as inward currents due to the change of E<sub>K</sub> towards 0 mV. These currents look similar to WT hERG currents recorded in 96 mM K<sup>+</sup> solution. The V<sub>0.5</sub> of activation for G648A was  $-23.5 \pm 1.7$  mV and the slope was  $13.6 \pm 1.6$  mV (n = 6) (Figure 3.8B). This mutation also appeared to have a statistically significant (p < 0.05) but minor effect on hERG activation gating, when compared to WT channels using the same recording conditions. This was however not consistent with a glycine hinge point that would be expected to induce a substantial change in energetics for opening.

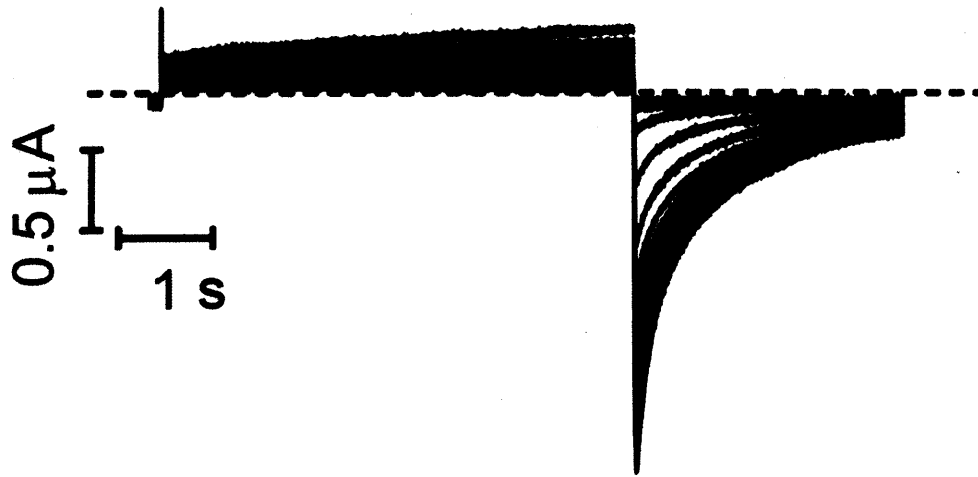
Figure 3.9 shows the activation time course of the alanine mutants at 0 mV compared to the WT currents with equivalent recording conditions. After fitting with a single exponential, the time constant of activation for G657A and G648A currents was  $154 \pm 2$  ms and  $305 \pm 67$  ms respectively (n = 5). Changes to the time dependent kinetics of activation with both alanine mutants were relatively minor but statistically significant (p < 0.05). Neither the voltage nor the time dependent kinetics of activation was dramatically altered in the presence of these alanine mutations at the putative glycine hinge sites. These findings were conflicting with roles of these glycines as gating hinges required for the opening of hERG channels.

To investigate effects on channel closure, the mean slow and fast time constants of deactivation for G657A and G648A currents were obtained at different voltages by using the 'fully-activated I-V protocol'. These values were plotted on a log<sub>10</sub> scale against test potentials (Figure 3.10). G657A currents had a slow deactivation time constant of  $229 \pm$

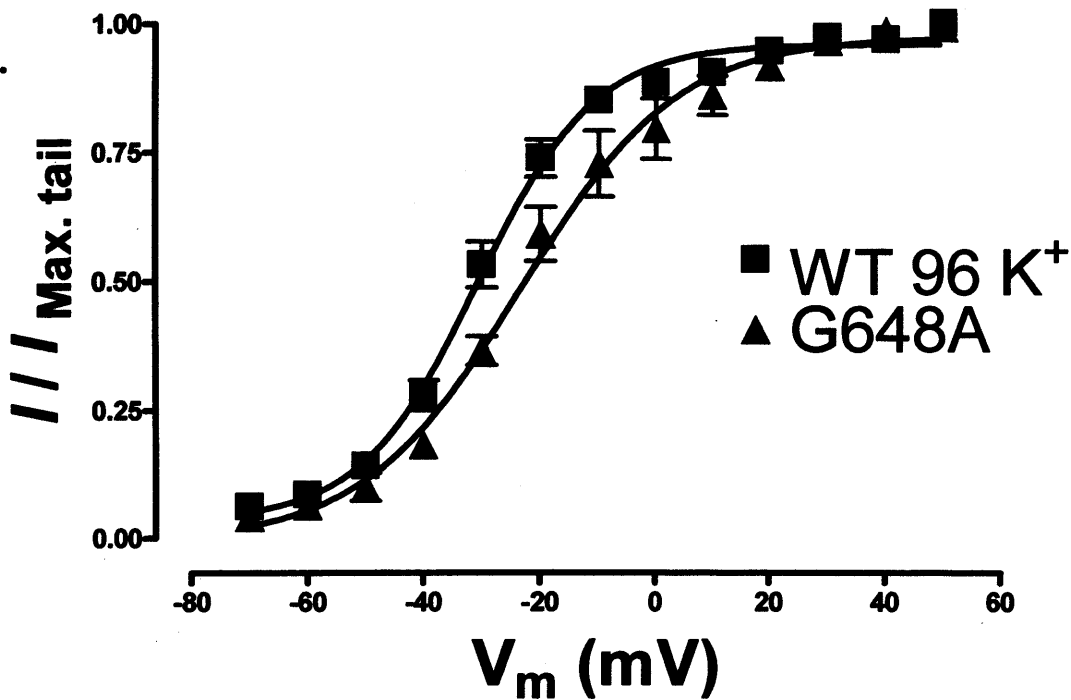
Chapter 3- Glycine hinge study

**Figure 3.8: Effects of G648A mutation on hERG currents.** A. Representative family of currents recorded using the I-V protocol, in 96 mM K<sup>+</sup> solution. The holding and tail current potential was -90 mV. B. Mean normalised peak tail currents plotted against test potential and fitted with a Boltzmann function (n = 6). The mean results for WT hERG, in the same recording conditions, are shown for comparison.

A.

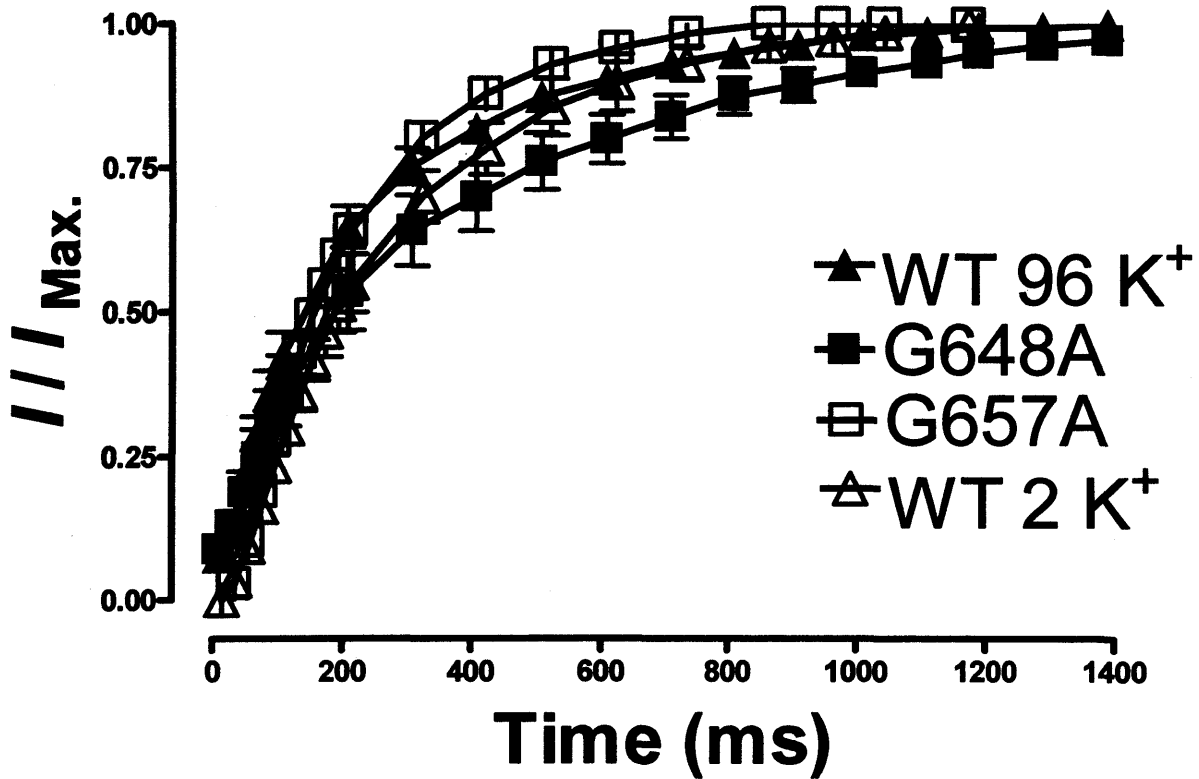


B.



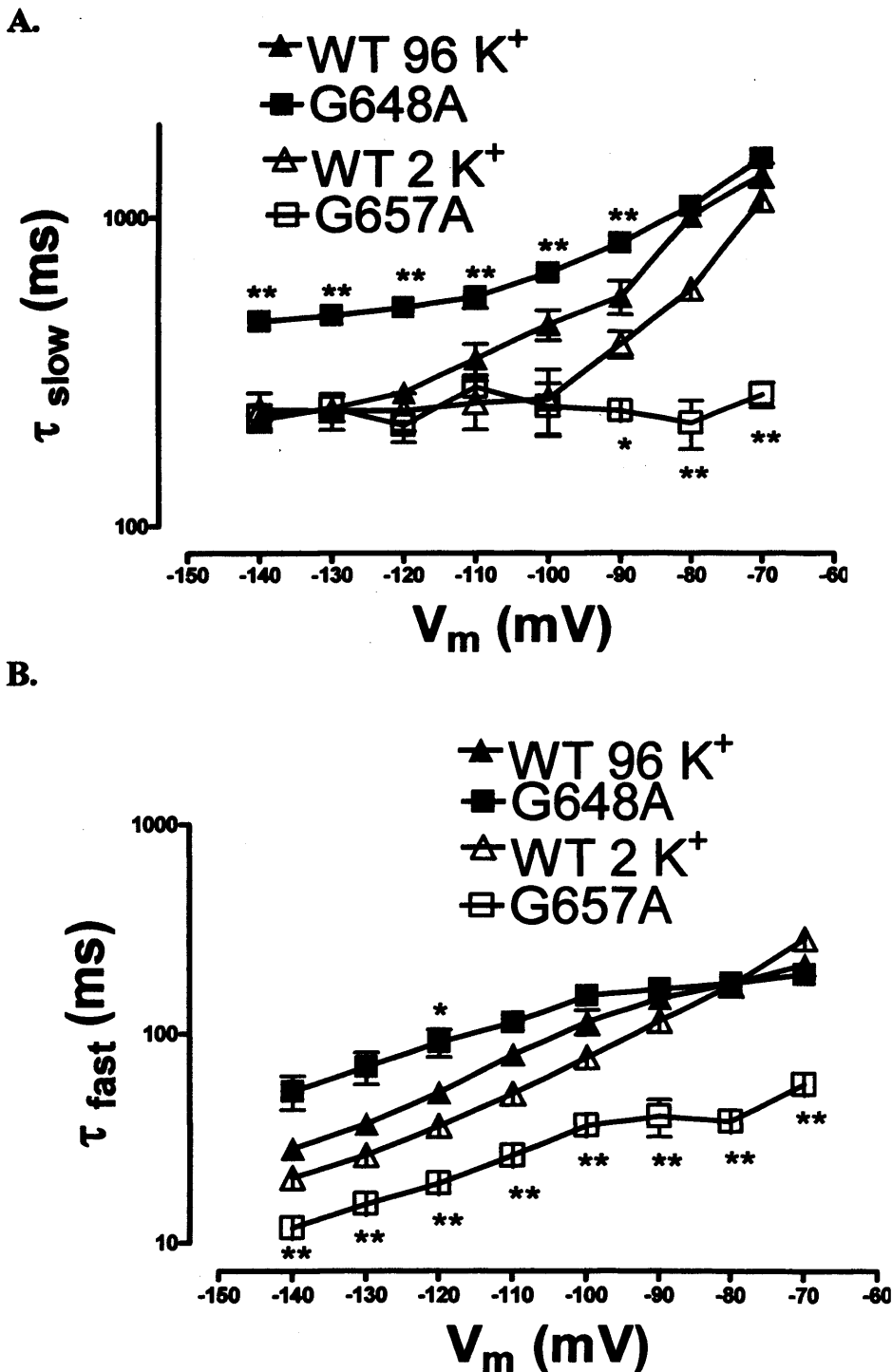
Chapter 3- Glycine hinge study

**Figure 3.9: Time dependent kinetics of activation of G657A and G648A hERG.** Mean normalised peak tail currents elicited using the 'envelope of tails' protocol with a test potential of 0 mV (refer to Figure 3.2). The time course of activation of G657A was compared to WT currents in 2 mM K<sup>+</sup> solution and G648A was compared to WT currents in 96 mM K<sup>+</sup> solution (n = 5).



Chapter 3- Glycine hinge study

**Figure 3.10: Voltage dependence of deactivation for G657A and G648A hERG.**  $\tau_{slow}$  (A.) and  $\tau_{fast}$  (B.) of deactivation were measured from currents elicited using the 'fully-activated I-V' protocol and plotted against test voltages on a  $\log_{10}$  scale ( $n = 5$ ). Values for WT hERG are shown for comparison. Statistical differences at different voltages between the alanine mutants and WT hERG under same recording conditions are shown, whereby (\*) indicates  $p < 0.05$  and (\*\*) indicates  $p < 0.01$ .



### Chapter 3- Glycine hinge study

5 ms and a fast deactivation time constant of  $48 \pm 2$  ms at -90 mV ( $n = 5$ ). It is interesting to note the apparent lack of voltage dependence of the slow time constant of deactivation of G657A hERG. G657A deactivation kinetics were significantly faster than WT currents ( $n \geq 5$ ,  $p < 0.05$ ), especially the fast time constants of deactivation which appeared to be statistically significantly faster than WT currents ( $n \geq 5$ ,  $p < 0.01$ ) at all voltages studied. G648A currents had a slow deactivation time constant of  $855 \pm 57$  ms and a fast deactivation time constant of  $163 \pm 14$  ms at -90 mV ( $n = 5$ ). The slow time constant was statistically significantly slower than WT deactivation kinetics ( $n \geq 5$ ,  $p < 0.01$ ), although prominent differences in the slow deactivation kinetics occurred at more negative voltages. The fast time constants however were similar to WT hERG. The relative proportion of slow and fast deactivation was also similar between both alanine mutants and WT hERG measurements under the identical recording conditions.

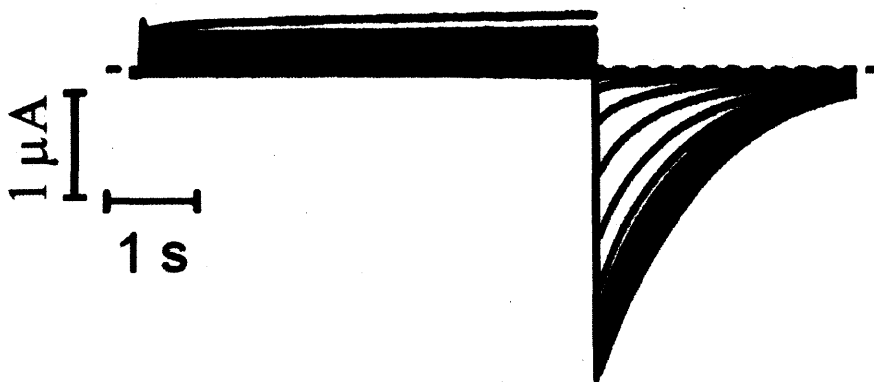
These results showed that substituting either glycine with an alanine gave functional channels whose voltage dependence was relatively similar to that of WT hERG. G657A did not seem to considerably affect the kinetics of channel opening but channel closure occurred more rapidly. On the other hand, G648A currents deactivated more slowly. These effects were not consistent with a role of glycine residues as gating hinges, as mutating each to an alanine could still render the channel functional.

It may be possible that when one glycine was mutated to an alanine, the other glycine, which was still intact, could be compensating for it and therefore the channel could still function relatively normally. To investigate this further, both glycine residues were simultaneously mutated to an alanine. Figure 3.11A shows representative current traces of G648A:G657A hERG elicited using an I-V protocol. As with G648A hERG, these currents had to be recorded in 96 mM  $K^+$  solution. The  $V_{0.5}$  of activation of  $-39.8 \pm 1.7$  mV and the slope was  $15.8 \pm 1.5$  mV ( $n = 6$ ). Figure 3.11B shows that, although there was a statistically significant change to the  $V_{0.5}$  of activation ( $p < 0.05$ ), the effect of the double mutation was relatively minor. The time course of activation at 0 mV was compared to WT hERG in the same recording conditions (Figure 3.11C). The time course of activation obtained for G648A:G657A hERG was  $304 \pm 21$  ms, which was a minor but

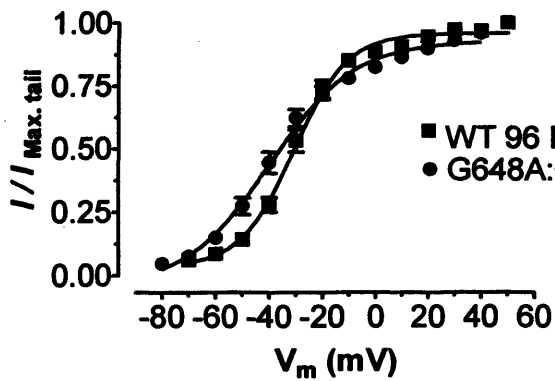
Chapter 3- Glycine hinge study

**Figure 3.11: Time and voltage dependence of activation of G648A:G657A hERG.** A. Representative G648A:G657A currents recorded in 96 mM K<sup>+</sup> solution. B. Voltage dependence of activation (n = 6). C. Time dependent kinetics of activation (n = 6). WT currents, under identical recording conditions, are shown for comparison.

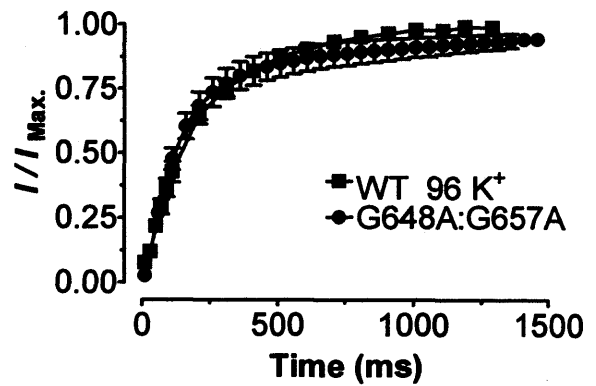
A.



B.



C.



### Chapter 3- Glycine hinge study

statistically significant reduction in activation kinetics compared to WT ( $p < 0.05$ ). Figure 3.12 compares the time constants of deactivation of G648A:G657A hERG to WT hERG in 96 mM  $K^+$  solution. At potentials between -140 and -70 mV, there were no significant changes to the slow kinetics of channel closure ( $n \geq 5$ ,  $p > 0.05$ ). The fast deactivating kinetics were only significantly faster ( $n \geq 5$ ,  $p < 0.05$ ), although minor, at more negative potentials.

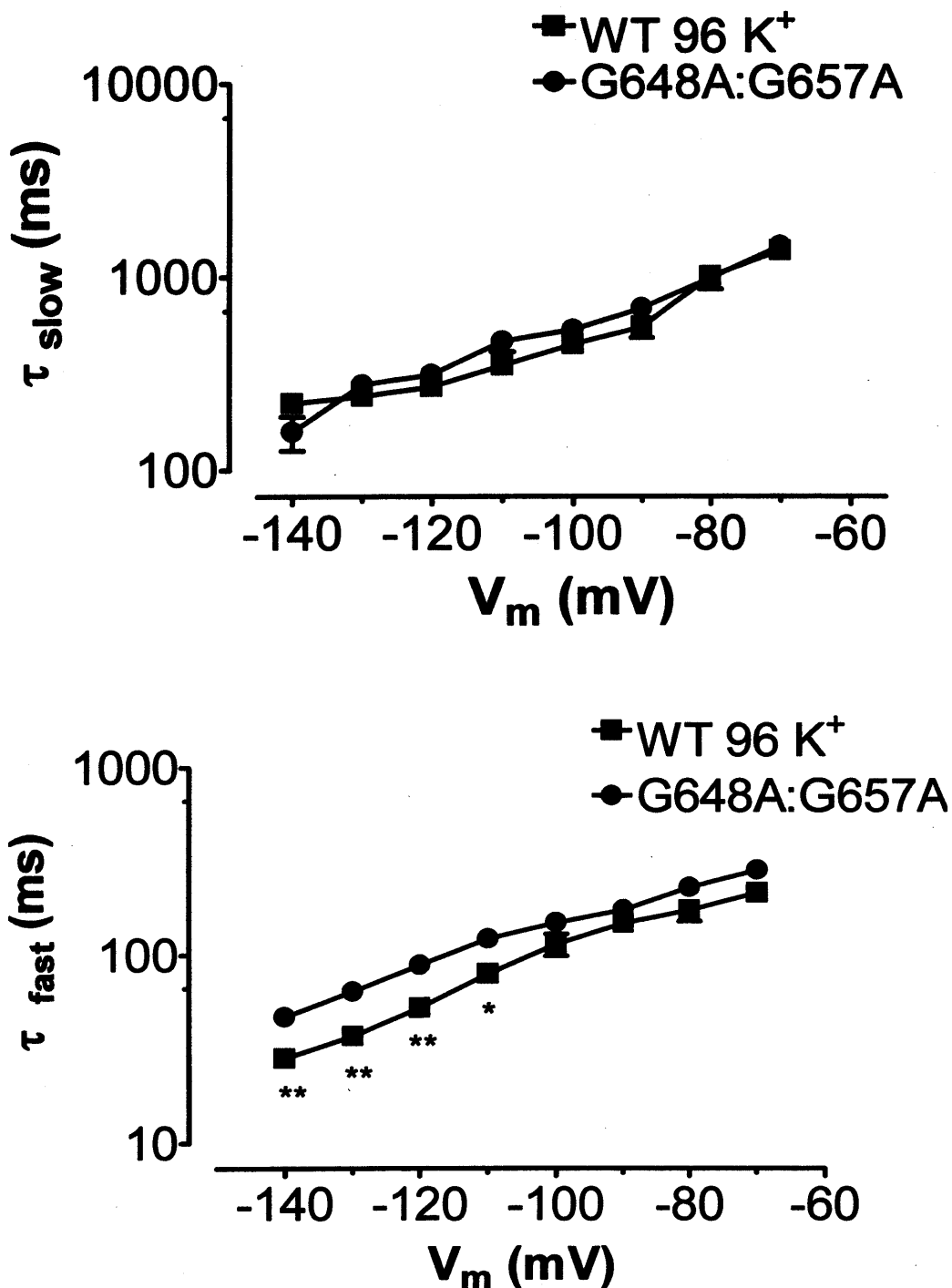
Removing both glycines was expected to substantially reduce S6 flexibility and therefore reduce channel open probability, either by shifting the voltage dependence of activation to more positive potentials or by dramatically slowing activation kinetics. On the contrary, the  $V_{0.5}$  of activation of G648A:G657A was shifted more negative by 9 mV, with minor changes to the time course of activation and deactivation. This suggested that Gly657 and Gly648 may not be acting as hinge sites for hERG activation gating or that hERG channels may not require the flexibility conferred by glycine residues for normal activation gating.

#### 3.3 Substituting the glycine residues with larger amino acid residues

The alternative role of glycine residues in S6 would be to enable protein folding and tight packing of  $\alpha$ -helices because of the small size of their side chain (Gimpelev *et al.*, 2004). According to homology models of hERG based on crystal structures of  $K^+$  channels in the open and closed state, Gly648 appears to be closely packed against the selectivity filter close to Thr623 residue (Mitcheson *et al.*, 2000a). In addition, G648A had effects on inactivation gating (Figure 3.8), which is proposed to involve a collapse of the selectivity filter. This is consistent with the assumption that glycine residues may be crucial for the normal packing of the channel. To investigate their role in packing, Gly657 and Gly648 were mutated to residues with larger side chain volumes. The hypothesis was that by mutating the small glycine residues to bulkier amino acid residues, the tight packing of the channel would be disrupted. The channel would then be unable to close properly or would be stabilized in the open state.

Chapter 3- Glycine hinge study

**Figure 3.12: Deactivation kinetics of G648A:G657A hERG.**  $\tau_{fast}$  and  $\tau_{slow}$  for deactivation of G648A:G657A channels were obtained from currents elicited using a 'fully-activated I-V' protocol and plotted against test potential on a  $\log_{10}$  scale ( $n = 5$ ). Values for WT hERG in 96 mM  $K^+$  solution are shown for comparison and statistical differences are denoted, whereby (\*) means  $p < 0.05$  and (\*\*) means  $p < 0.01$ .



### Chapter 3- Glycine hinge study

Functional currents were observed when Gly657 was mutated to Val or Ile (Figure 3.13A). These mutants were studied using 96 mM K<sup>+</sup> solution because of a leftward shift of inactivation. Mutant currents were recorded using an I-V protocol, from a holding potential of -120 mV. Depolarising pulses were applied between -120 and +30 mV and were followed by a repolarisation step to -140 mV. Large inward currents were observed at negative potentials due to the leftward shift of the voltage dependence of activation and the large K<sup>+</sup> driving force with E<sub>K</sub> being close to 0 in high K<sup>+</sup> solution. Figure 3.13B shows the voltage dependence of activation of G657V and G657I currents. For these mutant currents, activation threshold was -110 mV and increased with depolarization to reach steady state at -40 mV. The V<sub>0.5</sub> of activation for G657V was  $-84.8 \pm 1.6$  mV with a slope of  $6.9 \pm 1.3$  mV (n = 6) and the V<sub>0.5</sub> of activation for G657I was of  $-85 \pm 1.6$  mV with a slope of  $15.5 \pm 1.1$  mV (n = 6). Thus, G657V and G657I appeared to dramatically and significantly (p < 0.001, n = 6) shift the voltage dependence of activation to more negative potentials compared to WT hERG.

The kinetics of channel activation at 0 mV was also investigated (Figure 3.14). The time constants of activation were  $99 \pm 9$  ms for G657V and  $109 \pm 3$  ms for G657I hERG (n = 6). The kinetics of activation for G657V and G657I were significantly faster than WT hERG (p < 0.001, n = 6). These results suggested that these mutations enabled the channel to open more readily.

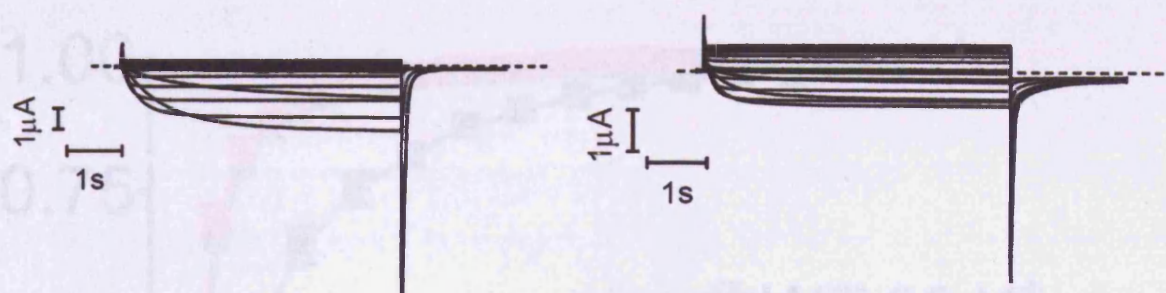
To investigate channel closure, the deactivation kinetics of the mutant channels were studied as described previously using the 'fully activated I-V' protocol. Deactivation was fit with a double exponential giving slow and fast time constants (Figure 3.15). The slow time constants of deactivation at -90 mV for each of these mutant channels were  $651 \pm 81$  ms and  $572 \pm 97$  ms for G657V and G657I respectively. The fast time constants of deactivation at -90 mV were  $120 \pm 14$  ms and  $106 \pm 10$  ms for G657V and G657I respectively (n = 6). These deactivation time constants were not significantly different to WT hERG (p > 0.05, n ≥ 6). These results showed that the voltage dependence and kinetics of activation gating were altered with the insertion of bulky residues at position 657 in hERG without affecting its deactivation kinetics. This provided evidence to

**Figure 3.13: Current-voltage relationship of the G657V and G657I mutants.** **A.** Representative current traces elicited using the I-V protocol and recorded in 96 mM K<sup>+</sup> solutions. These cells were held at -120 mV and the tail currents recorded at -140 mV following 5 s depolarising pulses to potentials between -120 and +30 mV. **B.** Mean normalised peak tail currents were plotted against membrane voltage then fitted with a Boltzmann function to give the voltage dependence of activation (n = 6).

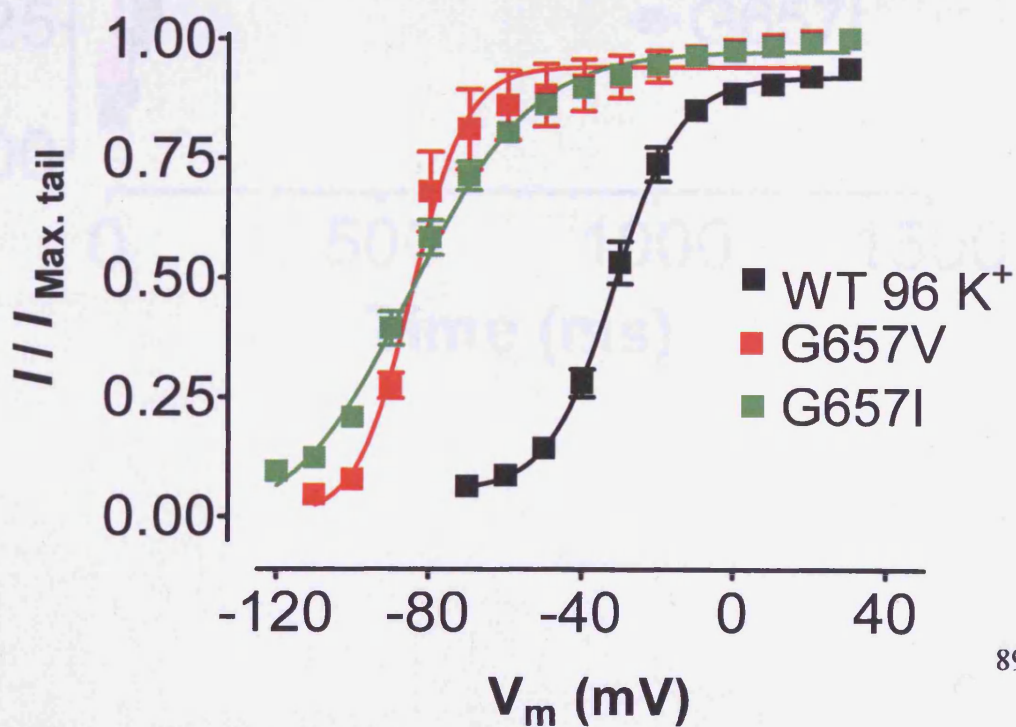
**A.**

G657V

G657I

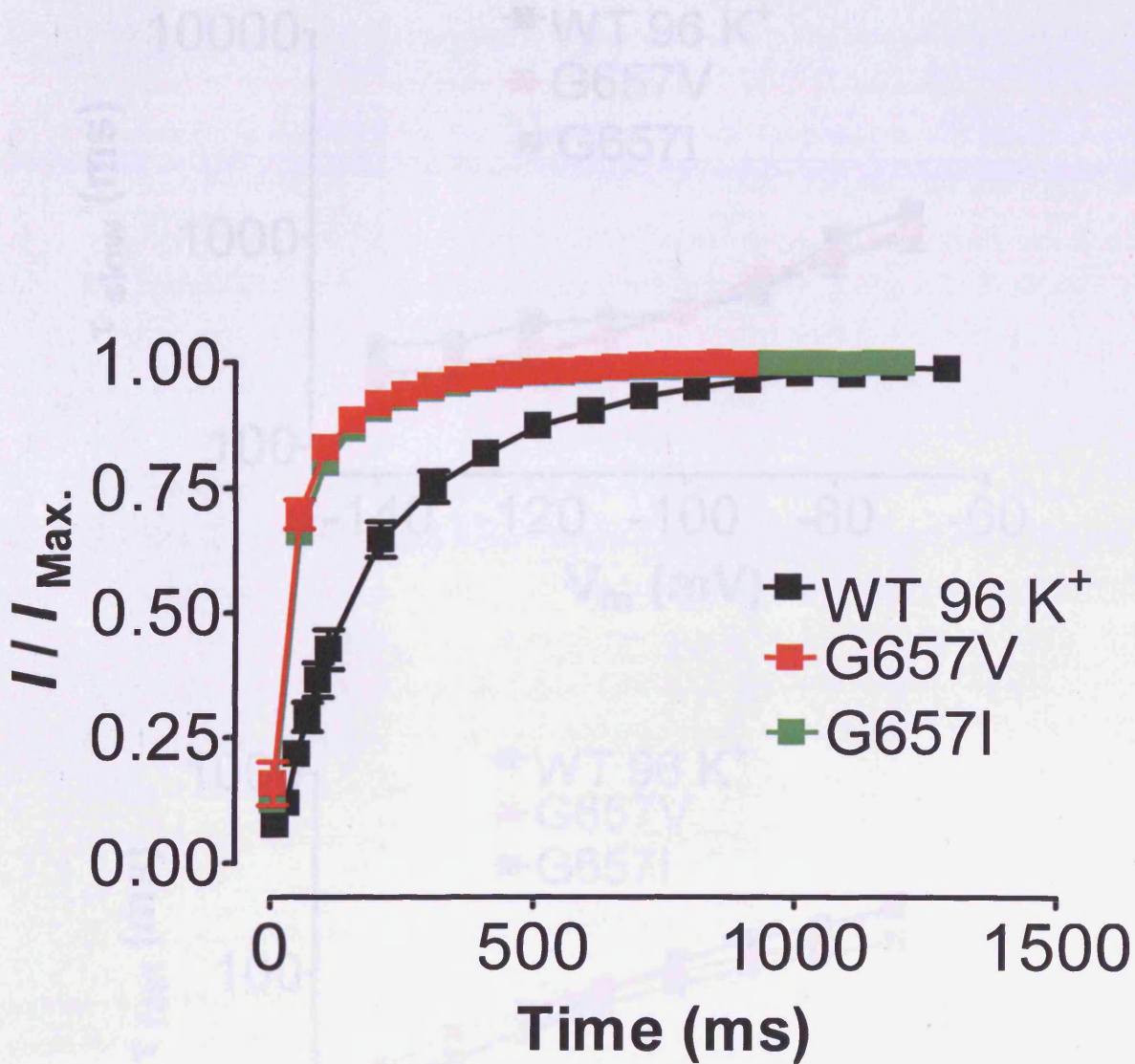


**B.**



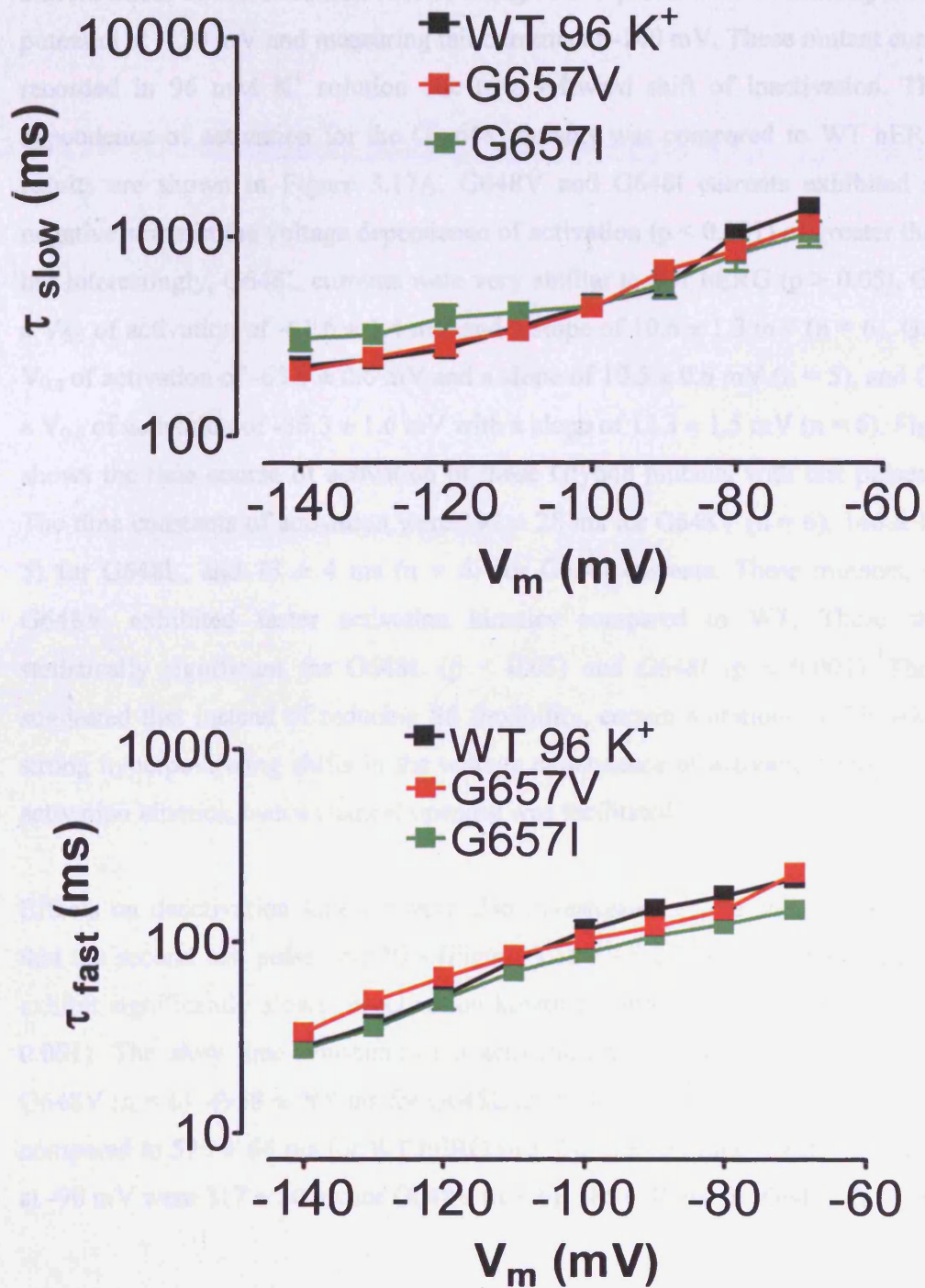
Chapter 3- Glycine hinge study

**Figure 3.14: G657V and G657I hERG exhibit rapid activation kinetics.** The time course of activation was measured using an 'envelope of tails' protocol by stepping from a holding potential of -120 mV to 0 mV for increasing time durations followed by a repolarising tail potential of -140 mV. Mean normalised peak tail currents were plotted against time and fitted with a single exponential and compared to WT hERG (n =6).



### Chapter 3- Glycine hinge study

**Figure 3.15: Time constants of deactivation of G657V and G657I ( $\tau_{\text{slow}}$  and  $\tau_{\text{fast}}$ ) were not different to WT hERG. A ‘fully-activated I-V’ protocol was applied and recordings were made in 96 mM  $\text{K}^+$  solution ( $n = 6$ ) and compared to WT hERG deactivation values.**



### Chapter 3- Glycine hinge study

support the view that mutations at Gly657 to larger residues altered channel packing and permitted entry into the open state more readily.

Similarly, Gly648 was mutated to a number of larger amino acid residues, Val, Leu, and Ile to investigate their effects on channel packing. Figure 3.16 shows representative current traces of these mutants elicited using an I-V protocol while holding the membrane potential at -120 mV and measuring tail currents at -140 mV. These mutant currents were recorded in 96 mM K<sup>+</sup> solution due to a leftward shift of inactivation. The voltage dependence of activation for the Gly648 mutants was compared to WT hERG and the results are shown in Figure 3.17A. G648V and G648I currents exhibited significant negative shifts in the voltage dependence of activation ( $p < 0.001$ ) of greater than 30 mV, but interestingly, G648L currents were very similar to WT hERG ( $p > 0.05$ ). G648V had a  $V_{0.5}$  of activation of  $-61.6 \pm 1.4$  mV and a slope of  $10.6 \pm 1.3$  mV ( $n = 6$ ), G648I had a  $V_{0.5}$  of activation of  $-65.9 \pm 0.6$  mV and a slope of  $10.5 \pm 0.6$  mV ( $n = 5$ ), and G648L had a  $V_{0.5}$  of activation of  $-36.3 \pm 1.6$  mV with a slope of  $13.3 \pm 1.5$  mV ( $n = 6$ ). Figure 3.17B shows the time course of activation of these Gly648 mutants with test pulses to 0 mV. The time constants of activation were  $192 \pm 28$  ms for G648V ( $n = 6$ ),  $146 \pm 16$  ms ( $n = 5$ ) for G648L, and  $73 \pm 4$  ms ( $n = 6$ ) for G648I currents. These mutants, except for G648V, exhibited faster activation kinetics compared to WT. These shifts were statistically significant for G648L ( $p < 0.05$ ) and G648I ( $p < 0.001$ ). These results suggested that instead of reducing S6 flexibility, certain mutations at Gly648 displayed strong hyperpolarizing shifts in the voltage dependence of activation and showed faster activation kinetics, hence channel opening was facilitated.

Effects on deactivation kinetics were also investigated as previously described, except that the second test pulse was 10 s (Figure 3.18). All of the Gly648 mutants seemed to exhibit significantly slower deactivation kinetics compared to WT channels ( $n \geq 5$ ,  $p < 0.001$ ). The slow time constants of deactivation at -90 mV were  $2754 \pm 214$  ms for G648V ( $n = 6$ ),  $4958 \pm 268$  ms for G648L ( $n = 5$ ), and  $5169 \pm 131$  ms for G648I ( $n = 6$ ) compared to  $579 \pm 66$  ms for WT hERG ( $n = 5$ ). The fast time constants of deactivation at -90 mV were  $317 \pm 30$  ms for G648V ( $n = 6$ ),  $388 \pm 40$  ms for G648L ( $n = 5$ ), and  $372$

### Chapter 3- Glycine hinge study

**Figure 3.16: Functional currents observed for the glycine mutants G648V, G648L, and G648I.** Representative current traces were elicited using an I-V protocol in 96 mM  $K^+$  solution. Cells were held at -120 mV and the tail currents recorded at -140 mV following 5 s depolarising pulses between -120 and +40 mV. The dashed line indicates the zero current line.

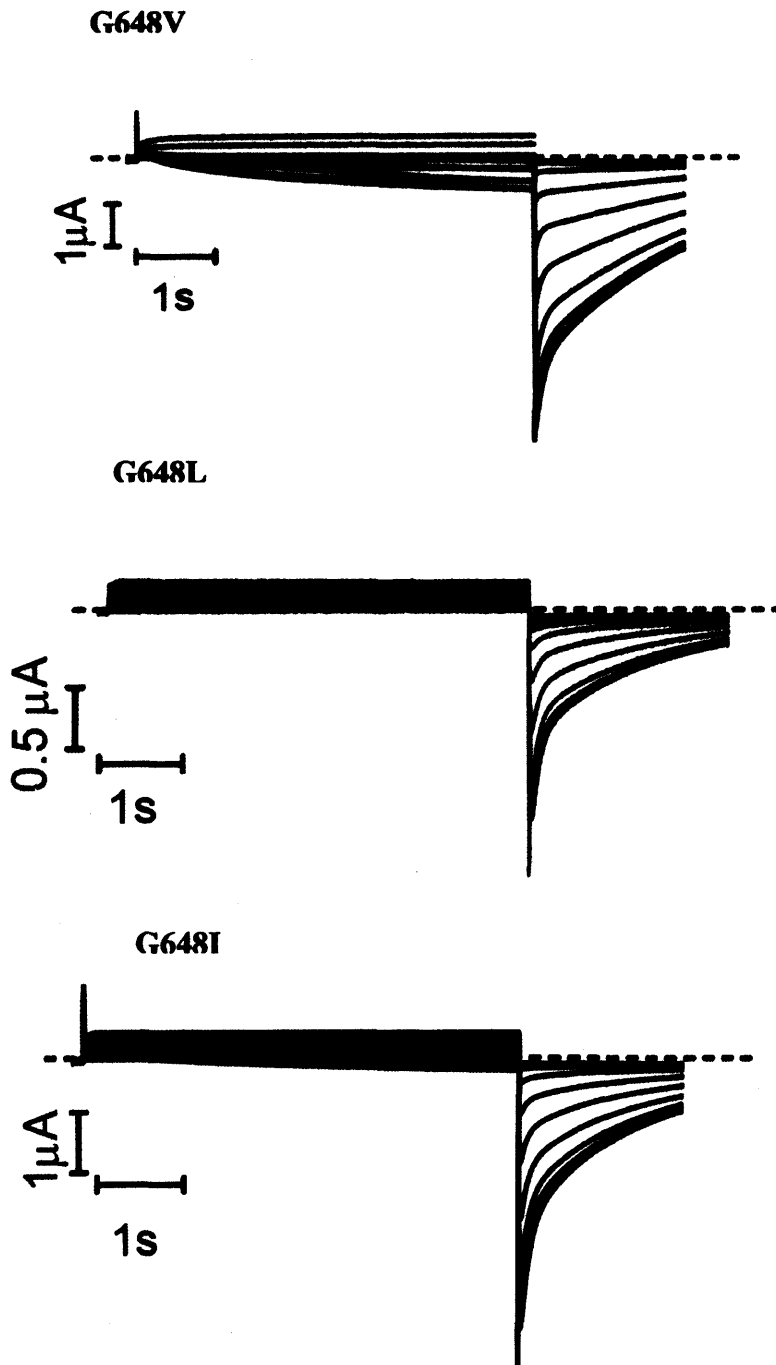
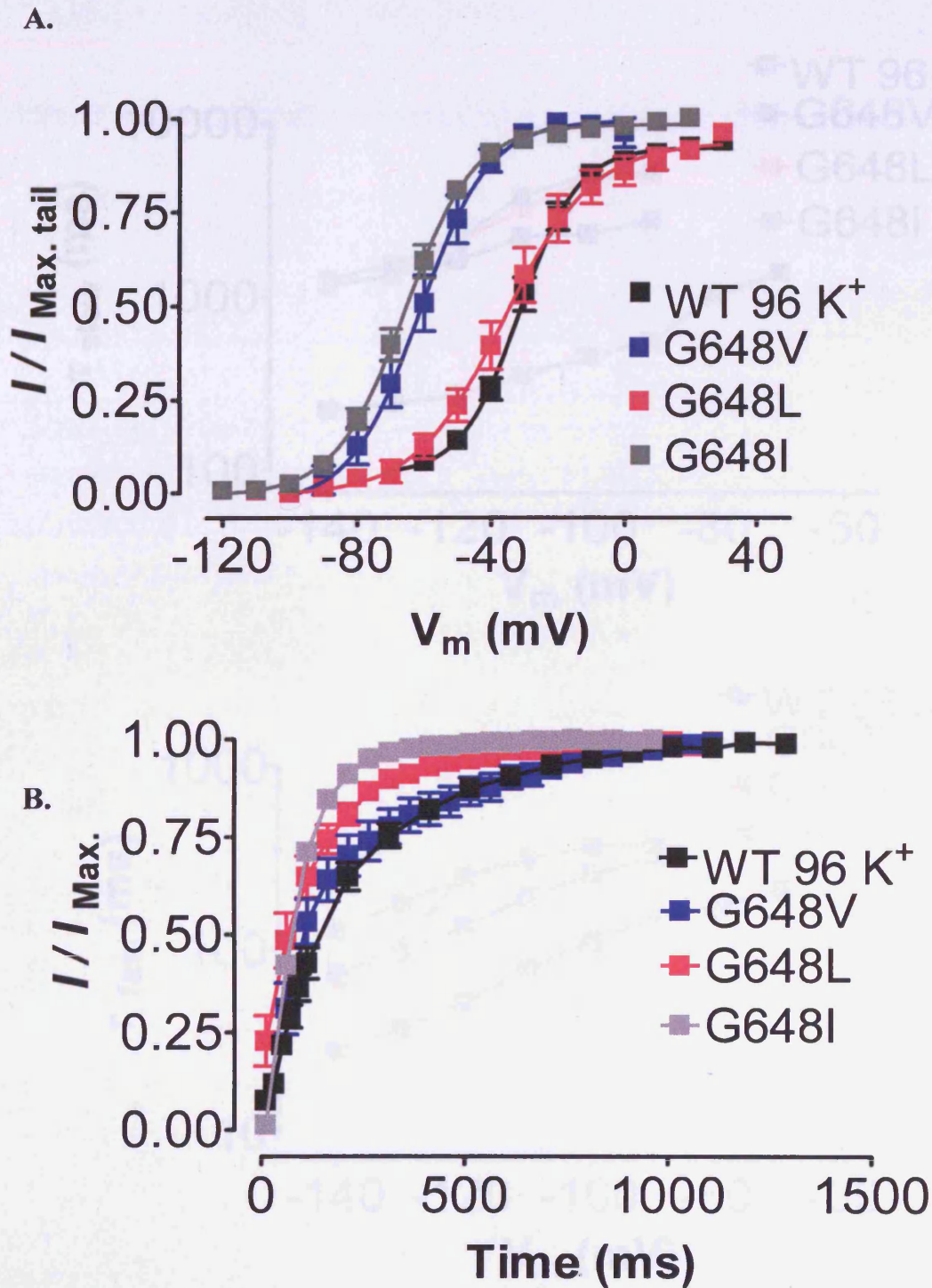
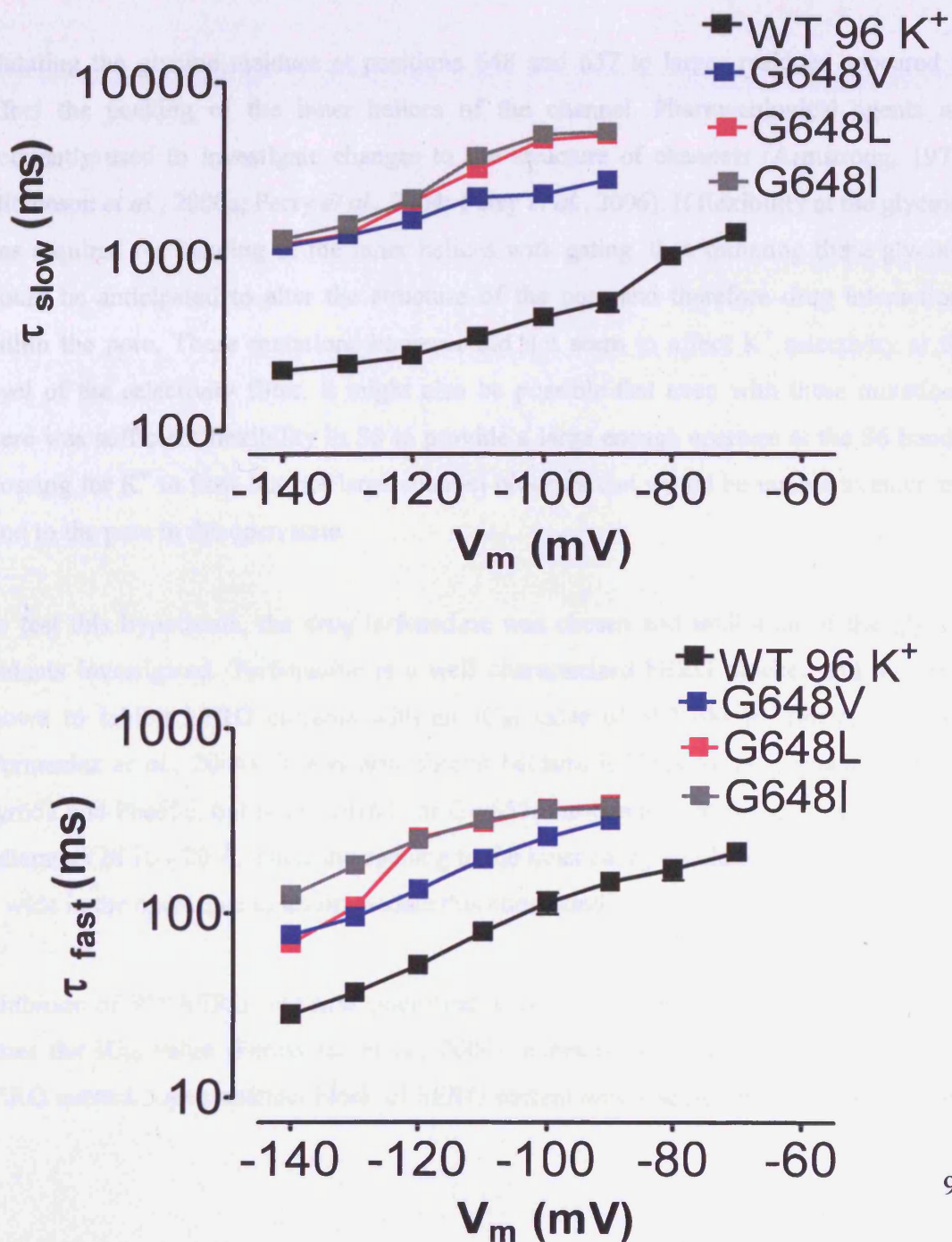


**Figure 3.17: Voltage and time dependent kinetics of activation of the G648V, G648L, and G648I currents.** A. The voltage dependence of the mutants was compared to WT hERG in 96 mM K<sup>+</sup> solution. Tail currents were recorded at -140 mV (n ≥ 5). B. Mean peak tail currents normalised to steady state maximal current and plotted against pulse duration at 0 mV. Mean results were fit with a single exponential function and compared to WT hERG in 96 mM K<sup>+</sup> solution (n ≥ 5).



### Chapter 3- Glycine hinge study

**Figure 3.18: Effects of G648V, L, and I mutations on deactivation kinetics.** Time constants ( $\tau$ ) of deactivation were determined as described previously (see Figure 3.3) except for a longer second pulse equal to 10 s.  $\tau$  values for WT hERG currents recorded in 96 mM  $K^+$  solution are shown for comparison ( $n \geq 5$ ). All Gly648 mutants exhibited statistically slower kinetics from WT at all voltages studied ( $n \geq 5$ ,  $p < 0.01$ ).



### Chapter 3- Glycine hinge study

$\pm 15$  ms for G648I ( $n = 6$ ) compared to  $108 \pm 33$  ms for WT hERG ( $n = 5$ ). These results suggested that the channel was prevented from closing normally as well as being able to open more readily in the presence of these bulkier residues. Thus, the data appears to be more consistent with the glycines at positions 648 and 657 being required to enable the tight packing of the inner helices rather than acting as gating hinges.

#### 3.4 Pharmacology of Gly657 and Gly648 mutants

Mutating the glycine residues at positions 648 and 657 to larger residues appeared to affect the packing of the inner helices of the channel. Pharmacological agents are frequently used to investigate changes to the structure of channels (Armstrong, 1971; Mitcheson *et al.*, 2000a; Perry *et al.*, 2004; Perry *et al.*, 2006). If flexibility at the glycines was required for bending of the inner helices with gating, then mutating these glycines would be anticipated to alter the structure of the pore and therefore drug interactions within the pore. These mutations however did not seem to affect  $K^+$  selectivity at the level of the selectivity filter. It might also be possible that even with these mutations, there was sufficient flexibility in S6 to provide a large enough aperture at the S6 bundle crossing for  $K^+$  to flow but not large channel blockers that would be unable to enter and bind to the pore in the open state.

To test this hypothesis, the drug terfenadine was chosen and inhibition of the glycine mutants investigated. Terfenadine is a well characterized hERG blocker and has been shown to inhibit hERG currents with an  $IC_{50}$  value of 300 nM in *Xenopus* oocytes (Fernandez *et al.*, 2004). It was also chosen because it binds to the aromatic residues Tyr652 and Phe656, but not to Gly648 or Gly657. Furthermore, terfenadine is large, with a diameter of 10 - 20 Å. Thus, the opening to the inner cavity would need to be at least 10 Å wide in the open state to accommodate this compound.

Inhibition of WT hERG was first quantified with 3  $\mu$ M terfenadine, a concentration ten times the  $IC_{50}$  value (Fernandez *et al.*, 2004), expected to inhibit the majority of the hERG current. Open channel block of hERG current was assessed by repetitive pulsing

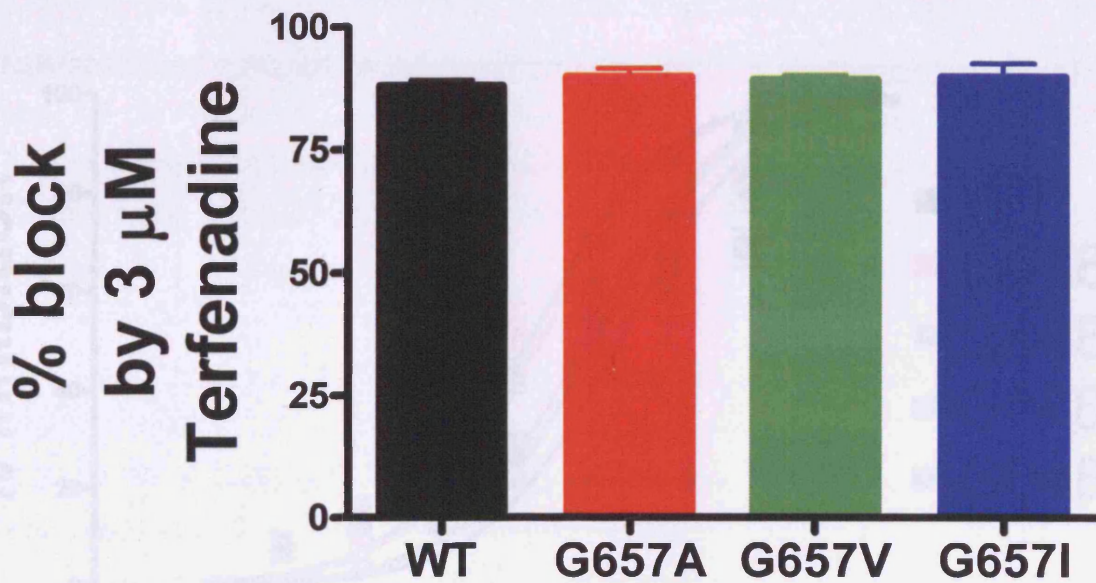
### Chapter 3- Glycine hinge study

from a holding potential of -90 mV to 0 mV for 5 s. Membrane potential was repolarised to -70 mV for 400 ms to elicit tail currents. The start-to-start interval was just 6 s. Recordings were stopped when the tail currents reached steady state amplitude. This protocol was used to investigate drug block as the channel was kept in the open/inactivated state for the majority of time allowing drug access to the inner cavity. The drug was applied for 2 minutes before pulsing to allow it to equilibrate across the membrane. Repetitive pulsing was continued until steady state inhibition was achieved. The amount of inhibition was comparable between WT and the Gly657 mutants. Drug inhibition was quantified by measuring peak tail current amplitudes after they have stabilised in control solutions and then after reaching steady state block at each drug concentration. Current amplitudes were also corrected for leak. The onset of current inhibition was just as fast in the Gly657 mutants as in WT hERG. Figure 3.19 shows that the percentage of inhibition obtained with 3  $\mu$ M terfenadine was the same for all currents ( $n = 6$ ). The mutant channels did not significantly alter block by terfenadine ( $p > 0.05$ ). Thus, mutations at Gly657 did not modify the structure of the drug receptor and presumably the inner cavity.

Similarly the effects of the Gly648 mutants on the potency of terfenadine were determined. If the structure of the pore was not disrupted by these mutations, then the  $IC_{50}$  value of terfenadine in WT and mutant channels should be similar. Terfenadine concentration-response relationships were determined for WT and mutant channels in 96 mM  $K^+$  solution and the results shown in Figure 3.20. The  $IC_{50}$  value obtained for WT hERG was 400 nM, which was slightly higher than the previously observed  $IC_{50}$  value in low  $K^+$  solution. The  $IC_{50}$  values of terfenadine obtained with the Gly648 mutants, reported in the table (Figure 3.20), were significantly different from the  $IC_{50}$  for terfenadine in WT hERG ( $p < 0.01$ ). The greatest shift in  $IC_{50}$  was seen with the G648V mutation that exhibited a 4-fold shift in  $IC_{50}$  compared to WT hERG. However, the overall fold change in  $IC_{50}$  with these mutations was relatively minor compared to the effects of the Y652A and F656A mutations, that demonstrated greater than a 100-fold change (Mitcheson *et al.*, 2000a). Therefore, the Gly648 mutations did not appear to dramatically alter the structure of the pore of the channel in the open state. These results

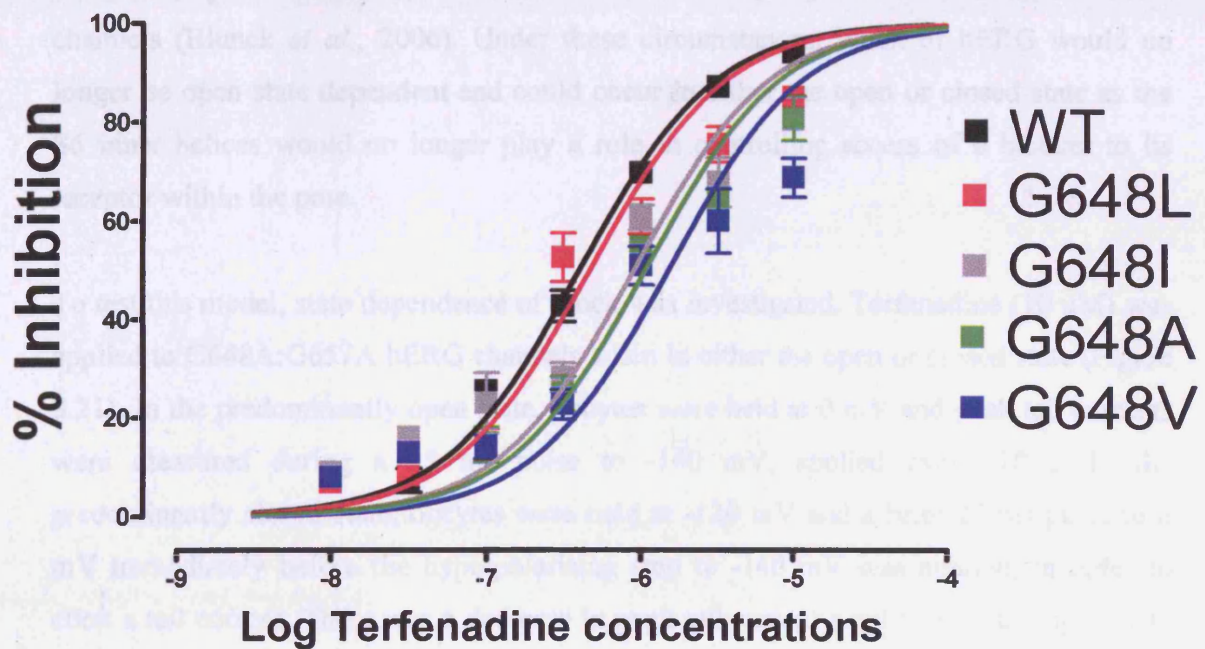
### Chapter 3- Glycine hinge study

**Figure 3.19: Inhibition of WT and Gly657 hERG currents by terfenadine.** Mean percentage of inhibition of WT and Gly657 mutant currents by 3  $\mu$ M terfenadine. Mutations did not significantly alter channel block ( $n = 6$ ,  $p > 0.05$ ).



Chapter 3- Glycine hinge study

**Figure 3.20: Concentration-response curves of terfenadine with Gly648 mutants.** Concentration-response relationships for terfenadine inhibition of WT and Gly648 mutant hERG currents shown fitted with a Hill function to obtain  $IC_{50}$  and hill slope values (see table). Drug block was established in 96 mM  $K^+$  solution. Changes in  $IC_{50}$  values for all mutant channels were statistically significantly different to WT  $IC_{50}$  values ( $n = 6$ ,  $p < 0.01$ ).



	$IC_{50}$ of Terfenadine (nM) in 96 mM $K^+$ solution	S.E.M	Hill slope	n
Wild-type	400	28	1	6
G648A	1060	49	0.9	6
G648V	1490	71	0.7	6
G648L	465	58	0.9	6
G648I	894	69	0.8	6

### Chapter 3- Glycine hinge study

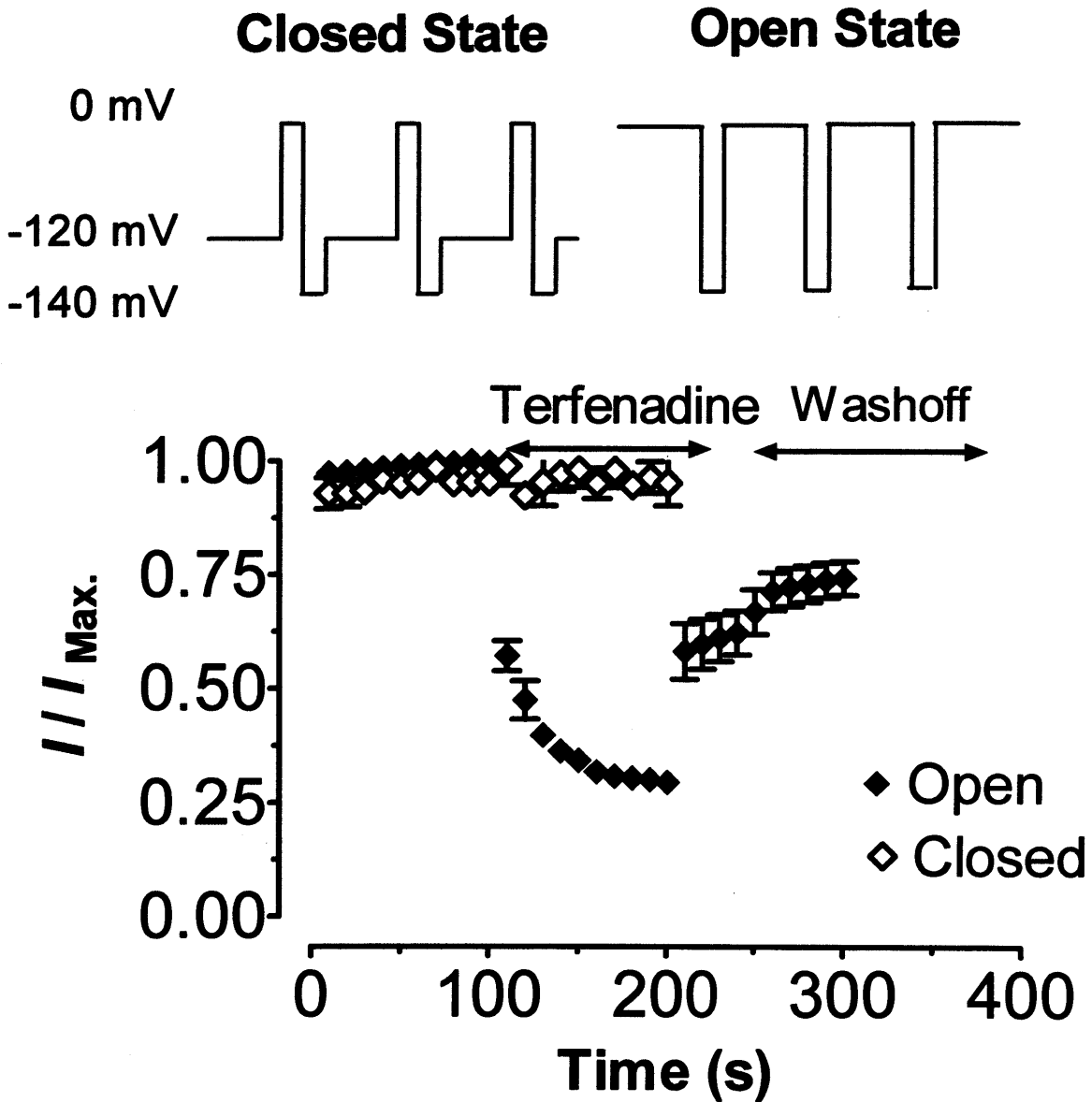
showed that the Gly657 and Gly648 mutants retained their sensitivity to block by terfenadine validating that the mutant channels had enough flexibility, even in the absence of glycines, to accommodate a large blocker.

The possibility that a second gate located at the selectivity filter, capable of mediating K<sup>+</sup> gating, could not be disregarded. In this case, loss of S6 flexibility could still result in K<sup>+</sup> flow through the selectivity filter if it was rendered predominantly open. The presence of a second gate at the selectivity filter has been proposed for cyclic nucleotide gated channels (Flynn *et al.*, 2001), inward rectifier channels (Claydon *et al.*, 2003), and KscA channels (Blunck *et al.*, 2006). Under these circumstances, block of hERG would no longer be open state dependent and could occur in either the open or closed state as the S6 inner helices would no longer play a role in controlling access of a blocker to its receptor within the pore.

To test this model, state dependence of block was investigated. Terfenadine (10 μM) was applied to G648A:G657A hERG channels when in either the open or closed state (Figure 3.21). In the predominantly open state, oocytes were held at 0 mV and peak tail currents were measured during a 25 ms pulse to -140 mV, applied every 10 s. In the predominantly closed state, oocytes were held at -120 mV and a brief 25 ms pulse to 0 mV immediately before the hyperpolarising step to -140 mV was applied, in order to elicit a tail current. There was a decrease in peak tail current amplitude in the open state that could then be partially recovered when the drug was washed off by switching back to the control recording solution. 10 μM terfenadine blocked G648A:G657A channels by 71.4 % (n = 6) compared to block of WT channels of 91.8 ± 1 %. This change in percentage of inhibition was statistically different to WT (p < 0.01). It was however similar to what was observed with the Gly657 and Gly648 mutations described previously and therefore relatively minor in comparison to other hERG mutants such as Y652A and F656A. When the drug was applied to channels predominantly kept in the closed state, no inhibition of current amplitude was observed. These results indicated that terfenadine still required the opening of the S6 inner helices to gain access to the pore of the G648A:G657A hERG channel. Because of this compound's large size, it can be

Chapter 3- Glycine hinge study

**Figure 3.21: The state dependence of G648A:G657A hERG current inhibition.** 10  $\mu$ M terfenadine was added to G648A:G657A hERG in either the predominantly open or closed state as shown in the inset. Recordings were made in control solution before switching to drug-containing solution. In the predominantly open state, there was a decrease in peak tail current due to terfenadine block. Recovery from block was measured upon switching back to control solution. However, no block was observed during the predominantly closed state.



### Chapter 3- Glycine hinge study

concluded that the channel was capable, even in the absence of the glycine residues, to form a significantly sized aperture to allow the normal binding of terfenadine in the open state. This further indicates that even in the absence of both glycines, the channel was capable of opening by at least 10 Å to allow terfenadine block within the inner cavity. Thus, the S6 glycines in hERG may not be required as gating hinges during hERG activation gating.

## Chapter 3- Glycine hinge study

### 3.5 Discussion

This chapter describes an investigation into the role of two glycine residues in hERG activation gating. I first began by characterizing the gating properties of WT hERG channels in 2 mM and 96 mM K<sup>+</sup> solutions, which would then enable direct comparisons to be made with mutant hERG channels. The rationale behind this study emerged from observations in crystal structures of bacterial channels as well as mutagenesis studies in a variety of different channels, which suggested that the transition from the closed to the open state is due to glycine residues which permit bending of the inner helices (Doyle *et al.*, 1998; Mitcheson *et al.*, 2000a; Jiang *et al.*, 2002a; Jiang *et al.*, 2002b; Long *et al.*, 2005). This is known as the glycine hinge hypothesis. hERG has two glycines in S6, Gly648 and Gly657, proposed to be involved in activation gating.

The results of this study show that mutating these residues, individually or simultaneously, to an alanine still results in a functional channel that is capable of opening and closing in a similar fashion to WT channels. Furthermore, substituting the glycines with bulkier residues resulted in channels with increased open probabilities, seen as shifts in the voltage dependence of activation to more negative potentials. Gly648 mutants significantly slowed the deactivation process indicating that these mutants stabilised the open state of the channel. Gly657 mutants did not appear to have dramatic effects on deactivation kinetics but they did have faster activation kinetics. This suggests that mutations at Gly657 destabilised the closed state of the channel. A summary of all the data is found in Table 3.22. Studies using terfenadine, a large hERG channel blocker, further confirms the ability of the channel to open relatively normally and allow open channel block by terfenadine even in the absence of both these glycine residues. This shows that the structure of the inner cavity was not dramatically altered by these mutations at the glycine positions. These results point to the importance of the small glycine residues in the close packing of the inner helices rather than as hinge points for gating. hERG channels appear likely to have sufficient inherent flexibility for the bending of the helices to occur with activation gating, even in the absence of the glycine residues. Thus, hERG activation gating does seem to be different from other Kv channels.

### Chapter 3- Glycine hinge study

**Table 3.22: Summary of the activation and deactivation properties of WT and mutant hERG channels.** WT hERG and G657A channels (in blue) were recorded in 2 mM K<sup>+</sup> solution, the rest (in black) were recorded in 96 mM K<sup>+</sup> solution. The values for V<sub>0.5</sub> of activation were obtained by fitting tail current-voltage relationships with a Boltzmann function. The activation time constants ( $\tau$ ) were determined from a single exponential fit to plots of peak tail current amplitude against time. Deactivation time constants ( $\tau_{slow}$  and  $\tau_{fast}$ ) were derived from double exponential fits to the decaying phase of the tail current at -90 mV ( $n \geq 5$  for each). Statistical comparisons were made for each mutant channel against WT channels under the same recording conditions.

\*  $p < 0.05$

\*\*  $p < 0.01$

	Activation		Deactivation@ -90 mV	
	V <sub>0.5</sub> of activation (mV)	Activation $\tau$ values (ms)	Deactivation $\tau_{slow}$ (ms)	Deactivation $\tau_{fast}$ (ms)
WT (2 mM K <sup>+</sup> )	-24.6 ± 0.7	248 ± 33	349 ± 30	84 ± 8
WT (96 mM K <sup>+</sup> )	-30.8 ± 0.9	214 ± 29	579 ± 66	108 ± 33
G648A	-23.5 ± 1.7 *	305 ± 67 *	855 ± 57 **	163 ± 14
G648V	-61.6 ± 1.4 **	192 ± 28	2754 ± 214 **	317 ± 30 **
G648L	-36.3 ± 1.6	146 ± 16 *	4958 ± 268 **	388 ± 40 **
G648I	-65.9 ± 0.6 **	73 ± 4 **	5169 ± 131 **	372 ± 15 **
G657A (2 mM K <sup>+</sup> )	-30.9 ± 0.5 *	154 ± 2 *	229 ± 5 *	48 ± 2 **
G657V	-84.8 ± 1.6 **	99 ± 9 **	651 ± 81	120 ± 14
G657I	-85 ± 1.6 **	109 ± 3 **	572 ± 97	106 ± 10
G648A:G657A	-39.8 ± 1.7 *	304 ± 21 *	692 ± 28	174 ± 12

## **Chapter Four**

## **Generation of stable cell lines**

A number of methods may be used to generate stable cell lines necessary for electrophysiological investigation. One novel approach which is described in this chapter involves the Flp-In system (Invitrogen, California, USA), which promised distinct advantages over other methodologies. Namely, it proposed a rapid and efficient way of generating isogenic stable cell lines expressing the gene of interest, without the need for clonal selection. This approach will be discussed in detail and compared to the standard method of making stable cell lines by utilising lipid reagents such as Lipofectamine 2000.

Generating stable cell lines was particularly desirable in this project in order to be used in the screening of a large number of hERG blockers by using a high throughput automated patch clamping system against WT as well as mutant hERG channels. In automated systems, cells are usually selected at random, thus having measurable currents in a high proportion of cells is essential. Stable expression in theory should be reproducible, exhibiting a stable current under electrophysiological conditions. It also eliminates the need for repeated transfections as in the case of transient systems. However, generating stable cell lines can also be problematic in many ways. Following transfection, only a small proportion of clones may express measurable currents. There may also be large cell-cell variability in expression levels, even within the same clone. Some ion channels may also be poorly tolerated giving rise to slowed cell growth and possibly loss of expression upon passaging.

Alanine-scanning mutagenesis revealed several amino acid residues on the S6 of hERG, which may be important in drug block (Mitcheson *et al.*, 2000a). The aromatic residues Phe656 and Tyr652 have been shown to be important for most drugs studied so far. Other residues near the selectivity filter, such as Thr623, Ser624, and Gly648, can also interact with some drugs. To further understand their roles in drug binding, stable cell lines carrying mutations to these various sites on S6 could then be used to test a large number

#### **Chapter 4- Generation of stable cell lines**

of drugs. This could result in the identification of important chemical groups on hERG blockers as well as elucidating the roles of these residues in hERG pharmacology.

In this chapter, I will begin by characterising the biophysical properties of the hERG mutants with the two-electrode voltage clamp method. This enabled us to identify the conditions and protocols needed to record from these currents using the patch clamp system. I will then reveal the strategy used in making stable cell lines by utilising the Flp-In system and the drawbacks to this method. Finally, I will evaluate this approach against a Lipofectamine-based method of generating stable cell lines.

## Chapter 4- Generation of stable cell lines

### 4.1 Characterisation of pore helix residues (Thr623 and Ser624)

The roles of a number of S6 residues in drug binding and/or activation gating in hERG are still unclear. Among these residues are the pore helix residues, Thr623 and Ser624, which are highly conserved among Kv channels. These residues are critical for the high affinity binding of some compounds (e.g. methanesulfonanilides) but not others as shown by alanine mutagenesis studies (Mitcheson *et al.*, 2000a).

To understand the effects of mutant hERG channels on pharmacological properties, it was important to understand first the effects of these amino acid substitutions on ionic currents. Using the two-electrode voltage clamp technique, the activation and deactivation properties of T623A and S624A hERG were characterised in *Xenopus* oocytes. These channels were previously characterised (Perry *et al.*, 2006) and hence, this data enabled us to validate the recording conditions and protocols used. Figure 4.1 shows a representative family of currents for S624A and T623A hERG using the I-V protocol described previously (see section 3.1.1). S624A hERG currents appeared to be very similar to WT hERG currents. T623A hERG currents were recorded in 96 mM K<sup>+</sup> solution due to a leftward shift in inactivation. These currents were also elicited with 5 s depolarising pulses from a holding potential of -90 mV, but with tail currents measured at -90 mV. The V<sub>0.5</sub> of activation was obtained by fitting peak tail current-voltage relationships with a Boltzmann function (Figure 4.1). The V<sub>0.5</sub> of activation of S624A hERG was  $-26.9 \pm 0.8$  mV, which was comparable to the V<sub>0.5</sub> of activation of WT hERG channels of  $-24.6 \pm 0.7$  mV in 2 mM K<sup>+</sup> solution (n = 5). T623A hERG had a V<sub>0.5</sub> of activation of  $-20.6 \pm 0.9$  mV, which was significantly shifted compared to WT currents with a V<sub>0.5</sub> of activation of  $-30.8 \pm 0.9$  mV in 96 mM K<sup>+</sup> solution.

The time constant of activation was also measured using an 'envelope of tails' voltage protocol. The current measured at 0 mV was normalised to maximum current then plotted against the time course of activation. It appeared to take longer for the S624A currents to reach maximal current. Figure 4.2 shows this data fit with a single exponential function to give a time constant of activation of  $368 \pm 30$  ms for S624A hERG and  $233 \pm 28$  ms

**Figure 4.1: Current-voltage relationships of T623A and S624A hERG.** **A.** Representative current traces of the S624A (i) and T623A (ii) hERG channels recorded using an I-V protocol in 2 mM and 96 mM  $K^+$  solutions respectively. A series of 5 s depolarising pulses from a holding potential of -90 mV to potentials between -60 and +50 mV were applied followed by a 2.5 s pulse to -70 mV (for S624A) or -90 mV (for T623A). The dashed line indicates the zero current line. **B.** The voltage dependence of activation of T623A and S624A hERG. Mean normalised data was fitted with a Boltzmann function ( $n = 5$ ).

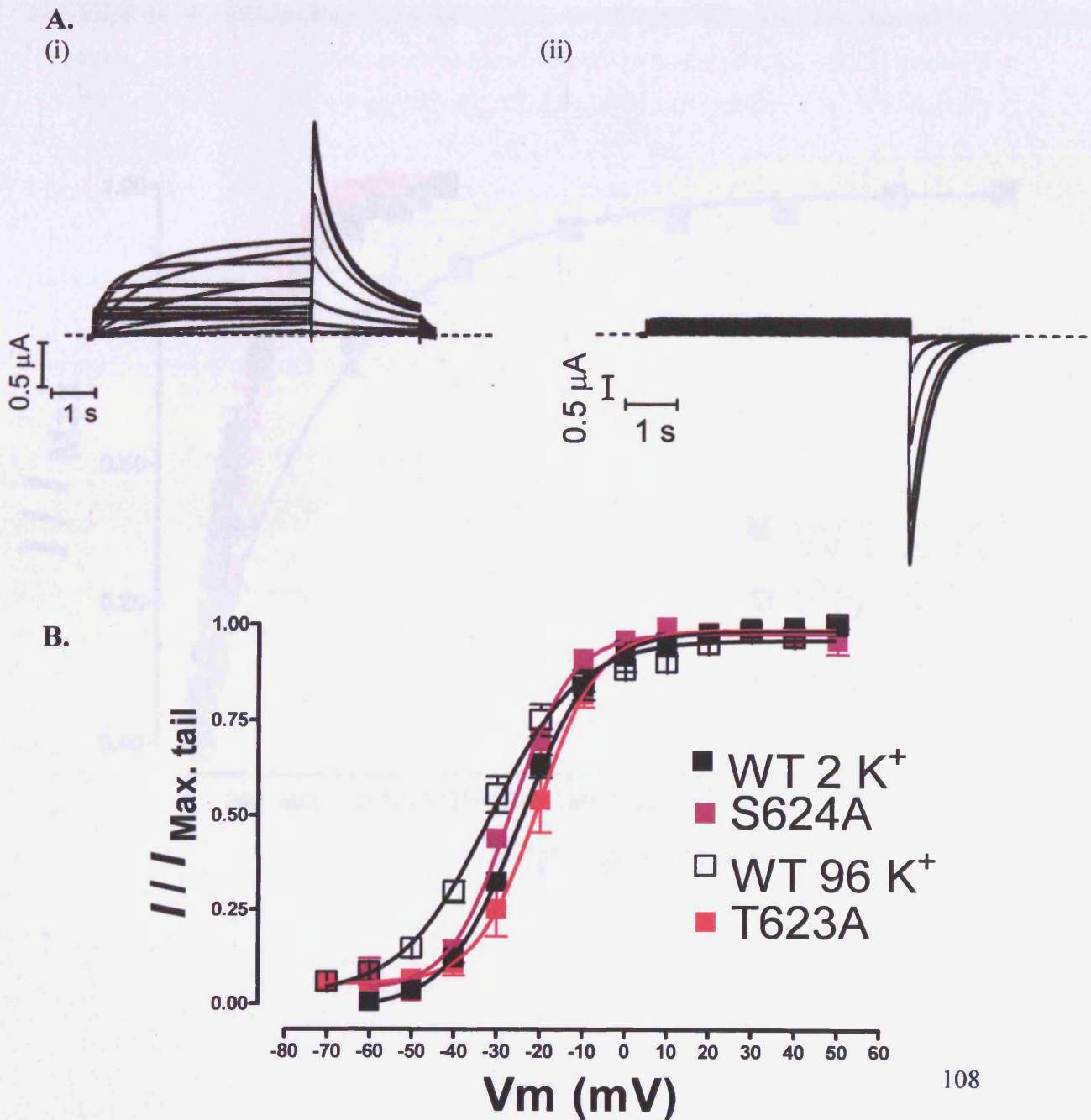
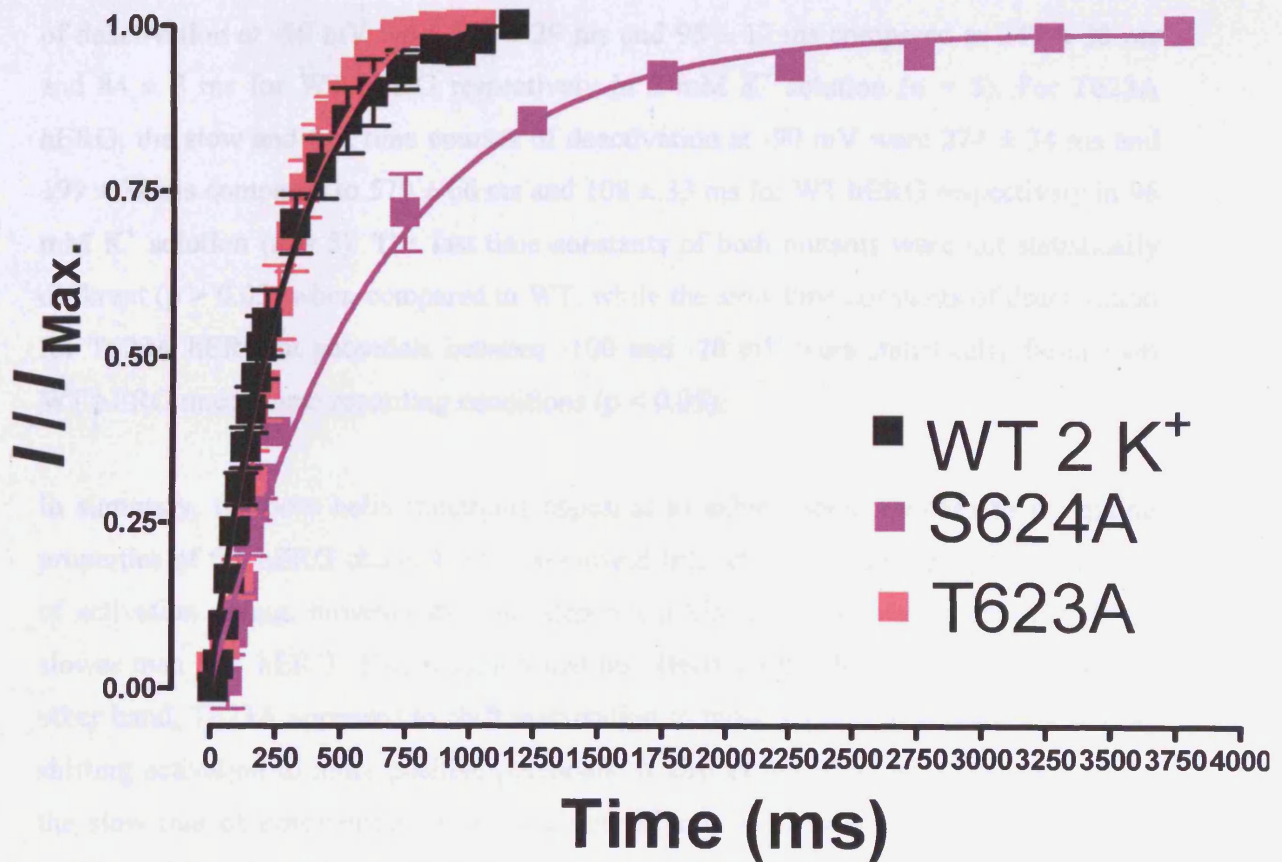


**Figure 4.2: Time dependent kinetics of activation of the S624A and T623A currents compared to WT hERG.** Mean normalised peak tail currents at 0 mV elicited using the 'envelope of tails' protocol and plotted against time (n = 5). For clarity, the activation time course of WT in 96 mM K<sup>+</sup> solution was not plotted as it is nearly superimposed on that for WT in 2 mM K<sup>+</sup> solution (see figure 3.2).



#### Chapter 4- Generation of stable cell lines

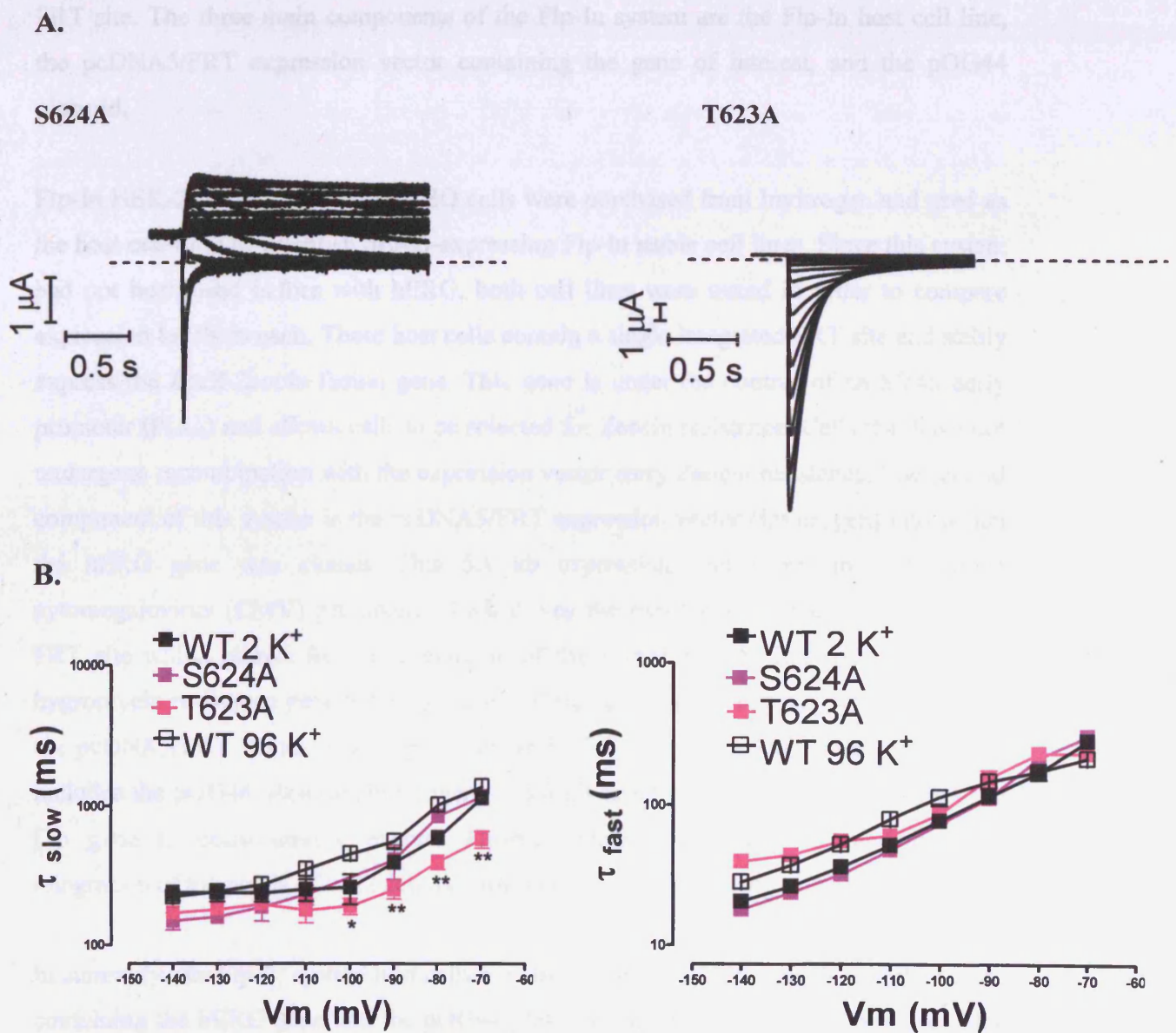
for T623A hERG compared to  $248 \pm 33$  ms and  $214 \pm 29$  ms for WT hERG in 2 mM and 96 mM  $K^+$  solution respectively ( $n = 5$ ).

A 'fully-activated I-V' protocol was used to compare the deactivation kinetics of T623A and S624A with WT hERG. Membrane potential was held at -90 mV and then stepped to +40 mV for 1 s. Test pulses were applied to varying potentials between +30 and -140 mV and Figure 4.3 shows representative current traces from this part of the protocol for S624A and T623A hERG. The time dependence of deactivation was measured from this protocol by fitting the decaying phase of the tail current with a double exponential function. The slow and fast rates of deactivation were plotted on a  $\log_{10}$  scale (Figure 4.3 (i) and (ii) respectively) for S624A and T623A hERG and compared to WT currents under the same recording conditions. For S624A hERG, the slow and fast time constants of deactivation at -90 mV were  $406 \pm 29$  ms and  $95 \pm 12$  ms compared to  $349 \pm 30$  ms and  $84 \pm 8$  ms for WT hERG respectively in 2 mM  $K^+$  solution ( $n = 5$ ). For T623A hERG, the slow and fast time courses of deactivation at -90 mV were  $274 \pm 34$  ms and  $199 \pm 38$  ms compared to  $579 \pm 66$  ms and  $108 \pm 33$  ms for WT hERG respectively in 96 mM  $K^+$  solution ( $n = 5$ ). The fast time constants of both mutants were not statistically different ( $p > 0.05$ ) when compared to WT, while the slow time constants of deactivation for T623A hERG at potentials between -100 and -70 mV were statistically faster than WT hERG under same recording conditions ( $p < 0.05$ ).

In summary, the pore helix mutations appeared to exhibit some changes to the gating properties of the hERG channel. S624A showed little change to the voltage dependence of activation gating, however the time dependent kinetics of activation appeared to be slower than WT hERG. This mutation had no effects on the deactivation rates. On the other hand, T623A appeared to shift inactivation to more negative potentials, as well as shifting activation to more positive potentials. It also exhibited a significant increase in the slow rate of deactivation at potentials positive to -100 mV. This reflects the tight packing of the channel, as substitutions at the pore helix seem to affect gating near the intracellular end of the channel.

Chapter 4- Generation of stable cell lines

**Figure 4.3: The ‘fully-activated I-V’ protocol measures the deactivation time constants for the S624A and T623A hERG channels.** A. Representative current traces from the ‘fully-activated I-V’ protocol for S624A and T623A hERG during the second test pulse between +30 and -140 mV. B. Deactivation was fit with a double exponential function giving the fast and slow time constants, which were plotted on a log<sub>10</sub> scale against membrane potential (n = 5). WT deactivation rates in 2 mM and 96 mM K<sup>+</sup> solutions were plotted and statistical comparisons made between mutants and WT under same recording conditions, whereby (\*) indicates p < 0.05 and (\*\*) indicates p < 0.01.



## Chapter 4- Generation of stable cell lines

### 4.2 Flp-In System for generating stable cell lines

The Flp-In system (Invitrogen, USA) was used to create stable cell lines expressing the hERG channel. This system is based on the *Saccharomyces cerevisiae*-derived DNA recombination system, which allows the integration of the hERG gene into a mammalian cell at a specific genomic location due to the presence of the Flp-Recombination Target (FRT) site in the mammalian cell line. An expression vector containing hERG can then be integrated into the genome via Flp recombinase-mediated DNA recombination at the FRT site. The three main components of the Flp-In system are the Flp-In host cell line, the pcDNA5/FRT expression vector containing the gene of interest, and the pOG44 plasmid.

Flp-In HEK-293 cells and Flp-In CHO cells were purchased from Invitrogen and used as the host cell lines to establish hERG-expressing Flp-In stable cell lines. Since this system had not been used before with hERG, both cell lines were tested in order to compare expression levels in each. These host cells contain a single integrated FRT site and stably express the *LacZ-Zeocin* fusion gene. This gene is under the control of an SV40 early promoter ( $P_{SV40}$ ) and allows cells to be selected for Zeocin resistance. Cells that have not undergone recombination with the expression vector carry Zeocin resistance. The second component of this system is the pcDNA5/FRT expression vector (Invitrogen) into which the hERG gene was cloned. This 5.1 kb expression vector contains the human cytomegalovirus (CMV) promoter, which drives the expression of the hERG gene, an FRT site which allows for the integration of the vector into the host cell line, and a hygromycin resistance gene for the selection of stable cell lines. The hygromycin gene on the pcDNA5/FRT vector lacks a promoter and ATG initiation codon. This system also includes the pOG44 plasmid (Invitrogen), a 5.8 kb expression vector which contains the Flp gene to constitutively express Flp-recombinase, necessary for mediating the integration of the pcDNA5/FRT into the host cell line via the pairing of FRT sites.

In summary, the Flp-In system host cells are co-transfected with the pcDNA5/FRT vector containing the hERG gene and the pOG44 plasmid. The pOG44 plasmid expresses Flp-

## Chapter 4- Generation of stable cell lines

recombinase which allows for the homologous recombination between the FRT sites on pcDNA5/FRT and the host cell line. Upon recombination, the hygromycin gene is activated while the *lacZ-Zeocin* gene is inactivated, due to the integration of the SV40 promoter and ATG initiation codon from the *lacZ-Zeocin* fusion gene into the expression vector. The stable cell lines can now express hygromycin resistance, zeocin sensitivity, as well as the hERG protein (Figure 4.4). The pcDNA5/FRT/CAT plasmid can be used as a positive control as it contains the chloramphenicol acetyltransferase (*CAT*) marker gene, which can be co-transfected with pOG44 into the Flp-In host cell line.

The advantages proposed by this system lie in its ability to generate stable cell lines rapidly and easily due to the integrated FRT sites present on the host cell lines and the pcDNA5/FRT expression vector. It allows the integration of the hERG gene at a specific and active genomic location, thus generating isogenic stable cell lines without the need for clonal selection, which is a time consuming process.

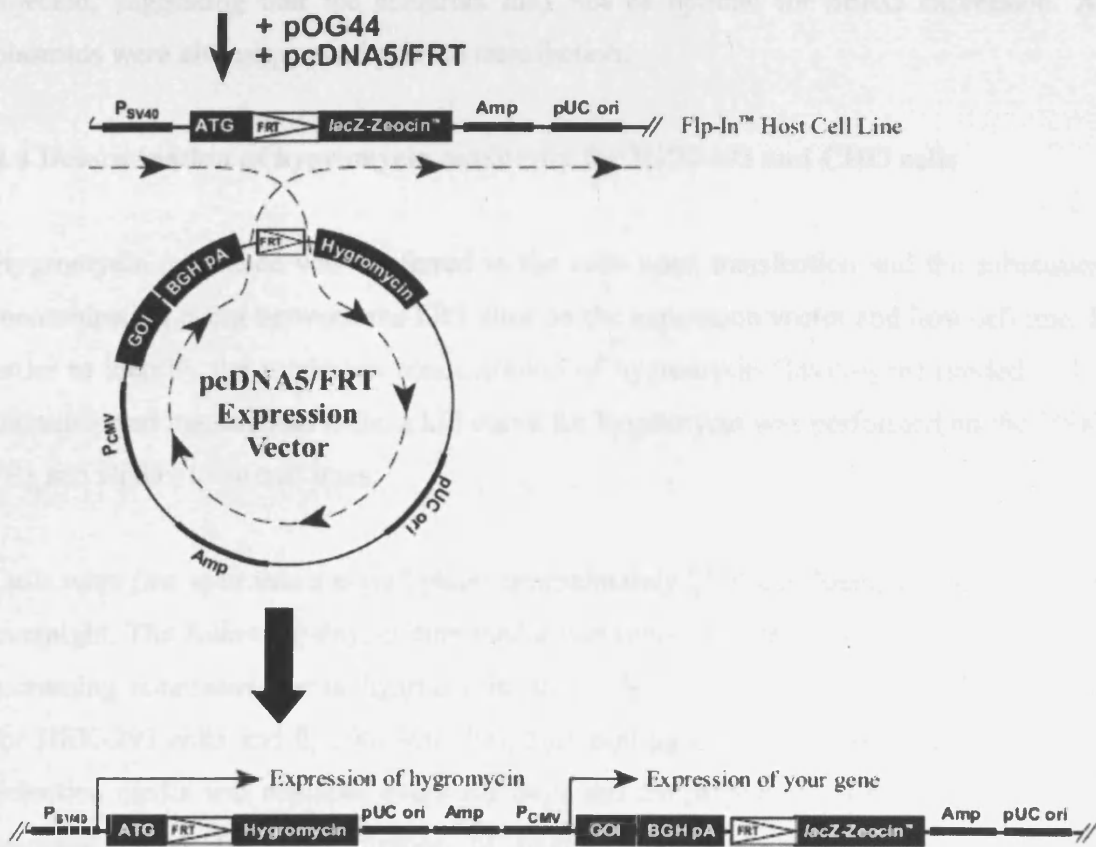
### 4.3 Preparation of the pcDNA5/FRT expression vector

The aim was first to subclone WT hERG from the pcDNA3 vector into the pcDNA5/FRT vector between the enzyme restriction sites of Hind III and BamHI. However, the pcDNA5/FRT expression vector also had a number of restriction sites, which were found in hERG. These restriction sites on pcDNA5/FRT included SalI (2881 and 5069), BglII (13), and XhoI (986), which had to be mutated by using PCR based site-directed mutagenesis techniques before hERG could be inserted. These restriction sites were not present in any of the vector's coding sequences and hence, could be removed.

In addition to WT hERG, *myc*-tagged hERG was similarly cloned into the pcDNA5/FRT vector and used for investigating levels of hERG expression in western blots. The *myc*-tag is a well characterised epitope tag that is useful for the labelling and detection of proteins. Its small size enables its fusion with the gene of interest, without interfering

## Chapter 4- Generation of stable cell lines

**Figure 4.4: Overview of the Flp-in system.** The pcDNA5/FRT expression vector containing the gene of interest (GOI) is co-transfected with pOG44 plasmid into the Flp-In host cell line. pOG44 constitutively expresses Flp-recombinase, which mediates the homologous recombination event between the FRT sites on the pcDNA5/FRT vector and that on the Flp-in host cell line. This process then allows the transcription of the hERG gene (GOI). The activation of the hygromycin resistance gene and inactivation of the *lacZ-Zeocin* gene permits cells that express the hERG gene to be selected for by gain of hygromycin resistance and loss of Zeocin resistance.



Obtained from Flp-In system online manual

[http://biochem.dental.upenn.edu/GATEWAY/Vector\\_manual/flpinsystem\\_man.pdf](http://biochem.dental.upenn.edu/GATEWAY/Vector_manual/flpinsystem_man.pdf)

## Chapter 4- Generation of stable cell lines

with its biochemical properties. Anti-*myc* antibodies may then be used to detect the *myc* sequence and therefore the protein associated with it. The *myc*-tag was added to the C-terminal end of hERG so that only fully transcribed proteins would be identified by the anti-*myc* antibodies. RNA was made to functionally test the hERG constructs, WT hERG in pcDNA5/FRT and *myc*-tagged WT hERG in pcDNA5/FRT, in *Xenopus* oocytes. Using the two-electrode voltage clamp technique, currents were obtained for both *myc*-tagged and WT hERG channels that were very similar to WT currents (Figures 4.5(i) and (ii) respectively). This confirmed that hERG was functionally expressing and that no additional mutations were present, which interfered with normal hERG function. Currents however were small in amplitude although maximal RNA concentration (30 ng) was injected, suggesting that the construct may not be optimal for hERG expression. All plasmids were also sequenced prior to transfection.

### 4.4 Determination of hygromycin sensitivity for HEK-293 and CHO cells

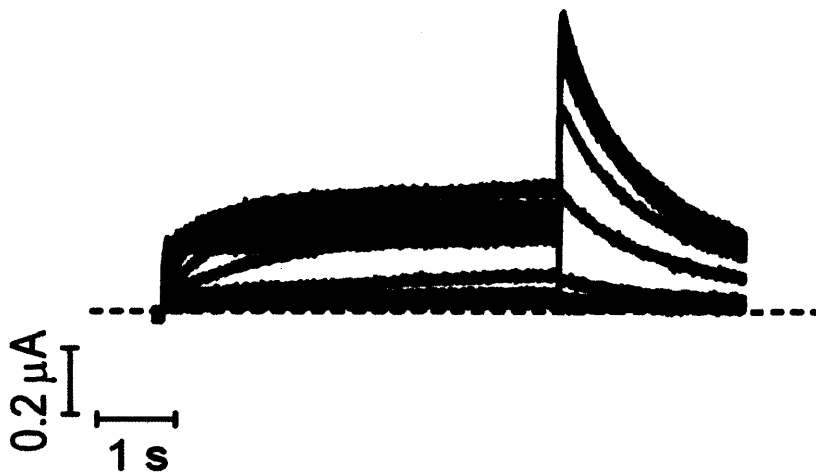
Hygromycin resistance was conferred to the cells upon transfection and the subsequent recombination event between the FRT sites on the expression vector and host cell line. In order to identify the minimum concentration of hygromycin (Invitrogen) needed to kill untransfected mammalian cells, a kill curve for hygromycin was performed on the HEK-293 and CHO Flp-In cell lines.

Cells were first split into a 6-well plate, approximately 25 % confluent, and left to adhere overnight. The following day, culture media was replaced with 3 ml of media containing increasing concentrations of hygromycin (0, 10, 50, 100, 150, 200  $\mu\text{g ml}^{-1}$  hygromycin for HEK-293 cells and 0, 200, 300, 400, 500, 600  $\mu\text{g ml}^{-1}$  hygromycin for CHO cells). Selection media was replaced every 2-3 days and the percentage of surviving cells was recorded daily. The concentration of hygromycin with optimal effectiveness was determined as 50  $\mu\text{g ml}^{-1}$  hygromycin for HEK-293 cells and 400  $\mu\text{g ml}^{-1}$  hygromycin for CHO cells. These concentrations led to total cell death after 3-4 weeks of hygromycin addition. Hence these concentrations were used to generate the stable cell lines.

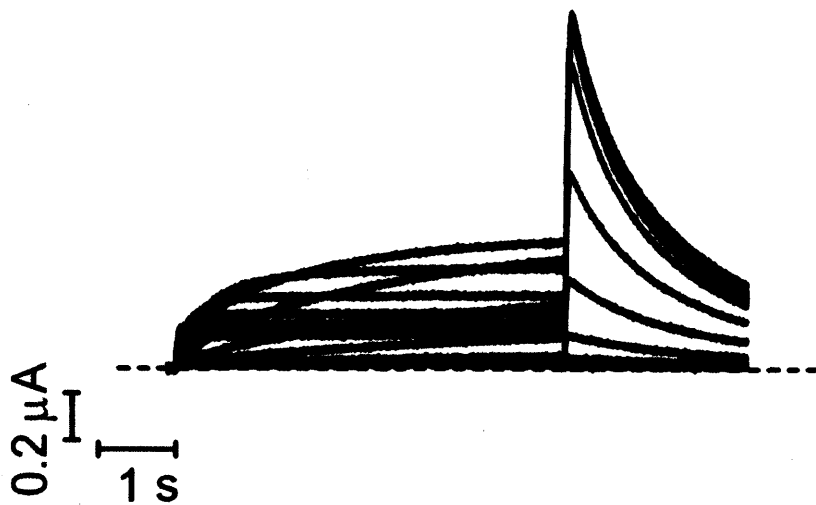
Chapter 4- Generation of stable cell lines

**Figure 4.5: Functional currents obtained for WT hERG in the pcDNA5/FRT expression vector.** WT hERG and *myc*-tagged WT hERG were subcloned into the pcDNA5/FRT expression vector. RNA was made and injected into *Xenopus* oocytes. Figures show representative currents using the I-V protocol of *myc*-tagged (i) and WT hERG (ii) in the pcDNA5/FRT vector.

(i)



(ii)



## Chapter 4- Generation of stable cell lines

### 4.5 Transfection methods

Following the manufacturer's recommendations, the HEK-293 and CHO Flp-In host cell lines were co-transfected with a 9:1 ratio of pOG44: pcDNA5/FRT/hERG plasmid DNA. A plate of untransfected cells was used as a negative control and the pcDNA5/FRT/CAT plasmid was used as a positive control. For each transfection sample, 10  $\mu$ l of Lipofectamine 2000 was diluted with 250  $\mu$ l of serum-free Opti-MEM media (Invitrogen) and incubated for 5 minutes at room temperature. In the meantime, 4  $\mu$ g of DNA made of a 9:1 ratio of pOG44: pcDNA5/FRT/hERG plasmid DNA was diluted to a total volume of 250  $\mu$ l in serum-free media Opti-MEM media. After the 5 minute incubation, the DNA was combined with the diluted Lipofectamine 2000 and incubated for 20 minutes at room temperature. The DNA-Lipofectamine complexes were added very slowly to cells in a 6-well plate, placed in culture media with serum but no antibiotics. 24 hours after transfection, fresh media was added to the cells. After 48 hours of transfection, cells were split into fresh media such that they were approximately 25 % confluent and incubated at 37 °C for 4-5 hours to adhere to the culture dish. Media was then replaced with 50  $\mu$ g ml<sup>-1</sup> hygromycin containing media for HEK-293 cells and 400  $\mu$ g ml<sup>-1</sup> hygromycin containing media for CHO cells. Media were changed every 3-4 days until hygromycin resistant colonies were evident. In theory, all of the hygromycin-resistant cells after co-transfection should be isogenic and expressing the hERG protein. Both WT hERG and *myc*-tagged WT hERG were transfected into HEK-293 as well as CHO Flp-In cell lines using this methodology.

### 4.6 Assay for hERG protein

Upon transfection into the mammalian cell lines, patch clamping experiments were carried out on antibiotic resistant cells. Unfortunately, these experiments showed no hERG currents. Colonies were also evaluated for hERG expression by western blot analysis on *myc*-tagged WT hERG with anti-*myc* antibody. No bands at 135 kDa (immature form of hERG) or 150 kDa (mature form of hERG) were observed, indicating the absence of hERG expression or else expression is too low to detect.

#### Chapter 4- Generation of stable cell lines

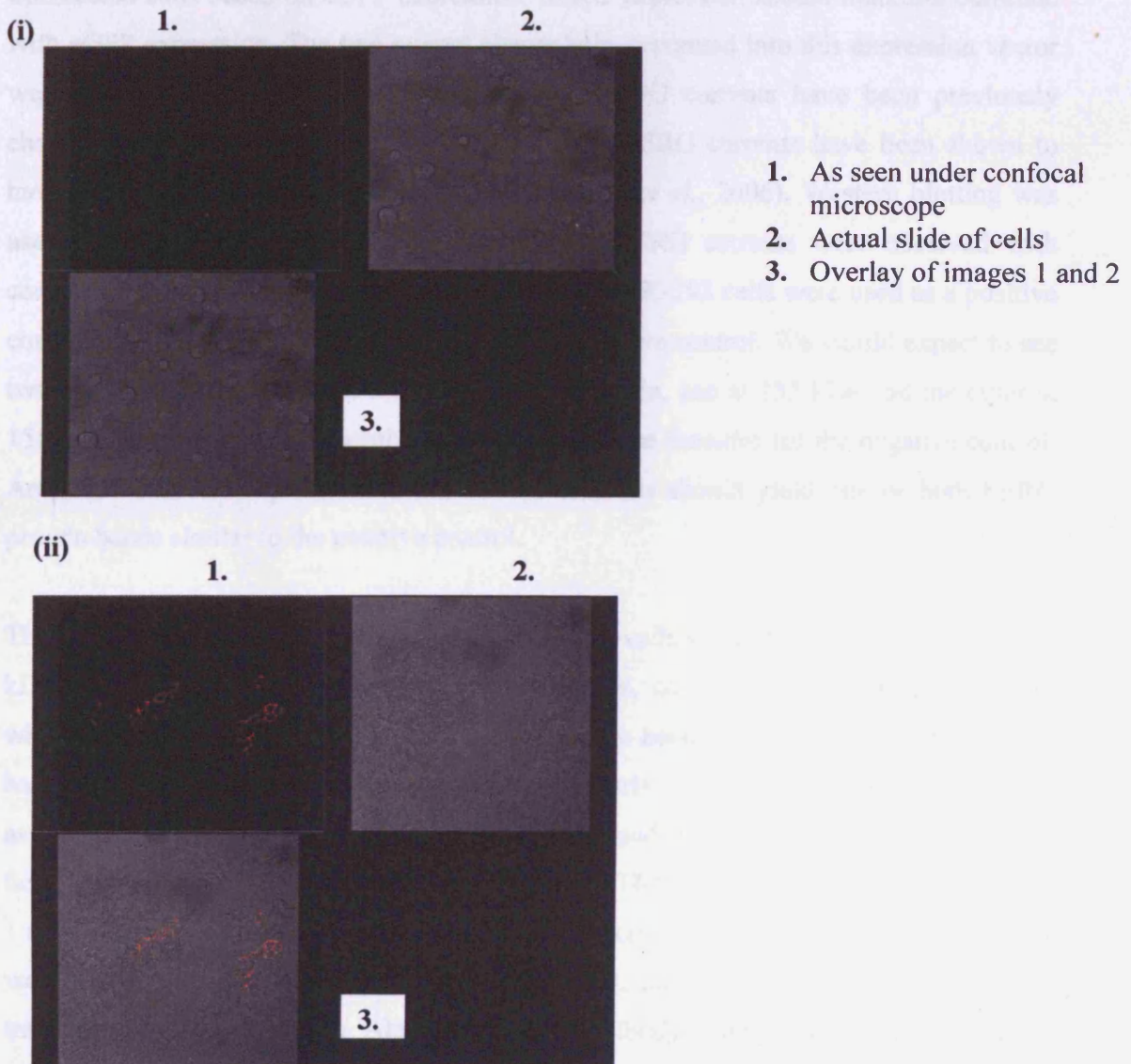
Immunocytochemistry staining was performed in order to detect the presence of any hERG protein in cells by using a fluorescent labelled antibody. This was done in the laboratory of Dr. Tania E. Webb (De Montford University, Leicester).

The staining protocol used was as follows. Cells stably transfected with *c-myc* hERG were seeded onto 0.1 % poly-lysine coated glass coverslips (15 mm in diameter) in 12-well plates at a concentration of  $2-3 \times 10^5$  cells per well. Cells were incubated overnight at 37 °C. The next morning, cells were fixed using 4 % neutral buffered formalin (NBF) at 4 °C for 15 minutes and 0.5 ml well<sup>-1</sup> of 0.2 % Triton in PBS for 5 minutes at room temperature. Subsequently, cells were washed 3 times with PBS and then blocked overnight at 4 °C using a 1 % BSA solution in PBS. Cells were then incubated for 2 hours at room temperature in the anti-*c-myc* primary antibody (Sigma Aldrich, USA) (1:500 using 1 % BSA), clone 9E10 from mouse (M5546). They were then washed 3 times with 0.5 ml PBS and incubated in secondary antibody for 1 hour in minimal ambient lighting. The secondary antibody was Cy3 sheep  $\alpha$ -mouse with an excitation peak at 550 nm and an emission peak at 570 nm (red fluorescent probe, Jackson ImmunoResearch). Confocal analysis was later performed on a Leica confocal microscope.

Cells in which incubation with primary antibody was omitted were used as a negative control and negligible fluorescence was detected on those slides. Unfortunately, experiments on stably transfected *myc*-tagged hERG Flp-In HEK-293 and CHO cells also failed to reveal detectable signals (Figure 4.6i). These cell lines therefore could not be used for the planned pharmacology studies using the high throughput patch clamping system. Figure 4.6(ii) shows similar experiments done on *myc*-tagged P2Y<sub>1</sub> receptors in HEK-293 Flp-In cells (courtesy of Dr. Rebecca Allsopp, De Montford University). These also showed low cell surface expression in only a few cells. This approach did not appear to work, as although cells were hygromycin resistant that did not correlate with expression of the hERG protein. This may be due to the decreased hERG expression in the pcDNA5/FRT vector or the possibility of random Flp-recombinase mediated integration into another genomic site resulting in hygromycin resistant cells, but not cells

#### Chapter 4- Generation of stable cell lines

**Figure 4.6: Confocal microscopy to investigate cell surface expression of *c-myc* hERG channels.** (i) These images are representative of experiments done on HEK-293 Flp-In transfected cells with *c-myc* hERG channels. Cells were grown on glass coverslips and after 48 hours fixed with 4 % NBF. Overnight blocking was in 1 % BSA solution. Immunofluorescence was detected with mouse anti-*c-myc* antibody, and Cy 3 (Ex 550 Em 570) conjugated secondary antibody. Similar results were obtained with the control and CHO Flp-In transfected cells. (ii) *Myc*-tagged P2Y<sub>1</sub> receptors in HEK-293 Flp-In cells were done under the same conditions and showed minimal fluorescence levels in only a few cells.



## Chapter 4- Generation of stable cell lines

that express the gene of interest. The fact that only a few cells expressed P2Y<sub>1</sub> receptors on the cell surface, further confirmed that this approach was not suitable for creating a stable cell line.

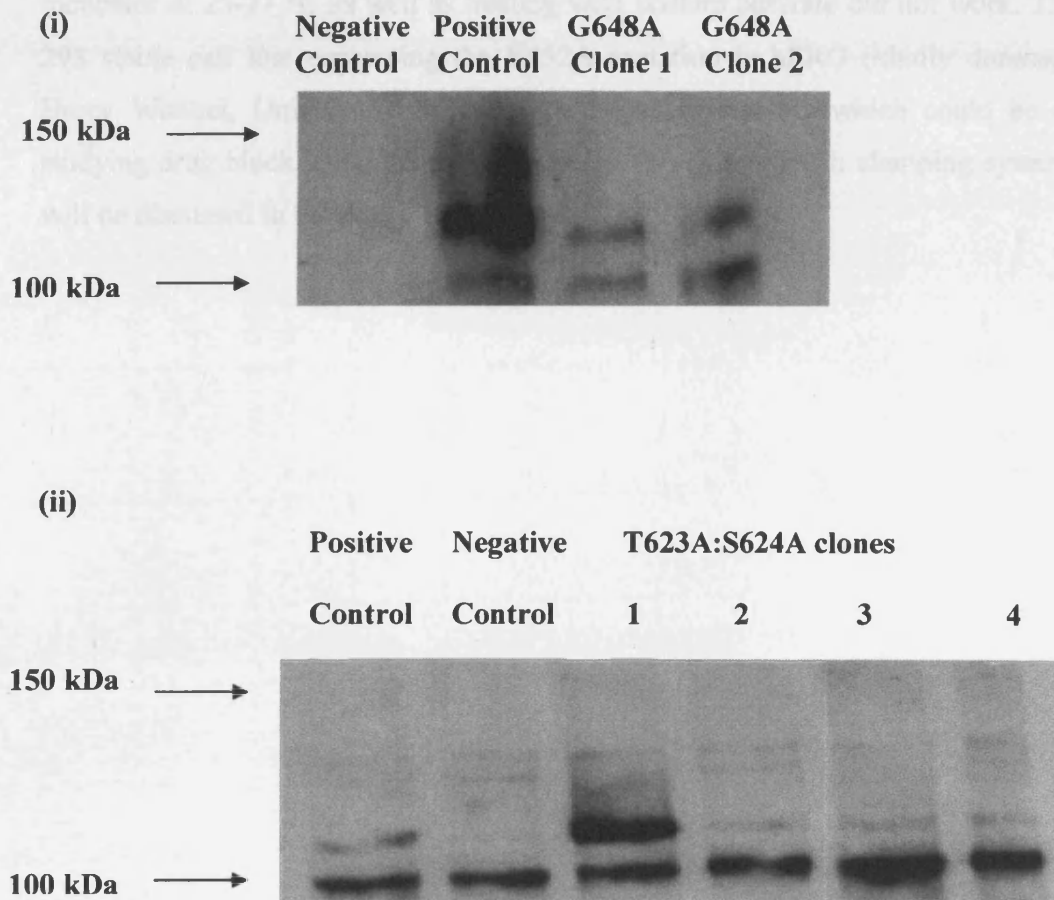
### 4.7 Generation of stable cell lines using Lipofectamine

Mutant stable cell lines were made using the pIRES2-eGFP-hERG construct, which was transfected into HEK-293 cells using Lipofectamine (as discussed in section 2.3.2). This vector allows the co-translation of hERG and the eGFP protein allowing the selection of transfected cells based on eGFP expression. hERG expression should therefore correlate with eGFP expression. The two mutant channels incorporated into this expression vector were G648A and T623A:S624A. The G648A hERG currents have been previously characterised in Chapter 3 and the T623A:S624A hERG currents have been shown to have similar characteristics to T623A hERG (Perry *et al.*, 2006). Western blotting was used to assess hERG expression, as no sizable hERG currents were observed with conventional patch clamping methods. WT hERG HEK-293 cells were used as a positive control and WT HEK-293 cells were used as a negative control. We would expect to see two bands indicating the presence of the hERG protein, one at 135 kDa and the other at 150 kDa, for the positive control and no bands at these densities for the negative control. Analysis of hERG expression in the mutant channels should yield one or both hERG protein bands similar to the positive control.

The positive control as well as the G648A HEK-293 cells showed mainly one band at 135 kDa indicating the presence of only the immature, core glycosylated hERG protein, which is located in the ER as well as a non-specific band at 100 kDa (Figure 4.7i). No bands were observed for the negative control. Similarly, the T623A:S624A clones as well as the positive control appeared to exhibit a single band at 135 kDa (Figure 4.7ii). A very faint band at 150 kDa could be seen in some of the T623A:S624A clones, such as clones 1 and 4. There was also a non-specific band at 100 kDa. We concluded that both mutants were likely to be expressed at the level of the ER, but did not seem to be efficiently transported to the cell surface. Alternatively, this antibody (kindly donated by Dr. Gail

Chapter 4- Generation of stable cell lines

**Figure 4.7: Western blotting analysis of hERG expression in the mutant cell lines. (i)** Representative western blot for the G648A HEK-293 cells transfected using the Lipofectamine 2000 methodology. Two different G648A clones with hERG HEK-293 cells as a positive control and WT HEK-293 cells as a negative control are shown. **(ii)** Representative western blot for a number of stably transfected T623A:S624A HEK-293 clones along with the same positive and negative controls.

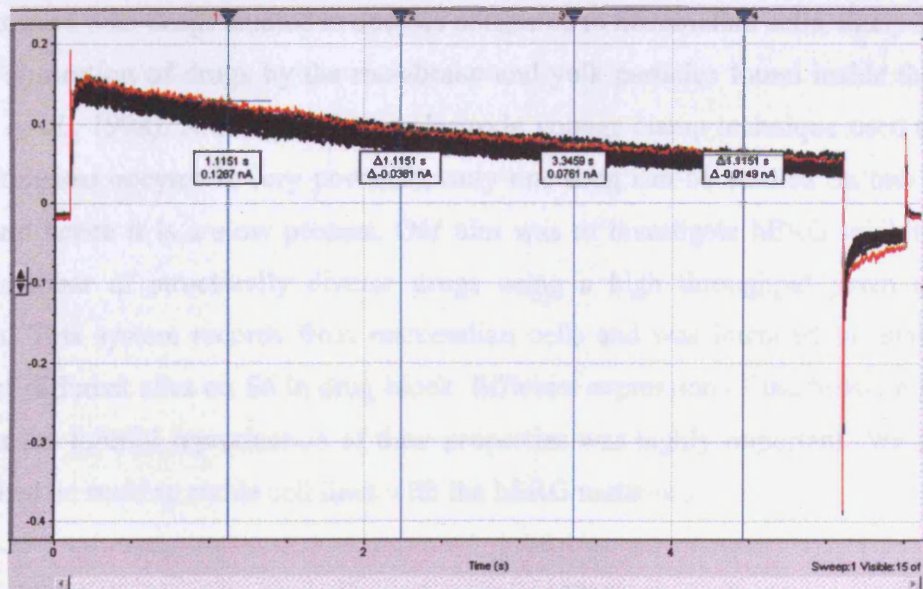


#### Chapter 4- Generation of stable cell lines

Robertson, University of Wisconsin) may not have been able to detect the mature, 150 kDa form of the hERG protein, in the control as well as the mutant HEK-293 cells as these cells exhibited good GFP expression. Cells were therefore tested for the presence of any hERG currents using a high throughput automated patch clamping system, the PatchXpress. Some samples showed very small hERG currents ( $< 200$  pA); however this was too little current to be used for pharmacological studies (Figure 4.8). Attempts to increase membrane expression (Robertson & January, 2006) by placing the cells in an incubator at 25-27 °C as well as treating with sodium butyrate did not work. The HEK-293 stable cell line expressing the Y652A mutation in hERG (kindly donated by Dr. Harry Witchel, University of Sussex) had sizable currents which could be used for studying drug block using the automated high throughput patch clamping system, which will be discussed in the next chapter.

## Chapter 4- Generation of stable cell lines

**Figure 4.8: Snapshot of T623A:S624A hERG currents using a high throughput patch clamping system.** This recording is representative of the T623A:S624A hERG currents obtained using a high throughput patch clamping system, the PatchXpress. An I-V protocol was elicited from a holding potential of -80 mV and with a tail potential of -150 mV in high extracellular  $K^+$  solution, giving a peak tail current of < 200 pA.



## Chapter 4- Generation of stable cell lines

### 4.8 Discussion

Expressing recombinant ion channels in heterologous systems is a powerful tool in the analysis of their biophysical and pharmacological properties. *Xenopus* oocytes have been extensively used in identifying the characteristics and structure-function relationships for a range of recombinant channels. Although this system is stable and robust, it can offer certain disadvantages. Optimal oocyte quality is critical for successful recordings and that may vary greatly between frogs. Ion channels may also exhibit biophysical properties in these systems that differ from mammalian channels found in their native environment, possibly due to the absence of accessory and regulatory proteins that would normally interact with these channels. In terms of pharmacological studies, lower drug potencies are observed with drugs studied in oocytes compared to mammalian cells, likely to be due to the absorption of drugs by the membrane and yolk particles found inside the oocyte (Zhou *et al.*, 1998). Although the two-electrode voltage clamp technique used to record from *Xenopus* oocytes is very powerful, only one drug can be studied on one cell at a time and hence it is a slow process. Our aim was to investigate hERG inhibition by a large number of structurally diverse drugs using a high throughput patch clamping system. This system records from mammalian cells and was intended to establish the roles of different sites on S6 in drug block. Efficient expression of the hERG mutants as well as the faithful reproduction of their properties was highly important. We therefore embarked on making stable cell lines with the hERG mutations.

To ensure that accurate properties of mutant hERG channels were reproduced in mammalian cells, these mutants were characterised using the two-electrode voltage clamp technique. In this chapter, we were interested in the roles of Gly648 and the pore helix residues (Thr623 and Ser624) in drug binding to hERG. It remains unclear why some drugs, such as ibutilide and clofilium (Perry *et al.*, 2004) are highly sensitive to Gly648 mutations while others are not. Similarly, the pore helix residues appear to be important for some drugs but not all. To address this issue, stable cell lines with hERG mutations at the pore helix and at the Gly648 residue were made in order to understand the structural basis that underlies these differences in drug binding. The effects of mutating Gly648 to

#### Chapter 4- Generation of stable cell lines

an alanine were studied and discussed in Chapter 3. In this chapter, I characterised the S624A and T623A hERG mutants. The S624A mutation had a similar midpoint of activation to WT hERG channels, although the time course of its activation was slower than WT channels. T623A hERG currents were recorded in 96 mM K<sup>+</sup> solution due to a negative shift in the midpoint of inactivation. Its activation and deactivation properties were shifted from WT channels; however this is not thought to be significant in altering drug block. The T623A:S624A hERG currents have also been previously shown to display similar characteristics to T623A hERG (Perry *et al.*, 2006).

Once the effects of these mutations on ionic currents were established in oocytes, it was then crucial to make stable cell lines, which would efficiently express the hERG protein with minimal cell-to-cell variation, optimal for high throughput electrophysiological recordings. The Flp-In system was therefore tested as an expression system to create stable cell lines expressing hERG. hERG was cloned into the pcDNA5/FRT expression vector, which is proposed to allow the integration of the hERG gene in a mammalian cell at the FRT site; creating isogenic clones. This should then ensure a rapid and efficient way of generating stable cell lines expressing hERG. Since expression could vary between cell lines, both CHO and HEK-293 Flp-In cell lines were used to identify the most highly expressing cell type. Both WT hERG and *myc*-tagged WT hERG (used for looking at hERG expression in western blots) were both cloned into the pcDNA5/FRT vector and RNA was made to confirm that these hERG constructs were functionally expressing by using the two-electrode voltage clamp. The currents obtained for both constructs in *Xenopus* oocytes were similar to WT hERG currents but smaller in amplitude. Co-transfecting the pOG44 plasmid, which constitutively expressed Flp recombinase, with the pcDNA5/FRT/hERG expression vector into the host cell line allowed the recombination between the FRT sites to occur. A stable cell line expressing hERG was generated and selected for hygromycin resistance. Patch clamping experiments, western blot analysis, as well as immunocytochemistry studies revealed no hERG expression in these cell lines. This was surprising since the cells would not have acquired hygromycin resistance if the recombination event had not occurred. However, it seemed that expression of hygromycin did not correlate with hERG surface expression,

#### Chapter 4- Generation of stable cell lines

and the possibility of a random Flp-recombinase mediated integration into another genomic site could not be excluded. In addition, the confocal images of the P2Y<sub>1</sub> receptor stably expressed in Flp-In HEK-293 cells revealed that not all cells were expressing the gene of interest, contrary to what was expected with this system in terms of the formation of isogenic cells. This system was therefore not suitable for making hERG expressing stable cell lines and did not seem to offer any advantages over other standard systems used.

We resorted to the standard lipid-based Lipofectamine method of transfection and the G648A and T623A:S624A mutant stable cell lines were generated using the pIRES2-eGFP-hERG construct. Clones were selected for using geneticin and resistant colonies picked according to GFP expression. The level of GFP expression however did not correlate well with mutant hERG surface expression when tested with patch clamping as well as western blotting techniques. It has been shown that there are a number of ways of increasing hERG trafficking to the cell surface (Robertson & January, 2006). Culturing cells at a reduced temperature (27 °C), the presence of pharmacological agents (E-4031, astemizole, and cisapride), and sodium butyrate treatment are a few ways of enhancing trafficking of functional channels into the plasma membrane. These processes are thought to stabilise intermediate states of the protein, thus promoting native protein folding and its export to the surface. Initial experiments were not effective in increasing hERG surface expression hence these cell lines were not used in pharmacological studies using the high throughput patch clamping system. It would be interesting though to investigate methodologies for improving expression of mutant hERG channels.



## Chapter Five- Structural determinants of hERG block

Developing ligand-based *in silico* models of hERG blockers depends greatly on the quality and reliability of the data on which the model was calculated. The consistency of this data is critical when building a good model. In this study, I investigated the action of a number of hERG blockers on channels stably expressing WT and Y652A hERG in HEK-293 cells. The Tyr652 residue has been identified as an important site of interaction for most hERG blockers (Mitcheson *et al.*, 2000a). All experiments were done under the same experimental conditions; thus cell type, voltage protocol, and recording solutions were all kept constant. An automated, medium-throughput patch clamp system, the PatchXpress 7000A (Axon Instruments, Molecular Devices Corporation, USA) was used to measure the concentration-response relationships of compounds against hERG. 24 LQT-associated compounds with various structures were chosen for this study. They appeared to encompass a range of potencies for hERG block as reported in the literature and had been investigated in numerous cell types. A larger number of compounds were tested than would have been possible with conventional patch clamping techniques. Inhibition of WT hERG currents was compared with Y652A hERG to investigate the importance of this mutation on the potency of compounds.

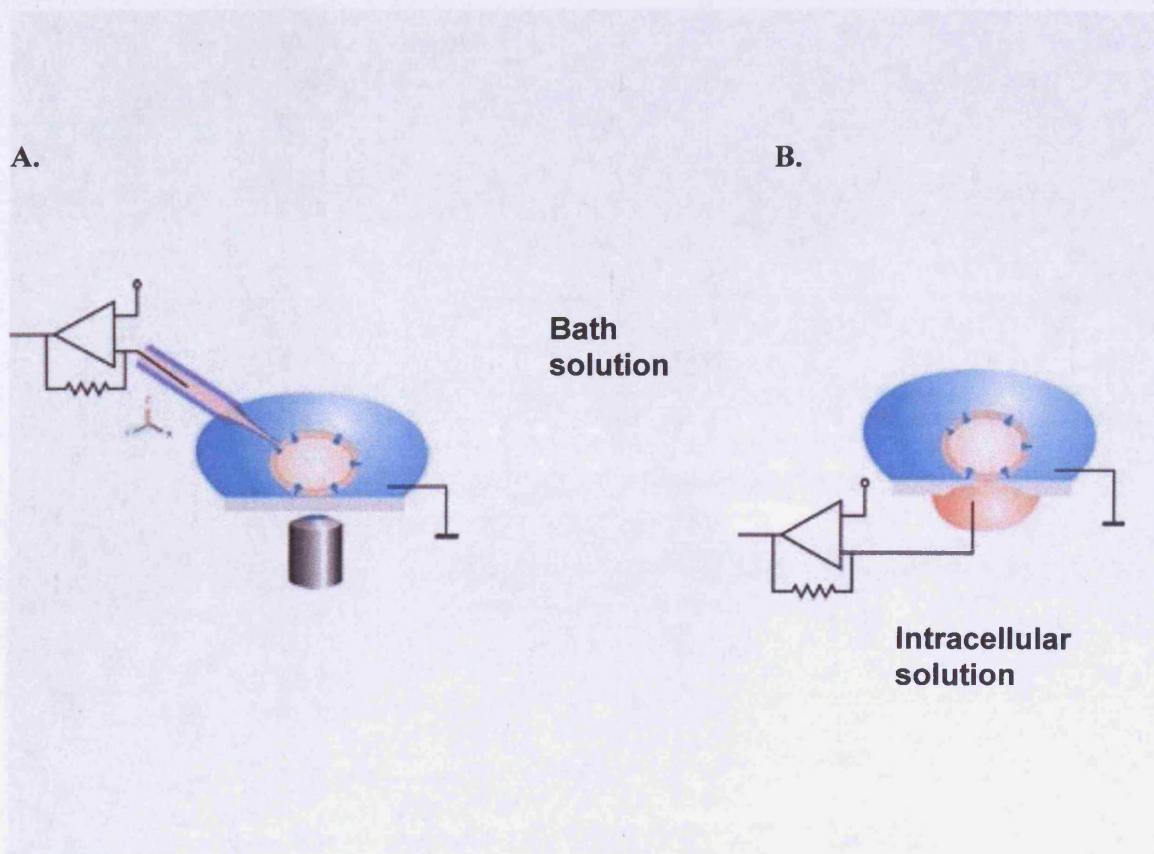
### 5.1 The PatchXpress 7000A

The PatchXpress is a fully automated patch clamping system used to make electrophysiological whole-cell recordings from individual cells. It makes use of the planar electrode technology, which has distinct advantages over conventional patch clamping methods (Figure 5.1). The classical patch clamping method involves the positioning of a glass pipette on a cell in order to form a tight electrical seal, which is then ruptured by suction to gain access into the cell. This technique requires skill and precise micromanipulation of the glass pipette under a high power microscope to record from one cell at a time. The automated device, on the other hand, consists of a planar chip with small apertures that replace the tip of the glass pipettes. A cell suspension is added onto the patch clamp chip and a number of pressure and suction protocols allow the formation of a seal through positioning of a cell on the aperture of the chip. High resistance seals are formed and whole cell access into the cell achieved by further suction. Since the chip has numerous apertures, recordings can be made from a number of cells in parallel. This device can be fully automated and is therefore less labour intensive with a much higher throughput rate, enhanced by the integrated recording software and automated fluidics.

The PatchXpress can perform parallel recordings on up to 16 cells simultaneously by using the *SealChip16* (AVIVA Biosciences, San Diego, CA). The *SealChip16* electrode consists of 16 holes, each 1-2  $\mu\text{m}$  in diameter, which act completely independently from one another (Figure 5.2). Each chamber is loaded with approximately 45  $\mu\text{l}$  of intracellular solution while extracellular solution is perfused from the top of the chamber through a 16-nozzle wash station. The electrode fits over an electrode base plate made up of 16 Ag/AgCl electrode tubes used for pressure control to seal, rupture, and hold the cells. Suction is used to achieve electrical access to the cells and high resistance (Gigaohm) seals can be formed. Other parameters such as capacitance and series resistance compensation can be controlled. The PatchXpress allows continuous whole cell recordings to be made during the whole process of compound addition and washoff and utilising diverse voltage protocols. Multiple drug concentrations can be added to a single cell allowing concentration-response curves to be generated for individual cells making

## Chapter Five- Structural determinants of hERG block

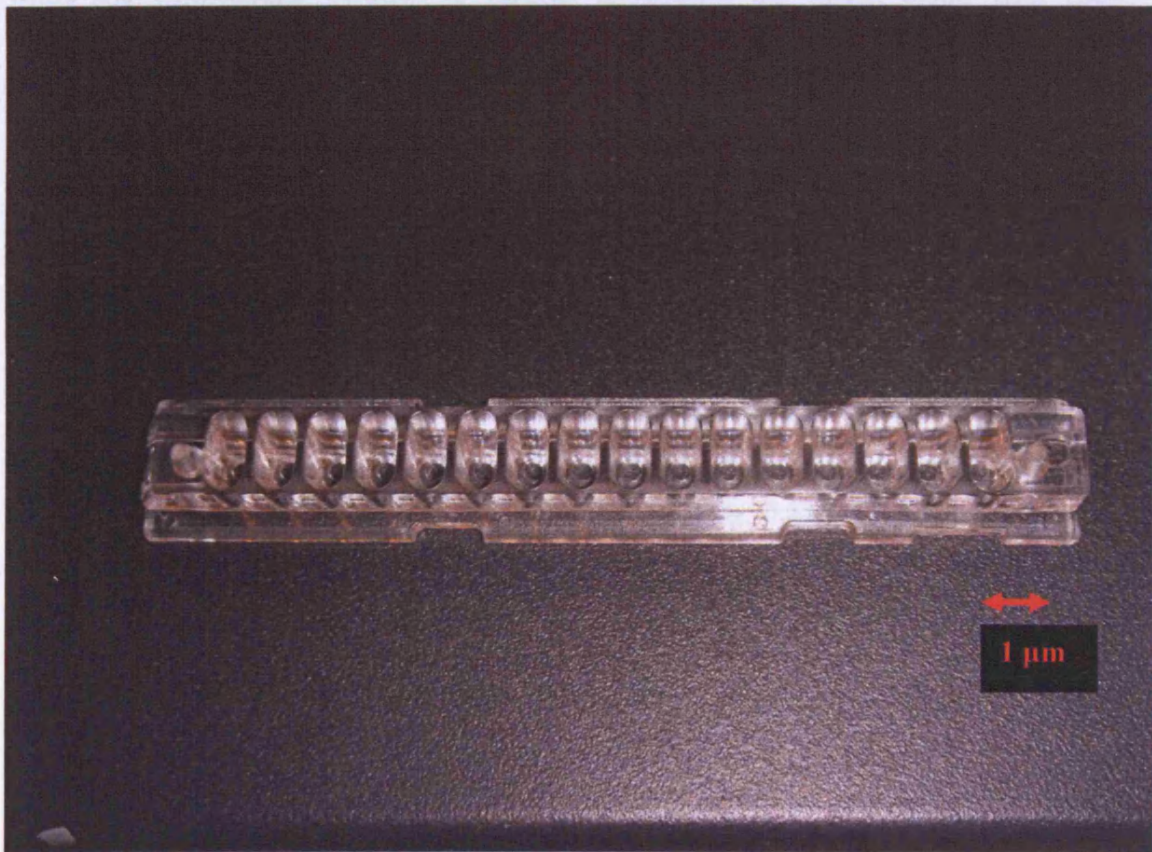
**Figure 5.1: Patch clamping methodologies: Conventional versus planar.** This is a diagrammatic representation of a conventional (A.) and a planar patch (B.), illustrating the differences between them. Instead of the manual manipulation of the glass pipette towards a cell in the conventional methodology, planar technology allows the cell to be attracted by suction to the aperture of an electrode chip. The cells are placed in bath solution and whilst pipettes in classical methods contain intracellular solution, in planar methods intracellular solution is loaded into the bottom of each chamber.



*Adapted from: <http://en.wikipedia.org/wiki/Electrophysiology>*

## Chapter Five- Structural determinants of hERG block

**Figure 5.2: SealChip16 electrode.** This is a top view picture of the *SealChip16* electrode used in the PatchXpress recordings. It consists of 16 wells which are independent from one another. Each well is  $\sim 1 \mu\text{m}$  in diameter, aligned 4.5 mm apart and can contain up to 250  $\mu\text{l}$  of solution.



## Chapter Five- Structural determinants of hERG block

it a high content automated system.

Other features of the PatchXpress include 8 MultiClamp amplifiers, a 16-channel 1322A digitiser, and a movable arm. A master controller is responsible for controlling the pressure and fluidics to the electrode chambers. It also has a separate vacuum pump (Edwards RV5) and air compressor (SilentAire). In the cabinet, there is an electrode holder and an electrode drying station, as well as waste chutes for used tips and electrodes. An intracellular solution filling station is located at the back of the cabinet while the extracellular solution is located underneath the bench along with fluid containers for waster and waste (Figure 5.3).

Multiple preparation stages are required for successful whole cell recordings to be made using the PatchXpress. These include the optimisation of cell preparation, solutions, and experimental procedure and will be discussed in detail in the sections to follow.

### 5.2 Solutions

The extracellular solution used was Hank's Balanced Salt Solution (Invitrogen) containing (in mM); CaCl<sub>2</sub>, 1.26; MgCl<sub>2</sub>-6H<sub>2</sub>O, 0.293; MgSO<sub>4</sub>-7H<sub>2</sub>O, 0.407; KCl, 5.33; KH<sub>2</sub>PO<sub>4</sub>, 0.441; NaHCO<sub>3</sub>, 4.17; NaCl, 137.93; Na<sub>2</sub>HPO<sub>4</sub>, 0.338; D-Glucose, 5.56 and was then supplemented with 5 mM HEPES, pH 7.4.

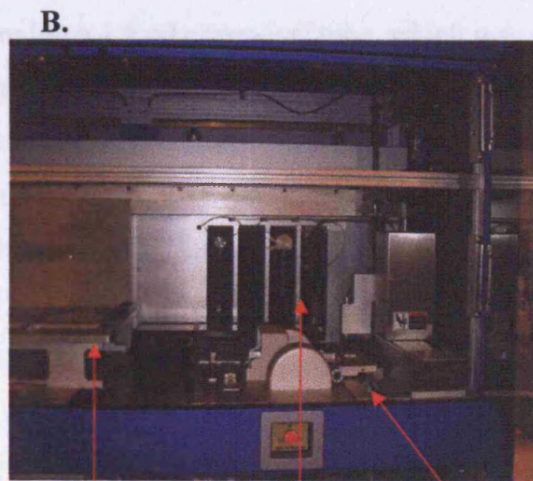
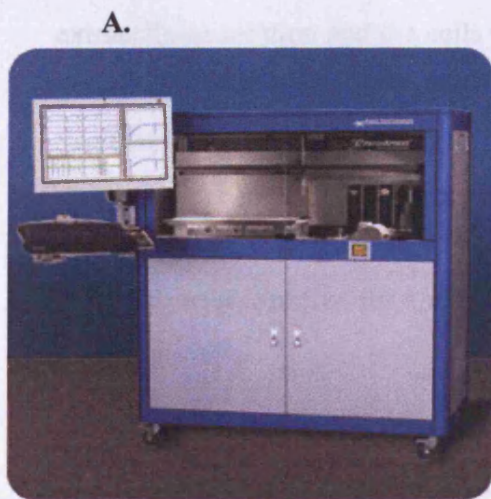
The intracellular solution contained (in mM); KCl, 130; MgCl<sub>2</sub>, 1; HEPES, 10; EGTA, 5; MgATP, 5; pH 7.2. 10 ml aliquots were stored at -20 °C to avoid degradation of ATP and thawed and kept on ice on the day of the experiment.

### 5.3 Cell Preparation

The cell preparation process is significantly different in planar electrophysiological techniques from conventional patch clamping methodologies. Optimising the cell culturing conditions for each cell line is also particularly important when using planar technology. Since it eliminates the step of choosing the best cell based on morphology, cell conditions therefore need to be optimal to ensure high success rates with these experiments.

Chapter Five- Structural determinants of hERG block

**Figure 5.3: The PatchXpress 7000A and its components.** A. This shows the PatchXpress with its upper and lower cabinets, movable arm and computer system. B. The upper cabinet contains an electrode holder and drying station, as well as an intracellular solution filling station. The compound plate and cells are also placed in this cabinet. C. The lower cabinet contains the fluid containers for water and waste, as well as waste chutes for used tips and electrodes. 8 MultiClamp amplifiers and a 16-channel digitiser are also located below the bench.



Compound plate and cells

Intracellular solution station

Electrode drying station



Waste chutes for tips and electrodes

MultiClamp Amplifiers

Fluid containers

## Chapter Five- Structural determinants of hERG block

HEK-293 cells stably expressing WT hERG (kindly provided by Dr. Craig January, University of Wisconsin) or Y652A hERG channels (kindly provided by Dr. Harry Witchel, University of Sussex) were used for this study. Cells were grown until 60 – 80 % confluent. Cells were harvested using 0.05 % trypsin from one T-25 flask per *SealChip16*. Trypsin was added to the cells for approximately 90 s and then inactivated by the addition of 5 ml of medium. Cells expressing WT hERG were then placed in a 15 ml falcon tube and left in the incubator at 37 °C with 5 % CO<sub>2</sub> with the lid loosely attached for approximately 30 minutes. After this incubation period, the cells were centrifuged at 1000 rpm for 1 minute. The pellet was then resuspended with 130 µl of extracellular solution and the cells transferred to a 1.5 ml eppendorf tube, which was then placed in the PatchXpress ready for dispensing into the individual chambers of the *SealChip16* by the robotic arm (3 µl per chamber). Cells stably expressing Y652A hERG channels were prepared in a similar manner except that they were not left in the incubator for 30 minutes, but were centrifuged immediately after the addition of 5 ml of medium following trypsinisation for 1 minute as they seemed to be too fragile.

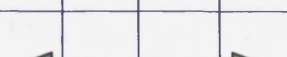
### 5.4 Compound preparation

Compounds were prepared by making up a stock solution of 100 mM for each compound in 100 % DMSO. Further DMSO stocks were prepared by serial dilution. Stock solutions were stored at 4 °C for no more than 2 weeks. On the day of the experiment, four concentrations of compound were prepared by a 1000-fold dilution into extracellular solution. Thus, the concentration of DMSO was always 0.1 %.

Compounds were prepared in a 96 well low-binding plate. The plate was divided in two (columns 1 - 6 and 7 - 12), ensuring that each compound could be applied to two different recording chambers (Figure 5.4). Each well contained 250 µl of solution. Columns 1 and 7 of the compound plate contained control solution with 0.1 % DMSO (vehicle control). Columns 2 - 5 and 8 - 11 contained increasing concentrations of the compounds being investigated. Finally, columns 6 and 12 contained 10 µM dofetilide, a concentration for

## Chapter Five- Structural determinants of hERG block

**Figure 5.4: Compound plate layout for use on the PatchXpress.** The 96 well plate was divided into two identical halves, containing a vehicle control (0.1 % DMSO) in columns 1 and 7, four increasing concentrations of the compound under investigation in columns 2 - 5 and 8 - 11 (Compound 1, Compound 2, Compound 3, or Compound 4), then a positive control containing dofetilide in columns 6 and 12. The second half of the plate was used for a second experiment using another electrode chip.

	1	2	3	4	5	6	7	8	9	10	11	12
<b>A</b>	DMSO					Dofetilide	DMSO					Dofetilide
<b>B</b>	DMSO					Dofetilide	DMSO					Dofetilide
<b>C</b>	DMSO					Dofetilide	DMSO					Dofetilide
<b>D</b>	DMSO					Dofetilide	DMSO					Dofetilide

## Chapter Five- Structural determinants of hERG block

maximal block for subtraction of leak from total ionic current. The second half of the plate (rows E – H) was identical to the first half and used for a second experiment on a different electrode chip, ensuring that at least 4 data points were obtained for each drug concentration on at least 2 different chips. The table in Figure 5.5 gives the list of the 24 compounds tested along with their structures.

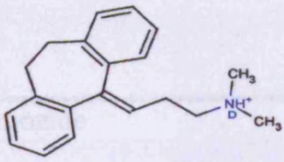
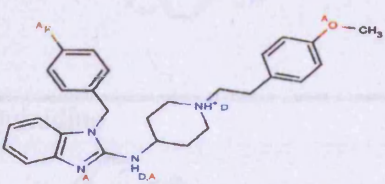
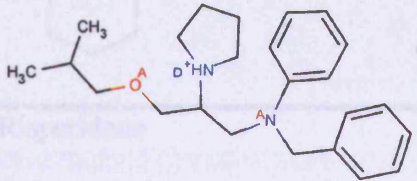
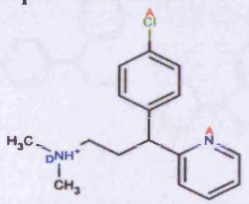
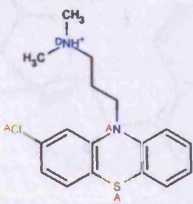
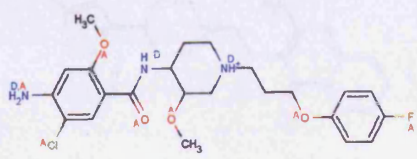
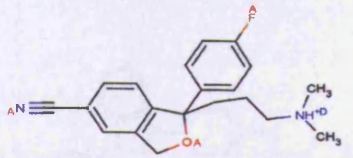
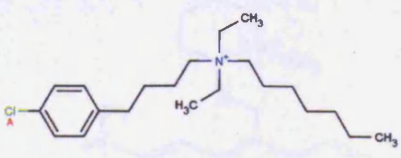
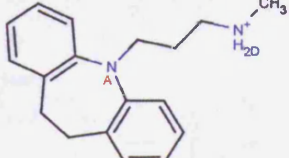
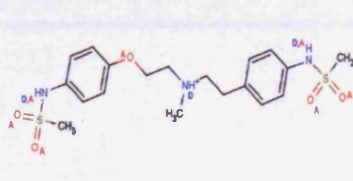
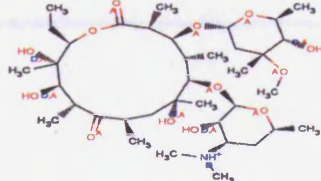
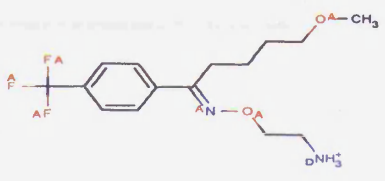
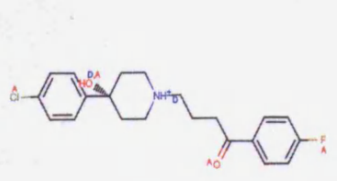
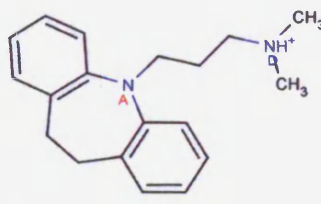
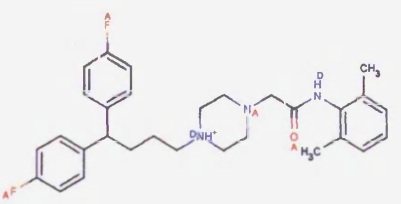
### 5.5 Seal formation

3  $\mu$ l of cell suspension was added to each chamber and a pressure of +10 mmHg (intracellular relative to extracellular chamber) was applied across the aperture to keep it free of debris. High resistance seals were made by the application of a series of pressure ramps/pulses to the chambers. The first pulse of pressure (-40 mmHg) attracted the cells to the apertures. Chambers were rejected if no cells were detected in a particular aperture after 90 s of cell addition. When the seal resistance exceeded 15 M $\Omega$ , a holding potential of -80 mV and a second pressure pulse (stabilisation pressure of 0 mmHg) was then applied. Seal formation was achieved by the application of repeated negative pressure ramps to -30 mmHg at a rate of -6 mmHg s<sup>-1</sup>. Whole cell access to rupture the patch was achieved by applying repeated pressure ramps to -200 mmHg at a rate of -13 mmHg s<sup>-1</sup>. If a cell entered the whole-cell configuration prior to achievement of a Giga-ohm seal, it was marked as “premature”. If a Giga-ohm seal was not achieved within 5 minutes of seal formation, then seal resistance for progression to whole cell was lowered to 250 M $\Omega$  and the cells were marked as “second chance seals”.

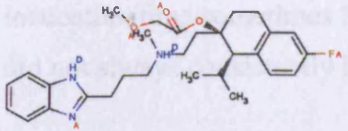
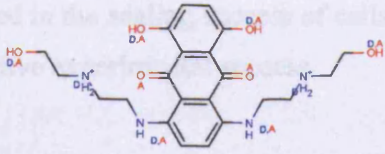
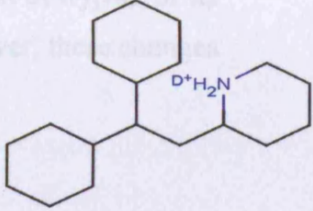
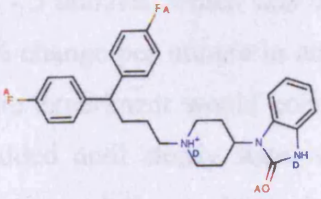
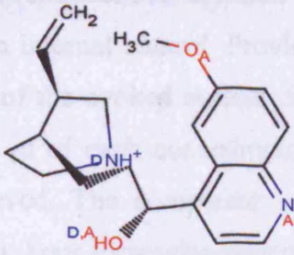
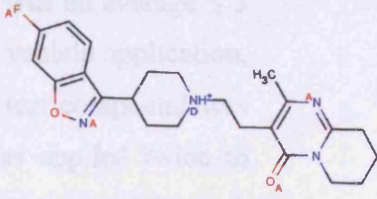
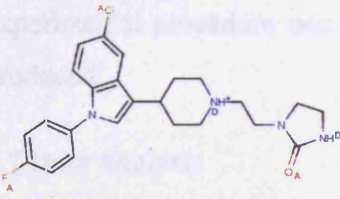
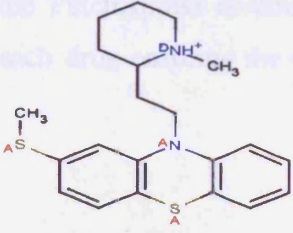
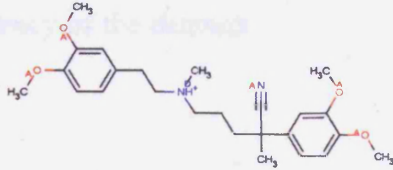
When the membrane capacitance ( $C_m$ ) was greater than 5 pF, the access resistance ( $R_a$ ) was less than 20 M $\Omega$ , and the membrane resistance ( $R_m$ ) was greater than 100 M $\Omega$ , the voltage protocol to record ionic currents was then initiated. The holding potential was -80 mV and a 5 s depolarising step to +20 mV ensured that the channels were kept in the open/inactivated state for a significant period of time. Peak tail currents were measured on return to -50 mV for 400 ms. The sweep start to start interval of this protocol was 6 s. Currents were filtered at 1 kHz and sampled at a frequency of 5 kHz. On days when the

Chapter Five- Structural determinants of hERG block

**Figure 5.5: LQT-compounds and their structures.** This table is a list of the 24 compounds chosen to be studied with WT and Y652A hERG channels. The structures of these compounds are also shown.

<p><b>Amitriptyline</b></p> 	<p><b>Astemizole</b></p> 	<p><b>Bepridil</b></p> 
<p><b>Chlorpheniramine</b></p> 	<p><b>Chlorpromazine</b></p> 	<p><b>Cisapride</b></p> 
<p><b>Citalopram</b></p> 	<p><b>Clofilium</b></p> 	<p><b>Desipramine</b></p> 
<p><b>Dofetilide</b></p> 	<p><b>Erythromycin</b></p> 	<p><b>Fluvoxamine</b></p> 
<p><b>Haloperidol</b></p> 	<p><b>Imipramine</b></p> 	<p><b>Lidoflazine</b></p> 

Chapter Five- Structural determinants of hERG block

<p><b>Mibefradil</b></p>  <p>The structure of Mibefradil features a central benzofuran core. It has a methyl group (H<sub>3</sub>C) and a propyl chain with a secondary amine (NH) attached to the benzofuran oxygen. The propyl chain is further substituted with a methyl group (H<sub>3</sub>C) and a piperazine ring. The piperazine ring is linked to a benzimidazole ring system. A fluorine atom (F) is attached to the benzimidazole ring.</p>	<p><b>Mitoxantrone</b></p>  <p>Mitoxantrone is a tetracyclic anthraquinone derivative. It has a central anthraquinone core with two hydroxyl groups (OH) at the 1 and 8 positions. The 4 and 5 positions are substituted with two propyl chains, each containing a secondary amine (NH) and a hydroxyl group (OH) at the end.</p>	<p><b>Perhexiline</b></p>  <p>Perhexiline consists of a central piperazine ring. The two nitrogen atoms of the piperazine ring are each substituted with a propyl chain. The propyl chains are further substituted with a methyl group (H<sub>3</sub>C) and a piperidine ring.</p>
<p><b>Pimozide</b></p>  <p>Pimozide has a central piperazine ring. One nitrogen of the piperazine ring is substituted with a propyl chain that is further substituted with a methyl group (H<sub>3</sub>C) and a piperidine ring. The other nitrogen of the piperazine ring is substituted with a propyl chain that is further substituted with a methyl group (H<sub>3</sub>C) and a piperidine ring. The piperidine rings are further substituted with a methyl group (H<sub>3</sub>C) and a piperidine ring.</p>	<p><b>Quinidine</b></p>  <p>Quinidine is a tetracyclic quinoline derivative. It has a central quinoline core with a methyl group (H<sub>3</sub>C) at the 8 position. The 4 and 5 positions are substituted with two propyl chains, each containing a secondary amine (NH) and a hydroxyl group (OH) at the end.</p>	<p><b>Risperidone</b></p>  <p>Risperidone features a central piperazine ring. One nitrogen of the piperazine ring is substituted with a propyl chain that is further substituted with a methyl group (H<sub>3</sub>C) and a piperidine ring. The other nitrogen of the piperazine ring is substituted with a propyl chain that is further substituted with a methyl group (H<sub>3</sub>C) and a piperidine ring. The piperidine rings are further substituted with a methyl group (H<sub>3</sub>C) and a piperidine ring.</p>
<p><b>Sertindole</b></p>  <p>Sertindole has a central piperazine ring. One nitrogen of the piperazine ring is substituted with a propyl chain that is further substituted with a methyl group (H<sub>3</sub>C) and a piperidine ring. The other nitrogen of the piperazine ring is substituted with a propyl chain that is further substituted with a methyl group (H<sub>3</sub>C) and a piperidine ring. The piperidine rings are further substituted with a methyl group (H<sub>3</sub>C) and a piperidine ring.</p>	<p><b>Thioridazine</b></p>  <p>Thioridazine is a tetracyclic thiazine derivative. It has a central thiazine core with a methyl group (H<sub>3</sub>C) at the 4 position. The 2 and 5 positions are substituted with two propyl chains, each containing a secondary amine (NH) and a hydroxyl group (OH) at the end.</p>	<p><b>Verapamil</b></p>  <p>Verapamil features a central piperazine ring. One nitrogen of the piperazine ring is substituted with a propyl chain that is further substituted with a methyl group (H<sub>3</sub>C) and a piperidine ring. The other nitrogen of the piperazine ring is substituted with a propyl chain that is further substituted with a methyl group (H<sub>3</sub>C) and a piperidine ring. The piperidine rings are further substituted with a methyl group (H<sub>3</sub>C) and a piperidine ring.</p>

## Chapter Five- Structural determinants of hERG block

cells were not sealing very well, sucrose was added to the intracellular solution to raise the osmolarity to approximately 300 mOsm. Changing the concentration of trypsin or its incubation time sometimes helped in the sealing success of cells. However, these changes did not always consistently improve experimental success.

### 5.6 Experimental procedure

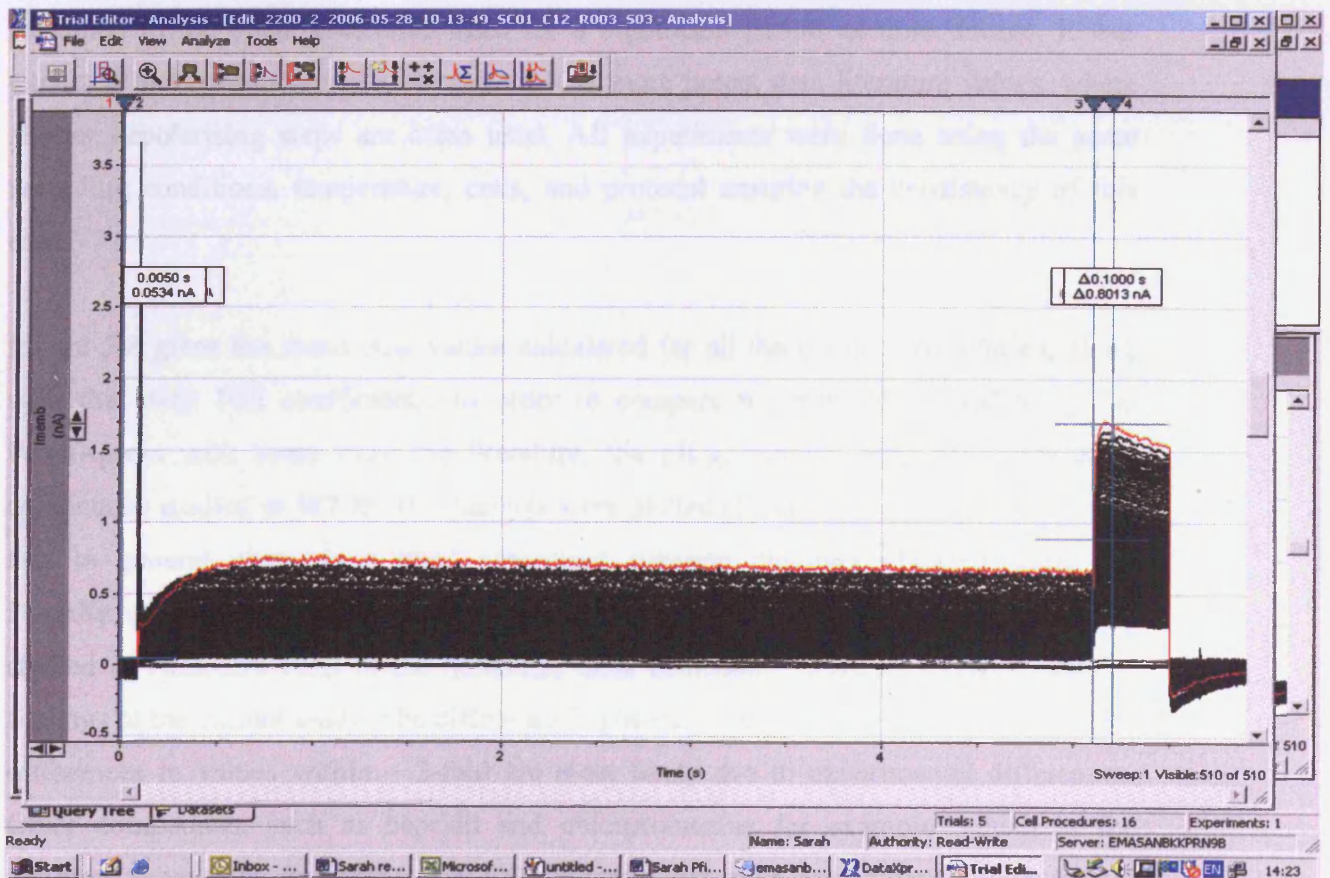
The automated microfluidics machinery would first apply extracellular solution for 2 minutes followed by vehicle control (extracellular solution containing 0.1 % DMSO) for 2 - 5 minutes, which was used as an internal control. Provided there was on average  $\leq 3$  % change per minute in amplitude of the evoked current during the vehicle application, the experiment would continue. 45  $\mu$ l of each concentration of the test compound was added until steady state was achieved. The compound solution was applied twice to ensure solution exchange in the well. Four increasing concentrations were tested for each cell, followed by 10  $\mu$ M dofetilide. The voltage protocol was repeated every 6 s and resulting currents were recorded by the PatchXpress commander software. The same experimental procedure was used for each drug ensuring the consistency of the datasets produced.

### 5.7 Data analysis

On completion of the experiment, data was automatically imported into the DataXpress database for further off-line analysis. Data was acquired and analysed using DataXpress software (Axon Instruments, Molecular Devices Corporation). Dofetilide-insensitive current was subtracted using the "Trial Editor" software facility. Cursors 1 and 2 were placed at 30 ms apart at the beginning of the sweep to measure baseline current. Cursors 3 and 4 were placed 100 ms apart to measure peak tail current. Figure 5.6 shows a representative current trace of WT hERG channels obtained using the PatchXpress with the cursors placed in their respective positions for analysis. Average values from 5 current traces were determined for controls and test compound concentrations. Constraints for minimum and maximum current block were 0.001 and 100 % respectively. The percentage inhibition was plotted against drug concentration and fitted

## Chapter Five- Structural determinants of hERG block

**Figure 5.6: WT hERG current traces using the PatchXpress.** Representative traces of WT hERG currents obtained using the PatchXpress. The currents were recorded in the presence of citalopram. Using "Trial Editor" in the DataXpress software, dofetilide insensitive current was subtracted, then cursors 1 and 2 were placed at the beginning of the sweep to monitor leak and current stability from measuring the holding current, while cursors 3 and 4 were used to measure peak tail current. The percentage of inhibition at each drug concentration was calculated and a concentration-response curve was fit with a Hill function to obtain the  $IC_{50}$  value for each drug.



## Chapter Five- Structural determinants of hERG block

using a Hill function, to give values for  $IC_{50}$  and Hill coefficient (Figure 5.7). The mean  $IC_{50}$  value for each drug was calculated for at least 4 cells, on at least 2 chips.

### 5.8 WT hERG concentration-response relationships

24 LQT compounds shown in the literature to block hERG channels were investigated using the PatchXpress. These compounds were chosen as their potencies covered a range of  $IC_{50}$  values that varied across 4 log units. They also had distinct structural properties and had been investigated in numerous cell types by utilising various voltage protocols. In this study, I measured the  $IC_{50}$  values for these compounds from concentration-response curves obtained using HEK-293 cells stably expressing WT hERG channels. The voltage protocol used was described in section 5.5 and ensured that the channel remained in the open/inactivated state for a significant period of time. Hence, it was expected that compounds would have an  $IC_{50}$  more potent than literature values, where shorter depolarising steps are often used. All experiments were done using the same recording conditions, temperature, cells, and protocol ensuring the consistency of this data.

Figure 5.8 gives the mean  $IC_{50}$  values calculated for all the compounds studied, along with the mean Hill coefficients. In order to compare the results obtained using the PatchXpress with those from the literature, the  $pIC_{50}$  values ( $-\log_{10} IC_{50}$ ) for these compounds studied in WT hERG channels were plotted (Figure 5.9). This plot illustrates that in general, there is a good agreement between the data obtained using the PatchXpress and conventional patch clamping methods. As expected for compounds studied in HEK-293 cells in the literature, most compounds were less potent than the findings of the current study. The difference in potencies ranged from 1.5 to 3-fold. These differences in values within ~ 3-fold are most likely due to experimental differences. Other compounds, such as bepridil and chlorpromazine for example, which in the literature have been investigated in COS-7 and CHO cells respectively, block hERG channels more potently using HEK-293 cells. Using the PatchXpress, bepridil had

Chapter Five- Structural determinants of hERG block

**Figure 5.7: Fluvoxamine concentration-response curve.** A. This table shows, for individual experiments (I, II, III, IV), the magnitude of WT hERG current inhibition in response to ascending concentrations of fluvoxamine and the resultant IC<sub>50</sub> and Hill slope obtained by analysis within DataXpress. The mean IC<sub>50</sub> and the Hill slope were then calculated. B. A typical concentration-response relationship showing the percentage of inhibition plotted against the log<sub>10</sub> drug concentrations and fitted with a Hill function to give values for IC<sub>50</sub> and Hill coefficient.

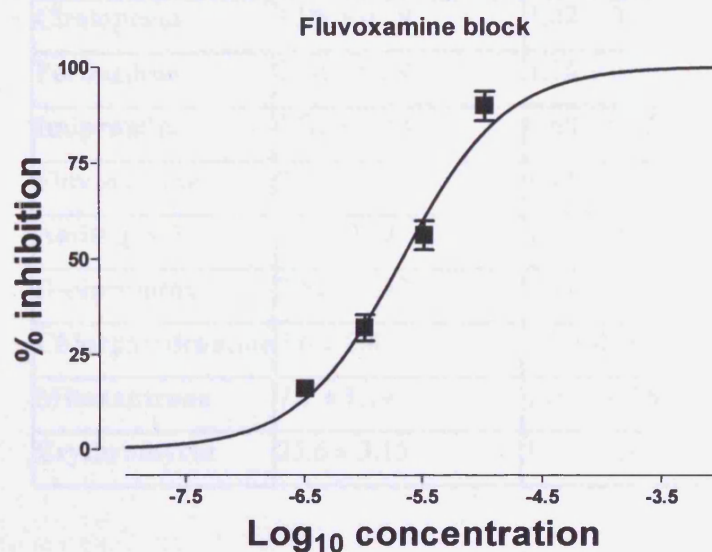
A.

Fluvoxamine concentrations (μM)	% inhibition (I)	% inhibition (II)	% inhibition (III)	% inhibition (IV)
0.3	10.16	17.73	15.92	20.04
1	23.02	37.19	37.47	29.66
3	57	65.99	52.44	48.42
10	100	83.39	91.23	84.06
IC <sub>50</sub> (μM)	2.186	1.623	1.922	2.439
Hill slope	1.799	0.939	0.981	0.881

Mean IC <sub>50</sub> (μM)	<b>2.043 ± 0.175</b>
Mean Hill slope	<b>1.15 ± 0.217</b>

B.



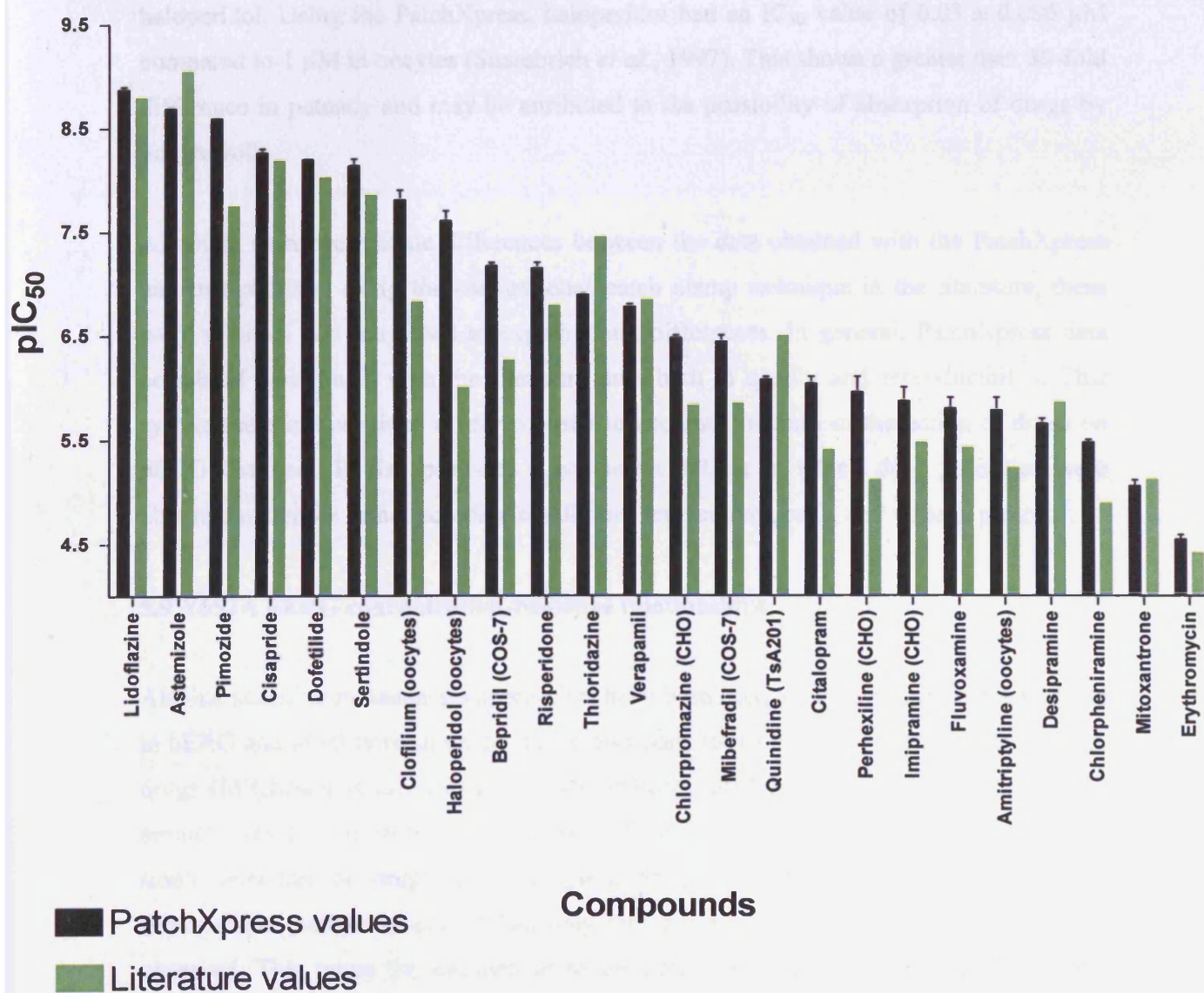
Chapter Five- Structural determinants of hERG block

**Figure 5.8: Results obtained on the PatchXpress using WT hERG channels. This table gives the mean IC<sub>50</sub> values (in ascending order), mean Hill coefficients, and n numbers for the 24 compounds studied on WT hERG channels using the PatchXpress.**

Compound	Mean WT IC <sub>50</sub> (μM)	Hill coefficient	n
Lidoflazine	0.00143 ± 0.0002	0.6 ± 0.065	4
Astemizole	0.0021 ± 0.00064	0.94 ± 0.23	5
Pimozide	0.0026 ± 0.001	0.55 ± 0.11	4
Cisapride	0.00598 ± 0.002	0.43 ± 0.07	5
Dofetilide	0.0064 ± 0.0013	1.1 ± 0.24	4
Sertindole	0.0084 ± 0.0018	0.87 ± 0.15	4
Clofilium	0.0192 ± 0.0037	0.87 ± 0.17	4
Haloperidol	0.031 ± 0.0059	0.91 ± 0.17	5
Bepriidil	0.074 ± 0.0099	1.1 ± 0.16	5
Risperidone	0.082 ± 0.004	1.001 ± 0.049	4
Thioridazine	0.132 ± 0.017	1.26 ± 0.22	4
Verapamil	0.179 ± 0.017	0.87 ± 0.084	4
Chlorpromazine	0.358 ± 0.036	1.31 ± 0.16	4
Mibefradil	0.42 ± 0.09	0.95 ± 0.2	4
Quinidine	0.9 ± 0.18	1.15 ± 0.26	4
Citalopram	1.08 ± 0.19	1.02 ± 0.19	4
Perhexiline	1.56 ± 0.29	1.36 ± 0.33	4
Imipramine	1.85 ± 0.48	0.68 ± 0.15	4
Fluvoxamine	2.04 ± 0.18	1.15 ± 0.22	4
Amitriptyline	2.2 ± 0.18	1.64 ± 0.22	4
Desipramine	2.52 ± 0.32	1.44 ± 0.25	4
Chlorpheniramine	3.6 ± 0.8	0.9 ± 0.19	4
Mitoxantrone	7.7 ± 1.14	1.03 ± 0.16	4
Erythromycin	25.6 ± 3.15	1.5 ± 0.26	5

## Chapter Five- Structural determinants of hERG block

**Figure 5.9: Comparison of pIC<sub>50</sub> values in WT hERG between the PatchXpress and literature data.** The IC<sub>50</sub> values for 24 LQT-compounds were determined using the PatchXpress in WT hERG HEK-293 cells. The pIC<sub>50</sub> (-log<sub>10</sub> IC<sub>50</sub>) values obtained using the PatchXpress were plotted in black and literature values were plotted in green. These values were very comparable. Most literature values were from experiments in HEK-293 cells. Other cell types used are indicated in brackets. Some of the error bars are very small.



## Chapter Five- Structural determinants of hERG block

an  $IC_{50}$  value of  $0.07 \pm 0.01 \mu\text{M}$  compared to  $0.55 \mu\text{M}$  in COS-7 cells (Chouabe *et al.*, 2000), while chlorpromazine had an  $IC_{50}$  of  $0.36 \pm 0.04 \mu\text{M}$  compared to  $1.5 \mu\text{M}$  in CHO cells (Kim & Kim, 2005). These larger shifts in  $IC_{50}$  equal to 4 and 8 fold differences for chlorpromazine and bepridil respectively are likely to be due to changes in the properties of each cell type. One possibility is that the transport of drugs into HEK-293 cells is more efficient than that into CHO and COS-7 cells, or that CHO and COS-7 cells express transporters, which extrude drugs. Even larger shifts in potency were also observed with some compounds, which had been previously studied in *Xenopus* oocytes, such as haloperidol. Using the PatchXpress, haloperidol had an  $IC_{50}$  value of  $0.03 \pm 0.006 \mu\text{M}$  compared to  $1 \mu\text{M}$  in oocytes (Suessbrich *et al.*, 1997). This shows a greater than 30-fold difference in potency and may be attributed to the possibility of absorption of drugs by oocyte yolk.

Although there were some differences between the data obtained with the PatchXpress and that obtained using the conventional patch clamp technique in the literature, these were minimal and attributed to experimental differences. In general, PatchXpress data correlated really well with the literature data both in quality and reproducibility. This system therefore provided a very robust and accurate measure of the action of drugs on hERG channels. It also provided a consistent dataset in which drug potencies were obtained under the same recording conditions, temperature, cells, and voltage protocol.

### 5.9 Y652A hERG concentration-response relationships

Alanine scanning mutagenesis approaches have been used to characterise the binding site in hERG and identify residues on the S6 and pore helix of the channel that interact with drugs (Mitcheson *et al.*, 2000a). For the majority of drugs tested to date, the Tyr652 aromatic residue on S6 has been shown to be a key site of interaction. However, for a small selection of drugs such as quinidine (Sanchez-Chapula *et al.*, 2003) and fluvoxamine (Milnes *et al.*, 2003a), only minor interactions with Tyr652 residue were observed. This raises the question as to the nature of binding to this residue and the reasons as to why it may be important for some drugs but not all.

## Chapter Five- Structural determinants of hERG block

Applying the same methodology, recording conditions, and voltage protocol as in WT hERG, the inhibition of Y652A hERG currents was also studied using the PatchXpress. The  $IC_{50}$  values of the same set of 24 compounds were determined and are reported in the table along with their Hill coefficients (Figure 5.10). In the literature, the effect of the Y652A mutation was tested on only a small sample of these compounds and often the  $IC_{50}$  values were not measured, instead only the percentage inhibition by a single concentration was reported. The data from this study could then be compared directly to WT values. The fold change in  $IC_{50}$  with the Y652A mutation was also calculated for these compounds. On the basis of this data, the compounds studied were divided into 2 groups, Group A and Group B (Figure 5.11). Group A compounds were the most potent compounds, with an  $IC_{50} < 100$  nM in WT hERG channels. Most Group A compounds exhibited a change in  $IC_{50} \geq 50$  fold in Y652A channels. On the other hand, Group B compounds were less potent with an  $IC_{50} > 100$  nM in WT hERG channels, and exhibited a change in  $IC_{50} < 10$  fold.

However, some exceptions to the trend were observed with several compounds such as haloperidol and bepridil in Group A. Although haloperidol and bepridil inhibited WT hERG currents with low nM potencies of 31 and 74 nM respectively, they only exhibited a 10 - 12 fold shift in  $IC_{50}$  in the presence of the Y652A mutation. This was dramatically smaller than the 50 - 400 fold change in  $IC_{50}$  seen with the other compounds in this group. Interestingly, thioridazine in Group B, blocked WT hERG with an  $IC_{50}$  only just over 100 nM, and exhibited only a 4.7 fold change in  $IC_{50}$  with the Y652A mutant.

It was expected that the most potent compounds would show the greatest change in  $IC_{50}$  with the Y652A mutation as their high affinity binding site would require the presence of this aromatic residue, in line with what has been previously reported in the literature. However, it was surprising that the Y652 mutation appeared to have little effects on the binding affinity of more than half the compounds studied. It was therefore important to then understand the structural basis of binding to the Tyr652 residue and provide an explanation to the exceptions seen.

Chapter Five- Structural determinants of hERG block

**Figure 5.10: Results obtained on the PatchXpress using Y652A hERG channels.** This table gives the mean IC<sub>50</sub> values, mean Hill coefficients, and n numbers for the 24 compounds studied on Y652A hERG channels using the PatchXpress.

Compound	Mean Y652A hERG IC <sub>50</sub> (μM)	Hill coefficient	n
Lidoflazine	0.57 ± 0.08	0.63 ± 0.04	4
Astemizole	0.24 ± 0.07	0.94 ± 0.13	4
Pimozide	0.59 ± 0.07	1.32 ± 0.28	4
Cisapride	1.67 ± 0.36	1.03 ± 0.09	4
Dofetilide	1.34 ± 0.4	1.32 ± 0.41	4
Sertindole	0.84 ± 0.4	1.12 ± 0.19	5
Clofilium	3.87 ± 0.7	1.57 ± 0.36	4
Haloperidol	0.38 ± 0.06	1.74 ± 0.13	4
Bepriidil	0.77 ± 0.21	1.14 ± 0.19	4
Risperidone	4.38 ± 1.41	0.69 ± 0.15	4
Thioridazine	0.63 ± 0.16	1.55 ± 0.31	4
Verapamil	0.68 ± 0.04	1.31 ± 0.06	4
Chlorpromazine	1.09 ± 0.19	1.05 ± 0.13	4
Mibefradil	1.07 ± 0.39	1.21 ± 0.34	4
Quinidine	0.15 ± 0.03	0.97 ± 0.41	7
Citalopram	1.28 ± 0.18	1.23 ± 0.8	4
Perhexiline	0.98 ± 0.4	1.44 ± 0.35	4
Imipramine	2.03 ± 0.47	1.39 ± 0.18	4
Fluvoxamine	11.22 ± 0.95	1.68 ± 0.14	4
Amitriptyline	2.11 ± 0.56	1.41 ± 0.25	4
Desipramine	2.58 ± 0.62	1.68 ± 0.17	4
Chlorpheniramine	6.01 ± 0.68	1.45 ± 0.3	4
Mitoxantrone	20.1 ± 4.7	1.24 ± 0.34	4
Erythromycin	248.69 ± 71.94	1.01 ± 0.25	4

## Chapter Five- Structural determinants of hERG block

**Figure 5.11: Compounds were divided into Groups A and B according to Y652A data.** Group A compounds were the most potent compounds, with an  $IC_{50} < 100$  nM in WT hERG channels, and which gave a fold change in  $IC_{50} \geq 50$  fold in Y652A channels (with 2 notable exceptions shown in red, haloperidol and bepridil). Group B compounds were less potent with an  $IC_{50} > 100$  nM in WT hERG channels, and which exhibited a fold change in  $IC_{50} < 10$  fold.

Group A			Group B		
Compound	WT $IC_{50}$ ( $\mu$ M)	Fold change Y652A $IC_{50}$	Compound	WT $IC_{50}$ ( $\mu$ M)	Fold change Y652A $IC_{50}$
Lidoflazine	0.00143	397.20	Thioridazine	0.132	4.76
Astemizole	0.0021	115.36	Verapamil	0.179	3.80
Pimozide	0.0026	228.37	Chlorpromazine	0.358	3.05
Cisapride	0.00598	278.34	Mibefradil	0.42	2.54
Dofetilide	0.0064	209.38	Quinidine	0.9	0.17
Sertindole	0.0084	100.17	Citalopram	1.08	1.19
Clofilium	0.0192	201.60	Perhexiline	1.56	0.63
Haloperidol	0.031	12.25	Imipramine	1.85	1.10
Bepridil	0.074	10.35	Fluvoxamine	2.04	5.55
Risperidone	0.082	53.41	Amitriptyline	2.2	0.96
			Desipramine	2.52	1.02
			Chlorpheniramine	3.6	1.67
			Mitoxantrone	7.7	2.61
			Erythromycin	25.6	9.71

## Chapter Five- Structural determinants of hERG block

### 5.10 Structural analysis of the PatchXpress data

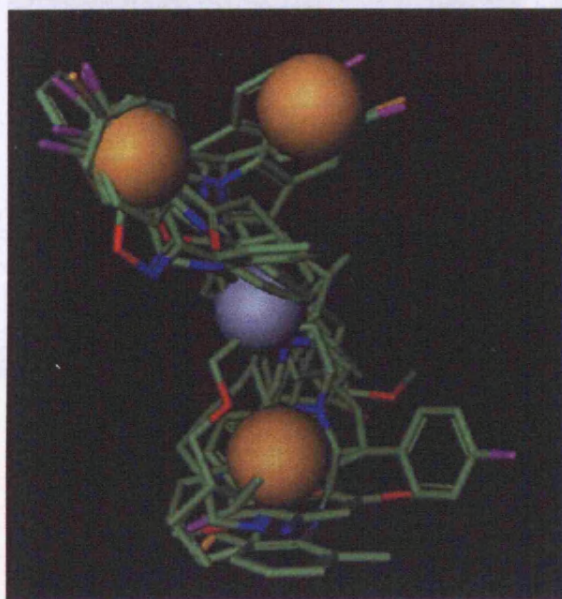
In an attempt to understand the interactions between each group of compounds and the hERG inner cavity, pharmacophoric analysis was performed at Pfizer using Phase software (version 2.02, Schrödinger, New York). A pharmacophore model gives a set of structural features and coordinates characteristic of a group of compounds. This can thus give an account of the molecular groups on drug molecules which may form particular interactions with its protein target. This tool is routinely used in the drug discovery process as a form of structure-based virtual screening for assaying a library of drug molecules rapidly and efficiently.

Default settings of this program were used throughout to generate pharmacophore hypotheses for each of our groups of compounds, which would incorporate the majority of compounds. The compounds in each group were first overlaid over each other to detect distinguishing characteristics of each group, with the exceptions of erythromycin and mitoxantrone in Group B, due to the bulkiness of their structures (Figure 5.12). The compounds in each group overlaid extremely well and an immediate structural difference was observed. Group A compounds had a long, extended conformation, in contrast to Group B compounds which appeared to be short and more compact. The molecular geometry of Group A compounds, for instance lidoflazine, could be described by the presence of a long molecular chain, with several aromatic, hydrophobic, and hydrogen-bonding groups. Group B compounds, such as amitriptyline, have much shorter molecular chains and some aromatic, hydrophobic, and hydrogen-bonding groups (see Figure 5.5). The overlays from each group in Figure 5.12 are shown within the pharmacophore that best described each set. The yellow spheres indicate hydrophobic groups, which may be aromatic, and the purple sphere indicates a basic nitrogen center. Both sets of compounds showed 2 hydrophobic regions and a basic centre. Although one or two compounds from each group may have extended to an extra hydrophobic region, the majority of compounds seemed to interact with 3 out of the 4 pharmacophoric groups. Figure 5.13 shows the 3-point pharmacophore developed for each group of compounds. However, only one of the hydrophobic groups found at position 1 and the basic nitrogen

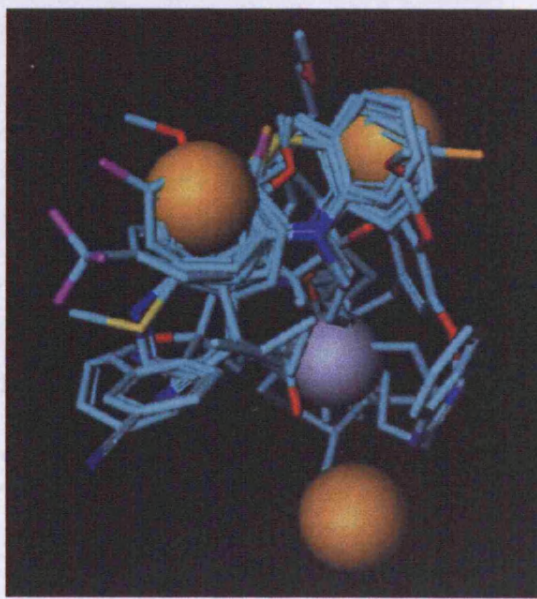
## Chapter Five- Structural determinants of hERG block

**Figure 5.12: Pharmacophoric overlay of compounds in Groups A and B.** Using Phase software, compounds in Group A and Group B (minus erythromycin and mitoxantrone) were overlaid on top of one another. Structural alignments for 10 compounds in Group A and 12 compounds in Group B are shown in green sticks and blue sticks respectively. The pharmacophore features common to most molecules are illustrated by yellow spheres (hydrophobic regions) and a purple sphere (basic central nitrogen group). Carbon atoms are shown in purple, oxygen atoms are seen in red, sulphur atoms in yellow, and nitrogen atoms in blue.

**Group A**



**Group B**

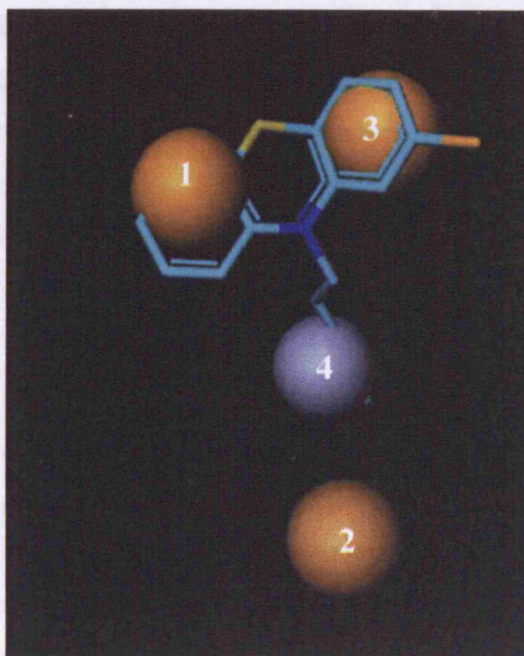
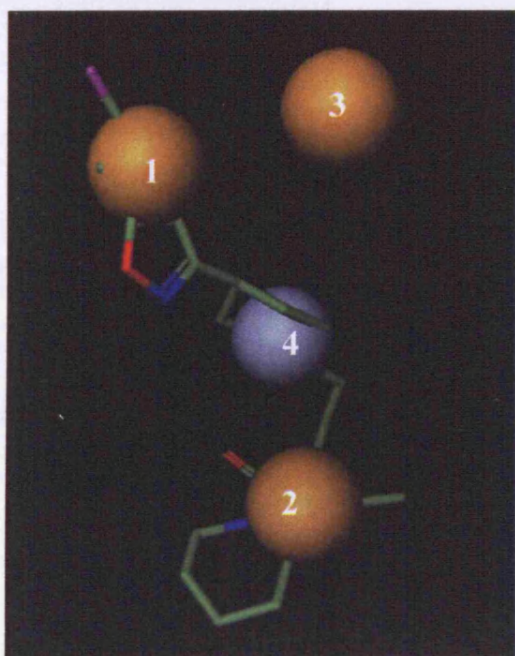


## Chapter Five- Structural determinants of hERG block

**Figure 5.13: Pharmacophore for Group A and Group B compounds.** A combined 4-point pharmacophore is shown with a representative compound from each group. The pharmacophore for Group A compounds is shown on the left with risperidone overlaid (in green sticks) showing that compounds from Group A exhibit pharmacophoric moieties at positions 1, 2, and 4. The pharmacophore for Group B compounds on the right is shown with amitriptyline overlaid (in blue sticks) and these compounds contain pharmacophoric moieties at positions 1, 3, and 4. Yellow spheres (1, 2, and 3) are hydrophobic regions and the purple sphere (4) is a basic nitrogen group.

**Group A**

**Group B**



## Chapter Five- Structural determinants of hERG block

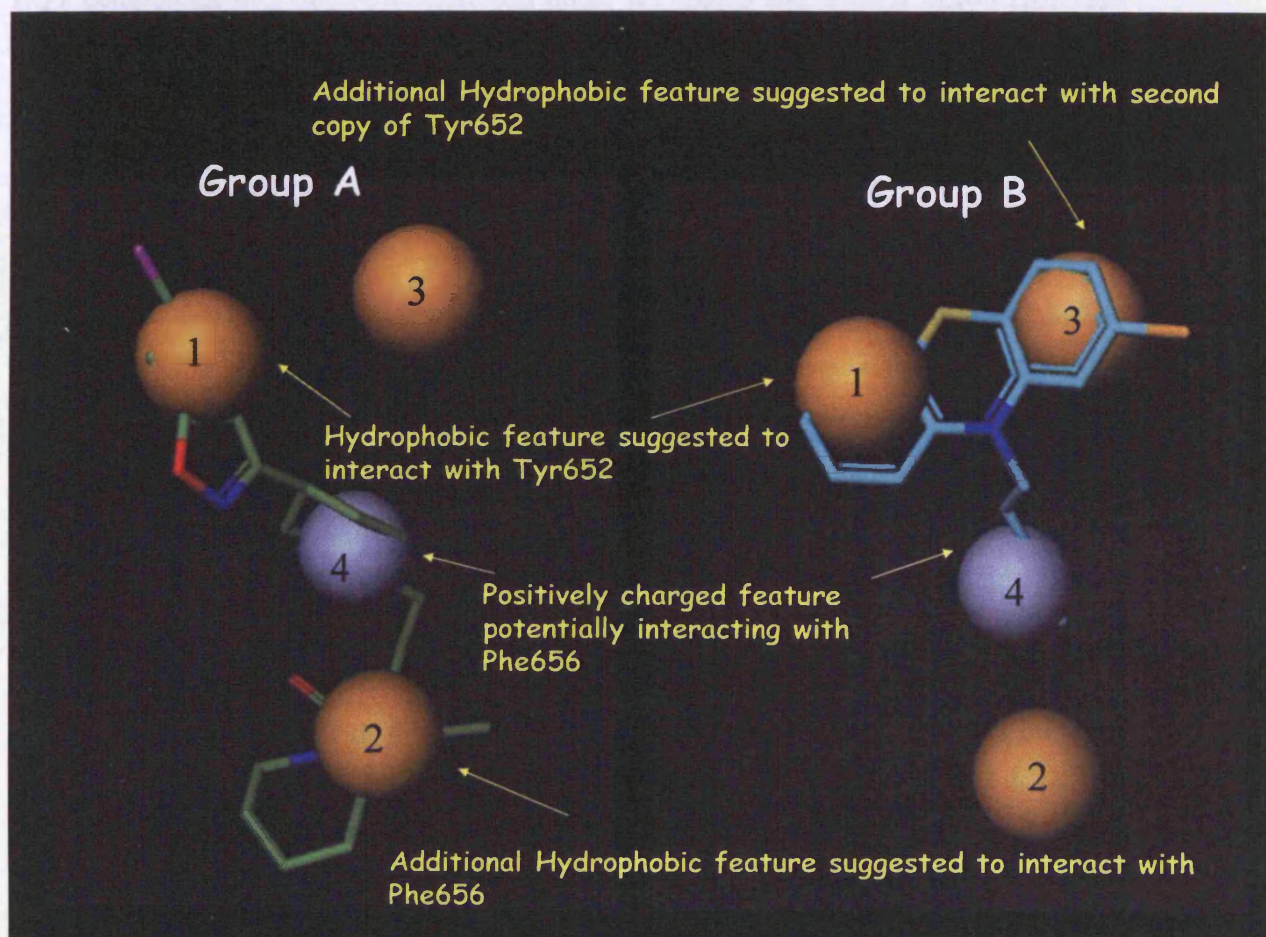
center were present in both sets. The position of the second hydrophobic feature differed. For the more elongated Group A compounds, this was located further away at position 2, whereas for the more compact Group B compounds, this was at position 3 adjacent to the first hydrophobic feature. The coordinates of the pharmacophores were as follows: groups 1 and 3 were 5 Å apart, groups 1 and 4 were 6 Å apart, groups 3 and 4 were 6.5 Å apart, and groups 4 and 2 were 4.5 Å apart.

Examining these pharmacophoric overlays within the homology model for hERG (Perry *et al.*, 2006), suggested possible interactions that these functional groups might form within the hERG channel (Figure 5.14). The hydrophobic feature at position 1, common to both groups of compounds, could form pi-pi interactions with the Tyr652 residue within the hERG inner cavity. The majority of Group A compounds also had a *para*-substituent, usually a halogen group, which could interact with pore helix residues. The charged nitrogen group also found in both pharmacophores could potentially form cation-pi interactions with the Phe656 residue in hERG. The second hydrophobic feature in Group A compounds found at position 2 might form pi-pi interactions with Phe656, while the hydrophobic feature at position 3 in Group B compounds might bind to a second copy of Tyr652 found on another subunit.

Our results indicated that the extended nature of Group A compounds made these compounds less flexible, therefore less likely to occupy other binding conformations. Hence, the absence of the Tyr652 residue would profoundly influence their binding affinity with the hERG channel. The more compact structure of Group B compounds would suggest that these drugs were able to change binding mode without much loss of binding energy and therefore, the absence of the Tyr652 residue did not make major changes to their binding affinity. The exceptions seen in the Group A compounds, haloperidol and bepridil, could be attributed to their symmetrical and less extended conformations respectively (see Figure 5.5), which would make them more flexible. As a consequence, this would permit multiple binding modes within the channel.

## Chapter Five- Structural determinants of hERG block

**Figure 5.14: The 3-point pharmacophore for each of the groups, A and B, and their possible interactions.** A combined 4-point pharmacophore is shown with the corresponding 3-point pharmacophore for each group. The hydrophobic feature (yellow sphere) at position 1 in both groups could interact with the Tyr652 residue. Most Group A compounds also had a *para*-substituent (purple stick) at position 1, which could interact with pore helix residues. The charged nitrogen group (purple sphere) also found in both pharmacophores could potentially interact with the Phe656 residue. The hydrophobic feature (yellow sphere) in Group A compounds found at position 2 was suggested to interact with Phe656, while the hydrophobic feature at position 3 (yellow sphere) in Group B compounds was suggested to bind to a second copy of Tyr652 found on another subunit. Risperidone (in green sticks) and amitriptyline (in blue sticks) are overlaid on the pharmacophore for Group A and Group B compounds respectively.



## Chapter Five- Structural determinants of hERG block

### 5.11 Discussion

An unwanted side effect to a considerable number of drugs is acquired LQTS and sudden cardiac death. This is a major concern for health regulatory authorities as well as the pharmaceutical industry, which strive to identify and remove drugs with these undesirable properties early on in the drug discovery process. The limited throughput of conventional electrophysiological methods that aim to measure currents through hERG channels and elucidate the actions of drugs on this channel has led to the investigation of more efficient, automated techniques. One of these devices which was described in this chapter, the PatchXpress, is a medium throughput patch clamping instrument that can record from up to 16 cells simultaneously, whilst each cell is completely independent from one another. This method allowed us to measure the drug binding affinity of 24 LQT compounds in 2 different stable cell lines, WT hERG and Y652A hERG HEK-293 cells. The aim was to generate a consistent dataset of drug potencies against WT and Y652A hERG channels using the same experimental procedure, voltage protocols, and solutions. This would then help us understand the importance of the Tyr652 residue on the potency of compounds.

The  $IC_{50}$  values obtained for these compounds in WT hERG were found to be slightly more potent than literature values, most likely due to the voltage protocol used, which ensured that the channel was in the open state for a significant period of time and in some cases also the type of cell line used. In general however, the data obtained with the PatchXpress was very comparable to literature values measured using conventional patch clamping methodologies, hence making this system a very robust and high content method to test the action of drugs on hERG. The  $IC_{50}$  values obtained using WT hERG channels were then compared to the values obtained in the Y652A hERG channels and the fold change in  $IC_{50}$  with this mutation was calculated. This revealed an interesting finding whereby more than half of the compounds studied had a fold change < 10 fold with the Y652A mutation. The majority of compounds studied to date had indicated that the presence of the Tyr652 residue was a requirement for high affinity hERG blockade, with the exception of some low affinity hERG blockers. Our results showed that even

## Chapter Five- Structural determinants of hERG block

relatively potent compounds such as thioridazine and verapamil, with  $IC_{50}$  values  $< 200$  nM in WT hERG channels, had minor effects when the tyrosine was substituted with an alanine. We divided the compounds into 2 groups, A and B, whereby Group A compounds were the most potent compounds with an  $IC_{50}$  value  $< 100$  nM and which exhibited large changes in  $IC_{50}$  with the Y652A mutation. On the other hand, Group B compounds were less potent and exhibited smaller changes in  $IC_{50}$  values with the Y652A mutation. Even amongst these groups, there were two notable exceptions, haloperidol and bepridil. Pharmacophore modelling was then utilised to structurally explain the data obtained using the PatchXpress.

3-point pharmacophore models were built for Group A and Group B compounds. These pharmacophores had a common central nitrogen group and a hydrophobic feature. In addition, each pharmacophore had another hydrophobic group but at different positions from one another. Group A compounds were longer and therefore less flexible, thus suggesting that the Tyr652 residue may be important for the interaction of these compounds. Exceptions in this group implied that, although some compounds may be very potent, their structural flexibility may render them able to conform to multiple binding modes within the channel. The Tyr652 residue seemed to be less important for the smaller, less potent compounds of Group B that may easily orientate to form other interactions within the pore. The pharmacophores generated from this study correlate well with hERG pharmacophore models in the literature and this will be discussed in chapter 7.

### 5.12 Comparisons between electrophysiological automated systems

During the course of this study, a number of other high throughput automated systems were investigated for potential use with hERG mutant channels. These systems incorporated the IonWorks Quattro (Axon Instruments, Molecular Devices, California) and the Roboocyte (Multi Channel Systems). Similar to the PatchXpress, these automated devices were used to record membrane currents and have been useful in a pharmaceutical setting as a high throughput screen for drug molecules. The IonWorks operates by

## Chapter Five- Structural determinants of hERG block

forming high resistance seals and performing whole cell recordings on mammalian cells using the planar patch clamp technology. It is able to record from parallel wells in a 384 well plate simultaneously. Although this is a much higher throughput than the PatchXpress, cells are not continuously voltage clamped. During pharmacological studies, unlike the PatchXpress where multiple concentrations of drugs are added to the same cell, the IonWorks adds different concentrations of compounds to different cells and the data then has to be compiled from several cells to obtain a dose-response curve. The quality of the data is therefore compromised. In addition, the experimental procedure had a duration of at least an hour compared to half an hour with the PatchXpress, and many cells died during this process. The seal success rates of the hERG cell line were also low suggesting that the cell preparation needed to be further optimised for use with this machine.

The Roboocyte is an automated oocyte recording system and can be used as an alternative to planar electrode systems. The course of the experiment using the Roboocyte is very similar to manual two-electrode voltage clamp experiments and its main advantage is in its throughput, as it can also be left to record unsupervised. This approach can be very useful for high throughput drug screening. I found current recordings with this system to be contaminated with electrical noise and so not ideal for generating publication quality data. Writing command scripts was also time consuming and often difficult, especially when utilising complex voltage protocols for characterising the gating properties of mutant hERG channels.

## **Chapter Six            The role of inner helix (Val659 and Ile662) residues in hERG gating and pharmacology**

To gain an understanding of the inner cavity of hERG, investigators have employed site-directed mutagenesis techniques to reveal key amino acid residues involved in channel gating and pharmacology. In an alanine scanning mutagenesis study by Mitcheson *et al* (Mitcheson *et al.*, 2000a), individual residues on S6 from Leu646 to Tyr667 and pore helix residues from Leu622 to Val625 were mutated and sensitivity to inhibition by MK-499 was determined. In most of the mutant channels, currents were inhibited in a similar manner to WT hERG indicating that the mutated residue was not involved in drug binding to MK-499. However, a number of residues showed substantially decreased sensitivity to block by MK-499, indicating that these residues could have either direct interactions with drugs or else allosteric effects on drug binding. This study also highlighted the profound effect V659A had on deactivation gating relative to its neighbouring residues. This mutation dramatically slowed channel deactivation. The position of this residue in the S6 helices is also critical. It is found at the bottom of the inner helices, near the proposed site for activation gating. Another residue, predicted to be at the narrowest point of the activation gate, possibly making it a critical component of the activation gate is Ile662. The I662A mutant was found to be non-functional in the alanine scan of S6.

The N-terminus has been shown to play an important role in slowing the deactivation process in hERG (Schonherr & Heinemann, 1996; Terlau *et al.*, 1997; Wang *et al.*, 1998; Chen *et al.*, 1999). Point mutations and deletions, particularly of the first 25 residues, resulted in the accelerated rate of deactivation (Terlau *et al.*, 1997). The N-terminus is thought to interact with the open activation gate at negative potentials stabilising the channel in the open state (Wang *et al.*, 2000). Destabilising this binding therefore leads to the acceleration of hERG deactivation. The N-terminus is also thought to bind to sites in the S4-S5 linker that are exposed following channel opening and slow the subsequent closure of the channel (Wang *et al.*, 1998; Tristani-Firouzi *et al.*, 2002). These studies have also shown that interactions between residues on the S4-S5 linker and the C-

## Chapter 6- Roles of inner helix residues

terminal end of S6 result in modulation of hERG gating (Tristani-Firouzi *et al.*, 2002). In particular, the mutation D540K on the S4-S5 linker exhibits electrostatic repulsion of Arg665 on S6, mediating hyperpolarisation dependent opening. R665A also exhibits slower deactivation kinetics similar to V659A, raising the possibility of potential interactions between the Val659 residue and the N-terminus.

We therefore propose the hypothesis that Val659 may directly bind or form part of the receptor to which the N-terminus binds, close to the S4-S5 linker, thus exerting its effects on deactivation gating. This may also involve other nearby residues, such as Ile662, that is one helical turn away from Val659. This chapter aims to understand the roles of Val659 and Ile662 in channel gating due to their key positions within S6, with particular emphasis on deactivation gating. Different sized mutant residues were used to gauge how the channel packs around that region. The roles of these residues in hERG pharmacology were also investigated. Changes to drug sensitivity with mutations may be due to reduced channel open probability rather than a loss of interaction with certain residues. This may be the case for V659A, which exhibited reduced sensitivity to MK-499, possibly due to its effects on hERG deactivation, and hence this was further investigated.

## Chapter 6- Roles of inner helix residues

### 6.1 Characterisation of the activation and deactivation kinetics of V659A currents

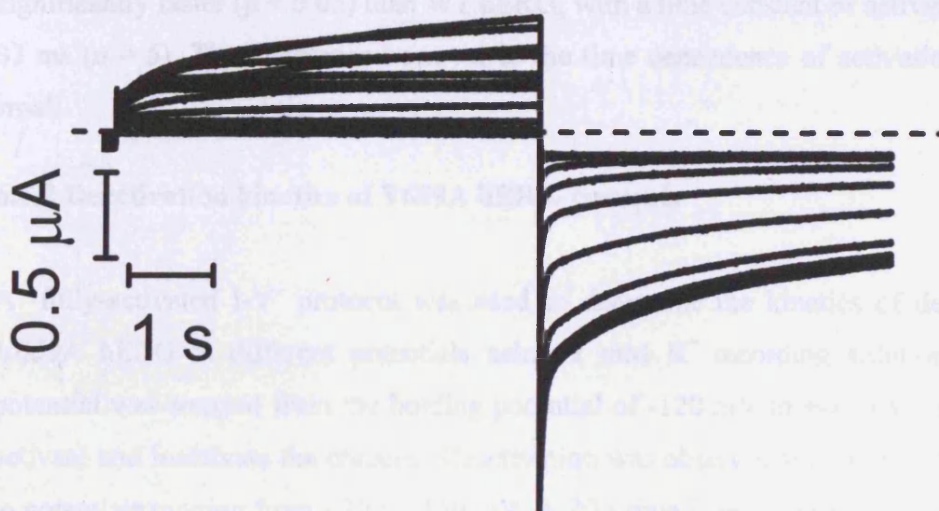
Recordings were made of V659A hERG currents, and directly compared to WT hERG currents recorded under the same conditions. V659A had been observed to have effects on channel deactivation in a previous study (Mitcheson *et al.*, 2000a). A more detailed characterisation was done with protocols that enabled us to investigate channel opening and closure.

#### 6.1.1 Activation kinetics of V659A hERG currents

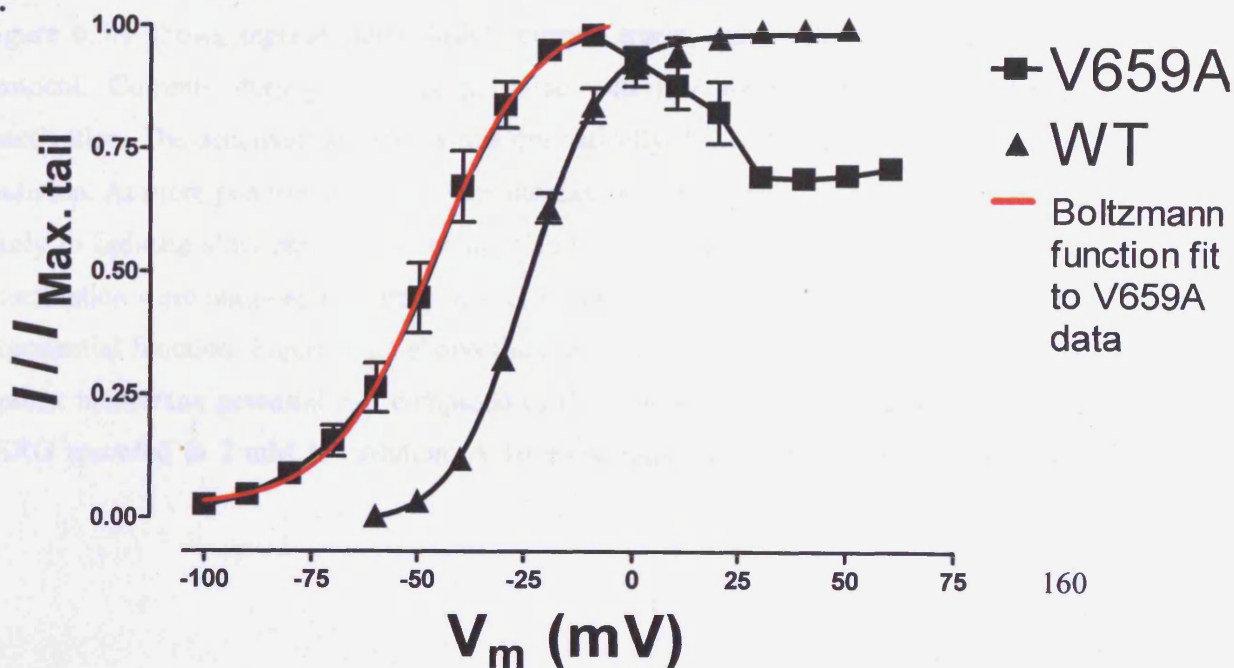
V659A hERG currents were recorded using an I-V protocol in 2 mM K<sup>+</sup> solution. Depolarising pulses were applied from a holding potential of -120 mV to potentials ranging between -100 and +60 mV for 5 s followed by a 5 s repolarising pulse to -140 mV. A duration of 50 s between sweeps allowed the channels to close between pulses and even this was insufficient for complete deactivation seen by the variable holding current before each test pulse. Figure 6.1A shows representative current traces for V659A hERG elicited using this protocol. Initially, activation and inactivation gating appeared relatively normal, although a clear slowing of deactivation could be observed. The peak tail currents obtained upon repolarisation to -140 mV were normalised to the maximum peak current value and plotted against the test potential to give the voltage dependence of activation (Figure 6.1B). Activation reached threshold at -90 mV and then increased with depolarisation to reach a maximum at approximately -10 mV. However upon further depolarisation, peak tail currents decreased by about 30 % and appeared to plateau at this lower value from +30 to +60 mV. This was very different to what was observed with WT currents, which increased with depolarisation from a threshold at -50 mV to reach a maximum steady state level at +20 mV. Data for V659A between -100 and -5 mV were fitted with a Boltzmann function and the  $V_{0.5}$  of activation and slope factor were calculated. The  $V_{0.5}$  of activation of V659A hERG was  $-46.7 \pm 1.9$  mV and the slope factor was  $11.7 \pm 1.9$  mV ( $n = 8$ ). The  $V_{0.5}$  of activation of WT hERG recorded in 2 mM K<sup>+</sup> solution was  $-24.6 \pm 0.7$  mV and the slope factor was  $8.4 \pm 0.6$  mV ( $n = 6$ ). Thus, the voltage dependence of V659A current was significantly shifted to negative potentials

**Figure 6.1: Current–voltage relationship of V659A currents.** **A.** Representative current traces recorded using an I-V protocol in 2 mM K<sup>+</sup> solution. A series of 5 s depolarising pulses from a holding potential of -120 mV to potentials ranging from -100 to +60 mV were applied followed by a 5 s pulse to -140 mV. The dashed line indicates the zero current line. **B.** Mean peak tail current normalised to maximum current and plotted against test potential. V659A data was only fit with a Boltzmann function between -100 and -5 mV (shown in red) to give the voltage dependence of activation (n = 8). The activation curve for WT hERG is shown for comparison.

A.



B.



## Chapter 6- Roles of inner helix residues

relative to WT hERG ( $p < 0.01$ ), with tail currents showing an unusual decrease in amplitude at potentials positive to 0 mV.

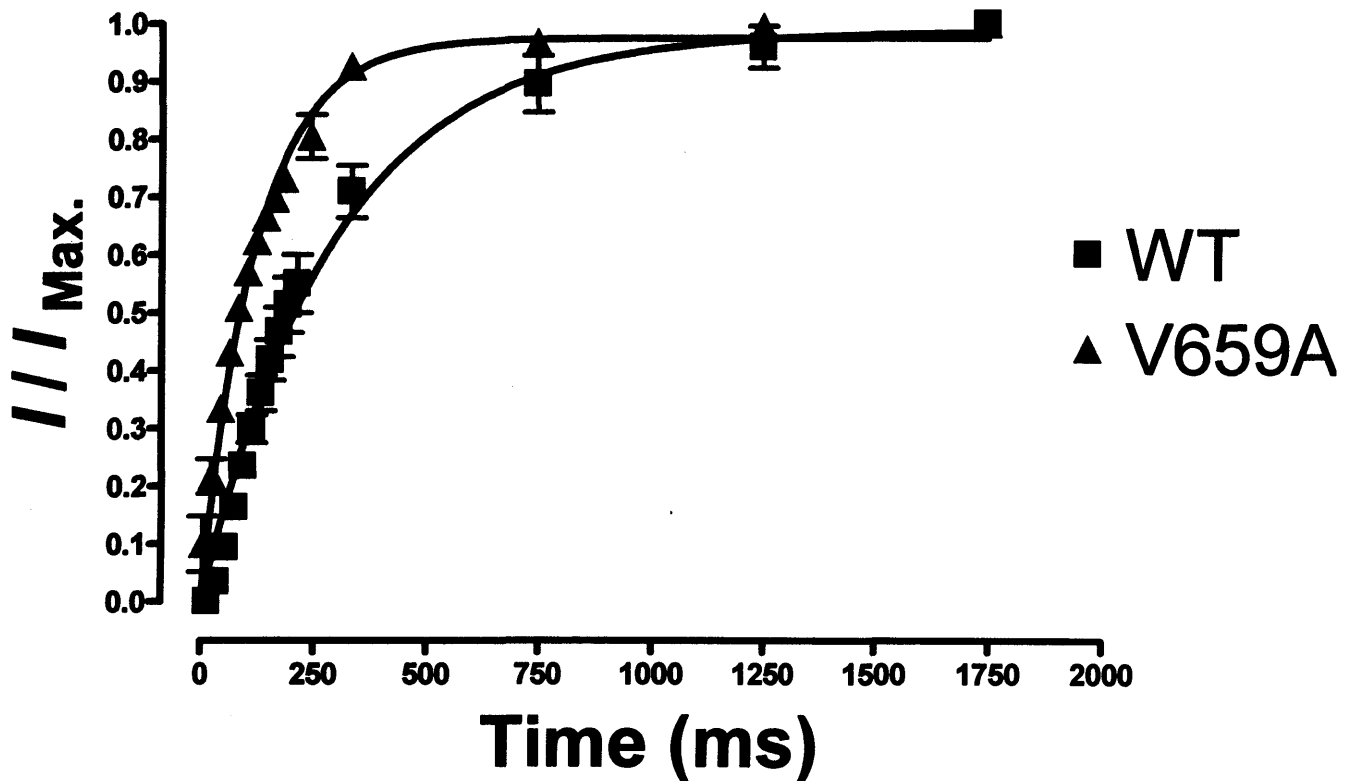
The time course of activation was measured using the 'envelope of tails' voltage protocol. Membrane potential was stepped from -120 mV to 0 mV for increasing time intervals from 20 ms to 2000 ms. The accumulation of channel activation was measured from the peak tail current amplitudes at -140 mV. A duration of 50 s was left between sweeps to allow the channel to close. The peak tail current from each time interval was normalised to steady state maximal current then plotted as a function of test pulse duration and fit with a single exponential function (Figure 6.2). The activation time constant obtained for V659A hERG current was  $118 \pm 18$  ms ( $n = 5$ ), which was significantly faster ( $p < 0.05$ ) than WT hERG, with a time constant of activation of  $248 \pm 33$  ms ( $n = 5$ ). The difference however in the time dependence of activation gating was small.

### 6.1.2 Deactivation kinetics of V659A hERG currents

A 'fully-activated I-V' protocol was used to determine the kinetics of deactivation of V659A hERG at different potentials using 2 mM  $K^+$  recording solution. Membrane potential was stepped from the holding potential of -120 mV to +40 mV for 1 s to fully activate and inactivate the channel. Deactivation was observed following 10 s test pulses to potentials ranging from +30 to -140 mV. A 30 s time interval was left between sweeps. Figure 6.3A shows representative hERG current traces, during the test pulses of this protocol. Currents during the first pulse to +40 mV were small due to channel inactivation. The deactivation process was dramatically slowed by the introduction of this mutation. At more positive potentials, the increase in current also appeared to be slowed, likely to indicate slow recovery from inactivation. The fast and slow time constants of deactivation were obtained by fitting the decaying phase of the tail current with a double exponential function. Figure 6.3B shows the mean time constants of deactivation plotted against membrane potential and compared to the time constants of deactivation of WT hERG recorded in 2 mM  $K^+$  solution. A 10 s test pulse was not long enough to obtain

## Chapter 6- Roles of inner helix residues

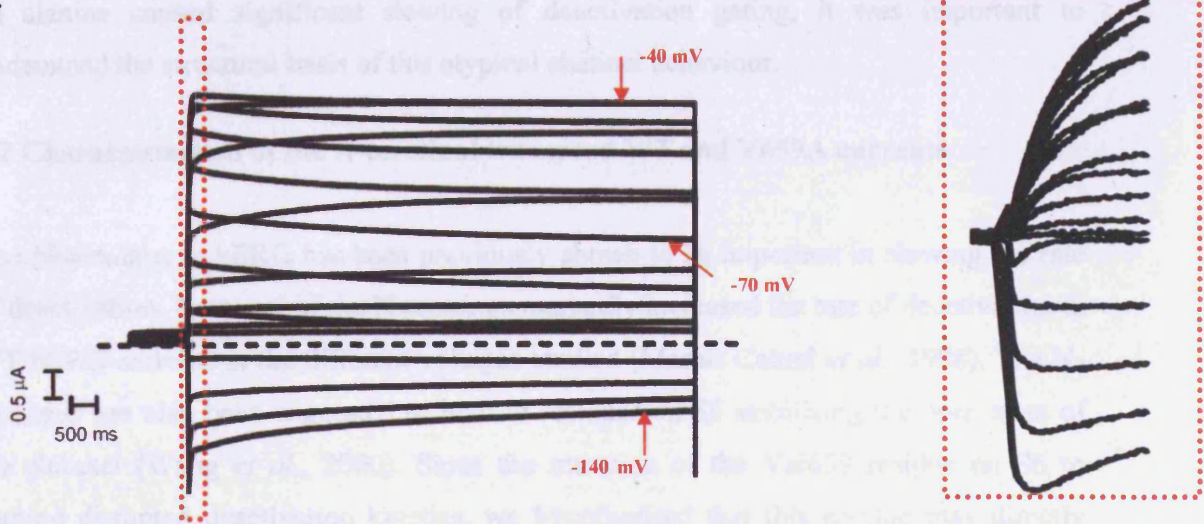
**Figure 6.2: The time dependence of activation of V659A hERG.** Mean peak tail current was normalised to maximal current and plotted against duration of pulse to 0 mV ( $n = 5$ ). Results were fit with a single exponential function and compared to the time course of activation of WT currents.



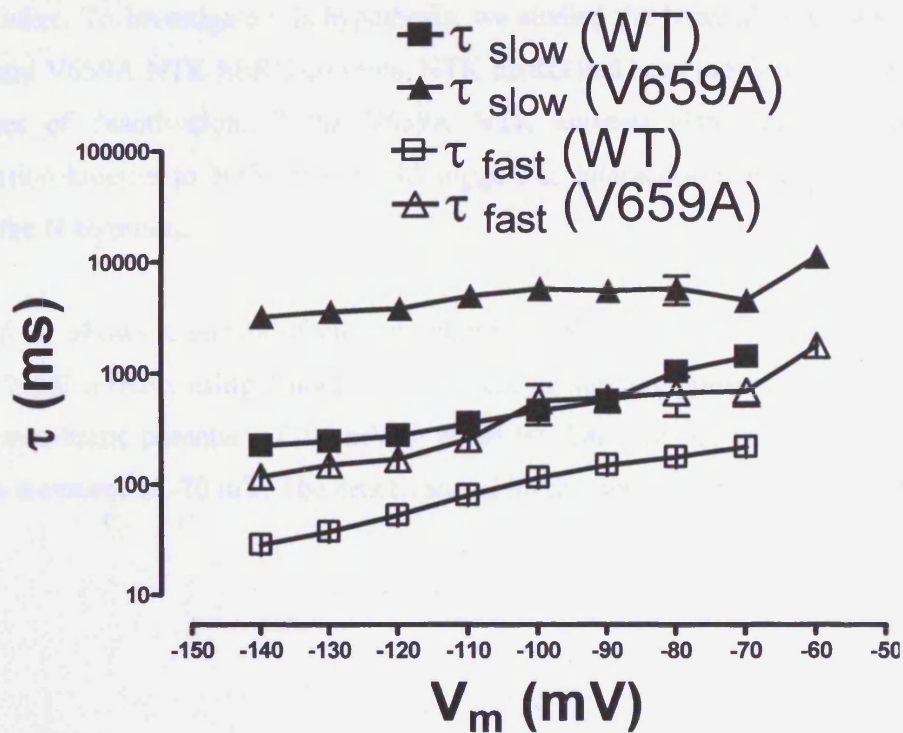
Chapter 6- Roles of inner helix residues

**Figure 6.3: Mean time constants of deactivation for V659A currents.** **A.** Representative current traces using the ‘fully-activated I-V’ protocol plotted from part of this protocol during the test pulses. It shows a fast and a slow deactivating component and the fast component is expanded and shown in the red dashed box. **B.** The time constants of deactivation ( $\tau_{fast}$  and  $\tau_{slow}$ ) were measured from this protocol and plotted on a  $\log_{10}$  scale against test voltages ( $n = 7$ ). Values for WT hERG are shown for comparison.

**A.**



**B.**



## Chapter 6- Roles of inner helix residues

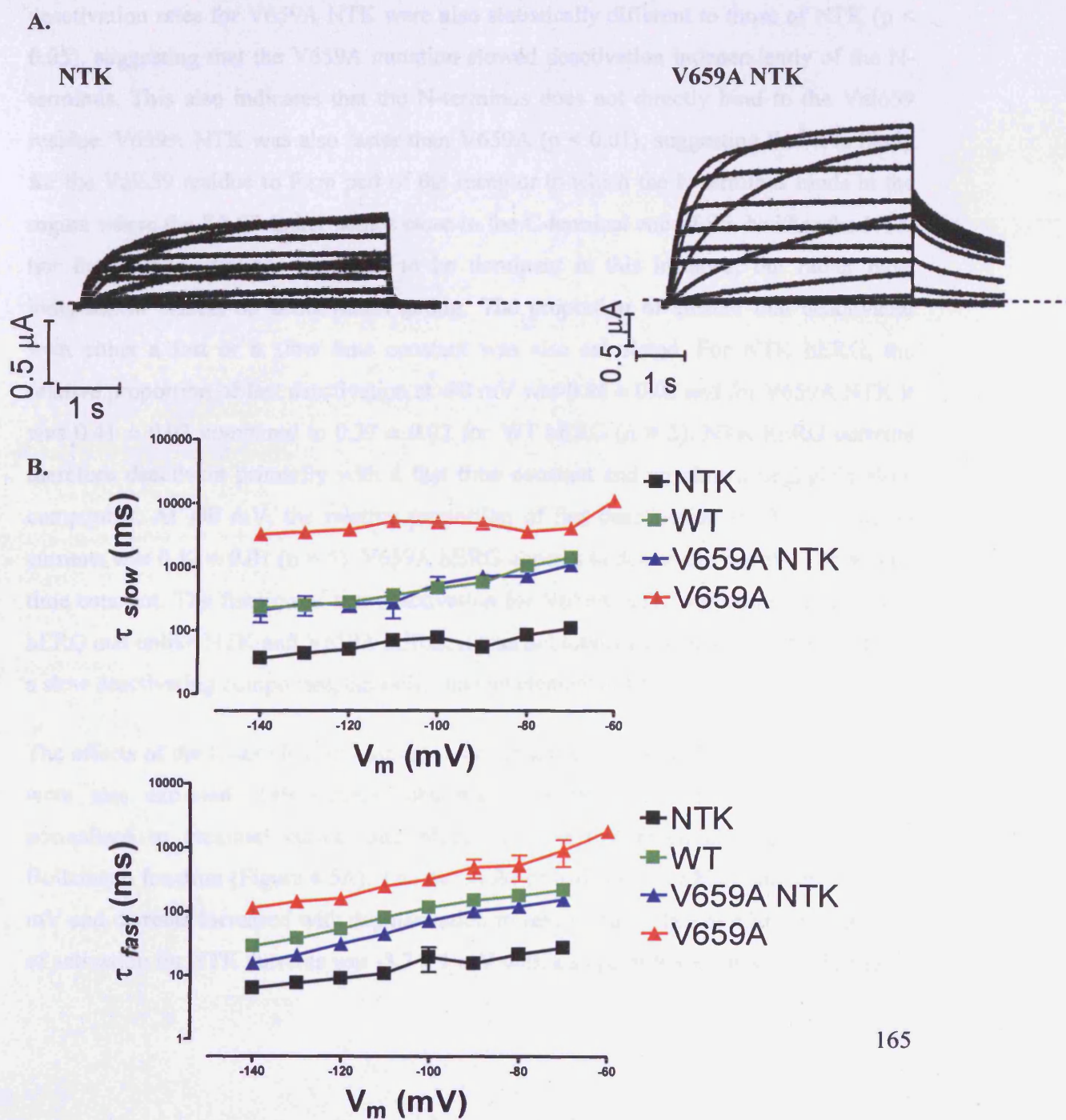
precise measurements, therefore the values given are underestimates particularly at the more positive potentials. At -140 mV, the  $\tau_{\text{slow}}$  and  $\tau_{\text{fast}}$  values for deactivation for the V659A currents were  $3181 \pm 156$  ms and  $117 \pm 13$  ms respectively ( $n = 7$ ). This compared to  $222 \pm 13$  ms and  $28 \pm 2$  ms respectively ( $n = 5$ ) for WT hERG. Both the slow and fast deactivating components of the V659A currents were statistically significantly slower than WT currents ( $p < 0.01$ ). The effect of this mutation on  $\tau_{\text{slow}}$  however, appears to be greater than for  $\tau_{\text{fast}}$ . These changes are too great to be due to the negative shifts on voltage dependent gating. Since the mutation of the Val659 residue to an alanine caused significant slowing of deactivation gating, it was important to understand the structural basis of this atypical channel behaviour.

### 6.2 Characterisation of the N-terminal truncated WT and V659A currents

The N-terminus in hERG has been previously shown to be important in slowing the rate of deactivation. Removal of the N-terminus markedly increased the rate of deactivation in WT hERG currents at the different voltages studied (Morais Cabral *et al.*, 1998). The N-terminus has also been suggested to bind to residues on S6 stabilising the open state of the channel (Wang *et al.*, 2000). Since the mutation of the Val659 residue on S6 to alanine disrupted deactivation kinetics, we hypothesised that this residue may directly interact with the N-terminus. Alternatively, it may form part of the receptor close to the S4-S5 linker. To investigate this hypothesis, we studied the N-terminal truncated (NTK) hERG and V659A NTK hERG currents. NTK hERG had been previously shown to have fast rates of deactivation. If the V659A NTK currents also exhibit similarly fast deactivation kinetics to NTK, this would suggest an interaction between this residue on S6 and the N-terminus.

Figure 6.4A shows a family of currents obtained using the I-V protocol for NTK and V659A NTK currents using 2 mM  $K^+$  solution. Depolarising pulses were applied from a resting membrane potential of -90 mV to potentials between -60 and +50 mV, with tail currents measured at -70 mV. The deactivation kinetics appeared to be much faster in the

**Figure 6.4: Effects of N-terminal truncation on hERG currents.** **A.** Representative current traces of NTK hERG and V659A NTK hERG currents recorded using an I-V protocol in 2 mM K<sup>+</sup> solution. The holding potential was -90 mV and the tail current potential was -70 mV. **B.**  $\tau_{fast}$  and  $\tau_{slow}$  of deactivation were measured for the NTK mutants from currents elicited using a 'fully-activated I-V' protocol and fit with a double exponential function. The mean time constants obtained were then plotted on a log<sub>10</sub> scale against test voltages (n = 5). The non-truncated channels are plotted for comparison.



## Chapter 6- Roles of inner helix residues

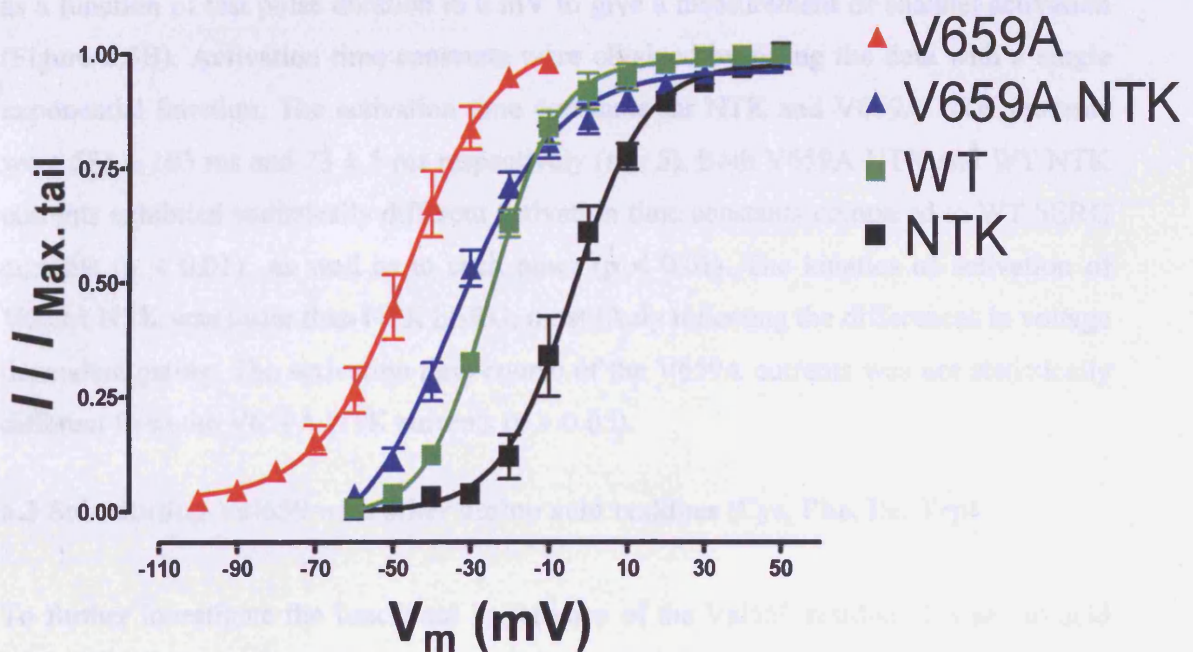
NTK channels compared to the full length channels. It was also apparent that NTK currents still had much faster deactivation kinetics than V659A NTK currents.

Tail currents decayed with two time constants. At -90 mV,  $\tau_{\text{slow}}$  and  $\tau_{\text{fast}}$  for V659A NTK hERG were  $702 \pm 94$  ms and  $100 \pm 4$  ms respectively ( $n = 5$ ) and for NTK hERG were  $54 \pm 8$  ms and  $15 \pm 2$  ms respectively ( $n = 5$ ). Deactivation kinetics were faster in the NTK channels compared to their corresponding non-truncated channels (Figure 6.4B). The deactivation rates for V659A NTK were also statistically different to those of NTK ( $p < 0.05$ ), suggesting that the V659A mutation slowed deactivation independently of the N-terminus. This also indicates that the N-terminus does not directly bind to the Val659 residue. V659A NTK was also faster than V659A ( $p < 0.01$ ), suggesting that it is likely for the Val659 residue to form part of the receptor to which the N-terminus binds in the region where the S4-S5 linker comes close to the C-terminal end of S6. Neither the NTK nor the alanine mutation appeared to be dominant in this instance, but rather have independent effects on deactivation gating. The proportion of current that deactivated with either a fast or a slow time constant was also calculated. For NTK hERG, the relative proportion of fast deactivation at -90 mV was  $0.86 \pm 0.02$  and for V659A NTK it was  $0.41 \pm 0.03$  compared to  $0.37 \pm 0.02$  for WT hERG ( $n = 5$ ). NTK hERG currents therefore deactivate primarily with a fast time constant and an almost negligible slow component. At -90 mV, the relative proportion of fast deactivation for V659A hERG currents was  $0.12 \pm 0.01$  ( $n = 5$ ). V659A hERG appears to deactivate mainly with a slow time constant. The fraction of fast deactivation for V659A NTK was comparable to WT hERG and unlike NTK and V659A hERG, it was not totally dependent on either a fast or a slow deactivating component, but rather had an element of both.

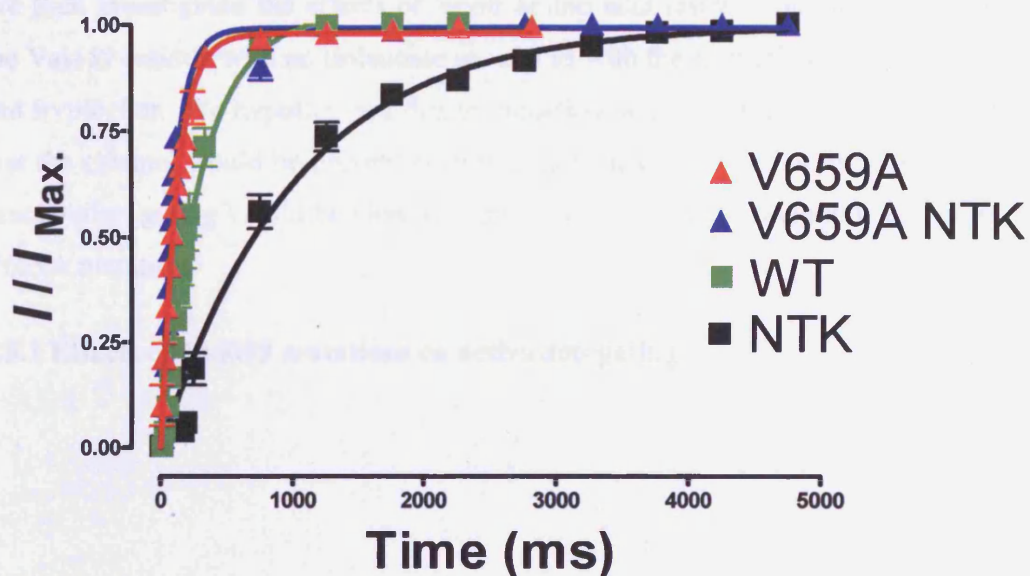
The effects of the N-terminal truncation on activation gating of WT and V659A currents were also explored. Tail currents obtained upon repolarisation to -70 mV were normalised to maximal current and plotted against test potentials then fit with a Boltzmann function (Figure 6.5A). The threshold of activation for both currents was -50 mV and currents increased with depolarisation to reach steady state at +20 mV. The  $V_{0.5}$  of activation for NTK currents was  $-3.7 \pm 1$  mV with a slope of  $9.3 \pm 1$  mV ( $n = 5$ ) and

**Figure 6.5: Effects of N-terminal truncation on hERG activation gating.** **A.** Mean normalised peak tail currents plotted as a function of test potential then fitted with a Boltzmann function to give the voltage dependence of activation of NTK and V659A NTK currents ( $n \geq 5$ ). **B.** Mean tail currents normalised to maximal steady state current were plotted against test pulse duration to 0 mV then fitted with a single exponential function. This gave the time constants of activation of the NTK mutant currents ( $n = 5$ ).

A.



B.



## Chapter 6- Roles of inner helix residues

the  $V_{0.5}$  of activation for V659A NTK currents was  $-34.1 \pm 2.2$  mV with a slope of  $13 \pm 1.5$  mV ( $n = 7$ ). The voltage dependence of activation for both NTK mutants was right-shifted relative to non-truncated hERG.

An 'envelope of tails' protocol was used to study the activation time courses of NTK and V659A NTK currents. A depolarisation to 0 mV for increasing time durations from 20 ms to 5000 ms was followed by a repolarising step to -70 mV to give a peak tail current. The peak tail current from each time interval was normalised to maximal current then plotted as a function of test pulse duration to 0 mV to give a measurement of channel activation (Figure 6.5B). Activation time constants were obtained by fitting the data with a single exponential function. The activation time constants for NTK and V659A NTK currents were  $581 \pm 103$  ms and  $73 \pm 5$  ms respectively ( $n = 5$ ). Both V659A NTK and WT NTK currents exhibited statistically different activation time constants compared to WT hERG currents ( $p < 0.01$ ) as well as to each other ( $p < 0.01$ ). The kinetics of activation of V659A NTK was faster than NTK hERG, most likely reflecting the differences in voltage dependent gating. The activation time course of the V659A currents was not statistically different from the V659A NTK currents ( $p > 0.05$ ).

### 6.3 Substituting Val659 with other amino acid residues (Cys, Phe, Ile, Trp)

To further investigate the functional importance of the Val659 residue, this amino acid was mutated to residues of different sizes and properties. We first mutated the Val659 residue to a cysteine, which is relatively small in size, comparable to the alanine mutant. We then investigated the effects of larger amino acid residues on gating by substituting the Val659 residue with an isoleucine as well as with the aromatic residues phenylalanine and tryptophan. We hypothesised that by inserting larger, bulkier residues at this position that the channel would be prevented from closing and stabilised in the open state. Hence deactivation gating would be slowed even further with these mutations compared to the V659A mutation.

#### 6.3.1 Effects of Val659 mutations on activation gating

## Chapter 6- Roles of inner helix residues

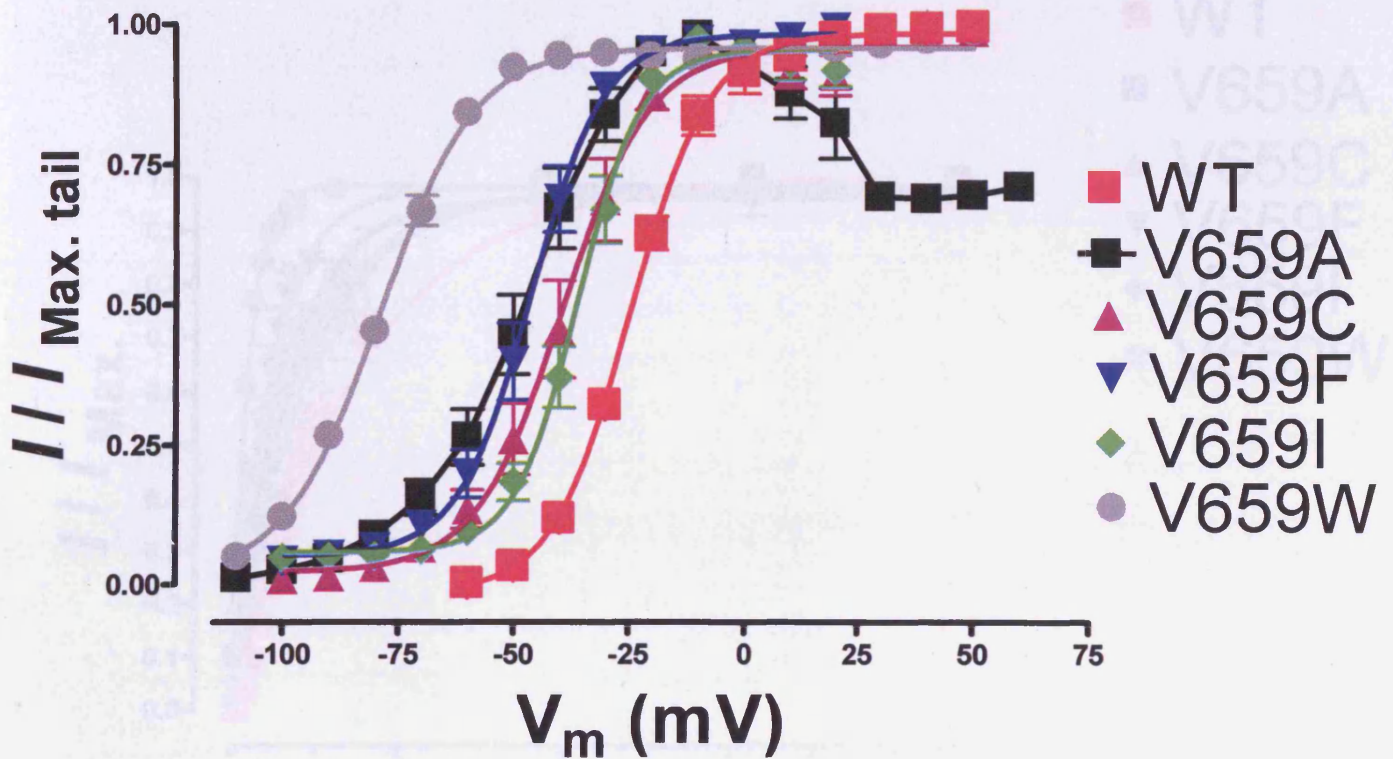
Currents from the mutant hERG channels, V659C, V659F, V659I, and V659W, were recorded using an I-V protocol in 2 mM K<sup>+</sup> solution. Mutant channels were held at a resting potential of -120 mV and 5 s depolarising steps between -100 and +50 mV were applied in 10 mV increments. Tail currents were elicited with a repolarising step to -140 mV for 2.5 s. An interval of 30 s was left between sweeps. Figure 6.6 shows the activation curves of the Val659 mutants compared to WT hERG. All mutants appeared to shift the voltage dependence of activation to more negative potentials compared to WT hERG. None of the mutant currents however exhibited the decrease in tail current amplitude at positive potentials observed with V659A hERG.

Similar to V659A hERG, the V659C, F, and I currents reached threshold at -90 mV and increased with depolarisation to reach a maximum at -10 mV. V659W currents were much more negatively shifted than the other mutants, with a threshold for activation at -100 mV and reaching steady state at approximately -40 mV. Although V659W hERG gave the largest negative shift in the voltage dependence of activation, there was no clear trend between residue size and the  $V_{0.5}$  of activation. The  $V_{0.5}$  of activation and slope factor was calculated for each of the mutant channels and reported in a table in Figure 6.6. The voltage dependence of activation of all these mutant currents was statistically significantly different to WT hERG currents ( $p < 0.05$  for V659I and  $p < 0.01$  for V659A, C, F, and W).

The effects of these mutations at the Val659 residue on the time course of activation gating were also assessed. The time constants of activation were measured using the 'envelope of tails' protocol by stepping to 0 mV for increasing time durations between 20 and 2000 ms and measuring peak tail current upon repolarisation to -140 mV (Figure 6.7). Results were fit with a single exponential function to give the mean time constants of activation of the mutant currents. These values are reported in the table in Figure 6.7. The time dependence of activation of the V659C and V659I currents were not statistically different to WT currents ( $p > 0.05$ ), but the time constants of activation of the V659F currents were statistically different to WT currents ( $p < 0.05$ ), as was the case for V659W currents ( $p < 0.01$ ). The time dependence of activation of all these mutants is

Chapter 6- Roles of inner helix residues

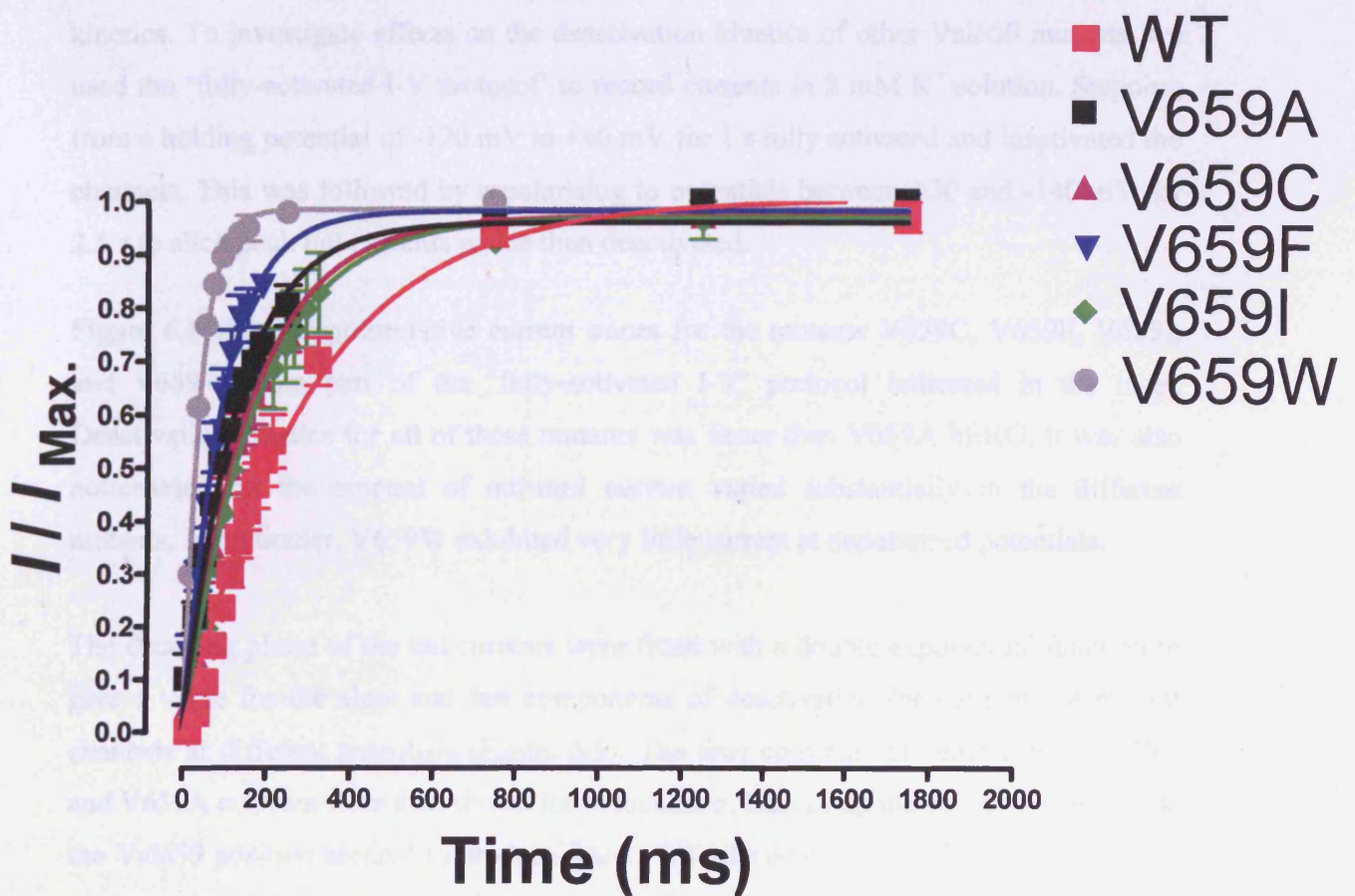
**Figure 6.6: Voltage dependence of activation of Val659 mutants.** Activation curves for V659C, V659F, V659I, and V659W currents. Mean peak tail currents normalised to maximal current were plotted against membrane voltage and fitted with a Boltzmann function ( $n = 6$ ). Activation curves for WT and V659A hERG are also plotted for comparison. All mutant currents were statistically different to WT hERG whereby (\*) means  $p < 0.05$  and (\*\*) means  $p < 0.01$ . Data from the curve fitting are shown in the table.



	$V_{0.5}$ of activation (mV)	Slope (mV)	n
WT	$-24.6 \pm 0.7$	$8.4 \pm 0.6$	6
V659A	$-46.7 \pm 1.9$ **	$11.7 \pm 1.9$	8
V659C	$-39.3 \pm 1.3$ **	$9.4 \pm 1.2$	6
V659F	$-46.2 \pm 0.9$ **	$7.9 \pm 0.8$	6
V659I	$-36 \pm 0.8$ *	$6.9 \pm 0.7$	6
V659W	$-79.3 \pm 0.9$ **	$9.6 \pm 0.7$	6

Chapter 6- Roles of inner helix residues

**Figure 6.7: Time dependence of activation at 0 mV of Val659 mutants.** An ‘envelope of tails’ protocol was used to measure the time constant of activation of V659C, V659F, V659I, and V659W currents. The time course of activation of WT and V659A hERG currents are also shown for comparison.  $\tau$  values are reported in a table and values which are statistically different to WT are denoted by (\*), whereby (\*) indicates  $p < 0.05$  and (\*\*) indicates  $p < 0.01$ .



	Time constant of activation $\tau$ (ms)	n
WT	$248 \pm 33$	5
V659A	$118 \pm 18$ *	5
V659C	$147 \pm 13$	6
V659F	$111 \pm 15$ *	6
V659I	$170 \pm 31$	6
V659W	$36 \pm 2$ **	6

## Chapter 6- Roles of inner helix residues

left-shifted compared to WT hERG, with V659W giving the fastest activation rate. Although there was no trend between residue size and activation kinetics, the changes in the time dependence of activation were concordant with the negative shifts in the voltage dependence of activation.

### 6.3.2 Effects of Val659 mutations on deactivation kinetics

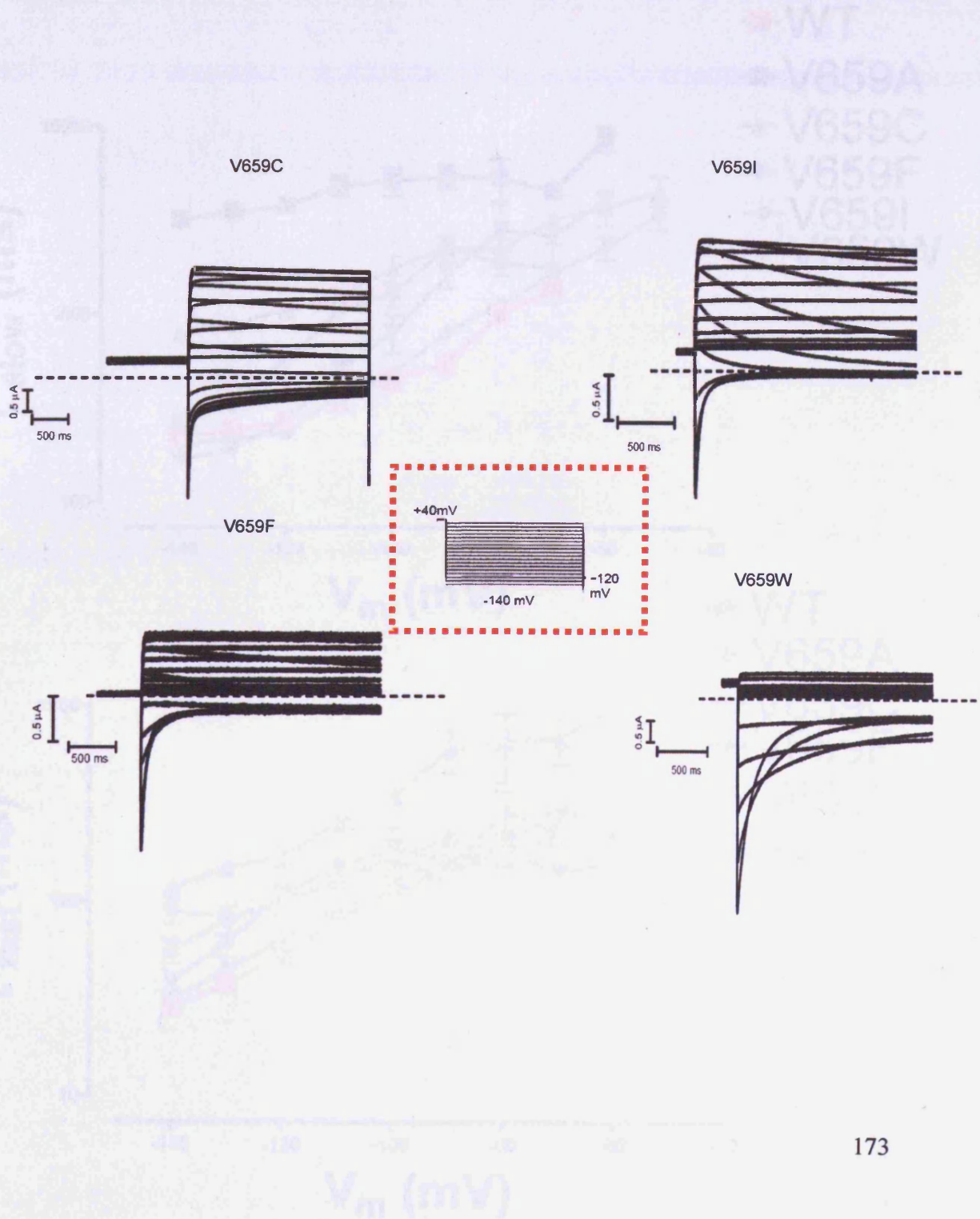
The substitution of the Val659 residue with an alanine dramatically slowed deactivation kinetics. To investigate effects on the deactivation kinetics of other Val659 mutants, we used the 'fully-activated I-V protocol' to record currents in 2 mM K<sup>+</sup> solution. Stepping from a holding potential of -120 mV to +40 mV for 1 s fully activated and inactivated the channels. This was followed by repolarising to potentials between +30 and -140 mV for 2.5 s to elicit peak tail currents which then deactivated.

Figure 6.8 shows representative current traces for the mutants V659C, V659F, V659I, and V659W from part of the 'fully-activated I-V' protocol indicated in the inset. Deactivation kinetics for all of these mutants was faster than V659A hERG. It was also noticeable that the amount of outward current varied substantially in the different mutants. In particular, V659W exhibited very little current at depolarised potentials.

The decaying phase of the tail currents were fitted with a double exponential function to give a value for the slow and fast components of deactivation for each of the mutant channels at different potentials (Figure 6.9). The time constants of deactivation for WT and V659A currents were also shown for comparison. Increasing the size of the residue at the Val659 position seemed to produce faster, WT-like deactivation kinetics. The effects of these mutations on the slow time constant of deactivation also appeared to be greater than for the fast time constant. The values of each of the deactivating time constants at -140 mV are reported in Figure 6.10A. The slow component of deactivation was statistically significantly different for V659A and V659C currents compared to WT currents ( $p < 0.01$ ) but not for the V659F, V659I, and V659W currents ( $p > 0.05$ ). The fast component of deactivation was statistically significantly different for V659A and

Chapter 6- Roles of inner helix residues

**Figure 6.8: Effects on deactivation with the Val659 mutants.** Representative family of currents using part of the 'fully-activated I-V protocol' illustrated in the inset (shown in red dashed box). These currents show the kinetics of deactivation of the V659C, V659F, V659I, and V659W hERG channels. The holding potential was -120 mV and the tail currents were recorded at potentials ranging from +30 to -140 mV.



Chapter 6- Roles of inner helix residues

**Figure 6.9:  $\tau_{fast}$  and  $\tau_{slow}$  of deactivation for Val659 mutants.** The fast and slow time constants of deactivation for the V659C, V659F, V659I, and V659W mutants were obtained at different voltages using the 'fully-activated I-V' protocol ( $n = 5$ ). Results were plotted on a  $\log_{10}$  scale against test potentials. Time constants for WT and V659A currents are also shown for comparison with other mutants.

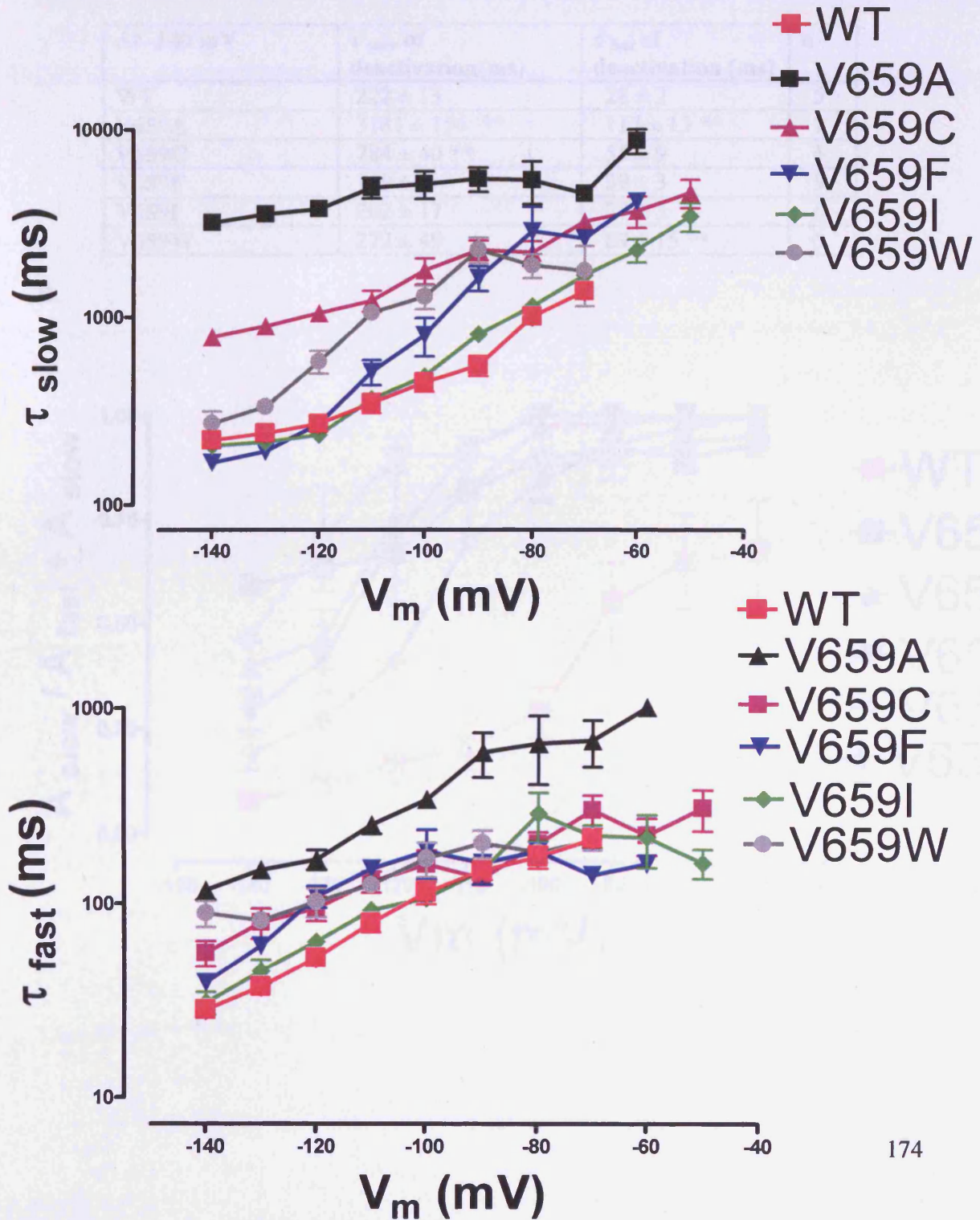
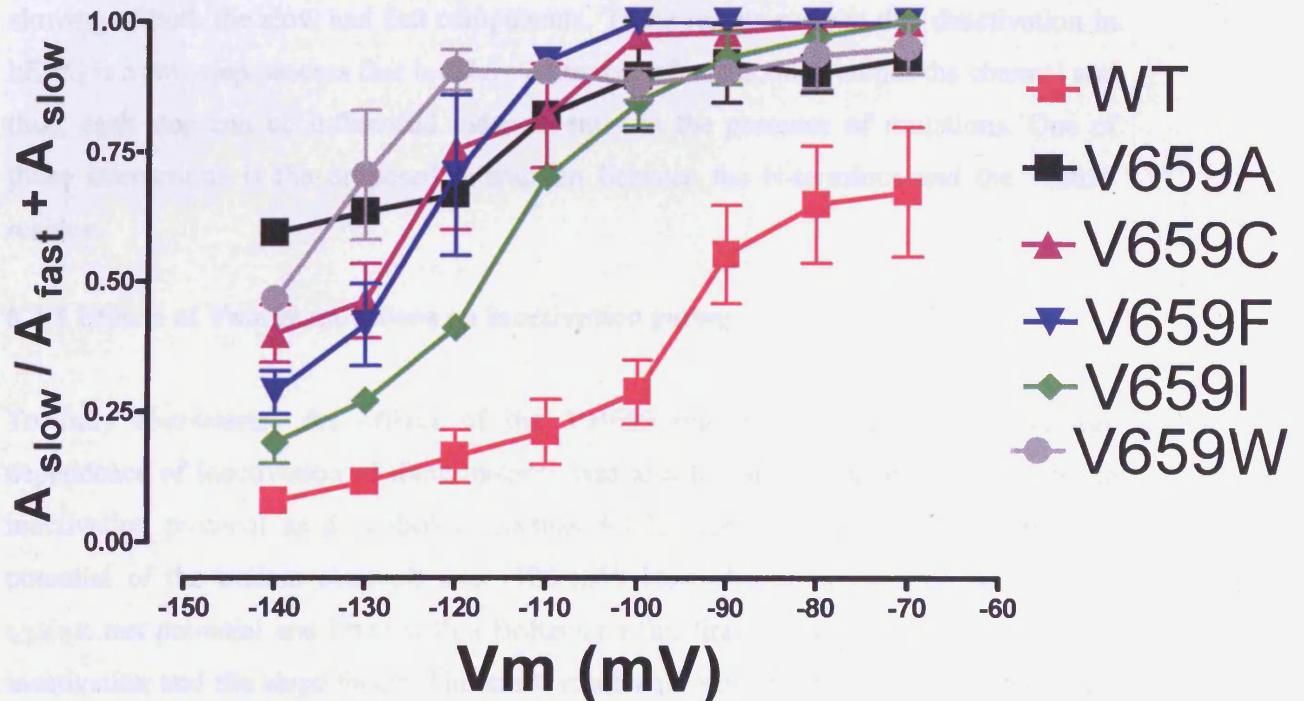


**Figure 6.10: Analysis of deactivating Val659 mutant hERG currents.** A. Values for  $\tau_{slow}$  and  $\tau_{fast}$  of deactivation for Val659 mutants and WT hERG at -140 mV ( $n \geq 5$ ). Values that are statistically different to WT hERG are denoted by (\*\*), which indicates  $p < 0.01$ . B. The fraction of slow deactivating current ( $A_{slow} / A_{fast} + A_{slow}$ ) plotted against membrane potential for Val659 mutants and compared to WT hERG.

A.

At -140 mV	$\tau_{slow}$ of deactivation(ms)	$\tau_{fast}$ of deactivation (ms)	n
WT	222 ± 13	28 ± 2	5
V659A	3181 ± 156 **	117 ± 13 **	7
V659C	784 ± 40 **	55 ± 9	5
V659F	169 ± 7	39 ± 3	5
V659I	202 ± 17	27 ± 3	6
V659W	272 ± 49	89 ± 15 **	5

B.



## Chapter 6- Roles of inner helix residues

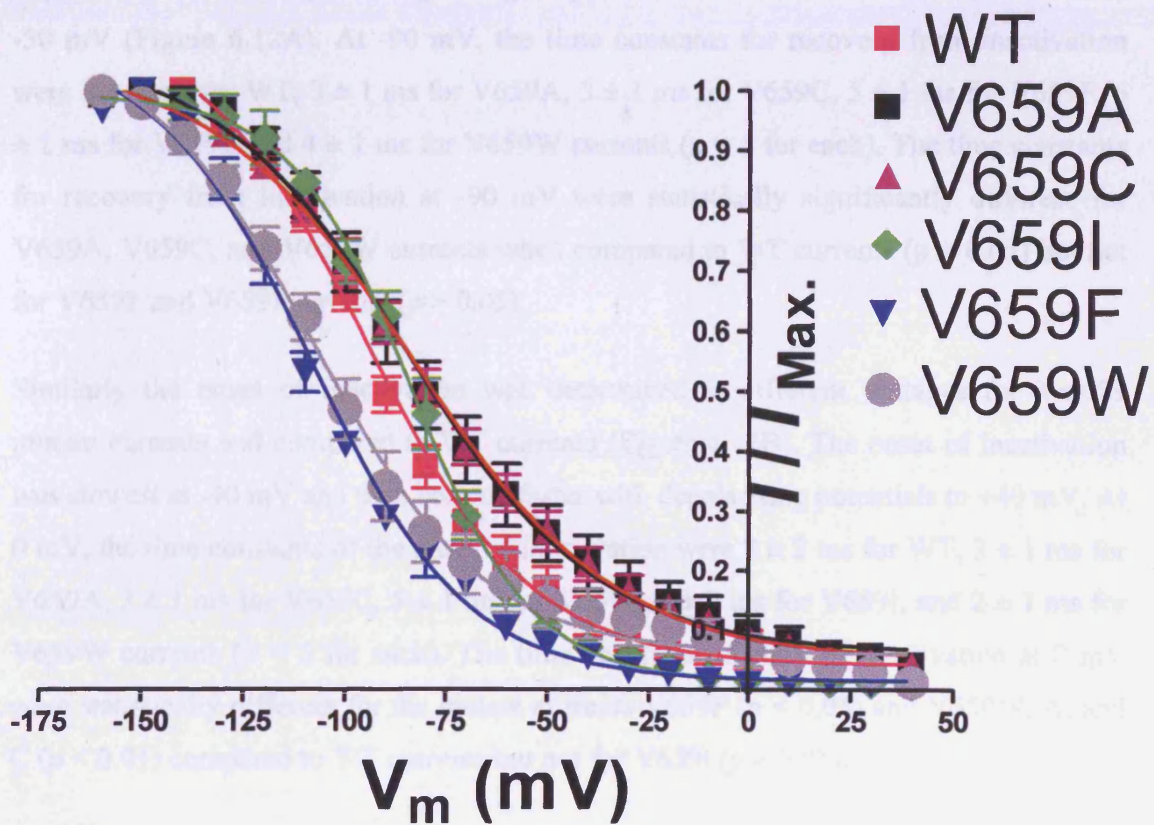
V659W currents compared to WT currents ( $p < 0.01$ ) but not for the V659C, V659F, and V659I currents ( $p > 0.05$ ).

The fraction of current deactivating with each time constant was also calculated. Figure 6.10B shows the fraction of the slow deactivating component for each of the Val659 mutants as well as for WT hERG at potentials between -140 and -70 mV. The data obtained appears to be strongly voltage dependent and for the Val659 mutants there is a clear loss of the fast deactivating component at the less negative potentials. This could explain the smaller effects observed on the fast time constants of deactivation (see Figure 6.9). V659C, F, I, and W exhibit a steep increase in the slow deactivating component with the application of depolarising potentials and the shifts from WT data loosely correlates with the negative shifts in the voltage dependence of activation (see Figure 6.6). The slowing of deactivation in these mutants is therefore mainly due to the increase of the slow deactivating component. V659A, on the other hand, appears to retain some of the fast deactivating component and in this mutation the effects on deactivation are due to slowing of both the slow and fast components. These results suggest that deactivation in hERG is a two-step process that involves a number of interactions within the channel and thus, each step can be influenced independently in the presence of mutations. One of those interactions is the proposed interaction between the N-terminus and the Val659 residue.

### 6.3.3 Effects of Val659 mutations on inactivation gating

To fully characterise the effects of the Val659 mutations on gating, the voltage dependence of inactivation of these mutants was also investigated using the triple pulse inactivation protocol as described in section 3.1.3, except that the resting membrane potential of the mutant channels was -120 mV. Normalised conductance was plotted against test potential and fitted with a Boltzmann function to give values for the  $V_{0.5}$  of inactivation and the slope factor. The mean results are shown for the V659 mutants and WT hERG in Figure 6.11. The amount of non-inactivating current for the V659F, I, and W as well as WT hERG appears to be very small at positive potentials compared to

**Figure 6.11: Voltage dependence of inactivation of Val659 mutants.** A triple pulse protocol was used to determine the voltage dependence of inactivation of the Val659 mutants compared to WT currents under the same recording conditions. Mean normalised data was plotted against membrane potential and fitted with a Boltzmann function ( $n = 5$ ). The values for  $V_{0.5}$  of inactivation and the slope factor are given in the table and show no statistical differences to WT hERG.



	$V_{0.5}$ of inactivation (mV)	Slope (mV)	n
WT	$-91 \pm 2.6$	$-20.8 \pm 1.9$	6
V659A	$-84.9 \pm 2.5$	$-24 \pm 2.3$	5
V659C	$-83.4 \pm 1.7$	$-25.1 \pm 1.6$	5
V659F	$-108.3 \pm 1.3$	$-19.4 \pm 0.9$	5
V659I	$-83.6 \pm 0.9$	$-15.1 \pm 0.8$	5
V659W	$-108 \pm 3.4$	$-21.4 \pm 2.5$	5

## Chapter 6- Roles of inner helix residues

V659A, and C. The voltage dependence of inactivation of all the mutant Val659 currents was not statistically significantly different to WT currents ( $p > 0.05$ ).

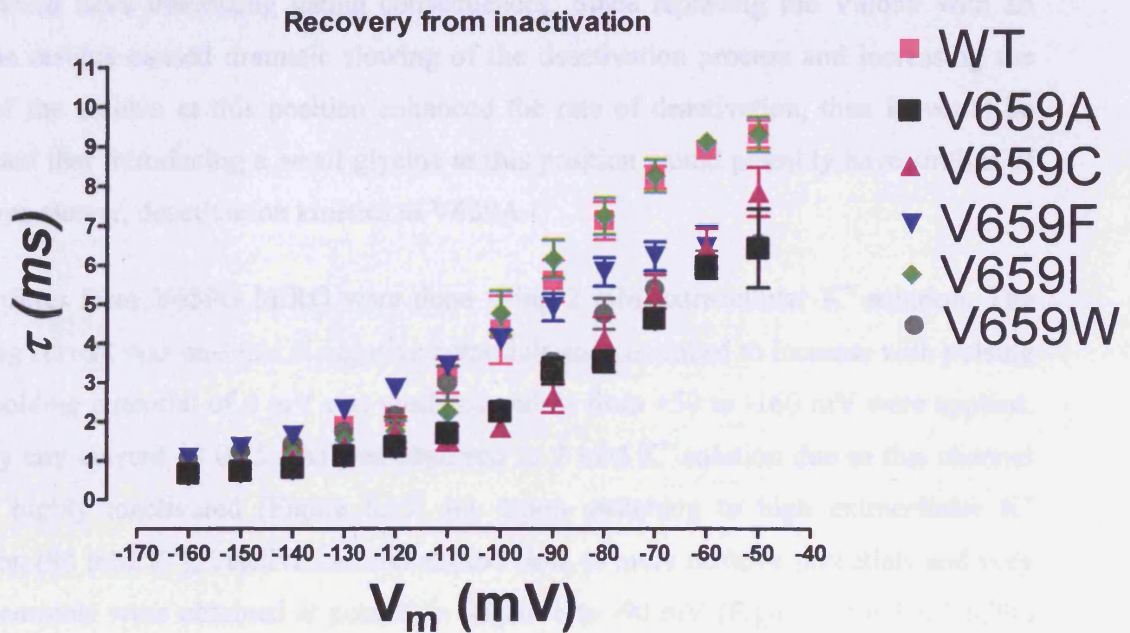
The time constants for the onset and recovery from inactivation were also determined at different voltages as described in section 3.1.3. The time constants for the recovery from inactivation for WT and Val659 mutants were plotted against membrane potential and became slower with depolarising voltages applied from -160 mV to reach maximum at -50 mV (Figure 6.12A). At -90 mV, the time constants for recovery from inactivation were  $6 \pm 1$  ms for WT,  $3 \pm 1$  ms for V659A,  $3 \pm 1$  ms for V659C,  $5 \pm 1$  ms for V659F,  $6 \pm 1$  ms for V659I, and  $4 \pm 1$  ms for V659W currents ( $n = 5$  for each). The time constants for recovery from inactivation at -90 mV were statistically significantly different for V659A, V659C, and V659W currents when compared to WT currents ( $p < 0.05$ ) but not for V659F and V659I currents ( $p > 0.05$ ).

Similarly the onset of inactivation was determined at different voltages for Val659 mutant currents and compared to WT currents (Figure 6.12B). The onset of inactivation was slowest at -40 mV and then became faster with depolarising potentials to +40 mV. At 0 mV, the time constants of the onset of inactivation were  $8 \pm 2$  ms for WT,  $3 \pm 1$  ms for V659A,  $3 \pm 1$  ms for V659C,  $5 \pm 1$  ms for V659F,  $8 \pm 2$  ms for V659I, and  $2 \pm 1$  ms for V659W currents ( $n = 5$  for each). The time constants of onset of inactivation at 0 mV were statistically different for the mutant currents V659F ( $p < 0.05$ ) and V659W, A, and C ( $p < 0.01$ ) compared to WT currents but not for V659I ( $p > 0.05$ ).

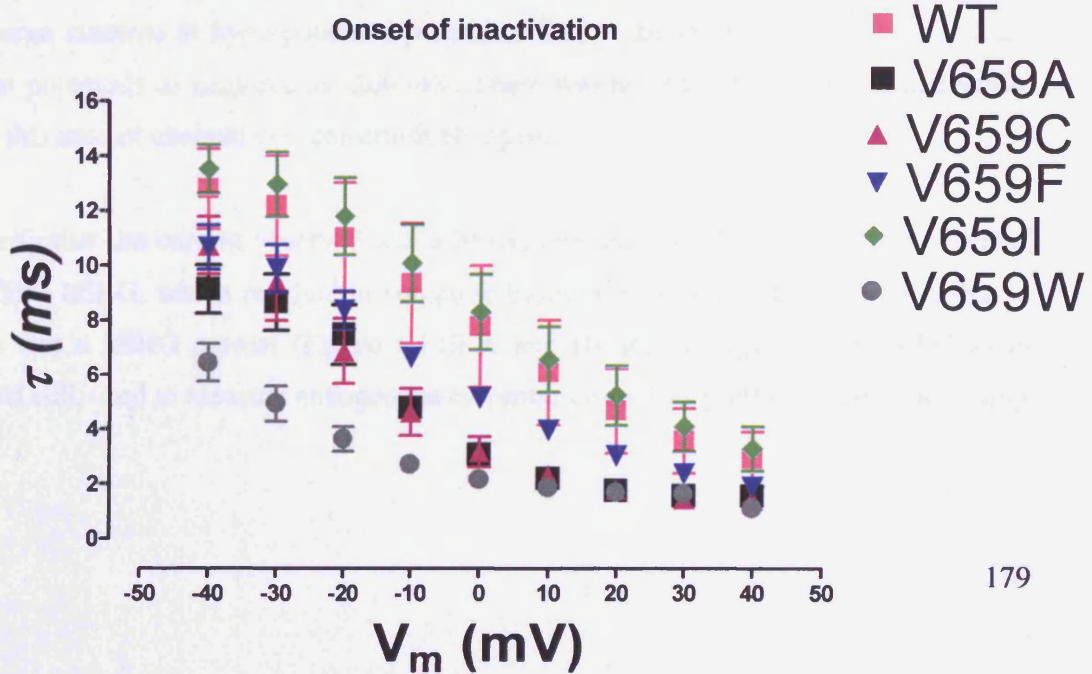
There was no clear trend with regards to residue size and the effects observed on the recovery and onset of inactivation. V659W however appeared to have very fast inactivation gating, with effects on both the kinetics of the onset and recovery of inactivation, and that could explain the small outward currents observed at more depolarised potentials (see Figure 6.8). V659A also exhibited faster inactivation kinetics compared to WT hERG, although a slow increase in outward current was observed at positive potentials (see Figure 6.3). This mutant may have another slow inactivating component that is stabilised at positive potentials and causes the unusual decrease in

**Figure 6.12: Time constants for the onset and recovery from inactivation for Val659 mutants.** A. A two pulse inactivation protocol was used to determine the time constants for recovery from inactivation for the Val659 mutants. Mean data were plotted against test voltages and compared to WT currents (n = 5). B. A triple pulse protocol was used to determine the time constants for onset of inactivation for the Val659 mutants. Mean data were plotted against test voltages from the second pulse and compared to WT currents (n = 5).

A.



B.



## Chapter 6- Roles of inner helix residues

amplitude of tail currents at potentials positive to 0 mV (see Figure 6.1). This stable inactivated state is also slow to recover from.

### 6.4 Substituting Val659 with a glycine residue

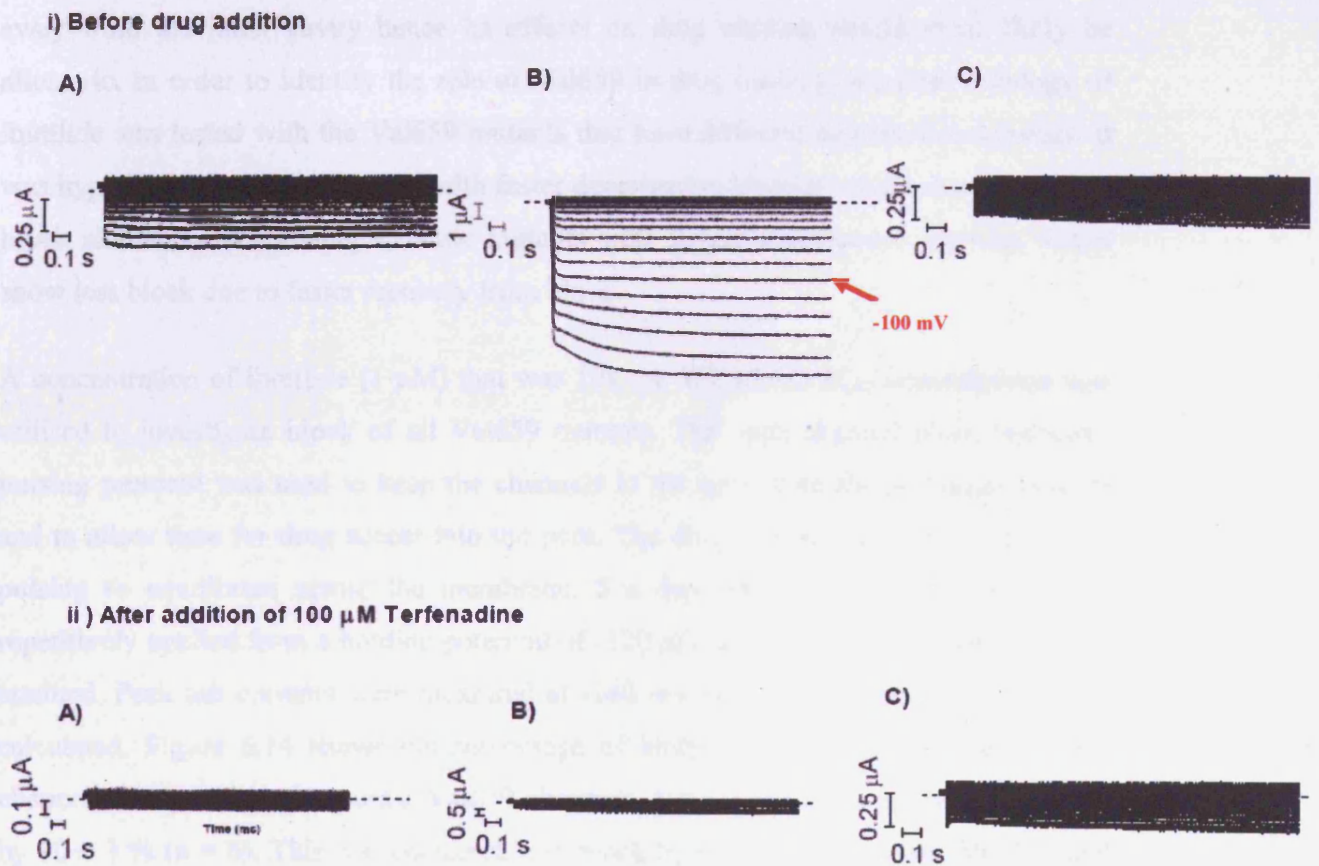
The Val659 residue was also substituted to a glycine to investigate its effects on gating. A glycine is the smallest amino acid residue and is thought to introduce flexibility within helices. Introducing a kink within this critical position on S6 near the putative activation gate could have interesting gating consequences. Since replacing the Val659 with an alanine residue caused dramatic slowing of the deactivation process and increasing the size of the residue at this position enhanced the rate of deactivation, then it would be expected that introducing a small glycine at this position would possibly have similar, if not even slower, deactivation kinetics to V659A.

Recordings from V659G hERG were done using 2 mM extracellular  $K^+$  solution. The holding current was unstable at negative potentials and continued to increase with pulsing so a holding potential of 0 mV was used and pulses from +50 to -160 mV were applied. Hardly any current ( $< 0.25 \mu A$ ) was observed in 2 mM  $K^+$  solution due to this channel being highly inactivated (Figure 6.13i A). Upon switching to high extracellular  $K^+$  solution (96 mM  $K^+$ ), inactivation was shifted back to more positive potentials and very large currents were obtained at potentials negative to -90 mV (Figure 6.13i B). V659G hERG was highly inward rectifying, displaying little current at depolarised potentials and very large currents at hyperpolarised potentials that continued to increase in amplitude even at potentials as negative as -200 mV. There was no indication of any deactivation; hence this mutant channel was constitutively open.

To verify that the current observed was a hERG current, 100  $\mu M$  terfenadine was added to V659G hERG, which resulted in complete block of these currents confirming that in fact it was a hERG current (Figure 6.13ii A and B). Recordings from a DEPC-water injected cell, used to measure endogenous currents, showed very little current when using

## Chapter 6- Roles of inner helix residues

**Figure 6.13: Gating properties of the V659G hERG currents.** i) Recordings were made with V659G hERG in 2 mM (A) then 96 mM  $K^+$  solution (B) by holding at 0 mV then stepping from +50 to -160 mV. The dashed lines indicate the zero current line. Endogenous currents in a DEPC-water injected cell are also shown (C). ii) 100  $\mu$ M terfenadine inhibited V659G hERG currents recorded from the same cells as (i) in 2 mM (A) and 96 mM  $K^+$  solution (B). Terfenadine had no effect on the current from the DEPC-water injected cell (C).



## Chapter 6- Roles of inner helix residues

the same voltage protocol (Figure 6.13i C). This current was also unaffected by the addition of 100  $\mu\text{M}$  terfenadine (Figure 6.13ii C). The mutation at this Val659 position to a glycine seemed to render the channel in a constitutively open state, possibly by uncoupling the S6 region from the S4-S5 linker and hence the voltage sensor.

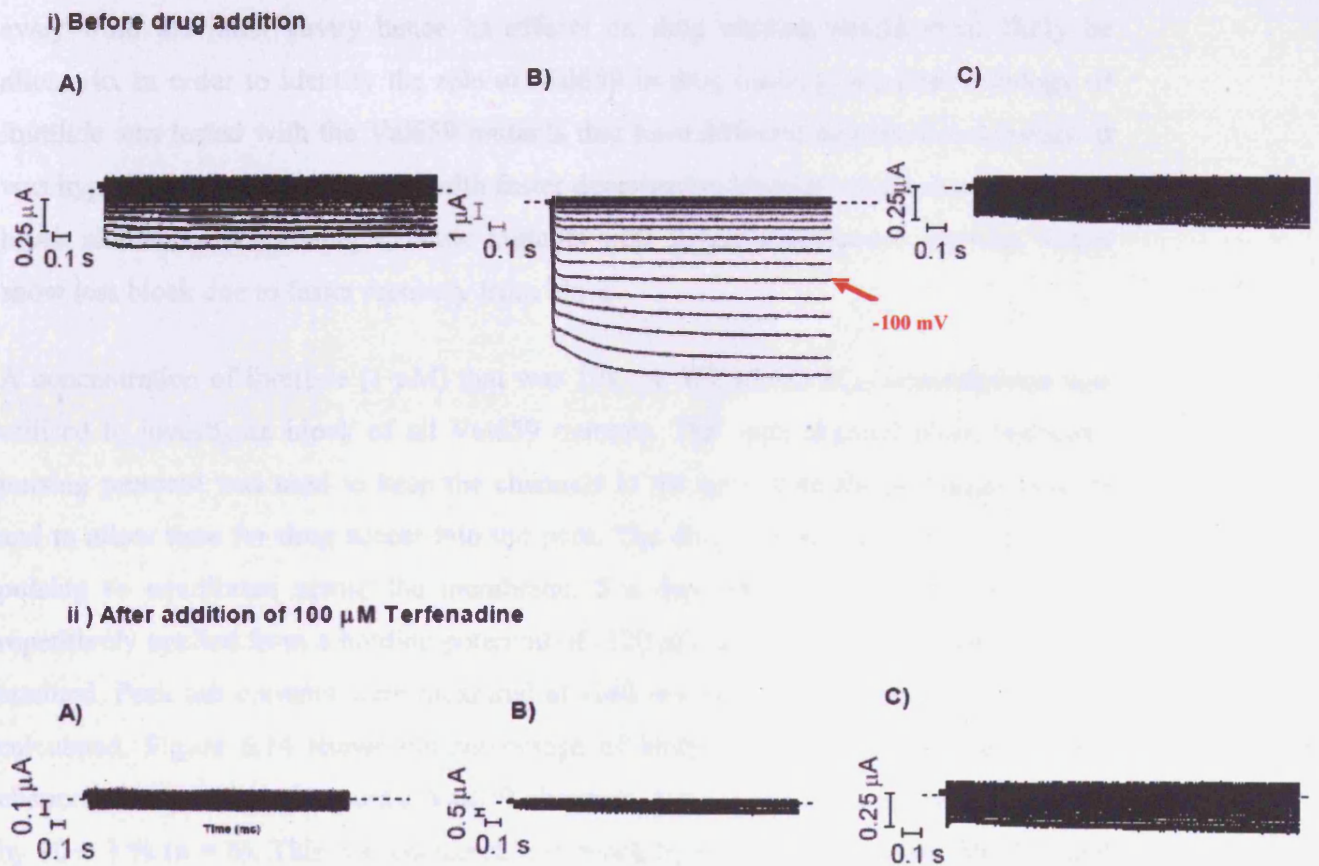
### 6.5 Pharmacology of Val659 mutants

Block of MK-499, in the alanine scan of S6 (Mitcheson *et al.*, 2000a), appeared to be sensitive to the V659A mutation. It was imperative to understand whether the observed changes in sensitivity to drugs were due to the effects of this mutation on the channel's deactivation kinetics. Homology models have suggested that the Val659 residue pointed away from the inner cavity hence its effects on drug binding would most likely be allosteric. In order to identify the role of Val659 in drug binding, the pharmacology of ibutilide was tested with the Val659 mutants that have different deactivation kinetics. It was hypothesised that the mutants with faster deactivation kinetics would show increased block similar to WT channels, while mutants with slower deactivation kinetics would show less block due to faster recovery from block.

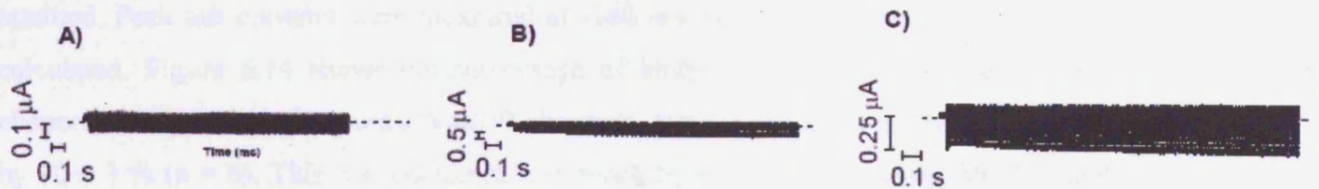
A concentration of ibutilide (1  $\mu\text{M}$ ) that was 10x the WT hERG  $\text{IC}_{50}$  concentration was utilised to investigate block of all Val659 mutants. The open channel block repetitive pulsing protocol was used to keep the channels in the open state for prolonged periods and to allow time for drug access into the pore. The drug was applied 2 minutes before pulsing to equilibrate across the membrane. 5 s depolarising pulses to 0 mV were repetitively applied from a holding potential of -120 mV until steady state inhibition was attained. Peak tail currents were measured at -140 mV and the percentage of inhibition calculated. Figure 6.14 shows the percentage of inhibition by 1  $\mu\text{M}$  ibutilide of WT channels compared to the mutant Val659 channels. 1  $\mu\text{M}$  ibutilide blocked WT currents by  $90 \pm 1\%$  ( $n = 6$ ). This was comparable to block by the fast deactivating V659W and V659I channels, which were blocked by  $83 \pm 3\%$  and  $77 \pm 2\%$  respectively ( $n = 6$  and  $p > 0.05$  for each). The slower deactivating currents exhibited significantly less block with percentages of inhibition of  $57 \pm 6\%$  for V659A,  $44 \pm 3\%$  for V659A NTK,  $54 \pm 5\%$

## Chapter 6- Roles of inner helix residues

**Figure 6.13: Gating properties of the V659G hERG currents.** i) Recordings were made with V659G hERG in 2 mM (A) then 96 mM  $K^+$  solution (B) by holding at 0 mV then stepping from +50 to -160 mV. The dashed lines indicate the zero current line. Endogenous currents in a DEPC-water injected cell are also shown (C). ii) 100  $\mu$ M terfenadine inhibited V659G hERG currents recorded from the same cells as (i) in 2 mM (A) and 96 mM  $K^+$  solution (B). Terfenadine had no effect on the current from the DEPC-water injected cell (C).



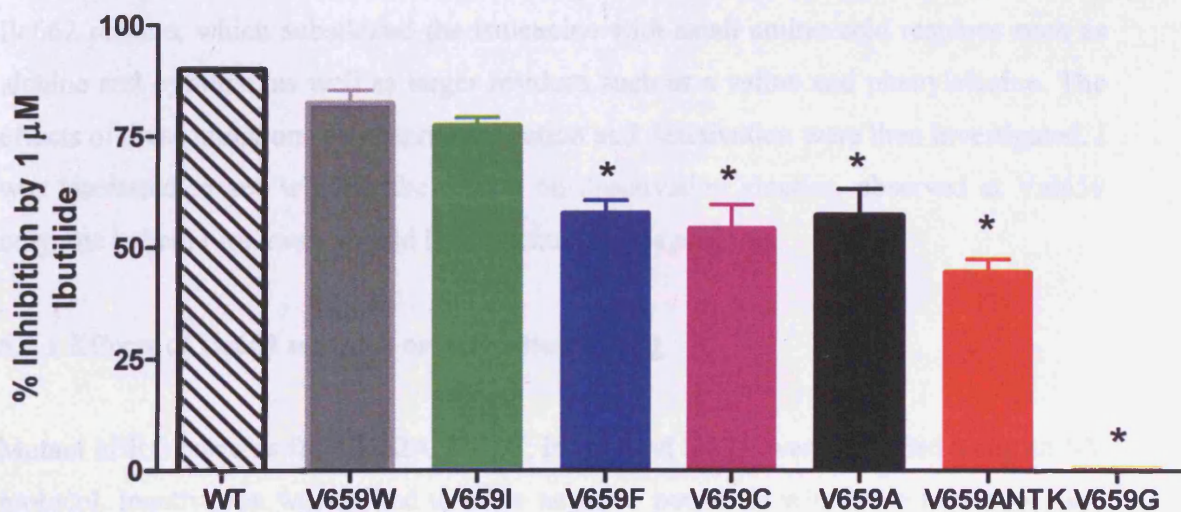
**ii) After addition of 100  $\mu$ M Terfenadine**



## Chapter 6- Roles of inner helix residues

**Figure 6.14: Block of Val659 mutants with ibutilide.** 1  $\mu$ M ibutilide was used to compare inhibition between WT and Val659 mutant channels. Mean percentage of inhibition obtained after the current reaches steady state is shown for WT and the Val659 mutants (n = 6). Some of the error bars, for instance for WT hERG, are very small.

\* p < 0.01



## Chapter 6- Roles of inner helix residues

for V659C, and  $58 \pm 3$  % for V659F hERG currents ( $n = 6$  and  $p < 0.01$  for each). V659G currents were not significantly inhibited by the addition of  $1 \mu\text{M}$  ibutilide ( $n = 6$  and  $p < 0.01$ ), suggesting that the binding site was modified by this mutation. Overall, the results support the view that the changes in sensitivity to drug block are related to changes to the open probabilities of channels rather than a direct interaction with the Val659 residue. This residue, thought to face away from the inner cavity, appears to exert allosteric effects on the hERG drug binding site.

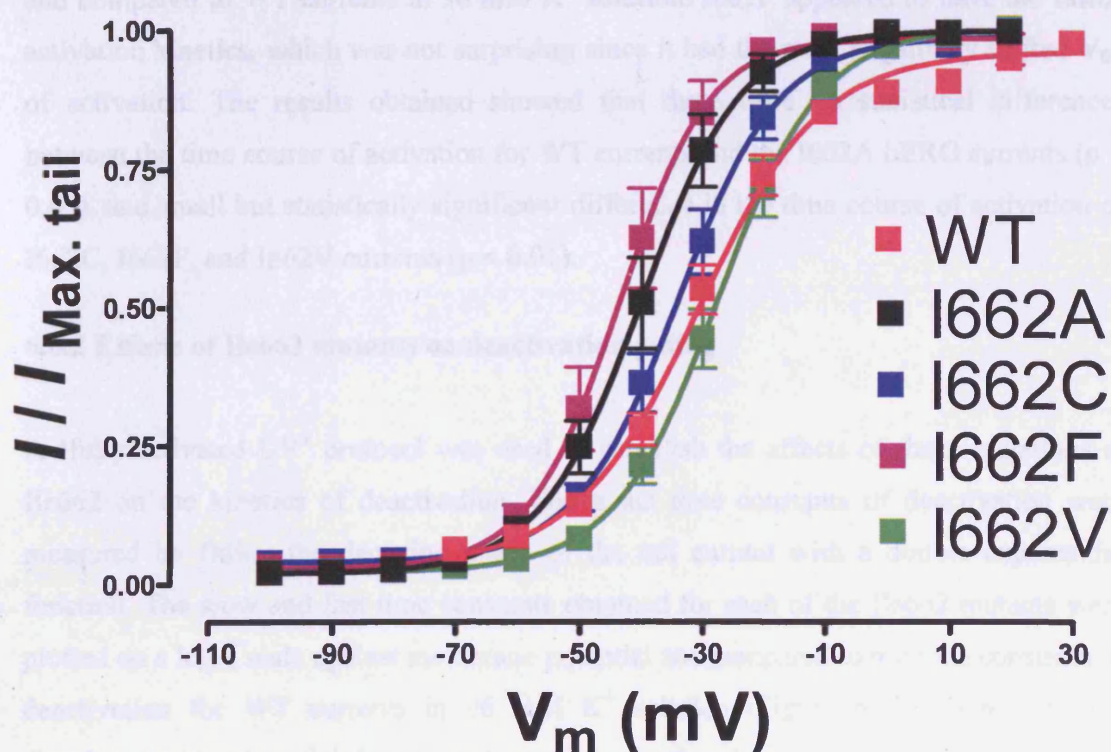
### 6.6 Effects of mutations at Ile662 on gating

Ile662 is one helical turn below Val659 and is predicted to be at the narrowest point of the pore in the closed state. Mutations at this position may also have profound effects on channel gating and packing around this region. A number of mutations were made at the Ile662 residue, which substituted the isoleucine with small amino acid residues such as alanine and cysteine, as well as larger residues such as a valine and phenylalanine. The effects of these mutations on channel activation and deactivation were then investigated. I was interested to see whether the effects on deactivation kinetics, observed at Val659 only one helical turn away, would be replicated at this position.

#### 6.6.1 Effects of Ile662 mutants on activation gating

Mutant hERG currents from I662A, I662C, I662F, and I662V were recorded using an I-V protocol. Inactivation was shifted to more negative potentials with these mutations, and functional currents had to be recorded in  $96 \text{ mM}$  extracellular  $\text{K}^+$  solution. Depolarising pulses were applied to potentials ranging from  $-100$  to  $+20 \text{ mV}$  from a holding potential of  $-120 \text{ mV}$  and were followed by a repolarising step to  $-140 \text{ mV}$  to elicit a tail current. With the exception of I662V, the voltage dependence of activation was negatively shifted with the Ile662 mutant currents compared to WT currents (Figure 6.15). I662F currents seemed to be the most negatively shifted. The voltage dependence of activation of I662A and I662F was significantly different from WT hERG ( $p < 0.01$ ), but I662C and I662V

**Figure 6.15: Current-voltage relationship of Ile662 mutant currents.** Peak tail currents for Ile662 mutant currents were normalised and plotted against membrane potential then fitted with a Boltzmann function ( $n \geq 5$ ). The voltage dependence of activation of WT currents in 96 mM  $K^+$  solution was plotted for comparison. The values obtained for the  $V_{0.5}$  of activation and slope factor are reported in the table and statistical differences are indicated by (\*\*), whereby  $p < 0.01$ .



	$V_{0.5}$ of activation (mV)	Slope (mV)	n
WT	$-30.8 \pm 0.9$	$10 \pm 0.8$	6
I662A	$-40.1 \pm 0.9$ **	$8.1 \pm 0.8$	6
I662C	$-34.1 \pm 0.7$	$8.3 \pm 0.7$	5
I662F	$-43.7 \pm 0.9$ **	$7.3 \pm 0.9$	5
I662V	$-27.6 \pm 0.7$	$8.5 \pm 0.6$	6

## Chapter 6- Roles of inner helix residues

were not ( $p > 0.05$ ). There was no particular trend between residue size and shifts to the voltage dependence of activation at this position.

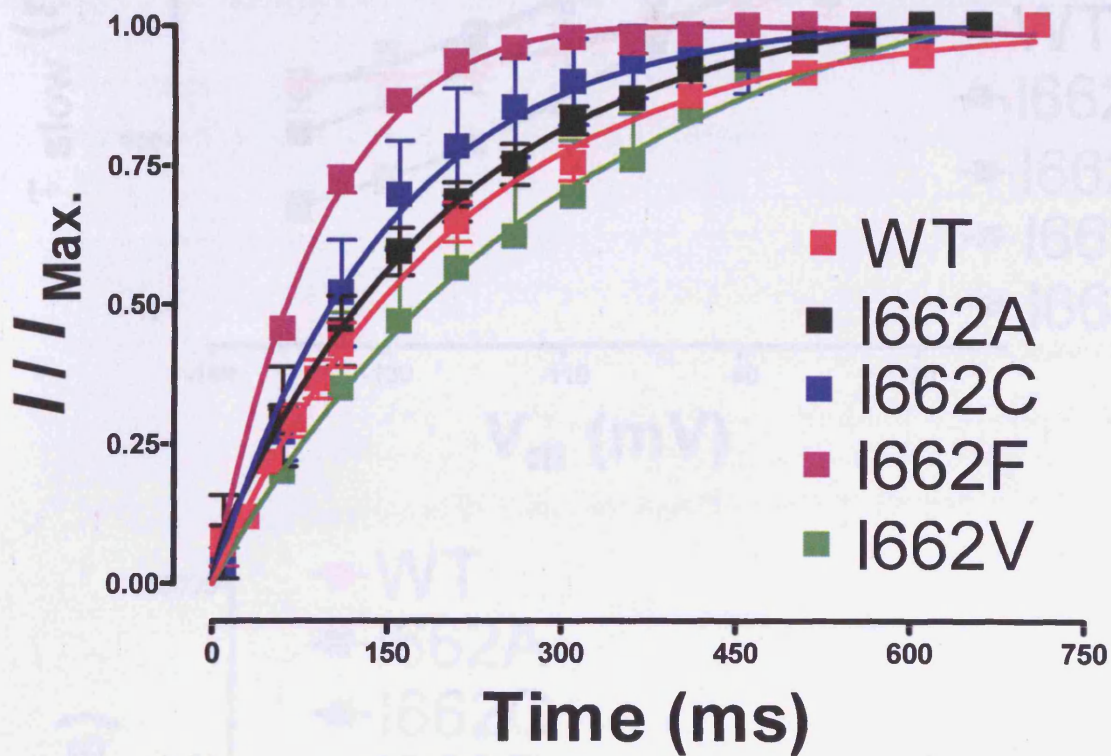
The time constants of activation were measured using an 'envelope of tails' protocol at 0 mV from a holding potential of -120 mV and a tail current at -140 mV. The peak tail currents obtained were normalised to maximal steady state current and plotted against duration of pulse to 0 mV (Figure 6.16). Mean results were fit with a single exponential and compared to WT currents in 96 mM  $K^+$  solution. I662F appeared to have the fastest activation kinetics, which was not surprising since it had the most negatively shifted  $V_{0.5}$  of activation. The results obtained showed that there were no statistical differences between the time course of activation for WT currents and the I662A hERG currents ( $p > 0.05$ ), and small but statistically significant difference in the time course of activation of I662C, I662F, and I662V currents ( $p < 0.01$ ).

### 6.6.2 Effects of Ile662 mutants on deactivation gating

A 'fully-activated I-V' protocol was used to establish the effects of these mutations at Ile662 on the kinetics of deactivation. The mean time constants of deactivation were measured by fitting the decaying phase of the tail current with a double exponential function. The slow and fast time constants obtained for each of the Ile662 mutants were plotted on a  $\log_{10}$  scale against membrane potential and compared to the time constants of deactivation for WT currents in 96 mM  $K^+$  solution (Figure 6.17). Generally, the deactivation kinetics of Ile662 mutants were slower than WT, and I662V had the slowest deactivation kinetics. It was apparent however that the dramatic slowing of deactivation observed with the Val659 mutants was not replicated with any of the Ile662 mutants.

At -90 mV, the slow time constants obtained in 96 mM  $K^+$  solution were  $922 \pm 144$  ms for I662A ( $n = 5$ ),  $1242 \pm 303$  ms for I662C ( $n = 5$ ),  $1961 \pm 258$  ms for I662V ( $n = 5$ ), and  $717 \pm 83$  ms for I662F ( $n = 5$ ) compared to  $579 \pm 66$  ms for WT currents ( $n = 5$ ). The fast time constants obtained at -90 mV were  $199 \pm 37$  ms for I662A ( $n = 5$ ),  $249 \pm 45$  ms for I662C ( $n = 5$ ),  $288 \pm 61$  ms for I662V ( $n = 5$ ), and  $116 \pm 35$  ms for I662F ( $n = 5$ )

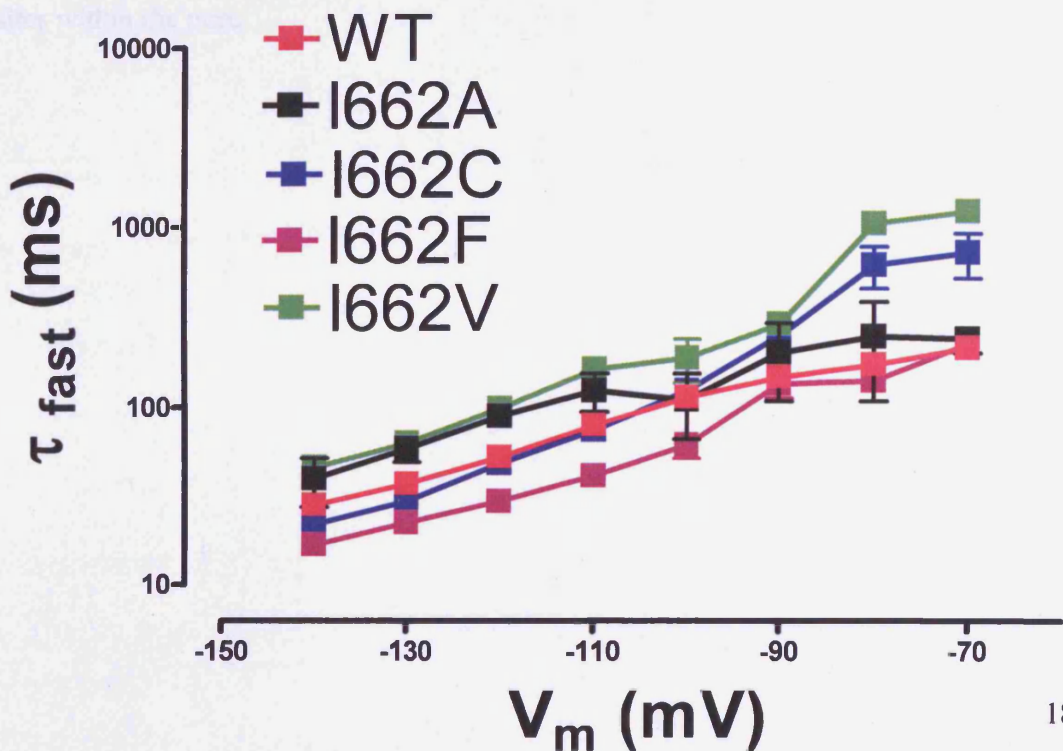
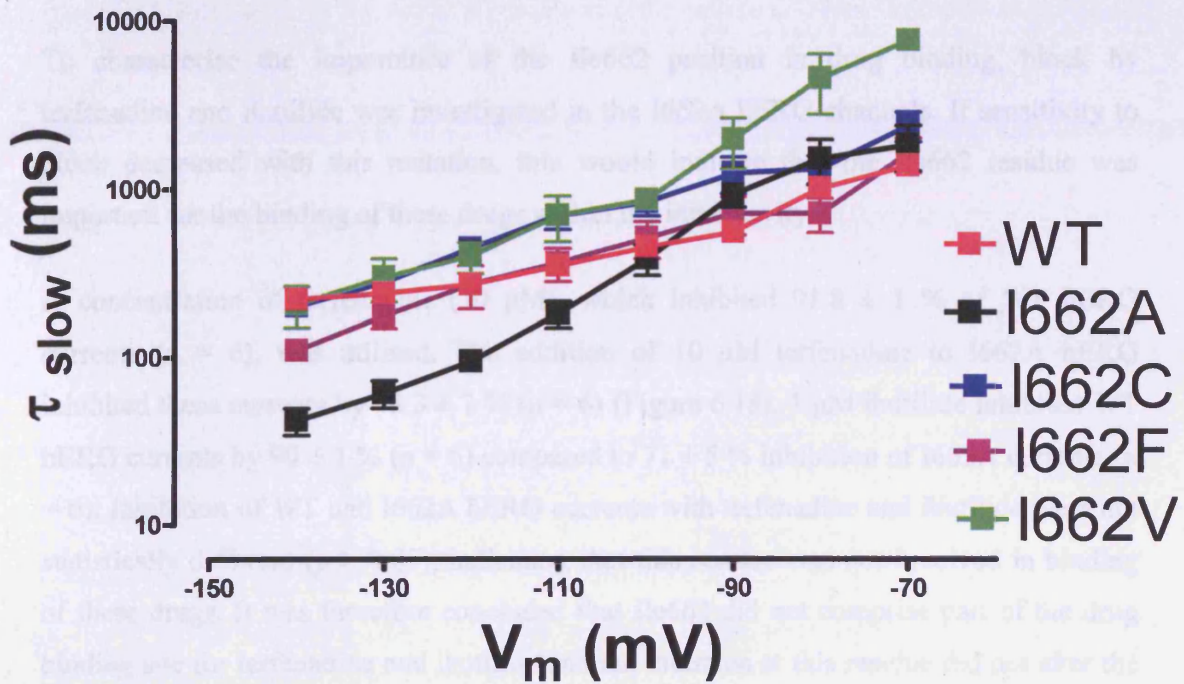
**Figure 6.16: Time dependence of activation of Ile662 mutant currents at 0 mV.** Mean peak tail currents at 0 mV of the Ile662 mutants were fit with a single exponential and compared to the time course of activation for WT currents in 96 mM K<sup>+</sup> solution (n = 5). Statistical differences between WT and Ile662 mutant hERG currents are indicated by (\*\*), whereby p < 0.01.



	$\tau$ of activation (ms)	n
WT	214 ± 29	5
I662A	191 ± 16	5
I662C	138 ± 19 **	5
I662F	76 ± 3 **	5
I662V	292 ± 31 **	5

Chapter 6- Roles of inner helix residues

**Figure 6.17: Mean time constants of deactivation for Ile662 mutants.**  $\tau_{fast}$  and  $\tau_{slow}$  of deactivation for Ile662 mutants were plotted on a log<sub>10</sub> scale against membrane potential and compared to WT currents in 96 mM K<sup>+</sup> solution (n = 5).



## Chapter 6- Roles of inner helix residues

compared to  $108 \pm 33$  ms for WT currents ( $n = 5$ ). Only I662V appeared to have significantly slower deactivation kinetics compared to WT hERG ( $p < 0.05$ ).

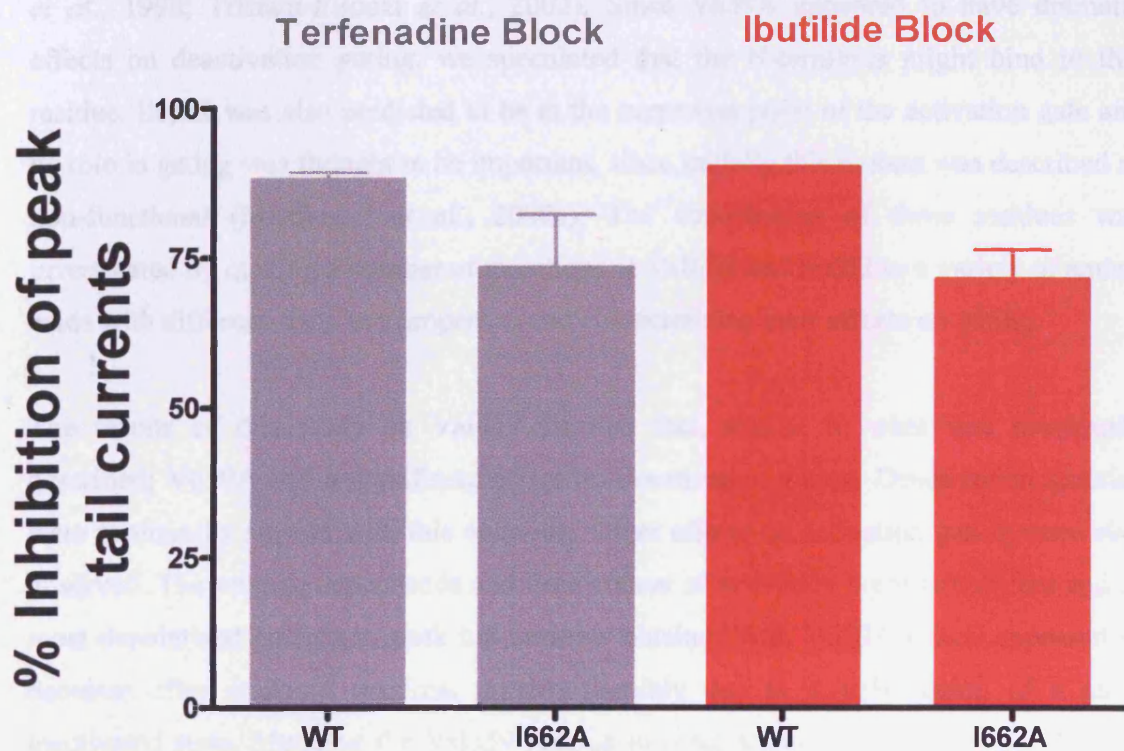
### 6.7 Effects of I662A on hERG pharmacology

To characterise the importance of the Ile662 position in drug binding, block by terfenadine and ibutilide was investigated in the I662A hERG channels. If sensitivity to block decreased with this mutation, this would indicate that the Ile662 residue was important for the binding of these drugs within the inner cavity.

A concentration of terfenadine ( $10 \mu\text{M}$ ), which inhibited  $91.8 \pm 1$  % of WT hERG currents ( $n = 6$ ), was utilised. The addition of  $10 \mu\text{M}$  terfenadine to I662A hERG inhibited these currents by  $73.3 \pm 7$  % ( $n = 6$ ) (Figure 6.18).  $1 \mu\text{M}$  ibutilide inhibited WT hERG currents by  $90 \pm 1$  % ( $n = 6$ ) compared to  $71 \pm 5$  % inhibition of I662A currents ( $n = 6$ ). Inhibition of WT and I662A hERG currents with terfenadine and ibutilide were not statistically different ( $p > 0.05$ ), indicating that this residue was not involved in binding of these drugs. It was therefore concluded that Ile662 did not comprise part of the drug binding site for terfenadine and ibutilide and the mutation at this residue did not alter the structure of the inner cavity to significantly change the binding of these drugs to other sites within the pore.

## Chapter 6- Roles of inner helix residues

**Figure 6.18: Pharmacology of the I662A hERG channel.** Recordings were made using the open channel block protocol with WT and I662A hERG channels. Terfenadine (10  $\mu\text{M}$ ) and ibutilide (1  $\mu\text{M}$ ) were used to assess inhibition. The mean percentage of inhibition with terfenadine is plotted for WT and I662A hERG currents in grey and inhibition with ibutilide for WT and I662A hERG currents is shown in red ( $n = 6$ ). Some of the error bars are very small.



## Chapter 6- Roles of inner helix residues

### 6.8 Discussion

This chapter describes the role of two particular residues, Val659 and Ile662 located on the S6 of hERG, on channel gating and pharmacology. Both these residues hold key positions within S6 by being at the bottom of the inner helices, close to the proposed bundle cross-over point and putative activation gate of hERG (Mitcheson *et al.*, 2000a). V659A was also shown in a previous study to affect deactivation gating by slowing it even further (Mitcheson *et al.*, 2000a). The N-terminus in hERG has been shown to be important in slowing the deactivation process in hERG (Schonherr & Heinemann, 1996; Terlau *et al.*, 1997; Wang *et al.*, 1998; Chen *et al.*, 1999) and is stabilised by binding to sites in the S4-S5 linker which interact with residues in the C-terminal end of S6 (Wang *et al.*, 1998; Tristani-Firouzi *et al.*, 2002). Since V659A appeared to have dramatic effects on deactivation gating, we speculated that the N-terminus might bind to this residue. Ile662 was also predicted to be at the narrowest point of the activation gate and its role in gating was thought to be important, since initially this mutant was described as non-functional (Mitcheson *et al.*, 2000a). The contribution of these residues was investigated by making a number of mutations at Val659 and Ile662 to a variety of amino acids with different sizes and properties and characterizing their effects on gating.

The results of this study on Val659 showed that, similar to what was previously described; V659A had a significant effect on deactivation gating. Deactivation kinetics were profoundly slowed with this mutation. Other effects on activation gating were also observed. The voltage dependence and time course of activation were left-shifted and at most depolarised potentials, peak tail currents obtained with V659A hERG appeared to decrease after reaching maximal current possibly due to a stabilisation of a slow inactivated state. Mutating the Val659 residue to other amino acids (Cys, Phe, Ile, and Try) did not show this property in their activation curves. They all however had a negative shift in their voltage dependence of activation. Increasing the size of the residue at Val659 appeared to increase the deactivation rate, although these currents were still slower than WT. These mutants increased the proportion of the slow deactivating component, and exhibited a loss of the fast component at more positive potentials.

## Chapter 6- Roles of inner helix residues

Surprisingly, the effects of V659A on deactivation were not totally due to changes in the slow deactivating component but rather to both the slow and fast components. V659A and V659C deactivated slowly possibly by stabilising the open state of the channel, while V659F, V659I, and V659W activated quickly and possibly destabilise the closed state of the channel. Interestingly, the V659G mutation resulted in a constitutively open channel. It appears to be important that a hydrophobic residue is present at this position on S6 for the channel to deactivate normally. The deactivation in hERG may involve a two-step process, one of which involves the proposed interactions between the N-terminus and the Val659 residue.

NTK mutants of WT and V659A channels were characterised. These two mutants had significantly different activation and deactivation kinetics from each other and it was thus concluded that the N-terminus did not seem to bind to this Val659 position. Deactivation kinetics for V659A NTK channels were faster than its non-truncated V659A counterpart, suggesting that Val659 forms part of the receptor to which the N-terminus binds close to the S4-S5 linker. The results obtained with V659G further support this hypothesis as this mutation appeared to uncouple the S4-S5 linker and hence the voltage sensor from S6, leading to a channel which did not close.

Val659 was also shown to have effects on hERG pharmacology by exhibiting reduced sensitivity to MK-499 in the presence of the V659A mutation (Mitcheson *et al.*, 2000a). The effects on drug binding were attributed to the changes observed to its deactivation kinetics. It was also proposed to face away from the inner cavity and therefore its effects would be allosteric rather than due to a direct binding of the drug to this residue on S6. Effects on current inhibition by ibutilide correlated with changes in deactivation kinetics and hence, channel open probabilities. The mutants with faster deactivation kinetics showed inhibition that was similar to WT, while mutants with slower deactivation kinetics showed less inhibition, presumably because of more rapid recovery from inhibition. Thus, Val659 appears to have allosteric effects on the hERG drug binding site.

## Chapter 6- Roles of inner helix residues

The effects of mutations at Ile662 were also characterised in order to understand its role in gating as well as packing around this region. No profound effects on activation gating or pharmacology were observed, although surprisingly inactivation gating was shifted to negative potentials. The dramatic slowing of channel deactivation with V659A was not observed with these mutations, although Ile662 is only one helical turn away. This could suggest that Ile662 does not form part of the receptor to which the N-terminus binds and packing around this position may not be as critical for gating as the Val659 residue.



## Chapter 7- General Discussion

& Yifrach, 2004; Zhao *et al.*, 2004a; Zhao *et al.*, 2004b; Ding *et al.*, 2005; Seebold *et al.*, 2006). Loss of channel function was not due to impaired membrane surface expression.

The possibility of another hinge site corresponding to the Pro-X-Pro motif, found near the bundle crossing, added another dimension to this gating mechanism. This second site was implicated in Shaker channels (Bright *et al.*, 2002) as well as in the eukaryotic Kv1.2 channel (Long *et al.*, 2005a). Prolines can also induce bending and flexibility into inner helices by disrupting the hydrogen bond backbone and inserting kinks into  $\alpha$ -helices. Thus, they may contribute to activation gating in eukaryotic channels (del Camino *et al.*, 2000; del Camino *et al.*, 2005). A study on the *Shaker* homologue Kv1.5, in which prolines at positions 509 and 511 of the Pro-X-Pro motif were both mutated to an alanine, resulted in non-functional channels (Labro *et al.*, 2003). Similarly, mutating Pro509 to an alanine or glycine resulted in non-functional channels, although the channels were trafficking to the cell surface. On the other hand, substituting Pro511 with alanine gave functional channels with an activation curve that was shifted more positively than the substitution with a glycine. The milder effects observed with the mutation to a glycine were not surprising as glycines can also induce flexibility into helices. This study implies a clear requirement for these prolines in normal channel gating. However, this motif is not fully conserved in  $K^+$  channels, and a second glycine residue analogous to the second proline residue is often observed. Interestingly, the non-functional mutants could be rescued by introducing prolines just a few amino acids upstream or downstream of position 509 indicating that the hinge point need not be conserved in a particular position but may be in different positions. In Shaker channels, the non-functional mutation at the hinge point (G466A) was rescued by introducing a glycine at position 467 (Ding *et al.*, 2005). It appears that the destabilisation of  $\alpha$ -helices, resulting from the presence of glycines or prolines, may be more essential than their exact position.

These findings raised the question as to the nature of activation gating in hERG channels. hERG has two glycines in S6, Gly648 analogous to the supposed gating hinge position and Gly657 corresponding to the second proline in the Pro-X-Pro motif in Kv channels.

## Chapter 7- General Discussion

An alanine scan of S6 reported that substitutions at either glycine had little effect on the properties of activation gating (Mitcheson *et al.*, 2000a).

The aim of my study was therefore, to elucidate the function of these S6 glycines in hERG activation gating. The question was whether either S6 glycine contributed to flexibility in gating or whether hERG channels opened via a different gating mechanism.

The results conveyed in chapter 3 of this thesis demonstrate that mutating these glycine residues, individually or simultaneously, to an alanine still results in a channel that is capable of opening and closing. This is surprising as alanine residues are known to stabilise  $\alpha$ -helices (Serrano *et al.*, 1992) and results were contrary to the effects of alanine substitutions on Shaker and other Kv channels (Magidovich & Yifrach, 2004; Ding *et al.*, 2005; Seebohm *et al.*, 2006). The small effect on hERG activation gating with these mutations was not consistent with a critical role of these glycine residues in hERG activation gating. Replacing the glycine residues with bulkier amino acid residues facilitated channel opening by causing a shift in the voltage dependence of activation to more negative potentials. Mutations at the Gly648 position also caused a significant slowing of the deactivation process, confirming a stabilisation of the open state. These results are not consistent with a gating hinge mechanism for activation gating in hERG, as the mutation of S6 glycines does not prevent channel gating. The data point to the importance of the small side chain volume of these glycine residues in the close packing of its inner helices. Studies using terfenadine, a large hERG channel blocker, further confirmed the ability of the channel to open relatively normally and allow open channel block by terfenadine, even in the absence of both glycines. Thus, despite removing both putative glycine hinges, the channel is able to open wide enough for terfenadine to access the inner cavity. These findings are very different to what has been observed with other channels, which usually result in a loss of channel function when the glycine is mutated to other amino acid residues. In addition, mutations of the putative glycine hinge point in Shaker channels result in channels that are slower to open, indicating that the mutations stabilise the closed state (Labro *et al.*, 2003; Ding *et al.*, 2005). My results show that mutations of the glycine residues increase the channel's open probability.

## Chapter 7- General Discussion

Further evidence to support this data includes work done in our laboratory by R.H. Hardman and P.J. Stansfeld (Hardman *et al.*, 2007). The glycine residues were substituted by a proline, which gave rise to terfenadine-sensitive currents that were unable to fully close. Thus, introducing prolines at these positions interfered with the tight packing of the inner helices and locked the channel in an open conformation. To provide further evidence that it was the size of the amino acid rather than polarity that resulted in the alteration of the channel's gating properties; glycines were substituted with serine residues. G657S and G648S had negatively shifted activation kinetics and dramatically slowed deactivation kinetics respectively. This is in line with what I observed with the other glycine mutants, in which I documented the different effects obtained depending on the position that was mutated. A good correlation was evident between side chain volume and gating properties. Larger side chain volumes at Gly648 shifted the voltage dependence of activation to the left (except for G648L) and dramatically slowed deactivation. This is consistent with mutants stabilising the open state. Mutations at Gly657 also shifted the voltage dependence to the left, but enhanced the rates of activation rather than deactivation, suggesting that these mutations destabilised the closed state. Both sets of findings strongly support a role for the glycine residues in packing, rather than bending. Molecular dynamics simulations of the kinking or swiveling motions of S6 were used to compare the conformational changes of the alanine mutants with WT channels. Analyzing the mobility of the S6 helices demonstrated that mutating the glycine residues had little impact on the flexibility of the helices (Hardman *et al.*, 2007). Unlike other Kv channels, hERG channels have sufficient inherent flexibility to allow gating movements of the S6 helices to occur, without the glycine residues acting as hinge points. It should also be stated that there are some K<sup>+</sup> and cyclic nucleotide gated channels, which lack a glycine in the equivalent position to the putative glycine hinge position. *Drosophila* EAG, KCNQ1, and some inward rectifier channels have an alanine at the hinge position and therefore function without the need for a glycine residue (Shealy *et al.*, 2003). In the case of KCNQ1, a Pro-X-Gly motif is likely to introduce flexibility and allow for movement of inner helices. Nevertheless, this is not the case for hERG channels as mutations at Gly657 enhance open probability. A number of recent studies also support our conclusion for a role of glycine residues in the tight packing of inner

## Chapter 7- General Discussion

helices. The heteromeric Kir4.1/Kir5.1 inward rectifier channels lack the conserved glycine at the proposed upper hinge position, but have a conserved glycine at the lower hinge position. Substituting the putative upper hinge positions (Thr154 and Ser157) with a glycine reduced channel opening and mutating the glycine at the lower hinge position with alanine gave functional currents with dramatically reduced whole cell currents compared to WT (Shang & Tucker, 2007). A homology model of the proposed lower hinge position showed that the small size of the glycine side chain allows for tight packing of the helices near the bundle crossing, hence mutations at this position affect channel activity by disrupting close packing in this region. Another study on a conserved glycine (Gly175) in Kir3.4 channels also favoured a role for glycines in tight packing within the channel due to their small size, rather than acting as a gating hinge (Rosenhouse-Dantsker & Logothetis, 2006). Replacing Gly175 with alanine resulted in a functional channel with substantially larger basal currents than WT, contrary to a role as a glycine hinge point. Non-functional mutants at Gly175 were rescued by substituting neighboring residues, leading the authors to conclude that this glycine is important for preventing interactions with residues around the selectivity filter that can impair channel function.

It has been suggested that activation gating may occur at the level of the selectivity filter in some channels, such as some inward rectifier and cyclic nucleotide gated channels (Flynn & Zagotta, 2001; Claydon *et al.*, 2003; Blunck *et al.*, 2006). In this model, the inner helices are not a barrier to ion flow, as the selectivity filter is the gate. I tested this model in hERG through state-dependent application of terfenadine. When terfenadine was applied to channels predominantly in the closed state, there was little block. Inhibition by terfenadine occurred only in the open state. Therefore, the motions of the S6 helices are likely to underlie the gate in hERG.

In conclusion, the results presented show the importance of glycines in hERG in the tight packing of the inner helices and that substitutions to bulkier residues result in channels with a higher open probability. The bacterial Na<sup>+</sup> channel NaChBac is also stabilised in the open state when the glycine is substituted with a proline (Zhao *et al.*, 2004a). Not

## Chapter 7- General Discussion

only did this proline substitution affect the voltage dependence of activation, but also reversed the polarity of channel gating, to give a hyperpolarisation-activated channel. This could have important implications for the mechanisms of gating of HCN channels. Interestingly, the D540K mutation on the S4-S5 linker of hERG allows entry into the open state readily upon hyperpolarisation due to the inability of interactions to form between residues on the S4-S5 linker and S6 that stabilise the closed state. It is possible that HCN channels may have altered polarity of opening compared with other Kv channels because of packing constraints in the pore and differences in the coupling between the S4-S5 linker and residues on S6 with other Kv channels. Interactions between the S4-S5 linker and post-S6 region have been shown to dictate polarity in these channels (Prole & Yellen, 2006). For instance, cross-linking interactions were shown to occur between F359C (on the S4-S5 linker) and K482C (on the C-linker) in the spHCN1 channel. With disulphide bond formation, an increase in current with depolarisation and a decrease in current in response to hyperpolarisation were measured. These effects were only observed upon cross-linking between these two regions, which then lead to a reversal in the channel's voltage dependence. Thus, changes in the polarity of channel gating are highly influenced by the differences in the coupling of the voltage sensor to the pore.

### 7.2 hERG deactivation gating

The crystal structure of Kv1.2 shed some light into the functional coupling between the voltage sensing domain and the pore region (Long *et al.*, 2005b). A striking feature was the relative independence of the voltage sensor in the X-ray structure and that its main coupling to the pore seemed to involve the simple use of the S4-S5 linker as a lever that pulls on the inner helices, thus constricting or dilating the pore. This 'electromechanical coupling' is crucial for voltage dependent gating in Kv channels. A number of studies support this concept of interaction between the S4-S5 linker and the pore. Functional chimeras were engineered by substituting the pore domain in Shaker with that of the voltage-independent KcsA channel, producing a voltage-sensitive channel. Mutations in either the S4-S5 linker or the C-terminal end of S6 resulted in a non-conducting channel,

## Chapter 7- General Discussion

indicating a clear requirement for both these regions to be present for voltage dependent gating (Lu *et al.*, 2001, 2002; Caprini *et al.*, 2005). Mutations of residues on the S4-S5 linker in Shaker (Isacoff *et al.*, 1991; Schoppa *et al.*, 1992; Slesinger *et al.*, 1993), Kv2.1 and Kv3.1 (Shieh *et al.*, 1997), and HCN channels (Chen *et al.*, 2001; Prole & Yellen, 2006) influence activation gating and gating charge movement. Similarly in hERG channels, studies have shown the importance of the S4-S5 linker in activation gating. A single charge reversal mutation of a residue on the S4-S5 linker (D540K) resulted in a channel exhibiting hyperpolarisation-dependent opening, by destabilising the closed state due to electrostatic repulsion with Arg665 on S6 (Tristani-Firouzi *et al.*, 2002). Moreover, D540C and L666C can form disulfide bridges in the closed state. Thus, specific interactions between certain residues on the S4-S5 linker and C-terminal end of S6 are necessary to stabilise the hERG channel activation gate in the closed conformation (Ferrer *et al.*, 2006).

The N-terminus in hERG has been shown to slow deactivation by stabilising the channel in the open state and increasing the channel's mean open time (Wang *et al.*, 2000), perhaps by binding to residues on the S4-S5 linker that are exposed upon activation (Wang *et al.*, 1998; Tristani-Firouzi *et al.*, 2002). A cysteine mutation of Gly546 on the S4-S5 linker in hERG was shown to mimic the phenotype of an N-terminal deletion, suggesting possible interactions between these two regions. The N-terminus is also thought to interact with residues on S6 at negative potentials, stabilising channel closure (Morais Cabral *et al.*, 1998; Wang *et al.*, 1998). N-terminal binding to its receptor site in hERG was shown to be sensitive to increasing extracellular K<sup>+</sup> concentration, suggesting that K<sup>+</sup> influx disrupts the binding of the N-terminus at a site located near the internal mouth of the pore. It may be possible that the N-terminal interactions within the channel hinder the formation of salt bridges between residues on the S4-S5 linker and S6, leading to a further slowing in the deactivation process. These results suggest that there is a complex network of interactions between these parts of the channel controlling its closure.

## Chapter 7- General Discussion

The aim of this study, discussed in chapter 6, was therefore to examine the complexities by which the N-terminus regulates channel deactivation. In an alanine scan of S6, the Val659 residue when mutated, resulted in a channel with extremely slowed deactivation kinetics (Mitcheson *et al.*, 2000a). I proposed a hypothesis that the Val659 residue may be a point of interaction between the N-terminus and the pore domain. Removal of the N-terminus of V659A hERG channels was expected to produce currents that deactivated at the same rate as NTK hERG. Although faster deactivating currents were attained, they were still slower than NTK hERG. It seems that V659A still slows deactivation, even in the absence of the N-terminus. This suggests that at least two mechanisms are in play to control deactivation; one mechanism which was influenced by the mutation at Val659, and another influenced by the N-terminus. These mechanisms may not be totally separate as Val659 may still contribute to the receptor site for the binding of the N-terminus. This receptor site is also likely to involve residues on the S4-S5 linker, as R665A on S6 has been shown to come into close proximity to D540K on the S4-S5 linker and also exhibits similar deactivation kinetics to V659A. It would be interesting to investigate any possible interactions between residues on the S4-S5 linker and Val659.

I substituted Val659 with differently sized residues and observed a negative shift in the voltage dependence of activation for all these mutants compared to WT hERG. Although all mutants had slower deactivation kinetics than WT hERG, a trend emerged whereby the small residues (Ala and Cys) had the slowest deactivation kinetics, whilst larger residues (Phe, Ile, Try) appeared to increase the deactivation rate. The main effects are owed to the increase in the slow time constant of deactivation and a tremendous reduction in the fraction of the fast deactivating current component at negative potentials. Although this was the case for most Val659 mutants, it was evident that V659A was different, exhibiting effects on both the fast and slow deactivating components. The varying effects on the two time constants of deactivation may have mechanistic implications. They may indicate that deactivation is a two-step process involving different sets of interactions with residues within the channel, which can also be modified independently by mutations.

## Chapter 7- General Discussion

Interestingly, V659G hERG is constitutively open and gated only by inactivation, perhaps by uncoupling the activation gate from the voltage sensor. Although the mutations to the smallest residue (V659G) and largest residue (V659W) increased open channel probabilities, the mechanisms are distinct. V659G appears to stabilise the open state, possibly by uncoupling the voltage sensor from the pore region, as the channel is constitutively open and does not deactivate even at very hyperpolarised potentials. In contrast, V659W destabilises the closed state, perhaps by disrupting packing of the inner helices in the closed state. Activation is rapid due to a large negative shift in the voltage dependence of activation but with little effect on the time dependent kinetics of channel deactivation. I postulate that a hydrophobic interaction between Val659 and residues on S4 or the S4-S5 linker may be necessary for normal deactivation.

V659A tail currents showed an interesting decrease in amplitude at potentials positive to 0 mV. This has been shown with a mutation of a residue found at the bottom of S4, Lys538, to cysteine (Hardman, R.H.; unpublished results). This mutant also exhibits slowed deactivation and it would be interesting to establish whether a possible link can be made between this position and Val659. The decrease in tail current amplitude may be attributed to a stable inactivated state. The conformational changes that unfold during inactivation gating are quite complex and not very well understood. It is thought that a fast P-type inactivation occurs leading to closure of the channel pore, followed by a slower yet more stable inactivated conformation known as C-type inactivation in which gating charge is immobilised. A recent study showed a clear separation between these inactivated states in hERG channels (Gang & Zhang, 2006). A Na<sup>+</sup> conductance could be measured through the hERG channel when extracellular Na<sup>+</sup> and K<sup>+</sup> ions were exchanged for N-methyl-d-glucamine (NMG) and intracellular K<sup>+</sup> was substituted for Na<sup>+</sup>. The Na<sup>+</sup> permeates only through the P-type inactivated conformation of the hERG channels. The inactivated state proposed for V659A appears to be extremely slow to recover from. Thus, V659A and K538C may exhibit a form of C-type inactivation that is more left-shifted or faster than in WT hERG. Other mutations at Val659 also had variable effects on P-type inactivation. V659W, for instance, exhibits fast kinetics for both the onset and recovery from inactivation, hence showing little outward current at depolarised

## Chapter 7- General Discussion

potentials. Regulation of hERG inactivation, as well as deactivation, is thought to involve the N-terminus as deletion of the N-terminus has been previously shown to slow C-type inactivation in hERG (Wang *et al.*, 1998). This earlier study also reported that the modification of G546C in the S4-S5 loop by MTS reagents disrupts both deactivation and inactivation gating, suggesting that both processes are influenced by the N-terminus binding to a site near that region. Based on my Val659 mutations, I would hypothesize that Val659 and other residues on S6 and the S4-S5 linker all contribute to a receptor site for the N-terminus in the open state. Different functional domains of the N-terminus may regulate deactivation and inactivation gating (Wang *et al.*, 1998). Thus, a complex network of interactions has evolved within the channel to mediate deactivation gating. This process may involve a sequential coupled movement of different parts of the channel. hERG is unusual because the disruption of interactions between the voltage sensor and the pore result in the channel not fully or stably closing. Unlike other Kv channels, hERG is energetically stable in the open state and interactions between the S4-S5 linker and S6 are required to keep it closed. Thus, the voltage sensor has to exert positive work to close the channel and there are latch-like mechanisms to keep the channel closed.

The results presented in this study give some insight into the mechanism behind the slowing of hERG deactivation gating. Additional experiments to consider would be those aiming at elucidating a precise network of interactions between S6, the S4-S5 linker, and the N-terminus. My data suggests a receptor site for the N-terminus at the intracellular mouth of the pore that may encompass the Val659 residue. The exact location of this receptor site may be established by mutating residues further downstream of Ile662 and investigating their effects on deactivation. I also proposed possible interactions between residues at the bottom of S4, such as Lys538, and the S4-S5 linker with Val659. A cysteine scan of this region would be necessary followed by an investigation into possible cross-linking interactions between cysteine-substituted residues on the S4-S5 linker and V659C. These further experiments may present a structural basis for hERG deactivation gating.

## Chapter 7- General Discussion

### 7.3 The hERG drug binding site

Studies have identified the inner cavity of hERG as being the main drug binding site. Consequently, residues lining the S6 inner helices are not only involved in different aspects of gating but are also fundamental in high affinity binding to hERG. A comprehensive characterisation of the drug binding site was achieved by an alanine-scanning mutagenesis approach (Mitcheson *et al.*, 2000a). Individual residues were mutated to alanine and the sensitivity to MK-499, cisapride, and terfenadine was assessed. This study revealed that the mutation of Phe656 and Tyr652 decreased the affinity of all three compounds. The mutations at the pore helix (Thr623, Ser624, and Val625) and those at Gly648 and Val659 located on the S6 domain, had variable effects on the potency of drugs. These residues therefore modify the drug binding site in different ways.

Gly648 in hERG, as discussed earlier, corresponds to the proposed hinge point in K<sup>+</sup> channels (Jiang *et al.*, 2002b). G648A had minor effects on hERG activation gating but did shift the voltage dependence of inactivation to more negative potentials. Changes to drug sensitivity may be attributed to changes in the inactivation properties; however the effects of G648A were not consistent between all drugs. Block by MK-499 appeared to be sensitive to the Gly648 mutation, but terfenadine and cisapride were not. My results also show that terfenadine can still block the inner cavity in the open state with various residues substituted at this position. Therefore, mutations at this position do not significantly alter the structure of the terfenadine binding site. An alternative scenario may be that a binding pocket formed between the pore helix and S6 can be occluded by mutations at this position. I have shown that Gly648 is highly critical in the close packing of the inner helices. It may also be possible that larger residues at this position obstruct interactions with the pore helix residues, Thr623 and Ser624. The hydroxyl groups of these two residues are directly involved in drug binding and are likely to be optimally positioned to form hydrogen bonds with compounds, such as ibutilide and clofilium (Perry *et al.*, 2004; Perry *et al.*, 2006). One of the aims of this project was to understand why Gly648 and the pore helix residues, Thr623 and Ser624, are important in the binding

## Chapter 7- General Discussion

of some drugs to hERG, but not all. The rationale was to use a large number of compounds in order to establish how structurally diverse drugs interact with these key residues in the inner cavity. Despite numerous attempts in making stable cell lines containing the G648A and T623A:S624A mutations, i was unable to obtain cell lines with high enough expression for use in these studies. It therefore still remains unclear why some drugs are highly sensitive to these mutations, while others are not. Although reducing temperature and using sodium butyrate did not enhance cell surface expression, it would be interesting to find other ways that may increase hERG expression in these cell lines.

On the other hand, my studies are able to establish that the effects observed with V659A on drug potency, can be ascribed to the changes in the channel's deactivation kinetics. I showed that the Val659 mutants with faster deactivation kinetics exhibited increased block similar to WT channels, while mutants with slower deactivation kinetics showed less block due to faster recovery from block. Hence, with V659A, the open probability of the channel was greater than WT, allowing faster recovery from block and therefore, affecting drug sensitivity. Homology models also suggest that Val659 points away from the inner cavity and therefore this residue does not directly interact with drugs, but rather has allosteric effects on drug binding to the hERG channel. The Ile662 residue, one helical turn away from Val659, is also not involved in drug binding.

The aromatic residues on S6, Phe656 and Tyr652, have been shown to be important in the binding of a large number of drugs within the inner cavity (Mitcheson *et al.*, 2000a; Perry *et al.*, 2004; Witchel *et al.*, 2004; Perry *et al.*, 2006; Sanguinetti & Tristani-Firouzi, 2006). These residues are not conserved in Kv channels. Most Kv channels have aliphatic isoleucine or valine residues in equivalent positions. The presence of aromatic residues in hERG therefore provides this channel with unique structural features aiding its pharmacological promiscuity. These aromatic residues on S6 can form hydrophobic as well as electrostatic  $\pi$ - $\pi$  interactions with aromatic groups on drug molecules and cation- $\pi$  interactions with charged amines. In particular, mutations at these positions showed that hydrophobicity was important for Phe656 whereas aromaticity was important for Tyr652

## Chapter 7- General Discussion

binding to three structurally diverse drugs (MK-499, cisapride, and terfenadine) (Fernandez *et al.*, 2004). This may not be true for all drugs. Although it was at first assumed that both residues would contribute to the binding site of most drugs, it now appears that for some compounds, one or neither is required (Milnes *et al.*, 2003a; Sanchez-Chapula *et al.*, 2003; Ridley *et al.*, 2004; Witchel *et al.*, 2004; Kamiya *et al.*, 2006; Milnes *et al.*, 2006). In order to further investigate the contribution of Tyr652, a stable cell line with the Y652A hERG mutation was used and experiments carried out on a set of 24 compounds using the PatchXpress 7000A. The planar electrode technology of this automated system is discussed in chapter 5 of this thesis and demonstrates a robust and accurate method for obtaining concentration-response curves for hERG blockers. A dataset of  $IC_{50}$  values was obtained for WT and Y652A hERG with 24 LQT-compounds and the fold change in  $IC_{50}$  in the presence of the tyrosine mutation was calculated. On the basis of this data, two groups of compounds emerged, termed Group A and Group B. Group A compounds were the most potent compounds with an  $IC_{50}$  value  $< 100$  nM in WT hERG and most were highly sensitive to the Y652A mutation by exhibiting a change in  $IC_{50} \geq 50$  fold. Whilst Group B compounds varied in potency between 100 nM and over 25  $\mu$ M and were less affected by this mutation giving a change in  $IC_{50} < 10$  fold. It was clear from this study that many more compounds than previously expected, did not require the Tyr652 residue for binding within the inner cavity. The question then became, what is the reason for this variability?

Pharmacophore modeling was then used to structurally explain this data. Three-point pharmacophore models were built for Group A and Group B compounds and show a common central nitrogen group and a hydrophobic group at position 1. The position of the second hydrophobic feature differs in each group. Group A compounds are more elongated and Group B compounds are shorter. My results suggest that in the absence of Tyr652, Group B compounds are more flexible and are capable of orientating within the channel to form other interactions, most likely with Phe656. The compact structure of these compounds may therefore enable them to occupy a variety of different binding modes. Group A compounds, on the other hand, have longer conformations that could make them less flexible and less likely to occupy other binding conformations. Hence, the

## Chapter 7- General Discussion

absence of the Tyr652 residue profoundly affects their binding affinity within the channel. I conclude that the Tyr652 residue is important for the interaction of the longer, more potent compounds within the hERG inner cavity, but is less important for the smaller, less potent compounds which may easily orientate to form other interactions within the pore. The main functional groups identified in the pharmacophoric overlays may form a number of interactions within the hERG channel. Based on examining these pharmacophores within a homology model of the hERG channel, the hydrophobic feature at position 1 was thought to form  $\pi$ - $\pi$  interactions with Tyr652. The second hydrophobic feature at position 2 in Group A compounds only was suggested to form  $\pi$ - $\pi$  interactions with Phe656, while the hydrophobic feature at position 3 in Group B compounds only was thought to bind to a Tyr652 from another subunit. Most Group A compounds also had a *para*-substituent, which usually was a halogen group, and was suggested to interact with pore helix residues. The charged central nitrogen could possibly form cation- $\pi$  interactions with Phe656. This study supports modifications proposed by others to reduce compound affinity for hERG, such as reducing the charge of the central amine and the hydrophobicity of the 'tail'-end of the molecule (Stansfeld *et al.*, 2007). Furthermore, modifications to the *para*-substituent on the phenyl ring were previously shown to reduce the potency of clofilium and some dofetilide analogs by 10 - 100 fold (Perry *et al.*, 2006). Interestingly, a *para*-substituent is evident on most Group A compounds and not on the less potent Group B compounds, verifying that alterations of the *para*-substituent may be highly desirable in reducing hERG blocking effects. Although these pharmacophore models initially help in structurally explaining patterns in my data, their predictive value is yet to be discovered. Further models using quantitative-structure activity relationships (QSAR) need to be derived and their predictive potentials investigated. More detailed analysis needs to be done to relate structural and chemical properties of the compounds to hERG potency. It may then be possible to determine differences in Tyr652 sensitive and insensitive compounds and define the nature of interactions of Tyr652 with compounds.

The pharmacophores proposed by my study are remarkably similar to other pharmacophores reported in earlier studies, namely the QSAR models for hERG blockers proposed by Ekins *et al.* (Ekins *et al.*, 2002), Cavalli *et al.* (Cavalli *et al.*, 2002), and

## Chapter 7- General Discussion

Pearlstein *et al.* (Pearlstein *et al.*, 2003). These consisted of a basic nitrogen group and 3 or 4 hydrophobic groups that may not all be present simultaneously. In this respect, all three models proposed similar properties of hERG blockers. The difference between these models was the position of the central moiety with regards to the surrounding hydrophobic functions. Ekins proposed a pyramidal structure with an ionizable moiety on top and hydrophobic groups located at similar distances from it. This structure had a smaller base and greater height than the pyramidal structure proposed by Cavalli. The difference in the shape of these models possibly represents the extended or folded conformation of the molecules studied. The Pearlstein pharmacophore was also similar to the Cavalli model, showing molecules in mainly the extended conformation. The pharmacophores discussed in the literature are very comparable to the ones proposed in this thesis, indicating common characteristics of hERG blockers. The pharmacophores for Group A and Group B compounds show both extended and folded conformations of hERG blockers and are unique in that they are built based on consistent, in-house datasets from structurally and therapeutically diverse drugs, instead of utilizing literature data. Although these pharmacophore structures are extremely useful, further efforts will be directed at marrying the mutagenesis, electrophysiological, and computational data in order to achieve an accurate predictive model for hERG channel behaviour and drug blocking activity.

### 7.4 Overall Summary

I first investigated the relevance of the glycine hinge hypothesis in hERG. This study revealed that the glycine residues have a role in ensuring the tight packing of the channel as opposed to acting as hinge points. Unlike other Kv channels, hERG is energetically more stable in the open than the closed state. I also presented further experimental evidence that the peptide bonds between amino acids in the inner helices are inherently flexible, enough to permit the bending necessary during channel activation. I also investigated possible molecular mechanisms behind the slow deactivation gating in hERG. This process appears to involve a network of interactions between the N-terminus, the S4-S5 linker, and the C-terminal end of S6. I showed that Val659 (but not Ile662)

## Chapter 7- General Discussion

may form part of the receptor to which the N-terminus binds. Further studies are required to test if normal deactivation requires hydrophobic interactions between Val659 and residues on S4 or the S4-S5 linker. Val659 was also shown to have allosteric effects on drug binding. However, Tyr652 appears to be important in the binding of longer, more potent compounds within the pore but is less important for smaller, less potent compounds, which may easily orientate to form other interactions within the pore. The pharmacophore models built show similarities to literature models, although QSAR models would need to be generated to further define the nature of interactions of compounds with this residue. The ultimate aim would be to produce an *in silico* model that accurately predicts potential hERG blocking activity. In order to do so, the contributions of other residues, such as Gly648, Thr623, and Ser624 to the hERG drug binding site would need to be elucidated.

- ABBOTT, G. W., SESTI, F., SPLAWSKI, I., BUCK, M. E., LEHMANN, M. H., TIMOTHY, K. W., KEATING, M. T. & GOLDSTEIN, S. A. (1999). MiRP1 forms IKr potassium channels with HERG and is associated with cardiac arrhythmia. *Cell* **97**, 175-187.
- AGGARWAL, S. K. & MACKINNON, R. (1996). Contribution of the S4 segment to gating charge in the Shaker K<sup>+</sup> channel. *Neuron* **16**, 1169-1177.
- ARCANGELI, A. (2005). Expression and role of hERG channels in cancer cells. *Novartis Found Symp* **266**, 225-232; discussion 232-224.
- ARMSTRONG, C. M. (1971). Interaction of tetraethylammonium ion derivatives with the potassium channels of giant axons. *J Gen Physiol* **58**, 413-437.
- BEZANILLA, F. (2000). The voltage sensor in voltage-dependent ion channels. *Physiol Rev* **80**, 555-592.
- BLUNCK, R., CORDERO-MORALES, J. F., CUELLO, L. G., PEROZO, E. & BEZANILLA, F. (2006). Detection of the opening of the bundle crossing in KcsA with fluorescence lifetime spectroscopy reveals the existence of two gates for ion conduction. *J Gen Physiol* **128**, 569-581.
- BRIGHT, J. N., SHRIVASTAVA, I. H., CORDES, F. S. & SANSOM, M. S. (2002). Conformational dynamics of helix S6 from Shaker potassium channel: simulation studies. *Biopolymers* **64**, 303-313.
- BROWN, A. M. (2004). Drugs, hERG, and sudden death. *Cell calcium* **35**, 543-547.
- BRUGADA, J., BRUGADA, R. & BRUGADA, P. (2007). Channelopathies: a new category of diseases causing sudden death. *Herz* **32**, 185-191.
- BRUGADA, R., HONG, K., CORDEIRO, J. M. & DUMAINE, R. (2005). Short QT syndrome. *Cmaj* **173**, 1349-1354.
- BRUGADA, R., HONG, K., DUMAINE, R., CORDEIRO, J., GAITA, F., BORGGREFE, M., MENENDEZ, T. M. & BRUGADA, J. E. A. (2004). Sudden death associated with short-QT syndrome linked to mutations in HERG. *Circulation* **109**, 30-35.
- CAPRINI, M., FAVA, M., VALENTE, P., FERNANDEZ-BALLESTER, G., RAPISARDA, C., FERRONI, S. & FERRER-MONTIEL, A. (2005). Molecular compatibility of the channel gate and the N terminus of S5 segment for voltage-gated channel activity. *J Biol Chem* **280**, 18253-18264.

## Chapter 8- Bibliography

- CAPRINI, M., FERRONI, S., PLANELLAS-CASES, R., RUEDA, J., RAPISARDA, C., FERRER-MONTIEL, A. & MONTAL, M. (2001). Structural compatibility between the putative voltage sensor of voltage-gated K<sup>+</sup> channels and the prokaryotic KcsA channel. *J Biol Chem* **276**, 21070-21076.
- CASIS, O., OLESEN, S. P. & SANGUINETTI, M. C. (2006). Mechanism of action of a novel human ether-a-go-go-related gene activator. *Mol Pharmacol.* **69**, 658-665.
- CAVALLI, A., POLUZZI, E., DE PONTI, F. & RECANATINI, M. (2002). Toward a pharmacophore for drugs inducing the long QT syndrome: Insights from a CoMFA study of hERG K<sup>+</sup> channel blockers. *J Med Chem.* **45**, 3844-3853.
- CHEN, J., MITCHESON, J. S., TRISTANI-FIROUZI, M., LIN, M. & SANGUINETTI, M. C. (2001). The S4-S5 linker couples voltage sensing and activation of pacemaker channels. *Proc Natl Acad Sci U S A* **98**, 11277-11282.
- CHEN, J., SEEBOHM, G. & SANGUINETTI, M. C. (2002). Position of aromatic residues in the S6 domain, not inactivation, dictates cisapride sensitivity of HERG and eag potassium channels. *Proc Natl Acad Sci U S A* **99**, 12461-12466.
- CHEN, J., ZOU, A., SPLAWSKI, I., KEATING, M. T. & SANGUINETTI, M. C. (1999). Long QT syndrome-associated mutations in the Per-Arnt-Sim (PAS) domain of HERG potassium channels accelerate channel deactivation. *J Biol Chem* **274**, 10113-10118.
- CHEN, Q., KIRSCH, G. E., ZHANG, D., BRUGADA, R., BRUGADA, J., BRUGADA, P., POTENZA, D., MOYA, A., BORGGREFE, M., BREITHARDT, G., ORTIZ-LOPEZ, R., WANG, Z., ANTZELEVITCH, C., O'BRIEN, R. E., SCHULZE-BAHR, E., KEATING, M. T., TOWBIN, J. A. & WANG, Q. (1998). Genetic basis and molecular mechanism for idiopathic ventricular fibrillation. *Nature* **392**, 293-296.
- CHENG, C. S., ALDERMAN, D., KWASH, J., DESSAINT, J., PATEL, R., LESCOE, M. K., KINRADE, M. B. & YU, W. (2002). A high-throughput HERG potassium channel function assay: an old assay with a new look. *Drug Dev Ind Pharm* **28**, 177-191.
- CHIU, P. J., MARCOE, K. F., BOUNDS, S. E., LIN, C. H., FENG, J. J., LIN, A., CHENG, F. C., CRUMB, W. J. & MITCHELL, R. (2004). Validation of a [<sup>3</sup>H]astemizole binding assay in HEK293 cells expressing HERG K<sup>+</sup> channels. *J Pharmacol Sci* **95**, 311-319.
- CHOI, K. L., ALDRICH, R. W. & YELLEN, G. (1991). Tetraethylammonium blockade distinguishes two inactivation mechanisms in voltage-activated K<sup>+</sup> channels. *Proc Natl Acad Sci U S A* **88**, 5092-5095.

## Chapter 8- Bibliography

- CHOI, K. L., MOSSMAN, C., AUBE, J. & YELLEN, G. (1993). The internal quaternary ammonium receptor site of Shaker potassium channels. *Neuron* **10**, 533-541.
- CHOUABE, C., DRICI, M. D., ROMÉY, G. & BARHANIN, J. (2000). Effects of calcium channel blockers on cloned cardiac K<sup>+</sup> channels IKr and IKs. *Thérapie* **55**, 195-202.
- CLANCY, C. E., KUROKAWA, J., TATEYAMA, M., LIU, H., WEHRENS, X. H. & KASS, R. S. (2003). K<sup>+</sup> channel structure-activity relationships and mechanisms of drug-induced QT prolongation. *Annu Rev Pharmacol Toxicol.* **43**, 441-461.
- CLARKE, C. E., HILL, A. P., ZHAO, J., KONDO, M., SUBBIAH, R. N., CAMPBELL, T. J. & VANDENBERG, J. I. (2006). Effect of S5P alpha-helix charge mutants on inactivation of hERG K<sup>+</sup> channels. *J Physiol* **573**, 291-304.
- CLAYDON, T. W., MAKARY, S. Y., DIBB, K. M. & BOYETT, M. R. (2003). The selectivity filter may act as the agonist-activated gate in the G protein-activated Kir3.1/Kir3.4 K<sup>+</sup> channel. *J Biol Chem* **278**, 50654-50663.
- CURRAN, M. E., SPLAWSKI, I., TIMOTHY, K. W., VINCENT, G. M., GREEN, E. D. & KEATING, M. T. (1995). A molecular basis for cardiac arrhythmia: HERG mutations cause long QT syndrome. *Cell* **80**, 795-803.
- DEL CAMINO, D., HOLMGREN, M., LIU, Y. & YELLEN, G. (2000). Blocker protection in the pore of a voltage-gated K<sup>+</sup> channel and its structural implications. *Nature* **403**, 321-325.
- DEL CAMINO, D., KANEVSKY, M. & YELLEN, G. (2005). Status of the intracellular gate in the activated-not-open state of shaker K<sup>+</sup> channels. *J Gen Physiol* **126**, 419-428.
- DELISLE, B. P., ANSON, B. D., RAJAMANI, S. & JANUARY, C. T. (2004). Biology of cardiac arrhythmias: ion channel protein trafficking. *Circ Res* **94**, 1418-1428.
- DING, S., INGLEBY, L., AHERN, C. A. & HORN, R. (2005). Investigating the putative glycine hinge in Shaker potassium channel. *J Gen Physiol* **126**, 213-226.
- DORN, A., HERMANN, F., EBNETH, A., BOTHMANN, H., TRUBE, G., CHRISTENSEN, K. & APFEL, C. (2005). Evaluation of a high-throughput fluorescence assay method for HERG potassium channel inhibition. *J Biomol Screen* **10**, 339-347.
- DOYLE, D. A., MORAIS CABRAL, J., PFUETZNER, R. A., KUO, A., GULBIS, J. M., COHEN, S. L., CHAIT, B. T. & MACKINNON, R. (1998). The structure of the potassium channel: molecular basis of K<sup>+</sup> conduction and selectivity. *Science* **280**, 69-77.

## Chapter 8- Bibliography

- EKINS, S., CRUMB, W. J., SARAZAN, R. D., WIKEL, J. H. & WRIGHTON, S. A. (2002). Three-dimensional quantitative structure-activity relationship for inhibition of human ether-a-go-go-related gene potassium channel. *J Pharmacol. Exp Ther.* **301**, 427-434.
- ELLIOTT, D. J., NEALE, E. J., AZIZ, Q., DUNHAM, J. P., MUNSEY, T. S., HUNTER, M. & SIVAPRASADARAO, A. (2004). Molecular mechanism of voltage sensor movements in a potassium channel. *Embo J* **23**, 4717-4726.
- FAN, J. S., JIANG, M., DUN, W., McDONALD, T. V. & TSENG, G. N. (1999). Effects of outer mouth mutations on hERG channel function: a comparison with similar mutations in the Shaker channel. *Biophys J* **76**, 3128-3140.
- FARLEY, J. & RUDY, B. (1988). Multiple types of voltage-dependent Ca<sup>2+</sup>-activated K<sup>+</sup> channels of large conductance in rat brain synaptosomal membranes. *Biophys J* **53**, 919-934.
- FEDIDA, D., MARUOKA, N. D. & LIN, S. (1999). Modulation of slow inactivation in human cardiac Kv1.5 channels by extra- and intracellular permeant cations. *J Physiol* **515** ( Pt 2), 315-329.
- FERNANDEZ, D., GHANTA, A., KAUFFMAN, G. W. & SANGUINETTI, M. C. (2004). Physicochemical features of the hERG channel drug binding site. *J Biol. Chem* **279**, 10120-10127.
- FERRER, T., RUPP, J., PIPER, D. R. & TRISTANI-FIROUZI, M. (2006). The S4-S5 linker directly couples voltage sensor movement to the activation gate in the human ether-a'-go-go-related gene (hERG) K<sup>+</sup> channel. *J Biol Chem* **281**, 12858-12864.
- FICKER, E., DENNIS, A. T., WANG, L. & BROWN, A. M. (2003). Role of the cytosolic chaperones Hsp70 and Hsp90 in maturation of the cardiac potassium channel HERG. *Circ Res* **92**, e87-100.
- FICKER, E., JAROLIMEK, W. & BROWN, A. M. (2001). Molecular determinants of inactivation and dofetilide block in ether a-go-go (EAG) channels and EAG-related K(+) channels. *Mol Pharmacol* **60**, 1343-1348.
- FICKER, E., JAROLIMEK, W., KIEHN, J., BAUMANN, A. & BROWN, A. M. (1998). Molecular determinants of dofetilide block of HERG K<sup>+</sup> channels. *Circ Res* **82**, 386-395.
- FICKER, E., KURYSHEV, Y. A., DENNIS, A. T., OBEJERO-PAZ, C., WANG, L., HAWRYLUK, P., WIBLE, B. A. & BROWN, A. M. (2004). Mechanisms of arsenic-induced prolongation of cardiac repolarization. *Mol Pharmacol* **66**, 33-44.

## Chapter 8- Bibliography

- FICKER, E., TAGLIALATELA, M., WIBLE, B. A., HENLEY, C. M. & BROWN, A. M. (1994). Spermine and spermidine as gating molecules for inward rectifier K<sup>+</sup> channels. *Science* **266**, 1068-1072.
- FINLAYSON, K., WITCHEL, H. J., MCCULLOCH, J. & SHARKEY, J. (2004). Acquired QT interval prolongation and HERG: implications for drug discovery and development. *Eur J Pharmacol* **500**, 129-142.
- FINLAYSON, K., TURNBULL, L., JANUARY, C. T., SHARKEY, J. & KELLY, J. S. (2001). [3H]dofetilide binding to HERG transfected membranes: a potential high throughput preclinical screen. *Eur J Pharmacol* **430**, 147-148.
- FLYNN, G. E. & ZAGOTTA, W. N. (2001). Conformational changes in S6 coupled to the opening of cyclic nucleotide-gated channels. *Neuron* **30**, 689-698.
- GANDHI, C. S. & ISACOFF, E. Y. (2002). Molecular models of voltage sensing. *J Gen Physiol* **120**, 455-463.
- GANDHI, C. S., LOOTS, E. & ISACOFF, E. Y. (2000). Reconstructing voltage sensor-pore interaction from a fluorescence scan of a voltage-gated K<sup>+</sup> channel. *Neuron* **27**, 585-595.
- GANG, H. & ZHANG, S. (2006). Na<sup>+</sup> permeation and block of hERG potassium channels. *J Gen Physiol* **128**, 55-71.
- GESSNER, G. & HEINEMANN, S. H. (2003). Inhibition of hEAG1 and hERG1 potassium channels by clofilium and its tertiary analogue LY97241. *Br J Pharmacol.* **138**, 161-171.
- GIMPELEV, M., FORREST, L. R., MURRAY, D. & HONIG, B. (2004). Helical packing patterns in membrane and soluble proteins. *Biophys J* **87**, 4075-4086.
- GONG, Q., JONES, M. A. & ZHOU, Z. (2006). Mechanisms of pharmacological rescue of trafficking-defective hERG mutant channels in human long QT syndrome. *J Biol Chem* **281**, 4069-4074.
- GURNEY, A. M. & JOSHI, S. (2006). The role of twin pore domain and other K<sup>+</sup> channels in hypoxic pulmonary vasoconstriction. *Novartis Found Symp* **272**, 218-228; discussion 228-233, 274-219.
- GURROLA, G., ROSATI, B., ROCCHETTI, M., PIMIENTA, G., ZAZA, A., ARCANGELI, A., OLIVOTTO, M., POSSANI, L. D. & WANKE, E. (1999). A toxin to nervous, cardiac, and endocrine ERG K<sup>+</sup> channels isolated from *Centruroides noxius* scorpion venom. *FASEB J* **13**, 953-962.

## Chapter 8- Bibliography

- GUTMAN, G. A., CHANDY, K. G., ADELMAN, J. P., AIYAR, J., BAYLISS, D. A., CLAPHAM, D. E., COVARRIUBIAS, M., DESIR, G. V., FURUICHI, K., GANETZKY, B., GARCIA, M. L., GRISSMER, S., JAN, L. Y., KARSCHIN, A., KIM, D., KUPERSCHMIDT, S., KURACHI, Y., LAZDUNSKI, M., LESAGE, F., LESTER, H. A., MCKINNON, D., NICHOLS, C. G., O'KELLY, I., ROBBINS, J., ROBERTSON, G. A., RUDY, B., SANGUINETTI, M., SEINO, S., STUEHMER, W., TAMKUN, M. M., VANDENBERG, C. A., WEI, A., WULFF, H. & WYMORE, R. S. (2003). International Union of Pharmacology. XLI. Compendium of voltage-gated ion channels: potassium channels. *Pharmacol Rev* **55**, 583-586.
- GUTMAN, G. A., CHANDY, K. G., GRISSMER, S., LAZDUNSKI, M., MCKINNON, D., PARDO, L. A., ROBERTSON, G. A., RUDY, B., SANGUINETTI, M. C., STUEHMER, W. & WANG, X. (2005). International Union of Pharmacology. LIII. Nomenclature and molecular relationships of voltage-gated potassium channels. *Pharmacol Rev* **57**, 473-508.
- HARDMAN, R. M., STANSFELD, P. J., DALIBALTA, S., SUTCLIFFE, M. J. & MITCHESON, J. S. (2007). Activation gating of hERG potassium channels: S6 glycines are not required as gating hinges. *J Biol Chem*.
- HILLE, B. (2001). *Ion channels of excitable membranes*, Sunderland, MA.
- HOLMGREN, M., SMITH, P. L. & YELLEN, G. (1997). Trapping of organic blockers by closing of voltage-dependent K<sup>+</sup> channels: evidence for a trap door mechanism of activation gating. *J Gen Physiol* **109**, 527-535.
- HOSHI, T., ZAGOTTA, W. N. & ALDRICH, R. W. (1990). Biophysical and molecular mechanisms of Shaker potassium channel inactivation. *Science* **250**, 533-538.
- HOSHI, T., ZAGOTTA, W. N. & ALDRICH, R. W. (1991). Two types of inactivation in Shaker K<sup>+</sup> channels: effects of alterations in the carboxy-terminal region. *Neuron* **7**, 547-556.
- HUANG, F. D., CHEN, J., LIN, M., KEATING, M. T. & SANGUINETTI, M. C. (2001). Long-QT syndrome-associated missense mutations in the pore helix of the HERG potassium channel. *Circulation* **104**, 1071-1075.
- ISACOFF, E. Y., JAN, Y. N. & JAN, L. Y. (1991). Putative receptor for the cytoplasmic inactivation gate in the Shaker K<sup>+</sup> channel. *Nature* **353**, 86-90.
- JAN, L. Y. & JAN, Y. N. (1997). Cloned potassium channels from eukaryotes and prokaryotes. *Annu Rev Neurosci* **20**, 91-123.
- JIANG, M., ZHANG, M., MASLENNIKOV, I. V., LIU, J., WU, D. M., KOROLKOVA, Y. V., ARSENIYEV, A. S., GRISHIN, E. V. & TSENG, G. N. (2005). Dynamic conformational changes of extracellular S5-P linkers in the hERG channel. *J Physiol* **569**, 75-89.

## Chapter 8- Bibliography

- JIANG, Y., LEE, A., CHEN, J., CADENE, M., CHAIT, B. T. & MACKINNON, R. (2002a). Crystal structure and mechanism of a calcium-gated potassium channel. *Nature* **417**; 515-522.
- JIANG, Y., LEE, A., CHEN, J., RUTA, V., CADENE, M., CHAIT, B. T. & MACKINNON, R. (2003a). X-ray structure of a voltage-dependent K<sup>+</sup> channel. *Nature* **423**, 33-41.
- JIANG, Y., LEE, A., CHEN, J. Y., CADENE, M., CHAIT, B. T. & MACKINNON, R. (2002b). The open pore conformation of potassium channels. *Nature* **417**, 523-526.
- JIANG, Y., RUTA, V., CHEN, J., LEE, A. & MACKINNON, R. (2003b). The principle of gating charge movement in a voltage-dependent K<sup>+</sup> channel. *Nature* **423**, 42-48.
- JIN, T., PENG, L., MIRSHAHI, T., ROHACS, T., CHAN, K. W., SANCHEZ, R. & LOGOTHETIS, D. E. (2002). The (beta)gamma subunits of G proteins gate a K(+) channel by pivoted bending of a transmembrane segment. *Mol Cell* **10**, 469-481.
- KAMIYA, K., MITCHESON, J. S., YASUI, K., KODAMA, I. & SANGUINETTI, M. C. (2001). Open channel block of HERG K(+) channels by vesnarinone. *Mol Pharmacol* **60**, 244-253.
- KAMIYA, K., NIWA, R., MITCHESON, J. S. & SANGUINETTI, M. C. (2006). Molecular determinants of HERG channel block. *Mol Pharmacol* **69**, 1709-1716.
- KANG, J., CHEN, X. L., WANG, H., JI, J., CHENG, H., INCARDONA, J., REYNOLDS, W., VIVIANI, F., TABART, M. & RAMPE, D. (2005). Discovery of a small molecule activator of the human ether-a-go-go-related gene (HERG) cardiac K<sup>+</sup> channel. *Mol Pharmacol* **67**, 827-836.
- KEATING, M. T. & SANGUINETTI, M. C. (2001). Molecular and cellular mechanisms of cardiac arrhythmias. *Cell* **104**, 569-580.
- KERSCHBAUM, H. H., GRISSMER, S., ENGEL, E., RICHTER, K., LEHNER, C. & JAGER, H. (2002). A Shaker homologue encodes an A-type current in *Xenopus laevis*. *Brain Res* **927**, 55-68.
- KIM, K. S. & KIM, E. J. (2005). The phenothiazine drugs inhibit hERG potassium channels. *Drug Chem Toxicol* **28**, 303-313.
- KLEMIC, K. G., SHIEH, C. C., KIRSCH, G. E. & JONES, S. W. (1998). Inactivation of Kv2.1 potassium channels. *Biophys J* **74**, 1779-1789.
- KUO, A., GULBIS, J. M., ANTCLIFF, J. F., RAHMAN, T., LOWE, E. D., ZIMMER, J., CUTHBERTSON, J., ASHCROFT, F. M., EZAKI, T. & DOYLE, D. A. (2003). Crystal

## Chapter 8- Bibliography

structure of the potassium channel KirBacl.1 in the closed state. *Science* **300**, 1922-1926.

KURYSHEV, Y. A., FICKER, E., WANG, L., HAWRYLUK, P., DENNIS, A. T., WIBLE, B. A., BROWN, A. M., KANG, J., CHEN, X. L., SAWAMURA, K., REYNOLDS, W. & RAMPE, D. (2005). Pentamidine-induced long QT syndrome and block of hERG trafficking. *J Pharmacol Exp Ther* **312**, 316-323.

LABRO, A. J., RAES, A. L., BELLENS, I., OTTSCHYTSCH, N. & SNYDERS, D. J. (2003). Gating of shaker-type channels requires the flexibility of S6 caused by prolines. *J Biol Chem* **278**, 50724-50731.

LAINE, M., LIN, M. C., BANNISTER, J. P., SILVERMAN, W. R., MOCK, A. F., ROUX, B. & PAPAZIAN, D. M. (2003). Atomic proximity between S4 segment and pore domain in Shaker potassium channels. *Neuron* **39**, 467-481.

LARSSON, H. P., BAKER, O. S., DHILLON, D. S. & ISACOFF, E. Y. (1996). Transmembrane movement of the shaker K<sup>+</sup> channel S4. *Neuron* **16**, 387-397.

LARSSON, H. P. & ELINDER, F. (2000). A conserved glutamate is important for slow inactivation in K<sup>+</sup> channels. *Neuron* **27**, 573-583.

LEDWELL, J. L. & ALDRICH, R. W. (1999). Mutations in the S4 region isolate the final voltage-dependent cooperative step in potassium channel activation. *J Gen Physiol* **113**, 389-414.

LEE, S. Y., LEE, A., CHEN, J. & MACKINNON, R. (2005). Structure of the KvAP voltage-dependent K<sup>+</sup> channel and its dependence on the lipid membrane. *Proc Natl Acad Sci USA* **102**, 15441-15446.

LEES-MILLER, J. P., DUAN, Y., TENG, G. Q. & DUFF, H. J. (2000). Molecular determinant of high affinity dofetilide binding to hERG1 expressed in *Xenopus* oocytes: involvement of S6 sites. *Mol Pharmacol*. **57**, 367-374.

LI, J., STEVENS, L., KLUGBAUER, N. & WRAY, D. (2004). Roles of molecular regions in determining differences between voltage dependence of activation of CaV3.1 and CaV1.2 calcium channels. *J Biol Chem* **279**, 26858-26867.

LI, J., STEVENS, L. & WRAY, D. (2005). Molecular regions underlying the activation of low- and high-voltage activating calcium channels. *Eur Biophys J* **34**, 1017-1029.

LIMAN, E. R., HESS, P., WEAVER, F. & KOREN, G. (1991). Voltage-sensing residues in the S4 region of a mammalian K<sup>+</sup> channel. *Nature* **353**, 752-756.

## Chapter 8- Bibliography

- LI-SMERIN, Y., HACKOS, D. H. & SWARTZ, K. J. (2000). A localized interaction surface for voltage-sensing domains on the pore domain of a K<sup>+</sup> channel. *Neuron* **25**, 411-423.
- LIU, J., ZHANG, M., JIANG, M. & TSENG, G. N. (2002). Structural and functional role of the extracellular s5-p linker in the HERG potassium channel. *J Gen Physiol* **120**, 723-737.
- LIU, J., ZHANG, M., JIANG, M. & TSENG, G. N. (2003). Negative charges in the transmembrane domains of the HERG K channel are involved in the activation- and deactivation-gating processes. *J Gen Physiol* **121**, 599-614.
- LIU, Y., HOLMGREN, M., JURMAN, M. E. & YELLEN, G. (1997). Gated access to the pore of a voltage-dependent K<sup>+</sup> channel. *Neuron* **19**, 175-184.
- LIU, Y., JURMAN, M. E. & YELLEN, G. (1996). Dynamic rearrangement of the outer mouth of a K<sup>+</sup> channel during gating. *Neuron* **16**, 859-867.
- LONG, S. B., CAMPBELL, E. B. & MACKINNON, R. (2005a). Crystal structure of a mammalian voltage-dependent *Shaker* family K<sup>+</sup> channel. *Science* **309**, 897-903.
- LONG, S. B., CAMPBELL, E. B. & MACKINNON, R. (2005b). Voltage sensor of Kv1.2: structural basis of electromechanical coupling. *Science* **309**, 903-908.
- LOOTS, E. & ISACOFF, E. Y. (1998). Protein rearrangements underlying slow inactivation of the Shaker K<sup>+</sup> channel. *J Gen Physiol* **112**, 377-389.
- LOPEZ-BARNEO, J., HOSHI, T., HEINEMANN, S. H. & ALDRICH, R. W. (1993). Effects of external cations and mutations in the pore region on C-type inactivation of Shaker potassium channels. *Receptors Channels* **1**, 61-71.
- LU, Z., KLEM, A. M. & RAMU, Y. (2001). Ion conduction pore is conserved among potassium channels. *Nature* **413**, 809-813.
- LU, Z., KLEM, A. M. & RAMU, Y. (2002). Coupling between voltage sensors and activation gate in voltage-gated K<sup>+</sup> channels. *J Gen Physiol* **120**, 663-676.
- LU, Z. & MACKINNON, R. (1994). Electrostatic tuning of Mg<sup>2+</sup> affinity in an inward-rectifier K<sup>+</sup> channel. *Nature* **371**, 243-246.
- MACKINNON, R., ALDRICH, R. W. & LEE, A. W. (1993). Functional stoichiometry of Shaker potassium channel inactivation. *Science* **262**, 757-759.
- MACKINNON, R. & YELLEN, G. (1990). Mutations affecting TEA blockade and ion permeation in voltage-activated K<sup>+</sup> channels. *Science* **250**, 276-279.

## Chapter 8- Bibliography

- MAGIDOVICH, E. & YIFRACH, O. (2004). Conserved gating hinge in ligand- and voltage-dependent K<sup>+</sup> channels. *Biochemistry* **43**, 13242-13247.
- MANNUZZU, L. M., MORONNE, M. M. & ISACOFF, E. Y. (1996). Direct physical measure of conformational rearrangement underlying potassium channel gating. *Science* **271**, 213-216.
- MCDONALD, T. V., YU, Z., MING, Z., PALMA, E., MEYERS, M. B., WANG, K. W., GOLDSTEIN, S. A. & FISHMAN, G. I. (1997). A minK-hERG complex regulates the cardiac potassium current I(Kr). *Nature* **388**, 289-292.
- MILLER, C. (2000). An overview of the potassium channel family. *Genome Biol* **1**, REVIEWS0004.
- MILLIGAN, C. J. & WRAY, D. (2000). Local movement in the S2 region of the voltage-gated potassium channel hKv2.1 studied using cysteine mutagenesis. *Biophys J* **78**, 1852-1861.
- MILNES, J. T., CROCIANI, O., ARCANGELI, A., HANCOX, J. C. & WITCHEL, H. J. (2003a). Blockade of HERG potassium currents by fluvoxamine: incomplete attenuation by S6 mutations at F656 or Y652. *Br J Pharmacol* **139**, 887-898.
- MILNES, J. T., DEMPSEY, C. E., RIDLEY, J. M., CROCIANI, O., ARCANGELI, A., HANCOX, J. C. & WITCHEL, H. J. (2003b). Preferential closed channel blockade of HERG potassium currents by chemically synthesised BeKm-1 scorpion toxin. *FEBS Lett* **547**, 20-26.
- MILNES, J. T., WITCHEL, H. J., LEANEY, J. L., LEISHMAN, D. J. & HANCOX, J. C. (2006). hERG K<sup>+</sup> channel blockade by the antipsychotic drug thioridazine: An obligatory role for the S6 helix residue F656. *Biochem Biophys Res Commun* **351**, 273-280.
- MITCHESON, J., PERRY, M., STANSFELD, P., SANGUINETTI, M. C., WITCHEL, H. & HANCOX, J. (2005). Structural determinants for high-affinity block of hERG potassium channels. *Novartis Found Symp* **266**, 136-150; discussion 150-138.
- MITCHESON, J. S., CHEN, J., LIN, M., CULBERSON, C. & SANGUINETTI, M. C. (2000a). A structural basis for drug-induced long QT syndrome. *Proc Natl Acad Sci U S A* **97**, 12329-12333.
- MITCHESON, J. S., CHEN, J. & SANGUINETTI, M. C. (2000b). Trapping of a methanesulfonanilide by closure of the HERG potassium channel activation gate. *J Gen Physiol* **115**, 229-240.
- MITCHESON, J. S. & HANCOX, J. C. (1999). An investigation of the role played by the E-4031-sensitive (rapid delayed rectifier) potassium current in isolated rabbit atrioventricular nodal and ventricular myocytes. *Pflugers Arch* **438**, 843-850.

## Chapter 8- Bibliography

- MORAIS CABRAL, J. H., LEE, A., COHEN, S. L., CHAIT, B. T., LI, M. & MACKINNON, R. (1998). Crystal structure and functional analysis of the HERG potassium channel N terminus: a eukaryotic PAS domain. *Cell* **95**, 649-655.
- NAKAJIMA, T., FURUKAWA, T., TANAKA, T., KATAYAMA, Y., NAGAI, R., NAKAMURA, Y. & HIRAOKA, M. (1998). Novel mechanism of HERG current suppression in LQT2: shift in voltage dependence of HERG inactivation. *Circ Res* **83**, 415-422.
- NEALE, E. J., ELLIOTT, D. J., HUNTER, M. & SIVAPRASADARAO, A. (2003). Evidence for intersubunit interactions between S4 and S5 transmembrane segments of the Shaker potassium channel. *J Biol Chem* **278**, 29079-29085.
- NEALE, E. J., RONG, H., COCKCROFT, C. J. & SIVAPRASADARAO, A. (2007). Mapping the membrane-aqueous border for the voltage-sensing domain of a potassium channel. *J Biol Chem*.
- NICHOLS, C. G. & LOPATIN, A. N. (1997). Inward rectifier potassium channels. *Annu Rev Physiol* **59**, 171-191.
- O'CONNELL, A. D., MORTON, M. J. & HUNTER, M. (2002). Two-pore domain K<sup>+</sup> channels-molecular sensors. *Biochim Biophys Acta* **1566**, 152-161.
- OLCESE, R., LATORRE, R., TORO, L., BEZANILLA, F. & STEFANI, E. (1997). Correlation between charge movement and ionic current during slow inactivation in Shaker K<sup>+</sup> channels. *J Gen Physiol* **110**, 579-589.
- ONO, K. & ITO, H. (1995). Role of rapidly activating delayed rectifier K<sup>+</sup> current in sinoatrial node pacemaker activity. *Am J Physiol* **269**, H453-462.
- ORTEGA-SAENZ, P., PARDAL, R., CASTELLANO, A. & LOPEZ-BARNEO, J. (2000). Collapse of conductance is prevented by a glutamate residue conserved in voltage-dependent K(+) channels. *J Gen Physiol* **116**, 181-190.
- PANYI, G. & DEUTSCH, C. (2007). Probing the cavity of the slow inactivated conformation of shaker potassium channels. *J Gen Physiol*. **129**, 403-418.
- PANYI, G., SHENG, Z. & DEUTSCH, C. (1995). C-type inactivation of a voltage-gated K<sup>+</sup> channel occurs by a cooperative mechanism. *Biophys J* **69**, 896-903.
- PAPAZIAN, D. M., TIMPE, L. C., JAN, Y. N. & JAN, L. Y. (1991). Alteration of voltage-dependence of Shaker potassium channel by mutations in the S4 sequence. *Nature* **349**, 305-310.

## Chapter 8- Bibliography

- PARDO-LOPEZ, L., GARCIA-VALDES, J., GURROLA, G. B., ROBERTSON, G. A. & POSSANI, L. D. (2002a). Mapping the receptor site for ergtoxin, a specific blocker of ERG channels. *FEBS Lett* **510**, 45-49.
- PARDO-LOPEZ, L., ZHANG, M., LIU, J., JIANG, M., POSSANI, L. D. & TSENG, G. N. (2002b). Mapping the binding site of a human ether-a-go-go-related gene-specific peptide toxin (ErgTx) to the channel's outer vestibule. *J Biol Chem* **277**, 16403-16411.
- PAUL, A. A., WITCHEL, H. J. & HANCOX, J. C. (2001). Inhibition of HERG potassium channel current by the class 1a antiarrhythmic agent disopyramide. *Biochem Biophys Res Commun* **280**, 1243-1250.
- PEARLSTEIN, R. A., VAZ, R. J., KANG, J., CHEN, X. L., PREOBRAZHENSKAYA, M., SHCHEKOTIKHIN, A. E., KOROLEV, A. M., LYSENKOVA, L. N., MIROSHNIKOVA, O. V., HENDRIX, J. & RAMPE, D. (2003). Characterisation of HERG potassium channel inhibition using CoMSiA 3D QSAR and homology modeling approaches. *Bioorg Med Chem Lett* **13**, 1829-1835.
- PEROZO, E., SANTACRUZ-TOLOZA, L., STEFANI, E., BEZANILLA, F. & PAPAZIAN, D. M. (1994). S4 mutations alter gating currents of Shaker K channels. *Biophys J* **66**, 345-354.
- PERRY, M., DE GROOT, M. J., HELLIWELL, R., LEISHMAN, D., TRISTANI-FIROUZI, M., SANGUINETTI, M. C. & MITCHESON, J. (2004). Structural determinants of HERG channel block by clofilium and ibutilide. *Mol Pharmacol* **66**, 240-249.
- PERRY, M., SACHSE, F. B. & SANGUINETTI, M. C. (2007). Structural basis of action for a human ether-a-go-go-related gene 1 potassium channel activator. *Proc Natl Acad Sci USA* **104**, 13827-13832.
- PERRY, M., STANSFELD, P. J., LEANEY, J., WOOD, C., DE GROOT, M. J., LEISHMAN, D., SUTCLIFFE, M. J. & MITCHESON, J. S. (2006). Drug binding interactions in the inner cavity of HERG channels: molecular insights from structure-activity relationships of clofilium and ibutilide analogs. *Mol Pharmacol* **69**, 509-519.
- PHARTIYAL, P., JONES, E. M. & ROBERTSON, G. A. (2007). Heteromeric assembly of human ether-a-go-go-related gene (hERG) 1a/1b channels occurs cotranslationally via N-terminal interactions. *J Biol Chem* **282**, 9874-9882.
- PIPER, D. R., HINZ, W. A., TALLURRI, C. K., SANGUINETTI, M. C. & TRISTANI-FIROUZI, M. (2005). Regional specificity of human ether-a-go-go-related gene channel activation and inactivation gating. *J Biol Chem* **280**, 7206-7217.

## Chapter 8- Bibliography

- PIPER, D. R., VARGHESE, A., SANGUINETTI, M. C. & TRISTANI-FIROUZI, M. (2003). Gating currents associated with intramembrane charge displacement in HERG potassium channels. *Proc Natl Acad Sci U S A* **100**, 10534-10539.
- PRIORI, S. G., NAPOLITANO, C., TISO, N., MEMMI, M., VIGNATI, G., BLOISE, R., SORRENTINO, V. & DANIELI, G. A. (2001). Mutations in the cardiac ryanodine receptor gene (hRyR2) underlie catecholaminergic polymorphic ventricular tachycardia. *Circulation* **103**, 196-200.
- PROLE, D. L. & YELLEN, G. (2006). Reversal of HCN channel voltage dependence via bridging of the S4-S5 linker and Post-S6. *J Gen Physiol* **128**, 273-282.
- RAJAMANI, S., ANDERSON, C. L., ANSON, B. D. & JANUARY, C. T. (2002). Pharmacological rescue of human K<sup>+</sup> channel long-QT2 mutations: human ether-a-go-go-related gene rescue without block. *Circulation* **105**, 2830-2835.
- RAJAMANI, S., ECKHARDT, L. L., VALDIVIA, C. R., KLEMENS, C. A., GILLMAN, B. M., ANDERSON, C. L., HOLZEM, K. M., DELISLE, B. P., ANSON, B. D., MAKIELSKI, J. C. & JANUARY, C. T. (2006). Drug-induced long QT syndrome: hERG K<sup>+</sup> channel block and disruption of protein trafficking by fluoxetine and norfluoxetine. *Br J Pharmacol* **149**, 481-489.
- RANGANATHAN, R., LEWIS, J. H. & MACKINNON, R. (1996). Spatial localization of the K<sup>+</sup> channel selectivity filter by mutant cycle-based structure analysis. *Neuron* **16**, 131-139.
- RASMUSSEN, R. L., MORALES, M. J., CASTELLINO, R. C., ZHANG, Y., CAMPBELL, D. L. & STRAUSS, H. C. (1995). C-type inactivation controls recovery in a fast inactivating cardiac K<sup>+</sup> channel (Kv1.4) expressed in *Xenopus* oocytes. *J Physiol* **489** ( Pt 3), 709-721.
- RASMUSSEN, R. L., MORALES, M. J., WANG, S., LIU, S., CAMPBELL, D. L., BRAHMAJOTHI, M. V. & STRAUSS, H. C. (1998). Inactivation of voltage-gated cardiac K<sup>+</sup> channels. *Circ Res* **82**, 739-750.
- RECANATINI, M., CAVALLI, A. & MASETTI, M. (2005). *In silico* modelling--pharmacophores and hERG channel models. *Novartis Found Symp* **266**, 171-181.
- RIDLEY, J. M., MILNES, J. T., WITCHEL, H. J. & HANCOX, J. C. (2004). High affinity HERG K(+) channel blockade by the antiarrhythmic agent dronedarone: resistance to mutations of the S6 residues Y652 and F656. *Biochem Biophys Res Commun* **325**, 883-891.
- ROBERTSON, G. A. & JANUARY, C. T. (2006). HERG trafficking and pharmacological rescue of LQTS-2 mutant channels. *Handb Exp Pharmacol*, 349-355.

## Chapter 8- Bibliography

- ROBERTSON, G. A., JONES, E. M. & WANG, J. (2005). Gating and assembly of heteromeric hERG1a/1b channels underlying I(Kr) in the heart. *Novartis Found Symp* 266, 4-15; discussion 15-18, 44-15.
- RODEN, D. M., BALSER, J. R., GEORGE, A. L. & ANDERSON, M. E. (2002). Cardiac ion channels. *Annu Rev Physiol*. 64, 431-475.
- ROE, S. M., PRODROMOU, C., O'BRIEN, R., LADBURY, J. E., PIPER, P. W. & PEARL, L. H. (1999). Structural basis for inhibition of the Hsp90 molecular chaperone by the antitumour antibiotics radicicol and geldanamycin. *J Med Chem*. 42, 260-266.
- ROSENHOUSE-DANTSKER, A. & LOGOTHETIS, D. E. (2006). New roles for a key glycine and its neighboring residue in potassium channel gating. *Biophys J* 91, 2860-2873.
- RUTA, V., CHEN, J. & MACKINNON, R. (2005). Calibrated measurement of gating-charge arginine displacement in the KvAP voltage-dependent K<sup>+</sup> channel. *Cell* 123, 463-475.
- SANCHEZ-CHAPULA, J. A., FERRER, T., NAVARRO-POLANCO, R. A. & SANGUINETTI, M. C. (2003). Voltage-dependent profile of human ether-a-go-go-related gene channel block is influenced by a single residue in the S6 transmembrane domain. *Mol Pharmacol*. 63, 1051-1058.
- SANGUINETTI, M. C., CURRAN, M. E., SPECTOR, P. S. & KEATING, M. T. (1996). Spectrum of HERG K<sup>+</sup> channel dysfunction in an inherited cardiac arrhythmia. *Proc Natl Acad Sci US A*. 93, 2208-2212.
- SANGUINETTI, M. C., JIANG, C., CURRAN, M. E. & KEATING, M. T. (1995). A mechanistic link between an inherited and an acquired cardiac arrhythmia: HERG encodes the I<sub>Kr</sub> potassium channel. *Cell* 81, 299-307.
- SANGUINETTI, M. C. & JURKIEWICZ, N. K. (1990). Lanthanum blocks a specific component of I<sub>K</sub> and screens membrane surface change in cardiac cells. *Am J Physiol* 259, H1881-1889.
- SANGUINETTI, M. C. & MITCHESON, J. S. (2005). Predicting drug-hERG channel interactions that cause acquired long QT syndrome. *Trends Pharmacol Sci* 26, 119-124.
- SANGUINETTI, M. C. & TRISTANI-FIROUZI, M. (2006). hERG potassium channels and cardiac arrhythmia. *Nature* 440, 463-469.
- SANGUINETTI, M. C. & XU, Q. P. (1999). Mutations of the S4-S5 linker alter activation properties of hERG potassium channels expressed in *Xenopus* oocytes. *J Physiol* 514, 667-675.

## Chapter 8- Bibliography

- SCHONHERR, R. & HEINEMANN, S. H. (1996). Molecular determinants for activation and inactivation of hERG, a human inward rectifier potassium channel. *J Physiol* **493**, 635-642.
- SCHONHERR, R., MANNUZZU, L. M., ISACOFF, E. Y. & HEINEMANN, S. H. (2002). Conformational switch between slow and fast gating modes: allosteric regulation of voltage sensor mobility in the EAG K<sup>+</sup> channel. *Neuron* **35**, 935-949.
- SCHOPPA, N. E., MCCORMACK, K., TANOUYE, M. A. & SIGWORTH, F. J. (1992). The size of gating charge in wild-type and mutant Shaker potassium channels. *Science* **255**, 1712-1715.
- SCHROEDER, B. C., WALDEGGER, S., FEHR, S., BLEICH, M., WARTH, R., GREGER, R. & JENTSCH, T. J. (2000). A constitutively open potassium channel formed by KCNQ1 and KCNE3. *Nature* **403**, 196-199.
- SEEBOHM, G., STRUTZ-SEEBOHM, N., URECHE, O. N., BALTAEV, R., LAMPERT, A., KORNICHUK, G., KAMIYA, K., WUTTKE, T. V., LERCHE, H., SANGUINETTI, M. C. & LANG, F. (2006). Differential roles of S6 domain hinges in the gating of KCNQ potassium channels. *Biophys J* **90**, 2235-2244.
- SEOH, S. A., SIGG, D., PAPAIZIAN, D. M. & BEZANILLA, F. (1996). Voltage-sensing residues in the S2 and S4 segments of the Shaker K<sup>+</sup> channel. *Neuron* **16**, 1159-1167.
- SERRANO, L., NEIRA, J. L., SANCHO, J. & FERSHT, A. R. (1992). Effect of alanine versus glycine in alpha-helices on protein stability. *Nature* **356**, 453-455.
- SHANG, L. & TUCKER, S. J. (2007). Non-equivalent role of TM2 gating hinges in heteromeric Kir4.1/Kir5.1 potassium channels. *Eur Biophys J*.
- SHEALY, R. T., MURPHY, A. D., RAMARATHNAM, R., JAKOBSSON, E. & SUBRAMANIAM, S. (2003). Sequence-function analysis of the K<sup>+</sup>-selective family of ion channels using a comprehensive alignment and the KcsA channel structure. *Biophys J* **84**, 2929-2942.
- SHI, W., WYMORE, R. S., WANG, H. S., PAN, Z., COHEN, I. S., MCKINNON, D. & DIXON, J. E. (1997). Identification of two nervous system-specific members of the *erg* potassium channel gene family. *J Neurosci.* **17**, 9423-9432.
- SHIEH, C. C., KLEMIC, K. G. & KIRSCH, G. E. (1997). Role of transmembrane segment S5 on gating of voltage-dependent K<sup>+</sup> channels. *J Gen Physiol* **109**, 767-778.
- SIGWORTH, F. J. (1994). Voltage gating of ion channels. *Q Rev Biophys* **27**, 1-40.

## Chapter 8- Bibliography

- SLESINGER, P. A., JAN, Y. N. & JAN, L. Y. (1993). The S4-S5 loop contributes to the ion-selective pore of potassium channels. *Neuron* **11**, 739-749.
- SMITH, P. L.; BAUKROWITZ, T. & YELLEN, G. (1996). The inward rectification mechanism of the HERG cardiac potassium channel. *Nature* **379**, 833-836.
- SMITH, P. L. & YELLEN, G. (2002). Fast and slow voltage sensor movements in HERG potassium channels. *J Gen Physiol* **119**, 275-293.
- SMITH-MAXWELL, C. J., LEDWELL, J. L. & ALDRICH, R. W. (1998a). Role of the S4 in cooperativity of voltage-dependent potassium channel activation. *J Gen Physiol* **111**, 399-420.
- SMITH-MAXWELL, C. J., LEDWELL, J. L. & ALDRICH, R. W. (1998b). Uncharged S4 residues and cooperativity in voltage-dependent potassium channel activation. *J Gen Physiol* **111**, 421-439.
- SPECTOR, P. S., CURRAN, M. E., KEATING, M. T. & SANGUINETTI, M. C. (1996a). Class III antiarrhythmic drugs block herg, a human cardiac delayed rectifier K<sup>+</sup> channel. Open channel block by methanesulfonamides. *Circ Res* **78**, 499-503.
- SPECTOR, P. S., CURRAN, M. E., ZOU, A., KEATING, M. T. & SANGUINETTI, M. C. (1996b). Fast inactivation causes rectification of the IKr channel. *J Gen Physiol* **107**, 611-619.
- SPLAWSKI, I., SHEN, J., TIMOTHY, K. W., LEHMANN, M. H., PRIORI, S., ROBINSON, J. L., MOSS, A. J., SCHWARTZ, P. J., TOWBIN, J. A., VINCENT, G. M. & KEATING, M. T. (2000). Spectrum of mutations in long-QT syndrome genes. KVLQT1, HERG, SCN5A, KCNE1, and KCNE2. *Circulation* **102**, 1178-1185.
- SPLAWSKI, I., SHEN, J., TIMOTHY, K. W., VINCENT, G. M., LEHMANN, M. H. & KEATING, M. T. (1998). Genomic structure of three long QT syndrome genes: KVLQT1, HERG, and KCNE1. *Genomics* **51**, 86-97.
- STANSFELD, P. J., GEDECK, P., GOSLING, M., COX, B., MITCHESON, J. S. & SUTCLIFFE, M. J. (2007). Drug block of the hERG potassium channel: insight from modeling. *Proteins* **68**, 568-580.
- STANSFELD, P. J., SUTCLIFFE, M. J. & MITCHESON, J. S. (2006). Molecular mechanisms for drug interactions with hERG that cause long QT syndrome. *Expert Opin Drug Metab Toxicol* **2**, 81-94.
- STARACE, D. M. & BEZANILLA, F. (2001). Histidine scanning mutagenesis of basic residues of the S4 segment of the shaker k<sup>+</sup> channel. *J Gen Physiol* **117**, 469-490.

## Chapter 8- Bibliography

- STARACE, D. M. & BEZANILLA, F. (2004). A proton pore in a potassium channel voltage sensor reveals a focused electric field. *Nature* **427**, 548-553.
- STARACE, D. M., STEFANI, E. & BEZANILLA, F. (1997). Voltage-dependent proton transport by the voltage sensor of the Shaker K<sup>+</sup> channel. *Neuron* **19**, 1319-1327.
- STARKUS, J. G., KUSCHEL, L., RAYNER, M. D. & HEINEMANN, S. H. (1997). Ion conduction through C-type inactivated Shaker channels. *J Gen Physiol* **110**, 539-550.
- SUBBIAH, R. N., CLARKE, C. E., SMITH, D. J., ZHAO, J., CAMPBELL, T. J. & VANDENBERG, J. I. (2004). Molecular basis of slow activation of the human ether-a-go-go related gene potassium channel. *J Physiol* **558**, 417-431.
- SUESSBRICH, H., SCHONHERR, R., HEINEMANN, S. H., ATTALI, B., LANG, F. & BUSCH, A. E. (1997). The inhibitory effect of the antipsychotic drug haloperidol on HERG potassium channels expressed in *Xenopus* oocytes. *Br J Pharmacol* **120**, 968-974.
- TANG, W., KANG, J., WU, X., RAMPE, D., WANG, L., SHEN, H., LI, Z., DUNNINGTON, D. & GARYANTES, T. (2001). Development and evaluation of high throughput functional assay methods for HERG potassium channel. *J Biomol Screen* **6**, 325-331.
- TERLAU, H., HEINEMANN, S. H., STUHMER, W., PONGS, O. & LUDWIG, J. (1997). Amino terminal-dependent gating of the potassium channel rat *eag* is compensated by a mutation in the S4 segment. *J Physiol* **502**, 537-543.
- TINEL, N., DIOCHOT, S., BORSOTTO, M., LAZDUNSKI, M. & BARHANIN, J. (2000). KCNE2 confers background current characteristics to the cardiac KCNQ1 potassium channel. *Embo J* **19**, 6326-6330.
- TOMBOLA, F., PATHAK, M. M. & ISACOFF, E. Y. (2005). Voltage-sensing arginines in a potassium channel permeate and occlude cation-selective pores. *Neuron* **45**, 379-388.
- TORRES, A. M., BANSAL, P. S., SUNDE, M., CLARKE, C. E., BURSILL, J. A., SMITH, D. J., BAUSKIN, A., BREIT, S. N., CAMPBELL, T. J., ALEWOOD, P. F., KUCHEL, P. W. & VANDENBERG, J. I. (2003). Structure of the HERG K<sup>+</sup> channel S5P extracellular linker: role of an amphipathic alpha-helix in C-type inactivation. *J Biol Chem* **278**, 42136-42148.
- TRISTANI-FIROUZI, M., CHEN, J., MITCHESON, J. S. & SANGUINETTI, M. C. (2001). Molecular biology of K(+) channels and their role in cardiac arrhythmias. *Am J Med* **110**, 50-59.

## Chapter 8- Bibliography

- TRISTANI-FIROUZI, M., CHEN, J. & SANGUINETTI, M. C. (2002). Interactions between S4-S5 linker and S6 transmembrane domain modulate gating of HERG K<sup>+</sup> channels. *J Biol Chem* **277**, 18994-19000.
- TRISTANI-FIROUZI, M. & SANGUINETTI, M. C. (2003). Structural determinants and biophysical properties of HERG and KCNQ1 channel gating. *J Mol Cell Cardiol* **35**, 27-35.
- TRUDEAU, M. C., WARMKE, J. W., GANETZKY, B. & ROBERTSON, G. A. (1995). hERG, a human inward rectifier in the voltage-gated potassium channel family. *Science* **269**, 92-95.
- TSENG, G. N. (2001). I(Kr): the hERG channel. *J Mol Cell Cardiol* **33**, 835-849.
- TSENG, G. N., SONAWANE, K. D., KOROLKOVA, Y. V., ZHANG, M., LIU, J., GRISHIN, E. V. & GUY, H. R. (2007). Probing the outer mouth structure of the HERG channel with peptide toxin footprinting and molecular modeling. *Biophys J* **92**, 3524-3540.
- VANDENBERG, J. I., TORRES, A. M., CAMPBELL, T. J. & KUCHEL, P. W. (2004). The HERG K<sup>+</sup> channel: progress in understanding the molecular basis of its unusual gating kinetics. *Eur Biophys J* **33**, 89-97.
- WANG, H., ZHANG, Y., CAO, L., HAN, H., WANG, J., YANG, B., NATTEL, S. & WANG, Z. (2002). HERG K<sup>+</sup> channel, a regulator of tumor cell apoptosis and proliferation. *Cancer Res* **62**, 4843-4848.
- WANG, J., MYERS, C. D. & ROBERTSON, G. A. (2000). Dynamic control of deactivation gating by a soluble amino-terminal domain in hERG K<sup>+</sup> channels. *J Gen Physiol* **115**, 749-758.
- WANG, J., TRUDEAU, M. C., ZAPPIA, A. M. & ROBERTSON, G. A. (1998). Regulation of deactivation by an amino terminal domain in human ether-a-go-go-related gene potassium channels. *J Gen Physiol* **112**, 637-647.
- WANG, M. H., YUSAF, S. P., ELLIOTT, D. J., WRAY, D. & SIVAPRASADARAO, A. (1999). Effect of cysteine substitutions on the topology of the S4 segment of the Shaker potassium channel: implications for molecular models of gating. *J Physiol* **521 Pt 2**, 315-326.
- WANG, Q., SHEN, J., LI, Z., TIMOTHY, K., VINCENT, G. M., PRIORI, S. G., SCHWARTZ, P. J. & KEATING, M. T. (1995a). Cardiac sodium channel mutations in patients with long QT syndrome, an inherited cardiac arrhythmia. *Hum Mol Genet* **4**, 1603-1607.

## Chapter 8- Bibliography

- WANG, Q., SHEN, J., SPLAWSKI, I., ATKINSON, D., LI, Z., ROBINSON, J. L., MOSS, A. J., TOWBIN, J. A. & KEATING, M. T. (1995b). SCN5A mutations associated with an inherited cardiac arrhythmia, long QT syndrome. *Cell* **80**, 805-811.
- WANG, S., MORALES, M. J., LIU, S., STRAUSS, H. C. & RASMUSSEN, R. L. (1997). Modulation of HERG affinity for E-4031 by [K<sup>+</sup>]<sub>o</sub> and C-type inactivation. *FEBS Lett* **417**, 43-47.
- WARMKE, J. W. & GANETZKY, B. (1994). A family of potassium channel genes related to eag in *Drosophila* and mammals. *Proc Natl Acad Sci USA* **91**, 3438-3442.
- WEERAPURA, M., NATTEL, S., CHARTIER, D., CABALLERO, R. & HERBERT, T. E. (2002). A comparison of currents carried by HERG, with and without coexpression of MiRP1, and the native rapid delayed rectifier current. Is MiRP1 the missing link? *J Physiol* **540**, 15-27.
- WIBLE, B. A., HAWRYLUK, P., FICKER, E., KURYSHEV, Y. A., KIRSCH, G. & BROWN, A. M. (2005). HERG-Lite: a novel comprehensive high-throughput screen for drug-induced hERG risk. *J Pharmacol Toxicol Methods* **52**, 136-145.
- WITCHEL, H. J. (2007). The hERG potassium channel as a therapeutic target. *Expert Opin Ther Targets* **11**, 321-336.
- WITCHEL, H. J., DEMPSEY, C. E., SESSIONS, R. B., PERRY, M., MILNES, J. T., HANCOX, J. C. & MITCHESON, J. S. (2004). The low-potency, voltage-dependent HERG blocker propafenone—molecular determinants and drug trapping. *Mol Pharmacol* **66**, 1201-1212.
- WITCHEL, H. J. & HANCOX, J. C. (2000). Familial and acquired long QT syndrome and the cardiac rapid delayed rectifier potassium current. *Clinical and Experimental Pharmacology and Physiology* **27**, 753-766.
- WITCHEL, H. J., MILNES, J. T., MITCHESON, J. S. & HANCOX, J. C. (2002). Troubleshooting problems with in vitro screening of drugs for QT interval prolongation using HERG K<sup>+</sup> channels expressed in mammalian cell lines and *Xenopus* oocytes. *J Pharmacol Toxicol Methods* **48**, 65-80.
- WRAY, D. (2004). The roles of intracellular regions in the activation of voltage-dependent potassium channels. *Eur Biophys J* **33**, 194-200.
- YELLEN, G. (1998). The moving parts of voltage-gated ion channels. *Q Rev Biophys* **31**, 239-295.
- YELLEN, G. (2002). The voltage-gated potassium channels and their relatives. *Nature* **419**, 35-42.

## Chapter 8- Bibliography

- YELLEN, G., SODICKSON, D., CHEN, T. Y. & JURMAN, M. E. (1994). An engineered cysteine in the external mouth of a K<sup>+</sup> channel allows inactivation to be modulated by metal binding. *Biophys J* **66**, 1068-1075.
- YUSAF, S. P., WRAY, D. & SIVAPRASADARAO, A. (1996). Measurement of the movement of the S4 segment during the activation of a voltage-gated potassium channel. *Pflugers Arch* **433**, 91-97.
- ZAGOTTA, W. N., HOSHI, T. & ALDRICH, R. W. (1990). Restoration of inactivation in mutants of Shaker potassium channels by a peptide derived from ShB. *Science* **250**, 568-571.
- ZHANG, M., KOROLKOVA, Y. V., LIU, J., JIANG, M., GRISHIN, E. V. & TSENG, G. N. (2003). BeKm-1 is a HERG-specific toxin that shares the structure with ChTx but the mechanism of action with ErgTx1. *Biophys J* **84**, 3022-3036.
- ZHANG, M., LIU, J., JIANG, M., WU, D. M., SONAWANE, K., GUY, H. R. & TSENG, G. N. (2005). Interactions between charged residues in the transmembrane segments of the voltage-sensing domain in the hERG channel. *J Membr Biol* **207**, 169-181.
- ZHANG, M., LIU, J. & TSENG, G. N. (2004). Gating charges in the activation and inactivation processes of the HERG channel. *J Gen Physiol* **124**, 703-718.
- ZHAO, Y., SCHEUER, T. & CATTERALL, W. A. (2004a). Reversed voltage-dependent gating of a bacterial sodium channel with proline substitutions in the S6 transmembrane segment. *Proc Natl Acad Sci USA* **101**, 17873-17878.
- ZHAO, Y., YAROV-YAROVY, V., SCHEUER, T. & CATTERALL, W. A. (2004b). A gating hinge in Na<sup>+</sup> channels; a molecular switch for electrical signaling. *Neuron* **41**, 859-865.
- ZHOU, J., AUGELLI-SZARAN, C. E., BRADLEY, J. A., CHEN, X., KOCI, B. J., VOLBERG, W. A., SUN, Z. & CORDES, J. S. (2005). Novel potent human ether-a-go-go-related gene (hERG) potassium channel enhancers and their in vitro antiarrhythmic activity. *Mol Pharmacol.* **68**, 876-884.
- ZHOU, Z., GONG, Q. & JANUARY, C. T. (1999). Correction of defective protein trafficking of a mutant HERG potassium channel in human long QT syndrome. Pharmacological and temperature effects. *J Biol Chem* **274**, 31123-31126.
- ZHOU, Z., GONG, Q., YE, B., FAN, Z., MAKIELSKI, J. C., ROBERTSON, G. A. & JANUARY, C. T. (1998). Properties of HERG channels stably expressed in HEK 293 cells studied at physiological temperature. *Biophys J.* **74**, 230-241.

## Chapter 8- Bibliography

- ZOU, A., CURRAN, M. E., KEATING, M. T. & SANGUINETTI, M. C. (1997). Single HERG delayed rectifier K<sup>+</sup> channels expressed in *Xenopus* oocytes. *Am J Physiol* **272**, H1309-1314.
- ZOU, A., XU, Q. P. & SANGUINETTI, M. C. (1998). A mutation in the pore region of HERG K<sup>+</sup> channels expressed in *Xenopus* oocytes reduces rectification by shifting the voltage dependence of inactivation. *J Physiol* **509** ( Pt 1), 129-137.